Mckeown, Andrew (2022) Comparison of pump cavitation mitigation techniques in micro scale organic Rankine cycle systems. PhD thesis.

https://theses.gla.ac.uk/83045/

Systems, Power and Energy Research Division

School of Engineering

University of Glasgow

Andrew Mckeown

Comparison of Pump Cavitation Mitigation Techniques in Micro Scale Organic Rankine Cycle systems

In partial fulfilment of the requirements for the degree of Doctor of Philosophy at the University of Glasgow

Abstract

The reduction of carbon dioxide emissions is becoming an ever increasing driving force in the development of innovative and technological solutions. The utilization of waste heat sources can help reduce carbon dioxide emissions. Various technological options exist, one of which is the Organic Rankine Cycle. Large scale commercial Organic Rankine cycles are already in operation, however, their transition into smaller scale systems is hindered by several technical challenges one of which is pump cavitation. Several cavitation mitigation techniques have been stated in the literature to reduce cavitation with three of the most practical being stored liquid column height, subcooling and pump bypass. The effects of all three of these techniques on the overall performance has been experimentally investigated on a micro scale ORC system designed for such purpose.

Initially, the effects of 2.1 meters of liquid column height and by virtue system mass was investigated to determine its influence on the ORC cycle at; four differing pump speeds (600, 800, 1000 and 1200 rpm), three cold sink temperatures (10°C, 15°C and 20°C) and three expander loads. The effects of stored liquid column height had significant effect on the operation of the system. The maximum output power of 300W occurred at 1000 rpm with an optimum expander output trend present in most cases. At the highest tested 1200 rpm case the maximum boundaries of the system where insufficient to result in stable system operation, resulting in a maximum output power of only 240W. A reduction in cold side temperature results in no observable change in the stored liquid column height, with a general increase in expander output as a result of increased pressure ratio across the expander. The expander load had negligible effect on the low pressure side of the system both in terms of stored height and pressure.

The experimental test rig was then modified to include a subcooler and pump bypass. The system was tested with increasing levels of system mass at various pump speeds with multiple degrees of subcooling and bypass valve angle. The combined influence of liquid column height with both subcooling and bypass effects was observed for each pump speed. The inclusion of the system bypass provided no observable benefit to the experimental test rig and only resulted in a deterioration in system performance. The combined interaction between subcooling and liquid column height is clearly observable in the data, with only the combined effect providing significant influence to allow the test rig to operate at its maximum pump speed and therefore with maximum output power of 370W. However, although the incorporation of subcooling extended the operational range of the test system. The system efficiency improvement was negligible, 3.7% compared with 3.6% for the

liquid height only system. The added system components and required additional lower temperature cold sink, provide further additional barriers. The practical implications of these findings highlight the continual struggle to improve the viability of micro scale ORC systems, where the performance of the pump remains a significant barrier.

Contents

List of Tables

List of Figures

Acknowledgements

A number of thanks are due for the completion of this thesis

I would firstly like to thank my supervisor Prof. Zhibin Yu, his support throughout the process has made the completion of this process possible.

I would like to thank EPSRC, who funded my research

The technical staff who have work tirelessly to assist in the creation of the experimental rig, particularly Bernard Hoey, Peter Miller, Dennis Kearns, Brian Robb and Wilson Macdougall.

Lastly, I would like to thank my family and friends.

Declaration

I declare that, unless explicitly stated to be the contribution of others, that this thesis is entirely my own work and has not been submitted for any other degree, at the university of Glasgow or elsewhere.

Elements of this research have previously been published by the following places

"Correction of cavitation with thermodynamic effect for a diaphragm pump in Organic Rankine cycle systems", Wenguang Li, Andrew Mckeown and Zhibin Yu, Energy Reports 6, November 2020.

Definitions and Abbreviations

<u>Abbreviations</u>

Diap	Diaphragm
Memb	Membrane
NPSHa	Net Positive Suction Head available
NPSHr	Net Positive Suction Head required
OF	Oil Free
ORC	Organic Rankine Cycle
PR	Pressure Ratio
SE	System Efficiency

<u>Symbols</u>

A	Surface area (m^2)	
a, b	Polynomial coefficients	
h	Specific enthalpy (J/kg)	
$\dot{m}$	Mass flow rate (kg/s)	
N	Shaft speed (rpm)	
P	pressure	
$\dot{Q}$	Heat flux (W)	
r_p	Pressure ratio	
T	Temperature	
V	Volume (m^3)	
$\dot{V}$	Volumetric flow (m^3/s)	
W	Work	
$\dot{W}$	Power (W)	
n	Efficiency (-)	
ρ	Density (kg/m^3)	

<u>Subscripts</u>

s	isentropic
pump	pump
expander	expander

Chapter 1 – Introduction

1.1. Background

It is now widely recognized worldwide that the burning of fossil fuels has a significant and direct impact on the rising global temperature as a result of greenhouse gases. These rising temperatures are having a drastic impact of the global climate resulting in disappearing polar ice caps, rising sea levels and an increased frequency of extreme weather events, to name a few. In 2015 the Paris climate agreement was struck which aimed to mitigate the catastrophic impacts of climate change by limiting the global rise in temperature to well below 2°C above pre-industrial levels, preferably to 1.5°C [1]. Since then governments around the world have produced targets and strategies to reach net zero carbon emissions. As of 2021 the UK government has set a target to reach net zero emissions by 2050 and is planning to do this by decarbonizing the power system by 2035, implementing no new gas boilers by 2035 and the end to new sales of petrol and diesel cars by 2030 [2]. In order to help meet these ambitious targets, reducing our energy consumption is an important step. Increased efficiency of energy systems and a better utilization of available energy sources is one means this can be done. Large amounts of waste heat is produced in many of our domestic and industrial processes, which in most cases is simply discarded to atmosphere. Utilization of this discarded energy could play an important role in limiting the impacts of climate change. In order to recover energy from waste heat a number of technologies and solutions exist including district heating schemes, combined heat and power, thermal acoustics, Stirling cycle, kalian cycle and many more. One of these promising potential solutions in the organic Rankine cycle (ORC) which has received significant research interest of the decades.

1.2. The Organic Rankine Cycle

The organic Rankine cycle is made up of the same four key processes as the conventional Rankine cycle namely an evaporation process, an expansion process, a condensation process and a recirculation or pump process. The four key components are shown in Figure 1.
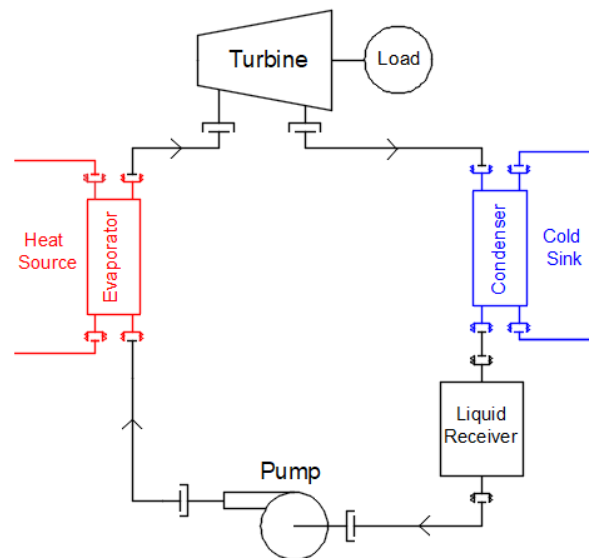
Figure 1: Basic Rankine Cycle system components

Starting from the inlet of the pump the working fluid is fed to an evaporator/boiler where it is vaporised. The vapour from the exit of the evaporator is then passed through an expander to extract mechanical work. If attached to a generator this work can be used to generate electricity. The vapour leaving the expander is then condensed to return it to a liquid state, before being recirculate back to the evaporator. If the working fluid is water then this cycle provides the basis for the conventional steam power plant. If the working fluid is an organic fluid, most commonly refrigerants, then this cycle provides the basis for organic Rankine cycle systems (ORC). The potentially lower vapour pressure of commonly used fluids like refrigerants results in lower evaporation temperatures, allowing lower temperature waste heat streams to be used to produce mechanical work or electricity. Although already implemented in larger scale systems there remains significant challenges in downsizing the process into smaller scale ORC applications. Some of these barriers centre around the ORC pump.

1.3. **Organic Rankine Cycle Pump**

The pump in the ORC system moves the liquid from the low pressure side of the system back to the evaporator at the higher pressure side of the system. The most common types of pumps used within the ORC community are gear pumps, centrifugal and diaphragm pumps which are normally commercially sourced. The commercially sourced components are designed to work with a vast range of working fluids across a wide range of engineering applications. This wide targeted working fluid approach can lead to various issues when adopted into ORC systems and ultimately leads to low efficiencies down below 35% [3] [4] [5] [6] [7]. These low efficiencies make a significant impact on the net

output of small and micro scale ORC systems which highlights the need for significant further improvements into ORC pumps.

1.4. **Pump Cavitation**

Cavitation is a phenomenon where the formation of bubbles in liquid occurs as a result of the pressure falling below the vapour pressure. Cavitation happens in many different industrial process and causes a problem generally in pumps. The inclusion of bubbles during the pump process causes a number of problems including mass flow changes and pump damage. The formed bubbles tend to collapse on surfaces which can cause significant erosion, vibration and noise issues [8], significantly reducing the working life of system components. Pump manufactures therefore specify a minimum pressure difference between the pump inlet pressure and the vapour pressure, to avoid cavitation issues. This minimum required pressure difference is known as the net positive suction pressure required (NPSHr). Its value is normally specified in vertical height in meters and is of the magnitude of several meters, depending on the pump. Due to the nature of the organic Rankine cycle, the working fluid leaves the condenser close to its vapour pressure resulting in a low available net positive suction head (NPSHa). This inherently low available net positive suction head (NPSHa) combined with generally high required net positive suction head (NPSHr) results in a high susceptibility of organic Rankine cycle systems to pump cavitation.

In terms of a closed loop organic Rankine cycle system, pump cavitation as well as general pump damage can have a significant effect on the ORC cycle as a result of mass flow changes. The mass flow rate has a significant effect on several aspects of the ORC system including: expander work, high side pressure, working fluid density, evaporator hold up heat transfer co-efficient etc [9] [7] [10] [11]. In general a drop in mass flow rate away from the design flow rate as a result of cavitation bubble formation results in a deterioration of performance. In extreme cases due to the closed loop cycle of the ORC variations in mass flow rate can develop into system instability as a result of pump surge and collapse, which has been observed in various ORC systems [12] [5] [13]. The author has also observed this phenomenon in a previous micro scale ORC system as well as in the development of this thesis.

Several techniques have been mentioned in the organic Rankine cycle literature as a means of mitigating pump cavitation: Increased liquid column height [13], pre feed pump [10] [14], pump bypass [15], nitrogen buffer [16] and most commonly sub-cooling [5] [13] [11]

[7] [4] [12]. However, within the research there remains a significant variation in the required level and effectiveness of cavitation prevention techniques, and their interaction between each other. For example in the literature the required degree of subcooling varies from 1°C [7] to upto 20°C [13]. Since the pump and mass flow play a significant role in the organic Rankine cycle performance, a further investigation into cavitation and mitigation techniques would be beneficial.

1.5. **Research Areas and themes for this thesis**

The broad reaching aim of this thesis is to investigate the effects of cavitation on the performance of micro scale ORC systems and evaluate the main techniques and their combined interaction for mitigating cavitation. A broad review of ORC literature, in general, as well as a more specific look at ORC cavitation has been carried out. The information from the review was used to develop a micro scale ORC experimental test rig. Initially investigating the interaction between system mass and stored liquid column height, and their interaction with several ORC system parameters: pump speed, condenser temperature and expander load. The initial rig was then modified to include a subcooler and pump bypass valve to evaluate the combined interaction between liquid column height, degree of subcooling and pump bypass. Their influence on the system performance was evaluated at different pump speeds.

Chapter 2 – Literature Review

A broad and wide reaching review of the organic Rankine cycle literature has been carried out and is presented initial. The purpose is to give a general background and overview of micro sized ORC systems. A more specific review of cavitation and its interaction with the organic Rankine cycle is then presented.

2.1. Broad Review of Organic Rankine cycle systems

2.1.1. Heat sources

The ability to effectively recover energy from heat is highly dependent on the heat source temperature/quality. The higher the available heat source temperature the higher the system efficiency which ultimately leads to a more financially viable ORC system. The heat sources are typically characterized into the following ranges [17]: high temperature (>650°C), medium temperature (230-650°C) and low temperature (<230°C). The composition and phase of the heat source medium can have a significant impact on the system with generally better heat transfer co-efficients for liquid mediums (pinch point temperatures 5-15 K [18]) compared with gases such as exhaust flue gases and air (pinch point temperatures 30 K [19]). In current ORC applications the main commonly utilized heat sources are biomass, solar, geothermal, industrial and power waste heat (including internal combustion engine and gas turbine).

Biomass

Biomass is normally a plant or animal based material that can be used to produce energy by either directly burning the material in a boiler such as wood pellets or converting the biomass material into a synthetic gas via a gasification process. The gas is then burned and the heat can be directly used for heating stream or used to generate electricity. Due to working fluid limitations, thermal stability limits the ORC system temperature to 330°C [20]. Biomass-organic Rankine cycle applications are normally combined as part of a combined heat and power plant (CHP), which results in higher ORC condenser temperatures of 80-120°C [21]. Commercial Biomass-ORC systems are already present in the market with companies such as Turboden, Rank, etc. There are various commercial biomass ORC plants with Turboden building a 6.5 MW plant in Holbrook industrial estate (Sheffield) [22] and Electratherma supplied an ORC system to Summerseat & Bradley fold garden centre which utilises 119°C heat [23]. The already commercialisation of biomass powered ORC systems shows that biomass already offers an effective heat source. Where

normally discarded by products can be converted into useful heat and power. The process by one means or another, however, still involves the burning of either a gas or product that releases emissions such as carbon dioxide into the atmosphere. Its use in future as a potential heat source is uncertain in a net zero society, where the release of carbon dioxide to the atmosphere is continually being restricted.

Solar

Solar panels converting light directly into electric (photovoltaic) is already a highly commercial industry, producing significant amounts of renewable energy around the world. An alternative to converting solar directly to electricity is to convert the solar energy into heat. In order to do this effectively a bank of solar reflectors are used to track the sun and concentrate the solar energy into a collector which transfers the energy into a fluid. The elevated temperature fluid can then be used either directly in a heating scheme or used to produce electricity via conventional power generation systems or using an Organic Rankine Cycle system. Commercial larger scale ORC systems already exist, with a significant amount of experimental systems outlined throughout the literature. A 1 MWe plant has been built in Arizona with a collector field of 10,000 m^2 [24] along with a 3 kWe plant in Lesotho with a 75 m^2 collector field area [25]. The use of solar power in any application either to provide heat or generate electricity is highly dependent on the amount of available solar radiation the system can absorb. The irradiation levels vary significantly around the world and within the Uk with areas in the north of Scotland around 70 Wm^2 (Annual Average) compared with approximately 120 Wm^2 in London and along the south coast of England [26]. A simulation based paper by Freeman evaluated the use of a solar-powered ORC system for combined heating and power applications for the UK domestic market. The result concluded that for a system using R245fa (120°C heat source, 10°C heat sink) and 15m^2 solar area: an annual average net power generation of 80-90 We was possible for an approximate capital cost of £4400-5500. The system also has the potential to provide 86% of domestic household hot water supply [27]. However, this high capital cost with low net power generation is potentially hindering commercial adoption.

Geothermal

Geothermal energy is the contained heat energy of the earth's interior. The earth has a geothermal gradient as the heat moves from the high temperature depths to the surface.

This gradient differs at different locations due to the local geology with some high temperature regions within drilling depth of the surface. In some circumstances water can collect in the regions, forming high temperature and pressure aquifers providing a source of extractable energy. The hot water or steam can then be used as a heat source before being reinjected back into the reservoir which helps prolong the commercial viability of a field. The temperatures, pressures, quantity and geothermal fluid properties of geothermal wells are highly dependent on the individual well, but can provide temperatures upto 300°C in some areas of the world [28]. This has led to multiply geothermal applications around the world including organic Rankine cycle systems. In the Uk the geothermal activity isn't as significant as some regions of the world, however, there are areas in which energy can be utilized. In Southampton a hot sediment aquifer is used to provide water less than 80°C in a district heating scheme [29]. Higher temperature geothermal sources of energy are possible in the UK with a Hot Dry Rock approach. HDR involves using two bore holes at either end of heated network of fractured rock. Water is injected into one of the bore holes and extracted from the other at a suggested 150°C for a drill depth of less the 5km depth (stated practical lower limit for utilising Hot Dry Rock) [30]. Although this temperature is higher and provides a better opportunity to extract energy the installation cost for both the extraction of heat from the rock and the power generation equipment makes commercial viability of this type of standalone ORC application low.

Industrial waste heat

Industrial processes consume large amounts of energy to produce heat, with a substantial quantity subsequently discarded into the environment. The temperature and medium in which the heat is discarded varies significantly with heavy industry such as glass, ceramics and steel, producing significant quantities of waste heat in the temperature range of between 300-400°C [31]. A case study on a cement industry carried out by Engin, demonstrated that approximately 40% of the energy consumed was lost in the hot flue gas, cooler stack and kiln shell (19.15%, 5.61% and 15.11% respectively) [32]. As well as high temperature waste heat sources, many industrial processes produce lower grade heat such as the whisky industry that makes use of steam boilers to heat stills. During the distillation process large quantities of ethanol are boiled off in stills maintained at temperatures of 78°C for periods of 4 to 7 hours per distillation. The type of still affects the processing but a typical still used in a malt distillery uses about 700-800 kW of heat from steam per still, which can be recovered into hot water at around 80°C. A grain distillery can produce in the

region of 40 metric tonne equivalents of steam per hour which is used for multiple applications including injection into a grain cooker, drying dark grains and in stills which have a spent wash temperature of 84-90°C. A significant amount of heat energy is therefore used throughout the distillation process. A case study of one Scottish distillery was noted to consume 1,646,320 litres of oil for one year to produce steam at 180°C and 8 barg [33]. In this one industrial process multiple ORC heat sources exist including the process steam, the exhaust gases from the steam boilers along with the condensation of distillate. Multiple potential heat source streams is synonymous with many industrial ORC applications and each case has to be taken in isolation to determine the best possible utilization of the heat due to the unavoidable process variations.

Power waste heat

Power waste heat can come from a variety of systems including gas turbines and internal combustion engines. With one significant application of ICE engines being transport. Generally in most cars and vans etc, approximately one third of energy converted from the total fuel energy is used for mechanical power, the majority of the remainder is lost as heat to the atmosphere through the radiator (80-100°C) and the exhaust gases (400-900°C) [34]. A significant amount of research has been carried out in the potential adoption of an ORC system with vehicle transport. Dual loop systems or systems that use engine cooling as a preheater can make much better use of the available heat source. However, effectively utilizing multiple heat sources can add significant complexity [19]. The current major factor in using ORC's in vehicle transport in the Uk is the ban on no new diesel or petrol cars/vans (including hybrids) from 2030 [2]. Although, other transportation options including larger commercial vehicles, ferries and other marine ICE's are not currently part of this ban. Song concluded that from a theoretical point of view a net power output 101.1 kW could be generated from a marine diesel engine [35]. Hoang also concluded in theory that recovery of waste heat from diesel engines saved up to 10% of the fuel consumption [36]. The major challenges faced with ORC-transport applications is the significant space and weight constraint, along with significantly varying load conditions.

2.1.2. Heat Sinks

The heat sink of the ORC is predominantly released to the environment either into air or water. Due to heat transfer coefficients, water is normally regarded as the better choice,

however, in certain applications a useable cold water supply may not be available. Mains water in the Uk is typically around 10°C and provides an attractive option. It should be considered that mains water in the Uk is treated to potable/drinkable standard. The process of treating the water to a standard well above that required for the purposes of heat transfer consumes a significant amount of energy and for this reason should be avoided if the water is to be discarded to the environment. The Uk has a significant network of streams, canals and reservoirs that can provide fresh water sources along with a significant coastline whereby salt water can be used. Fresh water sources are preferred to reduce corrosion problems, however depending on the source, it may be loaded with a significant biological content promoting fouling of the heat exchangers. It should also be noted that in Scotland and potentially some other countries the temperature of water discarded into the environment may be subjected to temperature restrictions [37]. Whether it be an air or water environmental heat sink, its temperature (which has a significant effect on the system) will vary throughout the day and sessions. A factor that is often overlooked during experimental system testing.

2.1.3. Working fluids

The principle of the Rankine cycle can be applied to a huge variety of fluids. The fluids are typically separated into three categories based on the shape of the saturation vapour curve: dry fluids have a positive slope, isentropic fluids have a close to vertical vapour saturation line and wet fluids have a negative slope. The main implication of this categorisation, is based around the expansion process. A fluid that enters the expander at a pressure and temperature close to the saturation curve will result in significantly different outlet conditions based on the working fluid category. A dry fluid with a positive slope will have an increased amount of superheating after an isentropic expansion process, an isentropic fluid having very similar amounts of superheating to the inlet condition. Both dry and isentropic fluids will remain in the vapour phase after isentropic expansion. A wet fluid on the other hand, will expand into the two phase region of the vapour dome producing condensation in the expander. The formation of condensate droplets can cause significant issues depending on the type of expander used. Due to this phenomena many ORC systems generally opted for dry and isentropic fluids. This working fluid categorisation is only one of many potential fluid selection criteria, with working fluid selection in general being investigated significantly within the ORC community [38] [39] [40] [41] [20] [42]. Generally, the fluid selection criteria is based on the application of the ORC system (sink

temperatures etc) and the individual fluid properties such as latent heat of vaporisation (lower latent heat of vaporisation leads to closer heat source temperature profile match, reducing heat exchanger irreversibility's [43]), heat transfer coefficients, toxicity, ozone depletion potential (ODP), global warming potential (GWP), decomposition temperature, flammability as well as cost. Unsurprisingly there is no one fluid that is optimal for all applications and fluid selection has to be done on a case by case basis.

A major factor that is resulting in a continual reduction in working fluid choice is due to environmental considerations under the Montreal Protocol [44]. The Montreal Protocol is an internationally recognised treaty that was introduced to protect the ozone layer, by a reduction in the production of substances that are contributing to ozone depletion. The protocol requires the ban on import and production of most chloroflurocarbons (CFS) by 1996, and the ban on import and production of hydrachloroflurocarbons (HCFCs) by 2030: which includes HCFC-123 used in some experimental ORC systems [14] [45] [46]. The Kigali Amendment added to the Montreal Protocol which came into force in 2019 added a further phasing down of hydrofluorocarbons (HFCs) by 80% over 30 years with the Uk government imposing a 79% reduction by 2030 [47]. HFC-134a is included in this list which again has been used in Organic Rankine Cycle systems [48] [49]. Although, these phase outs reduce the available selection of working fluids, there remains an extensive list of potential options.

2.1.4. ORC System layout

The Organic Rankine Cycle in its simplest form comprises of the four main elements of the pump, evaporator, expander and condenser. In practical terms, although possible to get a system running without one, a working fluid buffer/receiver is commonly part of the basic Organic Rankine Cycle system shown in Figure 2(left). The working fluid buffer is normally located before the pump and is used to store low pressure liquid working fluid after it has been condensed. The liquid receiver provides a mass buffer for the system to account for any system fluctuations. This simplistic system layout has very few components, providing a straightforward and low cost organic Rankine cycle solution. As mentioned in the previous section dry working fluids are commonly adopted in ORC systems which results in an increase in vapor superheat after expansion.This superheat can be used to preheat the liquid entering the evaporator, by means of the regenerator/recuperator. The preheating of the liquid reduces the demand from the heat source improving system efficiency [50] [51]. This leads to the regenerative cycle system

layout shown in Figure 2(right). However, the additional heat exchanger comes with increased financial cost along with a system pressure loss.
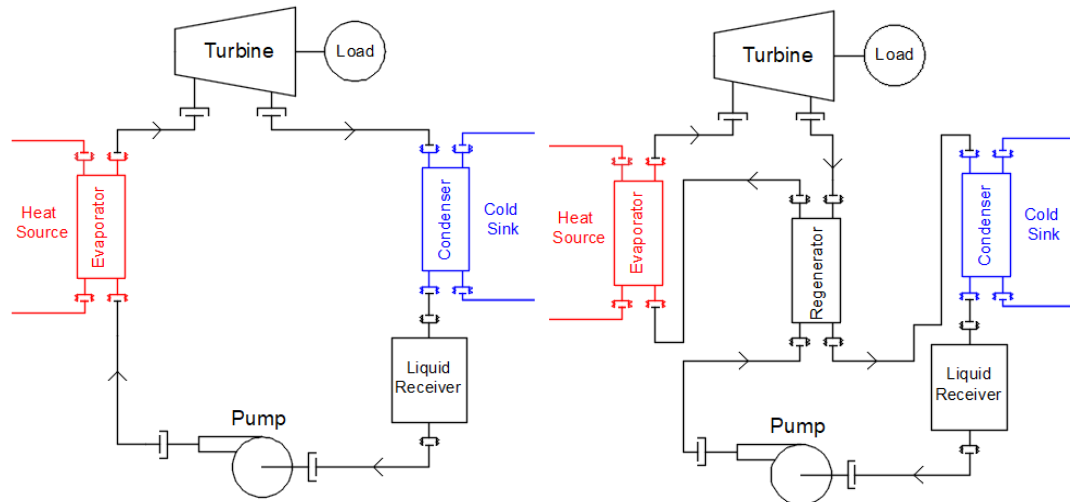
Figure 2: Basic Organic Rankine Cycle Layout (Left) with pump, evaporator, expander, condenser and liquid receiver. Regenerative Organic Rankine Cycle Layout (Right) which is the same as the basic layout with an additional heat exchanger used as pre heater for the evaporator.

2.1.5. ORC System Components

ORC systems are normally categorised based on the power output of the system, generally into micro (0.5-10 kW), small (10-100 kW), medium (100-kW – 1Mw) and large (>1MW) sized systems. Inevitably the system size has a significant effect on the type and size of the components. Although, overlaps do occur between various components and sizes, the experimental aspect of this thesis is based on a low temperature (below 100°C) micro scale ORC system. Therefore, the scope of this section of the literature review is primarily focused around system components and research in the micro to small region of the organic Rankine cycle spectrum. Table 1 contains a non-exhaustive list of microscale experimental research systems found in the literature.

Table 1 Non-Exhaustive list of micro Scale Organic Rankine Cycle Systems. Key: System efficiency (SE), Diaphragm (Diap), Membrane (Memb), Centrifugal (Cent). Derived from Compressor (DC), Oil-Free (OF), simulated expander (SME), Pressure Ratio (PR), Where possible the maximum reported values are presented in the table

Expander	volume ratio	Working fluid	Output power	Hot Side Temp	Cold Side Temp	SE	Pump type	
Scroll (DC, OF)	4.57	HCFC-123	187-256 W	-	22	7.2	Gear	[14]
Scroll (DC,OF)	4.05	HCFC-123	1.82 kW	-	-	-	Diap	[45]

Scroll	-	HCFC-123	3.2 kW	160	22-25	5.1	Piston	[10] [52]
Scroll (OF)	3.5	HCFC-123	2.8 kW	148-155	26-28	4.9	Diap	[13]
Scroll	-	HCFC-123	3kW	99-199	19	6.4	-	[11]
Scroll (DC)	2.44	HCF-134a	1-3.5 kW	80	5	-	Memb	[48]
a. Rotary-piston b. Scroll (DC)	a. 4 b. 2.7	R-123	a. 2kW b. 3kW	198	-	-	Gear/ Piston	[46]
Scroll (DC)	-	R113	450W	140	20	13	-	[53]
Scroll (DC)	-	HFC-134a	-	-	-	-	Diap	[49]
Scroll (DC)	PR - 3.5	HFC-245fa	100W	70	20	2.8	Gear	[54]
Scroll	3.5	HFC-245fa	1 kW	135	8	5.64	Gear	[55]
Scroll	3.5	HFC-245fa	160W	100-140	10-30	5.7	Plunger	[9]
Scroll	-	HFC-245fa R601a	550W	180	-	4.4%	Diap	[56]
Vane	-	HFE7000	860W	127	5	-	-	[57]
Vane	-	HFC-245fa	50W	60-90	7-12	-	Diap	[58]
Vane	-	HCFC-123	500W	40-90	-	5.8	-	[59]
Screw	-	HFC-245fa	-	115	10	-	Diap	[60]
Screw	-	HFC-245fa	3.5 kW	105-120	23-30	4.67	Diap	[61]
Piston	-	HFC-134a	1.2kW	50-90	16-25	4.5	Gear	[7]
(SME)	-	R600a	-	75-100	12.2	-	Cent	[62]

2.1.5.1. Expanders

There are various options for the choice of expansion device and they are normally separated into two defined categories, positive displacement and velocity/dynamic (Turbine) type. The main positive displacement machines comprise of scroll, single and twin screw, rotary vane and reciprocating piston. Positive displacement devices are defined primarily by a fixed volume change between the inlet and outlet of the expander due to the physical geometric volume constraints of the device. Turbomachines normally comprising radial or axial flow turbines, rely on a pressure differential across a series of blades to

generate a rotational force producing shaft work. Turbines are susceptible to increasing windage loss with reducing size, which is one of the main reasons positive displacement devices are better suited to smaller scale ORC systems [63]. Other reasons include higher pressure ratios, lower rotational speeds and lower flow rates compared to turbo machines [45] . Turbines are also much more sensitive to the formation of liquid droplets during expansion compared with positive displacement devices [64]. The turbine blades can suffer significant erosion as a result of liquid droplets striking the blades. During expansion the working fluid, therefore, has to remain in the superheated region. Generally, scroll and vane devices are used in the 1-10 kWe range, single and twin screws operate in the 15-200 kWe range, reciprocating pistons in the 20-100 kWe range and turbine type devices typically operating from the hundreds of kWe into the mega Watt range [65].

Positive displacement devices

Although positive displacement devices are generally better suited to smaller scale ORC applications there remains some significant practical issues with their adoption. The fixed internal volume change can result in under and over expansion losses. In both cases there is a mismatch between the internal pressure change of the device, and the system high and low pressure, which has a significant effect on the expander performance [45]. Lubrication of these devices helps reduce internal leakage and reduce wear. However, poor oil management can lead to reductions in expander efficiency and hinder heat transfer in heat exchangers [66]. The management of lubrication can be handled in numerous ways including direct high side injection, using the working fluid as the lubricant, etc. [67] [61]. Some expander systems are stated to be oil free, however, they generally have to adopt larger clearance distances, increasing leakage [68] [69] [70].

Scroll Expander

In a scroll expander two intermeshed scroll wraps create constrained pockets of vapour that move from the high pressure central region of the device to the low pressure area at the peripheral. An illustration of the expansion process is shown in Figure 3. The high pressure from the evaporator enters the expander in the central region, pushing outwards against the wrap causing the scroll to orbit outwards. This motion encloses a crescent shaped volume of vapour between the wraps that expands outwards around the scroll until it discharges to the low pressure side of the system. Multiple vapour pockets expand outward

simultaneously helping to smooth out the rotation of the device. This type of expander employs no valves which reduces their part count, improving reliability [64] [14]. The scroll expander was originally developed from scroll compressors that have been used extensively as refrigeration compressors and air compressors prior to their adoption as expanders. Many of the initial scroll expanders used in ORC prototypes where often converted scroll compressors [14] [45] [48].
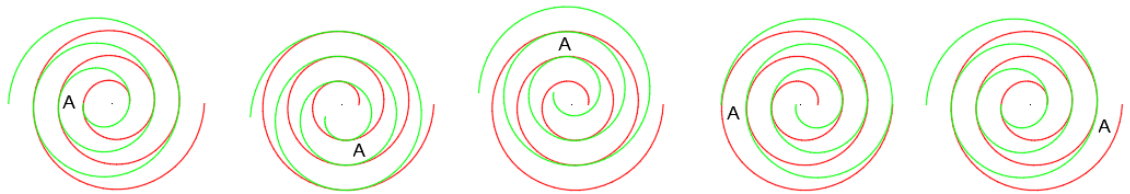
Figure 3: Illustration of the expansion process for a scroll expander following an enclosed volume 'A'. The enclosed volume bounded by the edge of the wraps moves outward from the central region to the scroll periphery.

Scroll expanders can be broken down into two types, kinematically rigid: which maintains a small clearance gap between the scrolls. Compliant type: whereby the wraps of the scroll are allowed to contact each other. Compliance in the radial and axial directions allows for sudden pressure spike and the presence of small amounts of foreign matter and liquid without damaging the device. The use of oil is therefore required in compliant type devices to reduce frication and wear between the wraps. Kinematically rigid devices can be run oil free, however, the addition of oil can help to seal the larger clearance gaps but too much oil can lead to a reduction in expander efficiency [66].

Screw Expander

Twin screw expanders consist of a male and corresponding female helical rotor that mesh together to form a seal. The high pressure vapour enters one end of the housing and pushes against the enclosed volume created by the pair of meshed rotors and the casing, causing the screws to rotate. As the screws rotate the enclosed volume moves through the device and increases in size, expanding the vapour as illustrated in Figure 4.
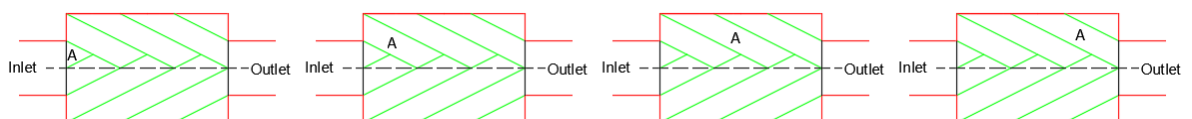
Figure 4: Illustration of the expansion process for a twin screw expander from left to right following an enclosed volume 'A'. The enclosed volume is created between the meshed rotors and the casing of the device.

Rotary Vane

Rotary vane expanders consist of a casing and a rotor which houses a set of sliding vanes as illustrated in Figure 5. The rotational movement of the rotor imparts a centrifugal force on the sliding vanes which forces the vanes against the casing creating a seal. In this example as the vanes rotate, from the inlet to the outlet, they move outwards with the increasing volume of the casing. The working fluid enters at the inlet of the expander and is enclosed between two vanes as it rotates. The fluid then expands around the device as the enclosed volume increases. The working fluid is then exhausted towards the end of the rotation.
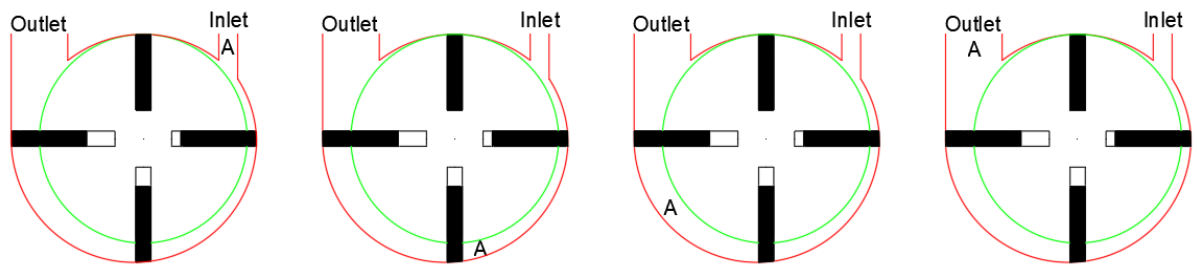
Figure 5: Illustration of the expansion process for a rotary vane expander from left to right following an enclosed volume 'A'. Centrifugal force causes the sliding vanes to press against the casing of the device. The vapour is enclosed between two vanes and expands as the volume increases.

Compared against an ideal expansion cycle, the most common expansion loses are attributed to: pressure drops due to filling and evacuation, frication including the contact of the sliding vanes with the casing, internal leakages and heat loss [59].

2.1.5.2. Heat exchangers

The transfer of heat to and from the system at the condenser and the evaporator can have a significant impact on system performance as well as cost. In terms of research, the use of heat exchangers are wide spread in a huge number of engineering applications, with journals including the journal of heat transfer containing leading edge modelling and heat transfer applications. In ORC experimental applications the vast majority of systems utilise commercially available heat exchangers. In general shell & tube type heat exchangers are normally adopted in larger ORC applications, with brazed plate heat exchangers used in smaller systems. The flow conditions and the composition of the two fluids are the major factors determining heat exchanger design. However, in some applications like automotive applications size and weight are important considerations.

2.1.5.3. Loads and Generators

In order to create resistance to rotation a load has to be applied to the expander to create the pressure difference in the system. The greater the resistance to rotation of the expander shaft the greater the potential pressure difference between the high and low side of the ORC system. In the experimental systems reviewed in the literature various techniques have been adopted with Table 2 outlining some different ORC loads. The load types fall mainly into two main categories mechanical and electrical loads. The electrical load types require a generator or alternator to convert the rotational movement of the expander into electrical energy, followed by an electrical circuit to control the electrical load on the generator. The downstream electrical load varies from a simple resistive load to direct grid connection [58] [46]. The resulting current and voltage draw on the generator has significant effect on rotational speed and resistance of the expander [57]. This poses a significant issue depending on the downstream application of the ORC system, with varying electrical demand resulting in significant changes to expander rotational speeds, pressures and performances. The mechanical loads used throughout the ORC literature normally involve direct coupling (or by means of pulleys and gears) of the expander shaft to an additional system or device. This can range from simple connection to torque sensors and brake motors for purely experimental ORC systems to direct coupling to additional systems such as the compressor of a refrigeration system or high pressure pump in a desalination system [49]. There is a significant variation in the adopted load types for Organic Rankine Cycle systems with the chosen load highly dependent on the application of the system.

Table 2: Non-exhaustive selection of different experimental ORC load types

Load type		Notes:	Reference
Electrical	3 phase asynchronous	Set of Capacitors, adjustable voltage transformer, fixed resistive load	[48]
Electrical	2 pole generator	The grid: Ohio State	[46]
Electrical	Alternator	Circuit to induce initial alternator electromagnets and various DC bulbs to provide resistive load	[57]

Mechanical	Torque meter	Torque meter connected to unspecified resistance	[53]
Mechanical	Oil Pump	The movement of oil around a tank provided the resistive load (experimental)	[71]
Mechanical	Desalination pump	Mechanical coupling to desalination pumps via gearing	[49]

2.1.5.4. Receivers and system fill

A significant amount of systems opt for ORC liquid receivers to balance the mass flow around the system, the receiver is most commonly placed before the pump. The purpose of the liquid receiver is to store any surplus working fluid, most commonly in liquid form, that isn't utilised by the ORC under prevailing system conditions. The receiver is most commonly a simple hold tank although, some experimental systems make use of the internal condenser volume to store the fluid [13]. A shell-tube heat exchanger was used as the condenser and to store the excess working fluid. The disadvantage of this approach is that increasing charge volume, reduces the available condenser heat transfer area which results in lower heat transfer coefficients and larger system back pressures. The liquid level and system mass fill is not normally stated in the vast majority of reported experimental findings, even though the system charge level can have a significant impact on system performance. Kim noted that increasing the mass in the system resulted in an increase in expander power output along with pump power consumption, which eventually reaches a net max power [54]. However, doesn't provide an explanation as to the reasons behind this trend. Cao expands this concept further and states that increasing the mass in the system, increases the expander outlet pressure (as a result of back pressure) and increases the pump inlet pressure resulting in an increase in system mass flow [60]. Liu notes that increasing the charge in the system will lead to an increase in evaporator and condenser pressures [13]. The level of mass or system charge, the size and shape and the location of the receiver in the system has a significant effect on the pump performance.

2.1.6. ORC Pumps

The pump in the ORC system moves the liquid from the low pressure side of the system back to the evaporator at the higher pressure side of the system. The most common types of pumps used within the ORC community are gear pumps, centrifugal and diaphragm pumps which are commercially available components. Some of the main performance aspects of the pump being pump efficiency, tightness, controllability and required Net Positive Suction Head [72]. The commonly used commercially available components are designed to work with a vast range of working fluids across a wide range of engineering applications. Therefore, their adoption into ORC can lead to a wide range of issues. For example, Mathias found that the low viscosity of the organic fluids resulted in a substantial amount of leakage back through the gears of a gear pump [46]. In addition these commercially bought pumps generally have NPSHr values in the range of several meters that has led to cavitation issues in a number of experimental ORC systems.

2.1.6.1. Pump types

The most commonly used pump types in the ORC community are diaphragm, gear and centrifugal pumps. Both diaphragm and gear pumps are of the positive displacement type and centrifugal pumps are of the "rotodynamic" type. A brief description of the different pump types is outlined as follows.

Diaphragm

A diaphragm pump is a positive displacement device that normally converts a reciprocating motion into a linear motion to drive a diaphragm. An illustration of a diaphragm pump is shown in Figure 6.
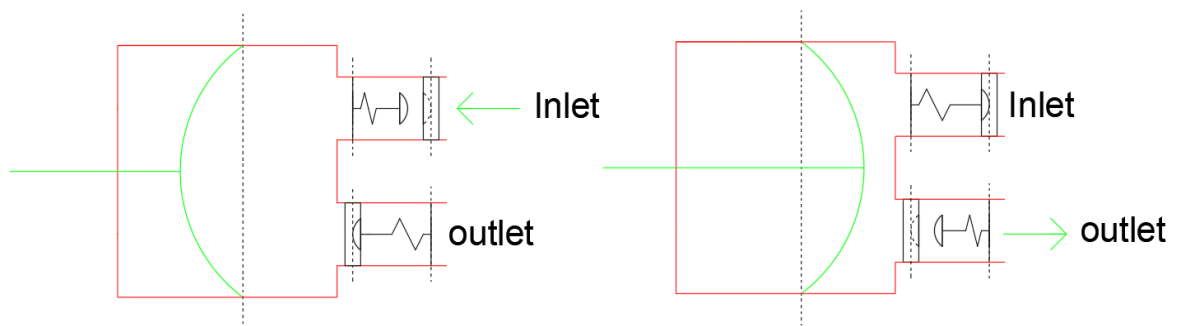
Figure 6: Simplified illustration of a single diaphragm pump during pump inlet stroke (left) and Outlet stroke (right)

The movement of the diaphragm can either be directly flexed using mechanical action (i.e by a piston) or by means of a hydraulic fluid that occupies one side of the diaphragm with the working fluid on the other. Similar to strokes of an internal combustion engine these pumps normally employ valves which are used to mitigate reverse flow. The reciprocating

motion of diaphragm style pumps can result in pulsation problems, which can cause issues in experimental pressure sensor fluctuations. Pulsation dampeners can, however, be employed to elevate the fluctuations. One of the main advantages of the diaphragm pump is the diaphragm material can provide a dynamic seal between the working fluid and the environment minimising loses to the environment [73] . Where environmental losses are strictly controlled when using fluorinated gases.

Gear

Gear pumps are another commonly used type of positive displacement pump with a simplified illustration shown in Figure 7. Rotating gears or cogs enclose a volume of working fluid between the casing of the pump and the teeth of the gears. The fluid is drawn from the inlet and forced out of the enclosed volumes by the meshing of the gears. The flow pattern is significantly smoother than diaphragm pumps. The clearances between the teeth and the casing, along with the viscosity of fluid impact the pump leakage. Gear pumps are generally suited to higher viscosity fluids, whereby Mathais found substantial leakage between the gears when using R123 in an experimental ORC, partly due to the low viscosity of the working fluid [46].
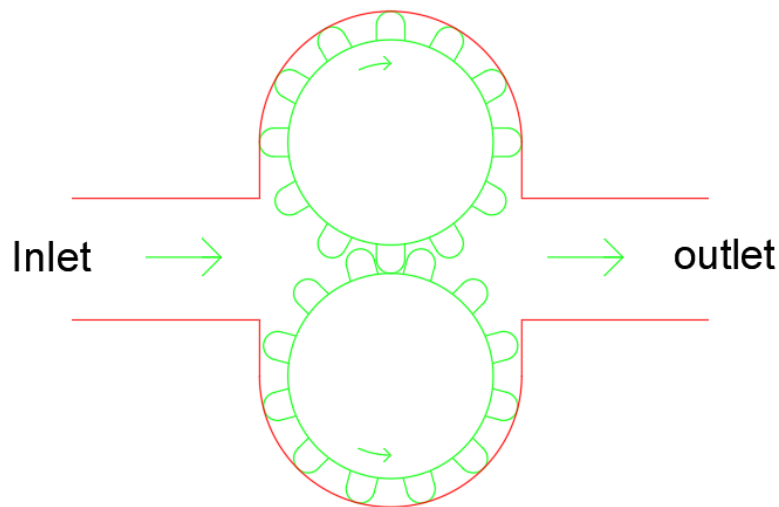
Figure 7: Simplified illustration of a gear pump

Centrifugal

Centrifugal pumps or rotodynamic pumps make use of a driven rotor otherwise known as an impeller to move liquid, in the case of Figure 8, from the central region of the pump to the peripheries. The fluid enters the central region, whereby the rotational motion of the impeller accelerates the working fluid along the vanes to the pump casing. The fluid

velocity is then slowed by means of a volute chamber or a diffuser. Centrifugal pumps are generally better suited to lower pressure applications using lower viscosity fluids. Although rotating at constant speeds the systems employ no valves, which can result in variable volumetric flow rates at fixed impeller speed depending on the system parameters.
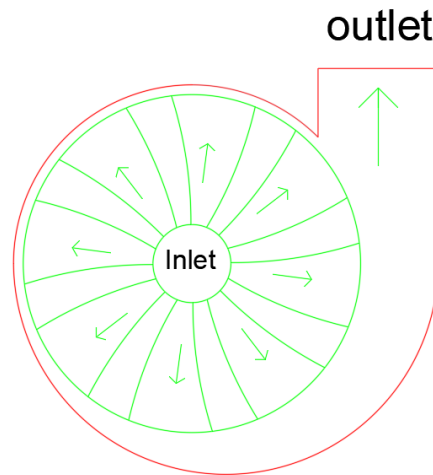
Figure 8: Simplified illustration of a centrifugal pump

2.1.6.2. Efficiency and Back Work Ratio

In theoretical modelling it has been common practice to assume pump efficiencies of greater than 50%. However, in small and micro scale applications the real efficiencies are often significantly lower with Quoilin achieving 25% [3], Landelle reported an average efficiency of 35% for small scale ORC applications [4] , Yang reported a maximum pump efficiency of 30% [5], Ziviani reported a maximum overall isentropic efficiency of below 5% [6] using R245fa in a centrifugal pump and Bianchi reported efficiencies of between 10-20% [7]. These significantly low efficiencies make a significant impact on the net output of small and micro scale ORC systems which highlights the need for significant further improvements into ORC pumps.

The back work ratio is the ratio of expander generated power to pump power consumption. An experimental investigation carried out by Bianchi found that the pump consumed 50% of the generated electricity for heat source temperatures of 65-85°C and sink temperatures around 20°C. Miao found that the pump consumed 11.5% and 30% of the produced work at 140 and 160°C heat source temperatures and sink temperatures of around 20°C [10].

Manolakos calculated the pump power based on the pressure difference and concluded the pump consumed one tenth of expander generated power. [49]

2.2. **Review of Cavitation and the Organic Rankine cycle**

In the last section a broad review of the organic Rankine cycle was presented to give some background and a general overview of the ORC system and the components most commonly used in a micro sized system. In this section a more specific review is presented centred on cavitation and its interaction with ORC systems.

2.2.1. Cavitation definition

The phenomenon of cavitation occurs across many different industries and applications which results in significantly varying definitions. Brennan defines cavitation as 'The process of nucleation in a liquid when the pressure falls below the vapor pressure, while boiling is the process of nucleation that occurs when the temperature is raised above the saturated vapor/liquid temperature' [8]. Davis opts for a more in depth definition by defining cavitation as 'Cavitation bubbles is the kind which grows in a liquid which is at a temperature sufficiently low so that the latent heat requirement for evaporation of the vapor may be neglected' [74]. The formation of bubbles and their dynamics has been researched at great length, with the vast majority of the published work in practical terms out with the scope of this research. The simplest analytical definition of cavitation defines that cavitation will not occur when the pressure of a fluid (p_i) is greater than or equal to the fluid vapour pressure (p_v) (Equation 1) [8].

$$p_i \geq p_v$$
Equation 1

The vapour pressure of a particular fluid is a strong function of the temperature. Equation 1 can be converted into units of height resulting in a definition for Net Positive Suction Head (NPSH).

Net Positive Suction Head (NPSH)

The Net Positive Suction Head (NPSH) is measure of pressure with the units most commonly stated in meters of water at a set of standard conditions. The Net Positive Suction head is normally separated into two distinct parts, Net Positive Suction Head available (NPSHa) and Net Positive Suction Head required (NPSHr). In terms of pumps;

NPSHa: Is the pressure at the inlet of the pump minus the vapor pressure and is a function of the system in which the pump is operating, in this case an ORC system.

NPSHr: Is the minimum amount of pressure difference required between the pump inlet pressure and the vapor pressure, in order for the pump to operate correctly. NPSHr is generally provide by the manufacture. For most variable speed pumps the curves plot NPSHr against rotational pump speed.

In order for the pump to operate within the manufacturing specifications the pressure available at the pump inlet (NPSHa) must be greater than minimum pressure required by the pump (NPSHr) (Equation 2)

$$NPSHa > NPSHr$$

Equation 2

When the criteria in Equation 2 isn't satisfied then the performance of the pump is effected which is most commonly attributed to pump cavitation.

2.2.2. Net Positive Suction Head required

The required net positive suction head for a given pump is supplied by the manufacture, normally in the form of graphs and referenced to water at a set of standard conditions. In order to use with alternative working fluids the curves have to be converted. Care must also be taken in the definitions used by manufactures to produce their curves. For example ANSI/HI 14.6: *Rotodynamic Pumps for Hydraulic Performance Acceptance Tests* defines Net Positive Suction head 3% (NPSH3) which is the minimum required pressure at the pump inlet, whereby the first-stage head drops by 3% [75]. Manufactures sometimes uses NPSH3 and NPSHr interchangeably.

2.2.3. Net Positive Suction Head available

The net positive suction head available at the pump inlet is determined by the system in which it operates, which in this case is a closed loop organic Rankine cycle. A large number of parameters effect the NPSHa in an ORC system including, system layout, mass, operating conditions etc. The available head of the system therefore becomes very condition sensitive and is discussed in more detail throughout this thesis.

2.2.4. Cavitation damage

Cavitation and the formation and subsequent collapse of bubbles during the pump operation can cause significant component damage. The bubbles tend to collapse on surfaces which cause localised high pressure shock waves which can cause significant

erosion, vibration and noise issues [8]. These effects can significantly reduce the working life of pumps, along with any potential vibration damage to other system components.

2.2.5. Cavitation mass flow effect

The formation of bubbles has a significant effect on the pumps mass flow rate. In the case of diaphragm pumps the average density of the fluid contained within the enclosed volume is reduced due to the incorporation of vapour bubbles, which in turn reduces the mass flow out of the pump. The changes in ORC mass flow results in a number of whole ORC system changes;

The mass flow rate has a significant effect on the high side pressure [9] [7]. The expander in the ORC system due to the load applied imparts a resistance which is a function of the ORC flow. An increase in mass flow results in and increase in resistance which results in a higher expander inlet pressure. A change in high side pressure has a significant impact on the system performance, effecting expander work output, including working fluid properties and degree of expander inlet superheating. It also results in a change in the liquid hold up in the evaporator [10] [11]. During evaporation the heat exchanger is arguably split into three sections a pre heat, evaporation and superheat section. Depending on the working fluid a rise in pressure, elongates the pre heating section of the exchanger [61] [13]. The increase in working fluid density at higher pressure may also increase the mass of working fluid entrained in the system high side. The change in liquid mass distribution changes the stored liquid height before the pump.

The mass flow rate effects the pressure drop and heat transfer coefficients of the heat exchangers. It's common knowledge that heat transfer coefficients and pressure drop are functions of flow rates. Changes in flow rate can therefore result in changes in the temperature and pressure of the low side of the system, effecting the pump.

In both the above cases due to the closed cycle nature of the ORC system, the onset of pump cavitation can result in changes to the conditions at the pump inlet causing system feedback. The potential creation of system feedback loops can result in system instability which is reported throughout the literature. Leontartis reported instability with the system producing significant oscillations in pressure when trying to get their experimental ORC system up and running and attributed the problem to pump cavitation [12]. Yang observed significant oscillating flow rates in an organic Rankine cycle system using a gear pump [5]. A system operated by Liu became unstable with oscillations of $\pm$ 100kg/h when the load on

the expander was increased which Liu attributed to pump cavitation [13]. The expander load is widely known to have a significant effect on the expander inlet pressure.

2.2.6. Cavitation mitigation techniques

The negative effects of cavitation and their influence on ORC systems can be severe either in terms of component damage or system instability. In order to mitigate the potential onset of pump cavitation several techniques have been stated in the literature: Increased vertical column height of the stored working fluid before the pump, pre feed pump, pump bypass, nitrogen buffer, and sub-cooling. All these techniques either aim to increase the pump inlet pressure away from vapour pressure or reduce the working fluid temperature away from the saturation temperature. Liu showed that increasing the charge level in the system increased the stored excess liquid working fluid, which increased the liquid column height and increased the pump inlet pressure [13]. However, due to system layout the increased charge flooded the ORC condenser. Miao used a centrifugal pump to pre feed a piston pump [10] and Peterson uses a small centrifugal pump to pre feed and sub cool the liquid entering a Sucton-shoe gear style pump [14]. Pei found pump cavitation to be a significant problem during system commissioning and attributed this to low vertical distance between liquid receiver and pump. Which was improved when they added a bypassline [15]. Although stated as a potential solution, to the best knowledge of the author at the time of writing no experimentally published ORC systems have adopted a nitrogen buffer as a cavitation mitigation technique. Nitrogen was used to pressurise the liquid in the receiver of an experimental system tested by Cao [16]. However, it is not stated if this addition was to mitigate or improve cavitation problems. The most commonly adopted technique for mitigating the effects of cavitation is sub-cooling. Sub-cooling in most cases involves the addition of an additional heat exchanger to reduce the temperature of the liquid working fluid away from the saturation temperature. Yang [5] reported having to use significant amounts of subcooling above 20.7°C in order to minimise the impacts of cavitation. Quoilin suggests subcooling in the range of 20-44°C. Liu [13] reported between 2-20°C of subcooling when operating one experimental system will maintaining 5°C in a previous experimental system [11]. Bianchi reported that 1°C was enough to prevent cavitation [7]. Landelle [4] noted that a minimum of 2.5°C to 4.4°C of subcooling was required for a pump speed of 20 to 100% of the maximum. Leontartis added a subcooler to the initial experimental system but the degree of subcooling has not been stated.

2.2.7. ORC Cavitation Literature Review Conclusion

Across the literature the onset of pump cavitation can result in both physical pump damage and changes in system mass flow, which can affect the ORC cycle performance and in severe cases cause cycle instability. A number of mitigation techniques have been stated in the literature including: increasing liquid column height, pre-feed pump, pump bypass, nitrogen buffer and most commonly subcooling. Even within the most commonly used mitigation technique there remains a significant degree of discrepancy between the stated required degree of sub-cooling. In addition all these systems will contain some degree of stored liquid refrigerant which will have an impact on the pump inlet conditions. A combined effect therefore exists between techniques which is scarcely commented upon in the literature. In order to investigate organic Rankine cycle cavitation and the influence of mitigation techniques further experimental evaluation would be beneficial.

Chapter 3 – Experimental Setup and Theory

In order to investigate the effects of cavitation mitigation techniques on ORC performance an experimental test rig was designed and constructed; to initial test the influence of mass and liquid column height, before being modified to test the combined interactions between subcooling, pump bypass, liquid column height and system charge.

During the process of experimentally investigating the effect of cavitation mitigation techniques, the experimental test rig had undergone a series of modifications before reaching "Test system 1" (used to test the sole effects of liquid column height) and "Test system 2" (used to test the combined effects of liquid column height, subcooling and pump bypass). A brief summary of the base system and the numerous system modifications to get to Test system 1 has been outlined initial before a more detailed account of Test System 1 and Test System 2 is presented.

3.1. Base Experimental Test system and major modifications

3.1.1. Initial base experimental test system.

The problem of cavitation has been tackled in various ways in the literature with subcooling, pump bypass or pre-feed pump. The simplest method to mitigate against the occurrence of cavitation is to increase the vertical distance between the pump and the top of the liquid of column. This in theory allows for control of the pump inlet pressure: without having to add an additional pump which increases energy consumption and capital cost, or imposes significant subcooling of the liquid refrigerant. The initial base experimental test system was therefore designed to accommodate the pump requirement NPSHr through liquid column height alone which was calculated at 2.5m. However, due to physical manufacturing constraints a maximum of 2.3m was achieved between the outlet of the condenser and the pump inlet. The calculation of this number is given in more detail in Test system 1. An illustration of the basic ORC layout and a more detailed layout of the low pressure side of the system is given in Figure 9 and Figure 10 respectively.
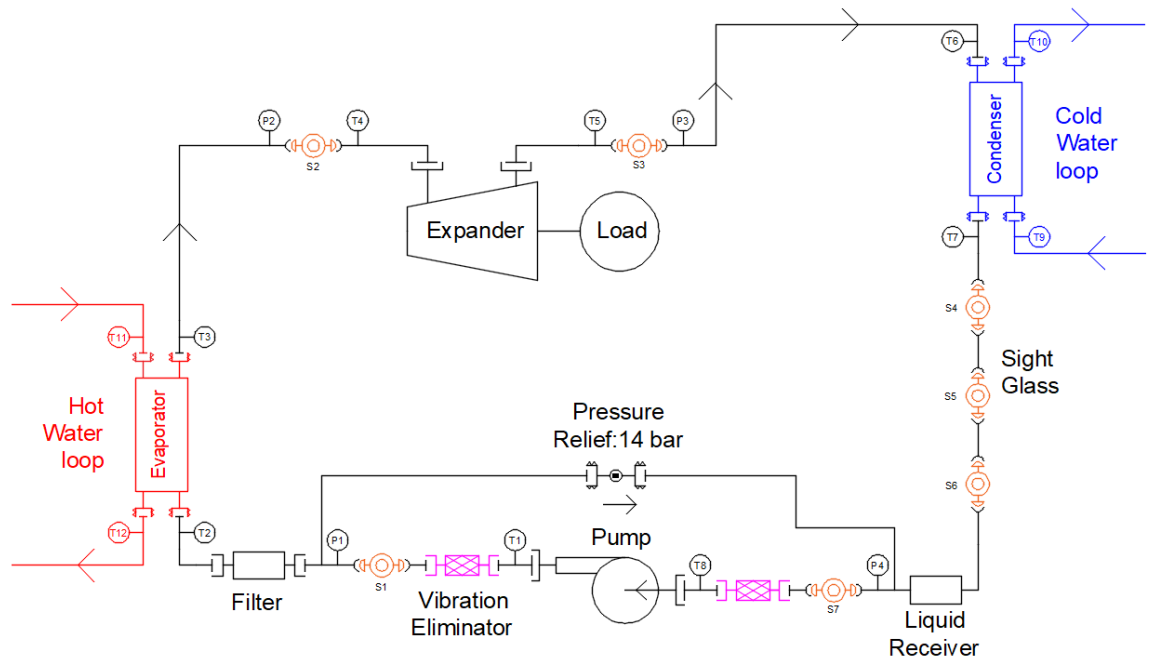
Figure 9: The initial base ORC experimental test system consisted of the basic Organic Rankine cycle components, with the exception of the significant vertical distance of 2.3m between the ORC pump and the condenser outlet.
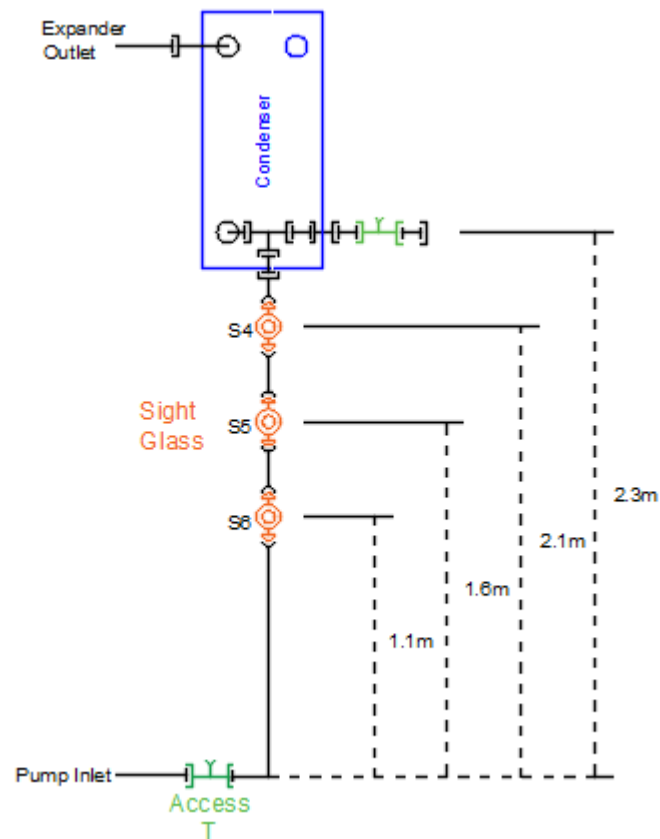
Figure 10: Illustration of vertical column at the low pressure side of the system

In order to minimize the amount of refrigerant required to increase the liquid column height, small bore 1/2" copper pipe was used as the column. However, it became apparent when testing began that due to the liquid column set up. The system was extremely sensitive to mass and for the most part uncontrollable. At even half the maximum pump

speed, as can be seen in Figure 11, the system became extremely unstable with drastic collapsing and surging of the system pressure.
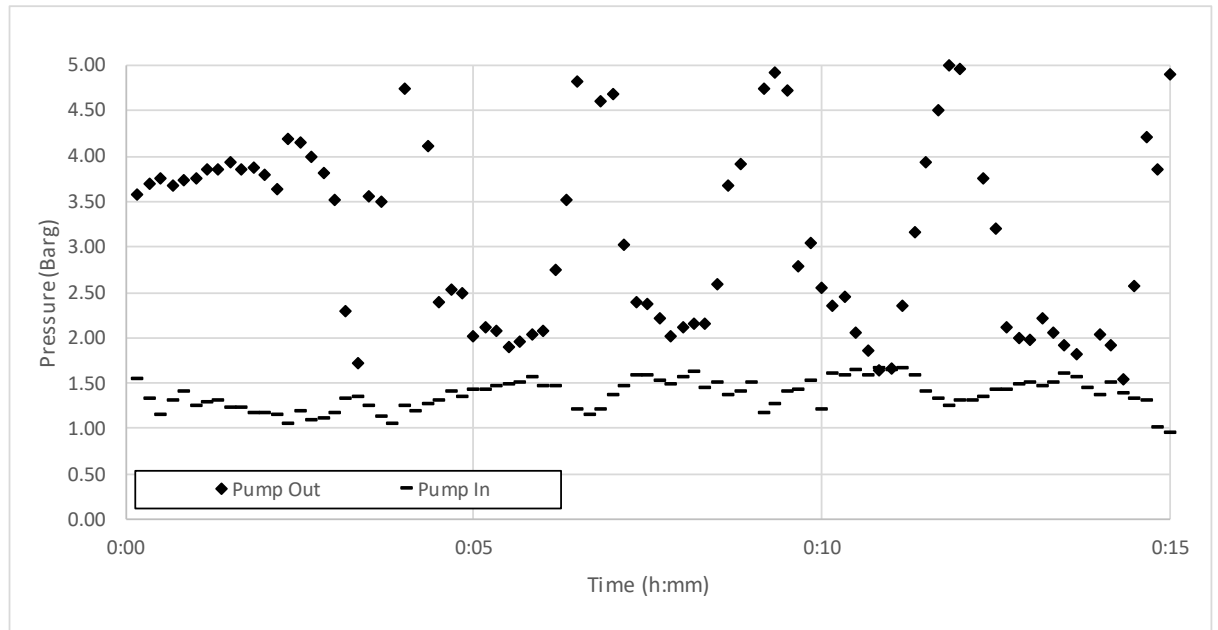
Figure 11: Initial base case experimental system: Pressure at the pump inlet and outlet at a pump speed of 35 Hz. The pump outlet has extreme oscillations in pressure varying from 5 bar to 2 bar over the span of a 2 min period. The pump inlet pressure also unstably fluctuates from 1 bar to just above 1.5 bar.

Sight Glass Observations

Figure 12: Images from Sight Glass S6 at 5mins (left) and 5 min 30 seconds (Right) for system pump speed running at 35 Hz.

Images taken from the lowest located sight glass on the column, sight glass (S6), shown in Figure 12 show the change in stored liquid level as the system surges and collapses.

It was concluded from various tests carried out. That the sensitivity of the system to stored mass resulted in any small variations in mass distribution significantly changing the liquid column height. The changing liquid height developed into system instability. In order to reduce the sensitivity and stabilise the system, it was concluded that additional liquid storage was required.

3.1.2. Modification 1: Increased liquid storage

In order to overcome the mass sensitivity and system instability of the base experimental system the layout between the outlet of the condenser and the inlet of the pump was modified to include additional liquid storage. A liquid buffer was added at the same height as each of the three sight glasses at 1.1, 1.6 and 2.1m, shown in Figure 13.
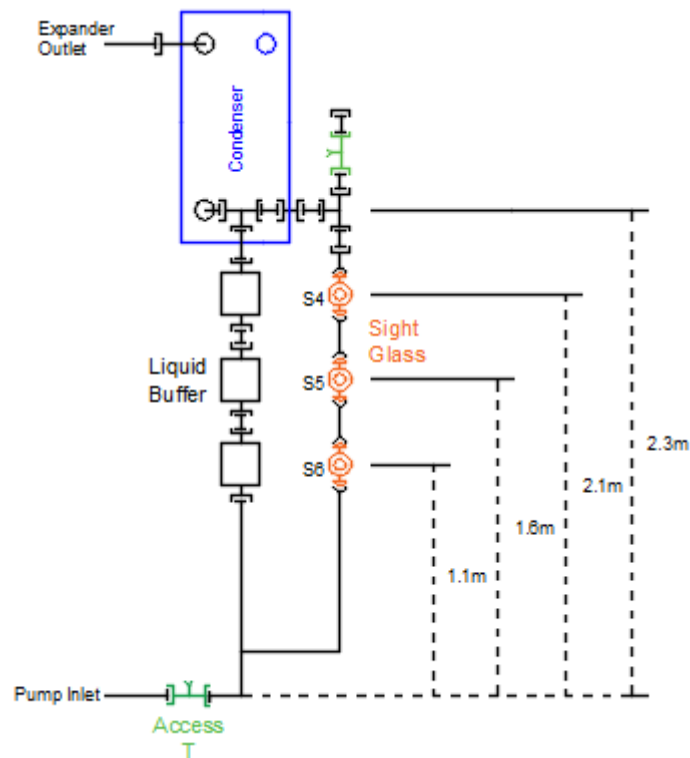
Figure 13: ORC Modification 1: The only system change was the addition of three liquid buffers in the liquid column.

The addition of the liquid buffers reduced the sensitive of the system and allowed it to operate in a more stable manner, for a series of tests to be carried out. However, during analysis of the results it became evident that natural fluctuations in the supply chilled water added significant uncertainty to the experimental results. An illustration of this is shown in Figure 14, the cold side of the system has a steady oscillation in temperature of around 3°C.
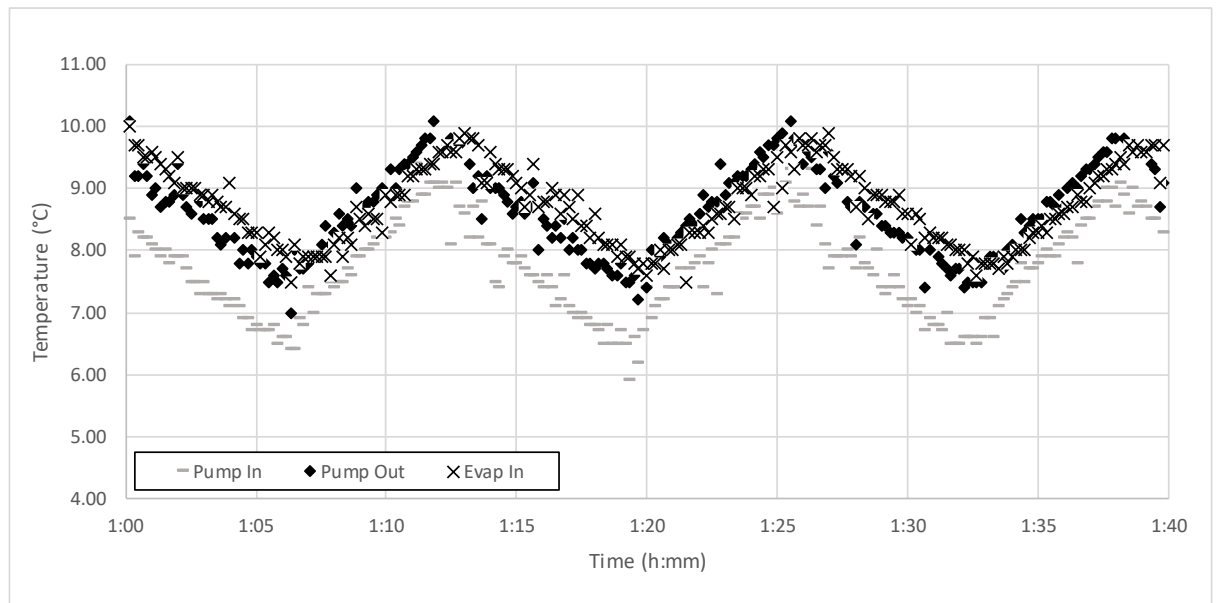
Figure 14: ORC modification 1: Pump Inlet, Pump Outlet and Evaporator Inlet Temperature 1 hour after system start up. The pump inlet temperature varies between 6 and 9 degrees. The pump outlet varies between 7 and 10 degrees Celsius.

This variation in temperature was as a result of the on/off control system of the large chiller used as the system cold sink. It was not possible to reduce this fluctuation with the chiller its self therefore further modification was required.

3.1.3. Modification 2: Cold sink improvements

Modification 1 to the initial base system helped to reduce the system instability but the 3°C variation in cold side temperature as a result of the supply chiller made analysis of the recorded data difficult. In order to provide a steadier supply temperature an additional temperature controlled water loop was added to the cold side supply as shown in Figure 15.
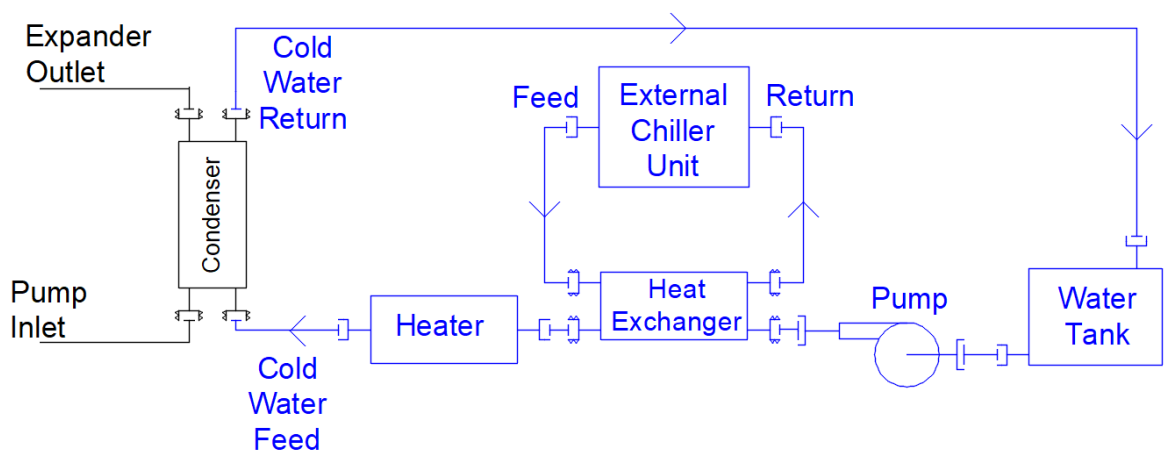
Figure 15: Simplified schematic diagram of the revised cooling circuit. The system has been split into a chiller loop which still provides 6-9 degrees chilled water which feeds into a temperature controlled water loop.

The original cooling loop has been split into the original external chiller circuit and a temperature controlled water loop. A water pump is used to pump water from a tank

through the chiller heat exchanger. The chiller heat exchanger cools the water loop temperature down to between 6-9 degrees before an immersion heater maintains the cold water feed temperature at a minimum of 10 degrees Celsius. A Titian mass flow meter is used to measure the water flowrate.
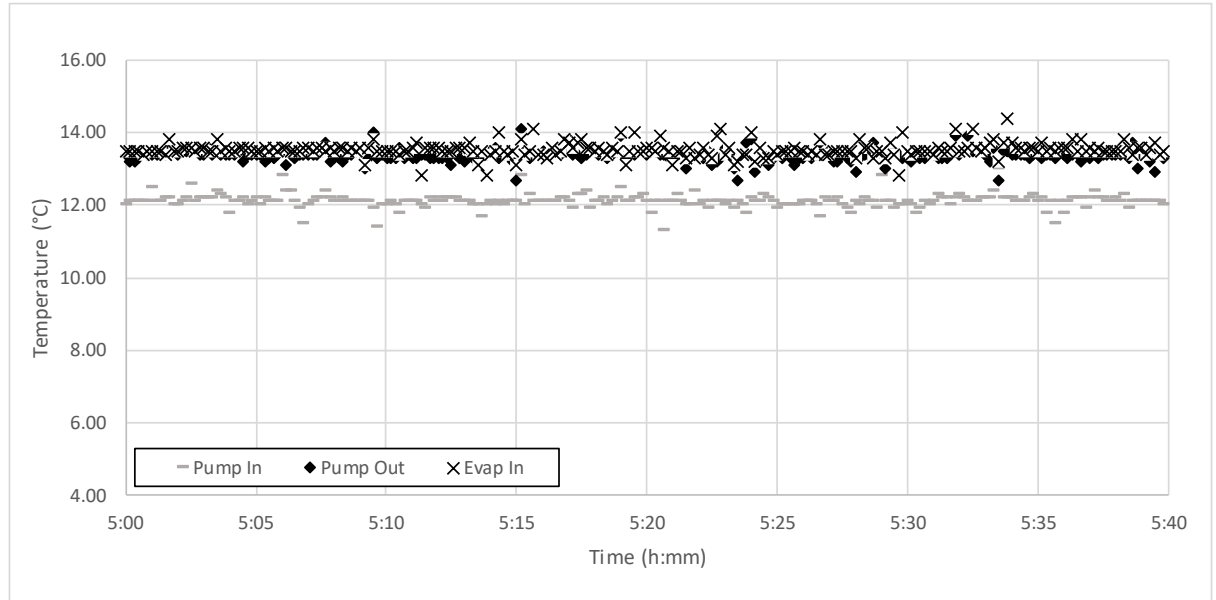
Figure 16: Pump inlet, pump outlet and evaporator inlet temperature after system start up. The average temperature values over this period are 12, 13 and 13 degrees Celsius respectively

The additional secondary cooling loop significantly stabilises the chilled water temperature as shown in Figure 16. This revised system layout forms the basis for test system 1 with more detailed system information outlined in the next section.

3.2. **Test System 1**

The experimental test rig used to test the effects of liquid column height on pump cavitation is outlined in detail in this section. An overview of the ORC layout is shown in Figure 17.
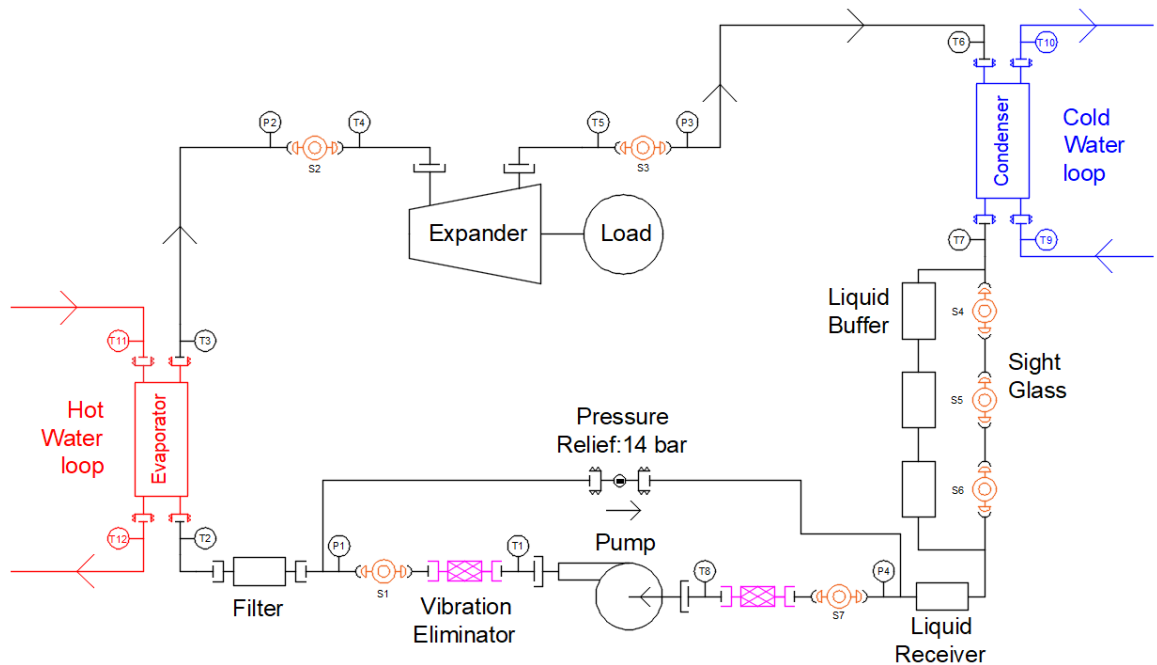
Figure 17: Organic Rankine Cycle schematic for experimental test system 1 (Top), used to test the effects of liquid column height on pump cavitation. Image (bottom)

3.2.1. General ORC components

The expander used in the ORC test system was an Air Squared scroll expander (E15H022A-SH) which is directly coupled to a single phase generator (Voltmaster: AB30L WEIPU). Any power generated by the ORC system was dissipated in 400W bulbs. A small diaphragm pump (Hydra-cell G20 EDSPHFEHG) attached to a three phase 6 pole motor (AEG: AM 80z AA 6), provided refrigerant flow. An inverter drive (Lenze: SMV) provided pump speed control. Brazed plate heat exchangers (Alfa Laval: AC-70X100M-F) where used in counter flow configuration for both the condenser and the evaporator. The remaining inline piping components including sight glasses, piping, vibration eliminators and pressure relief valves are all standard refrigeration components.

3.2.2. Liquid column

In order to test the effects of liquid column height the net positive suction head required by the pump is specified by the manufacture. The maximum motor range of the pump is 402-1200rpm which, using Equation 8, results in NPSHr of 2.5m and 3.5m of water respectively. Converting this to meters of R245fa, using Equation 9, with liquid density of R245fa (15°C) taken as $1373.1\frac{kg}{m^2}$ and water density at manufacture specified condition $998.2\frac{kg}{m^2}$. Results in 1.8m at 402 rpm and 2.5m at 1200 rpm of R245fa, respectively. Due to physical height limitations the condenser outlet height was set at 2.3m above the pump inlet as shown in Figure 18. In order to monitor the liquid level three sight glasses where set at height intervals of 1.1m, 1.6m and 2.1m respectively. Based on mass sensitivity issues, as discussed in the previous section, three liquid buffers where installed in parallel to the sight glasses. The sight glass line of piping consisted of ½" pipe with the liquid buffer line consisting of 7/8" pipe and three 300mm 1-1/8" inch pipe sections centered on the sight glasses.
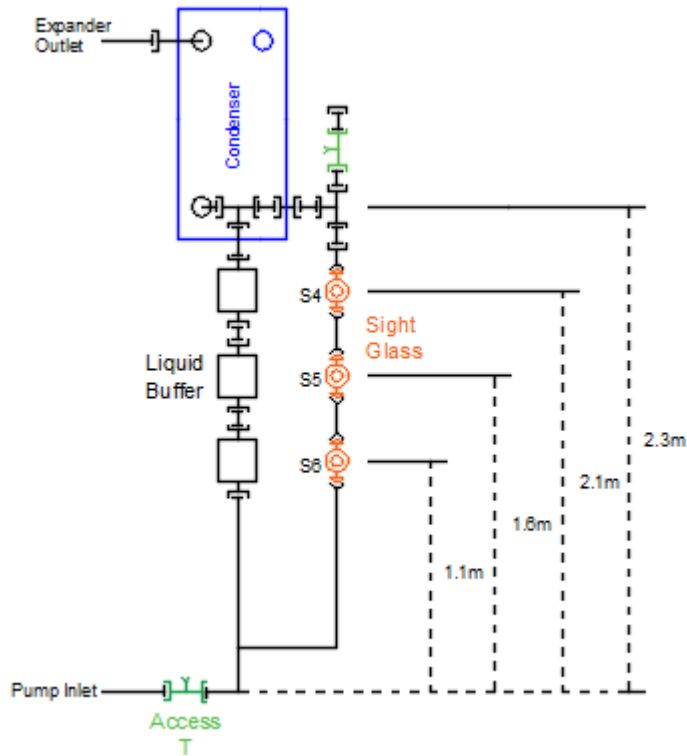
Figure 18: Schematic of ORC liquid column containing three sight glasses and liquid storage at 1.1m, 1.6m and 2.1m (left). Image (right).

3.2.3. Data Acquisition and Sensors

An Omega data acquisition board and accompanying software (DAQTEMP 14A, DAQView software) was used for data acquisition. The board has 7 analogue input channels, fourteen available temperature sensor inputs and four counter inputs with the allocation of channels shown in Table 3: Temperature Sensors and Table 4: Pressure Sensors.

Twelve k-type temperature sensors have been spread throughout the system with their acquisition channel number, label and location outlined in Table 3 with sensor layout also depicted in Figure 17.

Table 3: System temperature data acquisition channel number, label and system location

Data Acquisition Channel Number	Type	PID Label	Data Acquisition Label	System Location
0	-	-	CJC00-L	Daq Board: Cold Junction Temperature
1	WTF – K-type	T1	TPumpO	Pump Outlet
2	WTF – K-type	T2	TEvapIn	Evaporator Inlet: ORC
3	WTF – K-type	T3	TEvapO	Evaporator Outlet: ORC
4	WTF – K-type	T4	TExpIn	Expander Inlet
5	WTF – K-type	T5	TExpO	Expander Outlet
6	WTF – K-type	T6	TCondIn	Condenser Inlet: ORC
7	WTF – K-type	T7	TCondO	Condenser Outlet: ORC
8	-	-	CJC00-H	Daq Board: Cold Junction Temperature
9	WTF – K-type	T8	TPumpIn	Pump Inlet
10	-	-	-	**Not in use**
11	-	-	-	**Not in use**
12	MI – K-type	T9	TCi	Cold Water Feed
13	MI – K-type	T10	TCo	Cold Water Return
14	MI – K-type	T11	THi	Hot Water Feed
15	MI – K-type	T12	THo	Hot Water Return

Note: Welded Tip Fiberglass –WTF, Mineral Insulated - MI

Four Omega gauge pressure sensors are distributed throughout the system to monitor the ORC. The specification and location are outlined in Table 4 with sensor layout depicted in Figure 17.

Table 4: System pressure sensor data acquisition channel number, pressure sensor type and location

Data Acquisition Channel Number	Type	PID Label	Data Acquisition Label	System Location
1	PX-319	P1	Pump Out	Pump Outlet
2	PX-319	P2	Exp In	Expander Inlet
3	PX-319	P3	Exp Out	Expander Outlet
4	PX-319	P4	Pump In	Pump Inlet
5	PX-319	P5	Cond Out	Condenser Outlet

The electrical power used by the pump and generated by the expander is measured by electrical power meters. The consumed pump power, including the frequency converter, is measured by a HOBUT M880-DMF-RS-Pro power meter. The generated power from the expander/ generator combination is measured also by a HOBUT (149333/6/002) power meter.

3.2.4. Heater Circuit
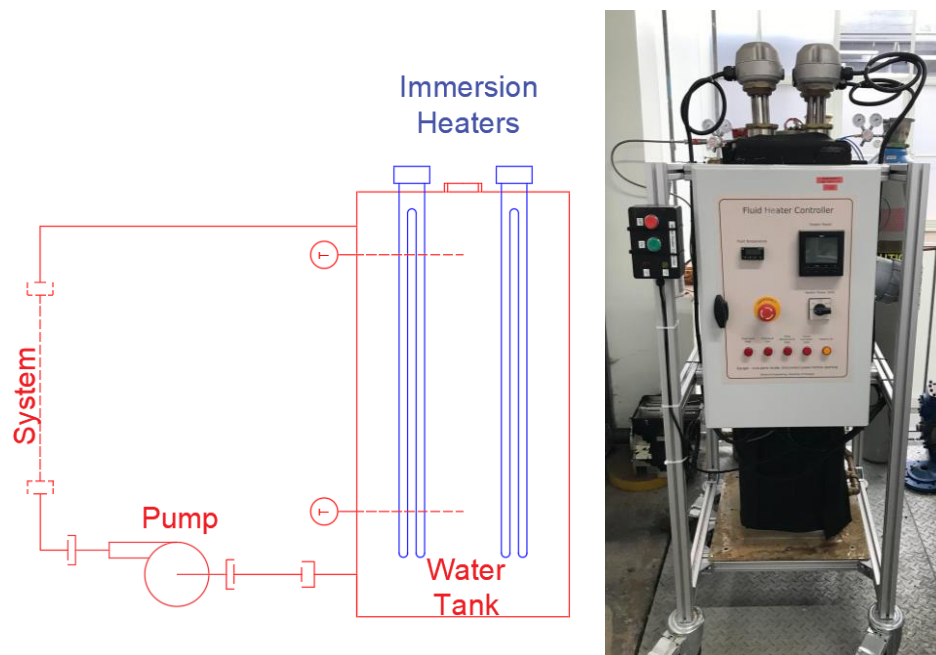
Figure 19: Heating circuit schematic diagram (Left), Image (right)

The supply of heat to the evaporator is via a water heating loop shown in Figure 19. The system makes use of a small water pump (Grundfos: UPS2 15-50/60) to circulate water through the ORC evaporator. The flow rate of water was set to 1.8 m^3/h. The temperature of the water is maintained via four 9kW immersion heaters, which are submerged into a 110 litre stainless steel water tank.

3.2.5. Chiller Circuit

The revised chiller circuit as mentioned previously is shown in Figure 20. A 40L stainless steel water tank provides a buffer tank for the system. A flowrate controllable Grundfos centrifugal pump (MagNa3 25-120 180) is used to pump water from the buffer tank through the chiller heat exchanger. The measured flow rate produced by the pump due to system losses is 17 litres/min of water. The chiller heat exchanger cools the water loop

temperature down to between 6-9 degrees before an immersion heater (EX HEAT: MLH18L) maintains the cold water feed temperature at a minimum of 10 degrees Celsius.
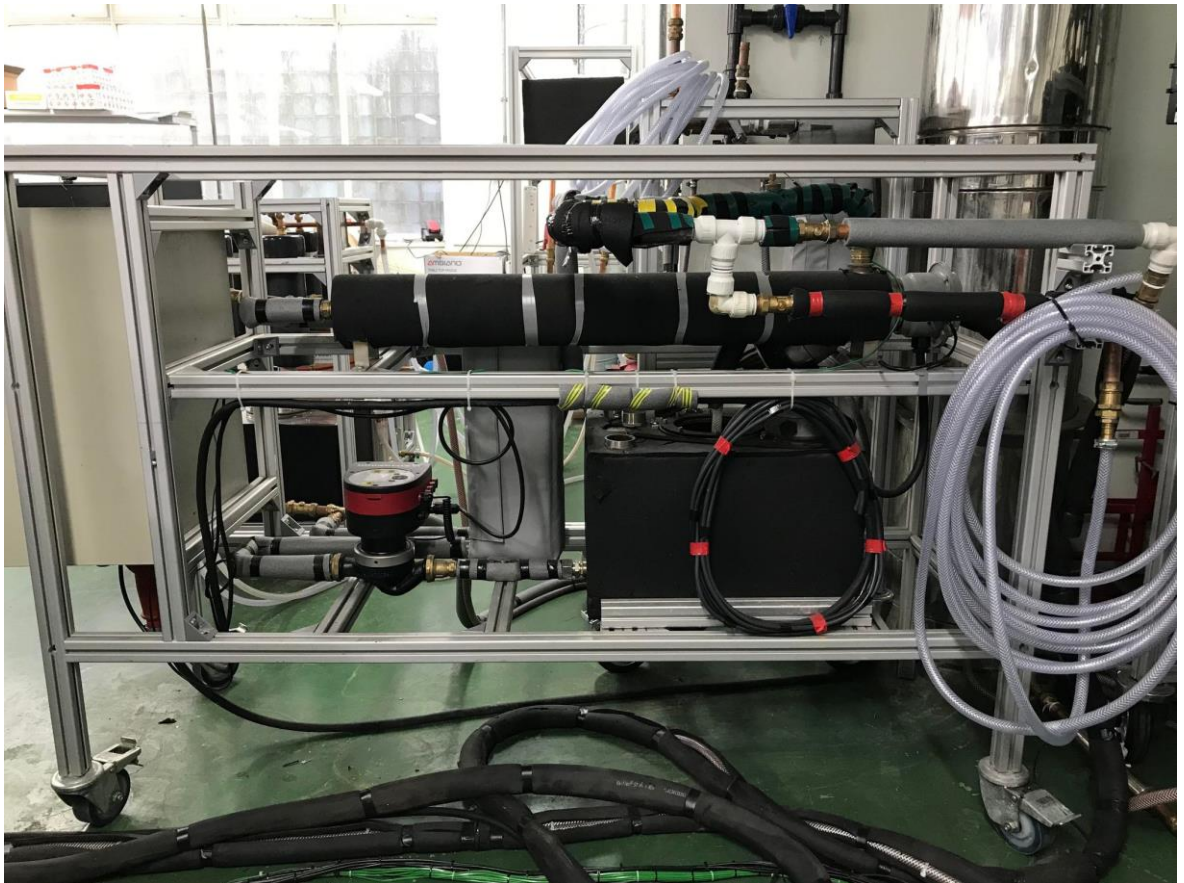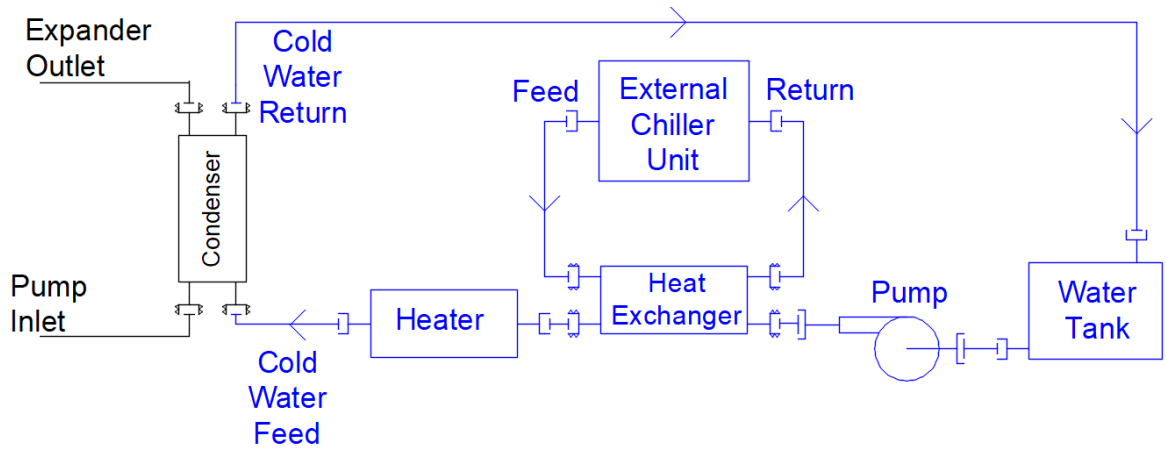
Figure 20: Simplified schematic diagram of revised cooling circuit (top). The system consists of an external chiller unit and a temperature controlled secondary loop. Image of the revised cooling circuit (bottom).

3.3. **Test System 2**

After the testing of system 1 was completed the system was modified to include a subcooler and pump bypass. The overall modified system layout is shown in Figure 21.

Unless otherwise stated the system components and test set up remain the same as test system 1.
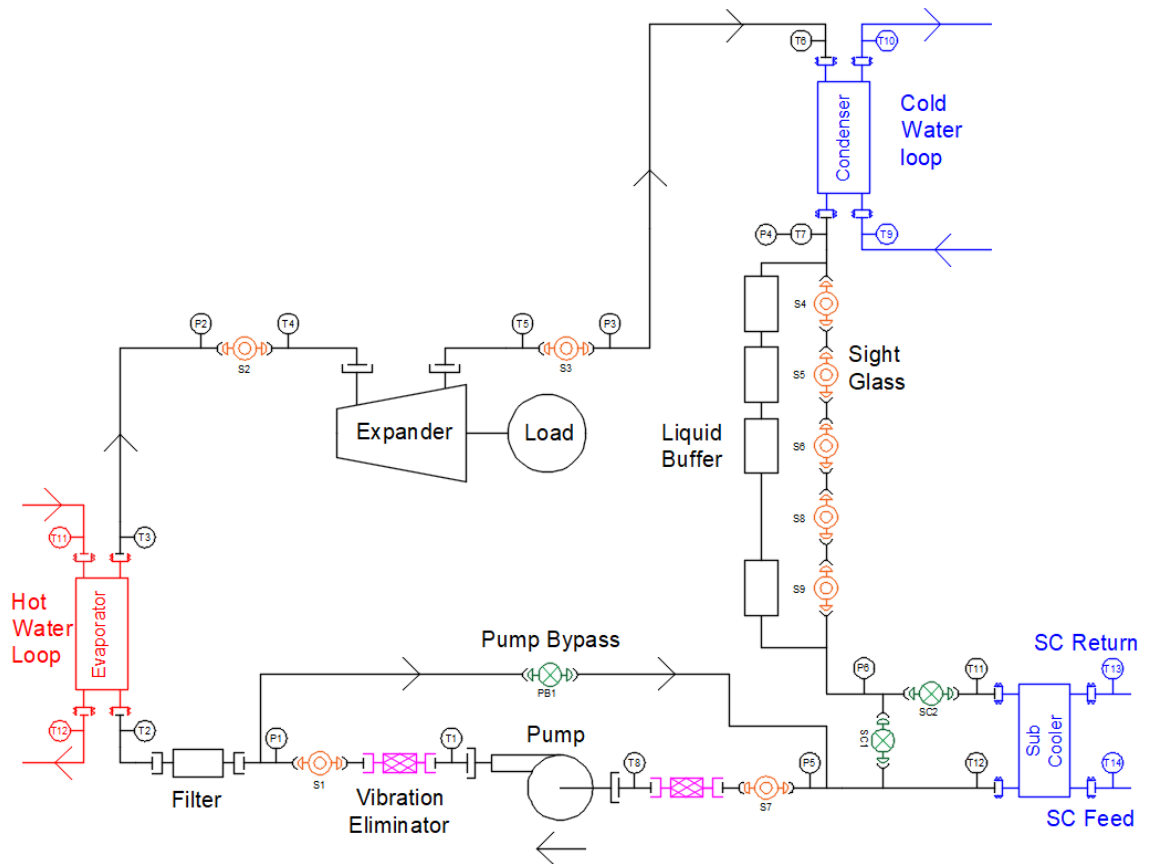
Figure 21: The Organic Rankine cycle overall schematic for Test system (Top). Image of additional subcooler and pump bypass addition (bottom).

The original internal pressure relief valve of test system 1 was replaced with a ½" ball valve which provided a manual pump bypass (PB1). A brazed plate heat exchanger (Sondex: SL23TL-30-AA) was installed at the bottom of the liquid column, with an optional bypass, to act as a sub cooler. A separate portable chiller unit (Thermo scientific: ThermoFlex7500) was used to supply the subcooler with 1.6 m^3/h of cold water glycol mixture at varying temperatures. The ORC liquid column was also modified to include an additional liquid buffer and sight glass pair 0.5m meters below S6, as shown in Figure 22. An additional sight glass was added midway between the bottom two sight glasses.
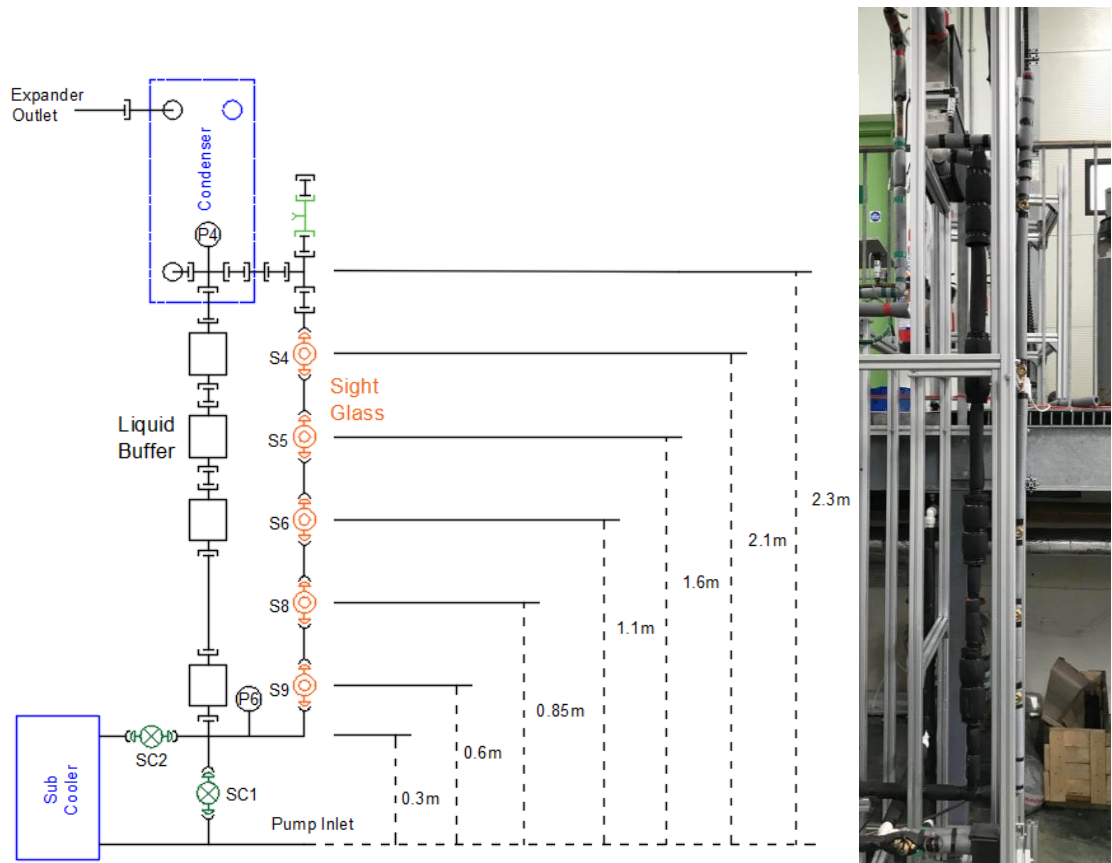
Figure 22: Test system 2 revised layout of ORC liquid column (Top). Drawing is not to scale and it should be noted that S4, S5, S6 and S9 sight glasses are equally spaced and S8 is added at the midpoint between S6 and S9. Image (right)

3.4. **Experimental Analysis**

This section outlines the equations that have been used to evaluate the experimental results produced by the ORC test systems.

3.4.1. First Law of Efficiency

The first law efficiency is the simplest analysis of the cycle and used extensively in the research. It calculates the net work output of the cycle and divides it by the heat input.

$$n_{cycle} = \left(\frac{W_{expander} - W_{pump}}{Q_{evaporator}} \right)$$

Equation 3

3.4.2. Back Work Ratio

The back work ratio is the ratio of the expander outlet power to the consumed pump power.

$$BWR = \left(\frac{\dot{W}_{pump}}{\dot{W}_{expander}} \right)$$

Equation 4

3.4.3. Net Positive Suction Head

In order to satisfy the pump cavitation criteria the net positive suction head available (NPSHa) must be greater than the net positive suction head required (NPSHr)

$$NPSH = NPSH_a - NPSH_r$$

Equation 5

$$NPSH_a > NPSH_r$$

Equation 6

Net positive suction head available

The net positive suction head available is a function of the system and is calculated from experimental data using

$$NPSA = P_{pump,Inlet} - SatP_{pump,Inlet}$$

Equation 7

The pump inlet pressure is taken directly from experimental data and the saturation pressure is calculated from pump inlet temperature.

Net positive suction head required

The required net positive suction head is pump dependent and is supplied by the manufacture. The pump used in this thesis is a diaphragm pump (Hydra-cell G20 EDSPHFEHG). The supplied manufacturing curves for the pump are shown in Figure 23 which has been curve fitted using a 2nd order polynomial given in Equation 8.
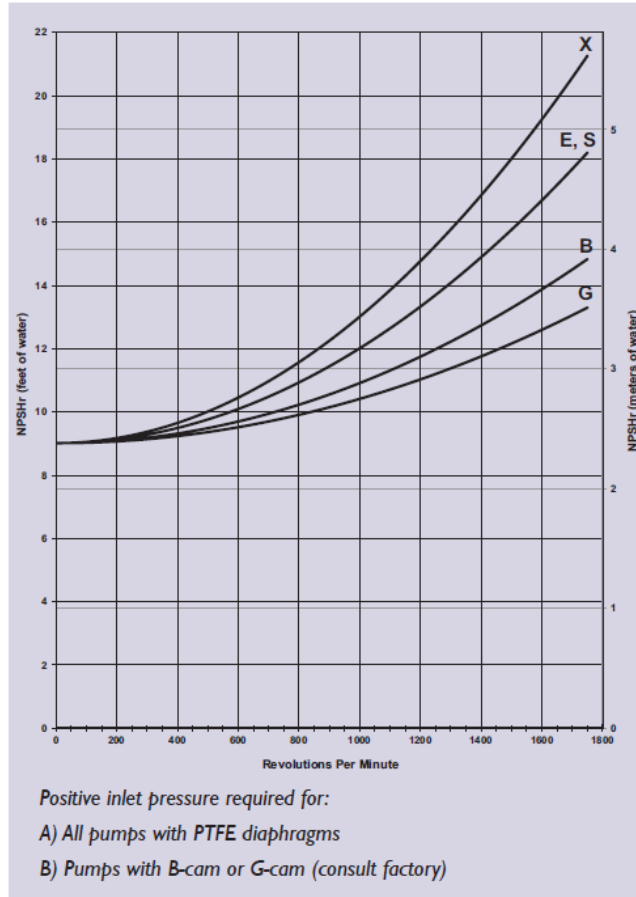
Figure 23: Hydra-cell G20 manufacturer supplied technical data for Net Positive Suction Head required (NPSHr). The graph shows the NPSHr specified in meters of water against pump rotational speed in RPM [76]

$$NPSHr(water) = 8x10^{-7}n^2 - 6x10^{-5}n + 2.3993 \qquad \text{Equation 8}$$

The manufacturing data is specified in terms of meters of water, however, the working fluid in the ORC system is R245fa. The conversion has been carried out using

$$NPSH_{ref} = NPSH_{water} \times \frac{\rho_{water}}{\rho_{ref}} \qquad \text{Equation 9}$$

The experimental testing of the pump occurs at four speeds: 600, 800, 1000 and 1200 Rpm.

3.4.4. Analysis Software and Error Analysis

Experimental analysis was carried out using Microsoft excel with fluid properties generated using NIST RefProp 10. The potential error within the data was calculated based on the population standard deviation of each data set recorded by the data acquisition

system. Due to the nature of the available equipment the pump and expander power where recorded manually at a single point at the mind point of the test run.

3.5. **Summary**

The details of the experimental test rigs used for the testing of pump cavitation mitigation techniques are outlined in this chapter. The initial system build was unable to provide sufficient stability to enable reliable system testing therefore a series of modifications were made to increase the liquid storage capacity of the rig and reduce the temperature variation of the cold water feed to the condenser. After modification this experimental setup was then used to test the effects of liquid column height on ORC performance, the results of which are outlined in chapter four. After testing was complete the experimental test setup was further modified to include a subcooler and pump bypass. This modified setup was then used to test the combined effects of liquid column height, pump bypass and subcooling on pump cavitation. The results are outlined in chapters five and six.

Chapter 4 – Effect of Liquid Column Height on ORC System performance

In order to investigate the cavitation phenomenon and evaluate if simply increasing liquid column height would be sufficient to elevate the cavitation problem. An ORC test rig was specifically built with a significant vertical distance between the condenser outlet and the pump inlet. The mass of the system was varied in order to adjust the liquid column height under several steady state test conditions.

The distribution of mass around the ORC cycle varies depending on the operational conditions of the system. For a set of stable operating conditions the excess refrigerant in the system is stored in the low pressure, cold side of the system normally in a liquid receiver. Depending on the location, shape and size of the receiver a relationship exists between the mass of the system and height of stored refrigerant. The stored liquid column height is therefore a function of the operational conditions and the system charge level. In order to investigate how these parameters interact with each other a series of tests have been conducted.

— Firstly: The effect of system charge is evaluated for a single set of ORC operational conditions
— Secondly: The effect of system charge is evaluated at various pump speeds
— Thirdly: The effects of system charge is evaluated at three cold side temperatures
— Finally: The effects of system charge is evaluated for at three load

Key: The observed liquid height at and between the system sight glasses has been included in the graphs as data symbol changes. The data in this chapter follows

Table 5: Experimental Liquid level Indication: Liquid column only

Symbol style	Liquid level (m)	Sight glass number
△	< 1.1	< S6
▲ 1	1.1	S6
▲	1.1-1.6	S6-S5
▲ 2	1.6	S5
▲	1.6-2.1	S5-S4
▲ 3	2.1	S4

4.1. **System Charge/liquid column effect on a single set of ORC operational conditions at a single pump speed**

For a set of stable conditions, the liquid height within the system will maintain a constant level. In order to vary the liquid column height R245fa was added in 100g mass increments, while the system was operated at 800rpm, 3 light resistive load, 15°C cold sink temperature and 93°C heat source temperature.

4.1.1. Experimental results

Experimental results observation summary: For a single set of ORC conditions increasing the system mass increases the ORC output up to a peak value. Further additional charge past this value results in a decline in system output. The power consumed by the pump shows no significant variation with charge. Likewise there is no significant changes in the recorded system temperatures with mass, with the exception of the expander outlet temperature which shows sustained increase with increasing mass. However, the system charge has significant effect on both the high side and low side pressures.

Overall performance:

The overall effect of changing the system mass on the ORC performance under a single set of conditions is shown in Figure 24 and Figure 25. Expander rotational speed (Figure 24) and, pump and expander power (Figure 25) plotted against mass. The rotational expander speed increases from an initial 2902 rpm upto a maximum of 2977rpm at 3.78kg of system mass. Further, additional system charge results in a decline in rotational speed down to a value of 2913 rpm at the last data point. Since the expander rotational speed is linked to the electrical power output, the output power follows the same trend as the rotational speed. Increasing from 0.14kW to 0.19kW at 3.78kg of system charge followed by a decline in expander output power as the charge level is increased. The power consumed by the pump shows no significant variation with mass and fluctuates around an average power consumption of approximately 0.08 kW.
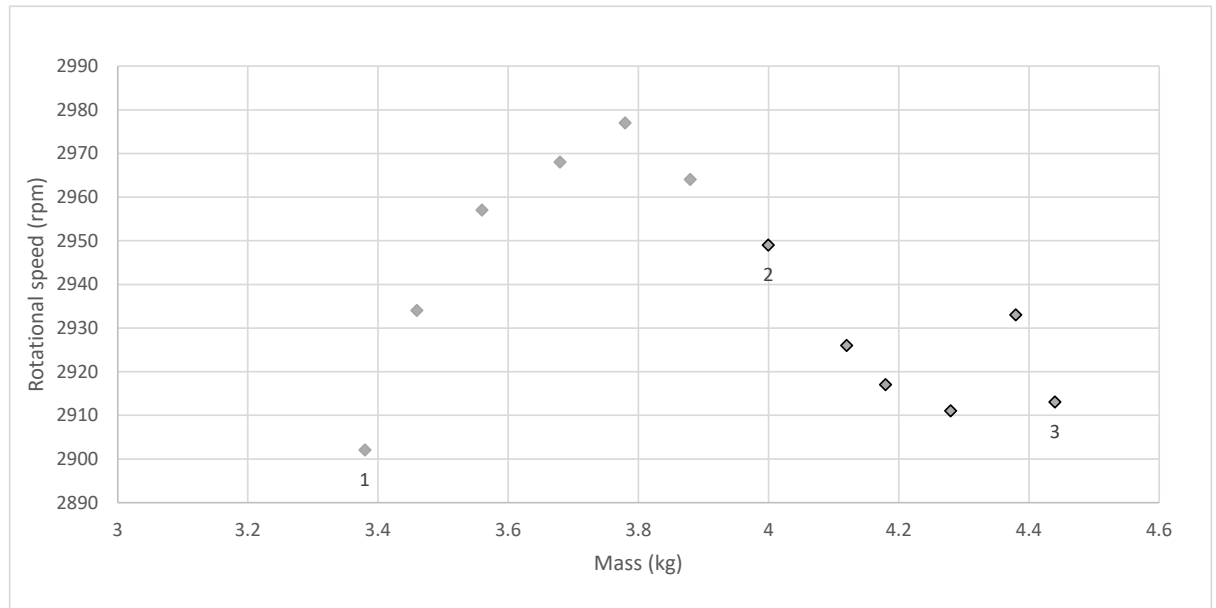
Figure 24: Expander Rotational speed for various system charges at 800 rpm pump speed. The visible liquid level at each of the three sight glasses is noted on the chart, along with marker changes to indicate in between levels. The expander rotational speed increases with system charge before reaching a peak at approximetly 3.8 kg of system charge. Further increase in system mass results in a deterioation in expander roatational speed.
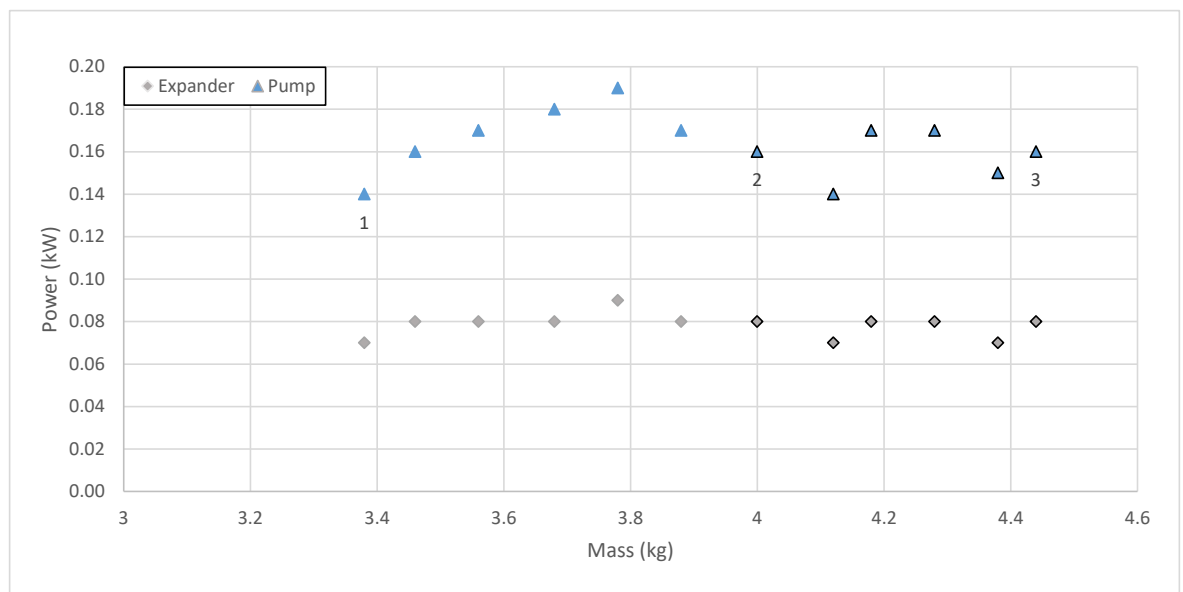
Figure 25: Expander and Pump power for various system charges at 800rpm pump speed. The expander power increases with the mass up to a maximum of 0.19 kW at approximately 3.8 kg of system charge.

Pressure:

Increasing the system charge results in an increase in both high side and low side pressures. Both the pump out and expander inlet pressure follow a very similar trend as shown in Figure 26. The pressures both increase initially from 4.06 bar at the pump outlet and 4.24 bar at the expander inlet. To an initial peak value of 4.45 bar and 4.64 bar at the pump outlet and expander inlet respectively. The pressure plateaus around these pressures

with a potential slight decline from a system charge of 3.68 to 4.12kg, after this there is a further gradual increase in pressure with system charge. It is worth noting here that the plateau in high side pressure is close to the system charge level of peak ORC output.
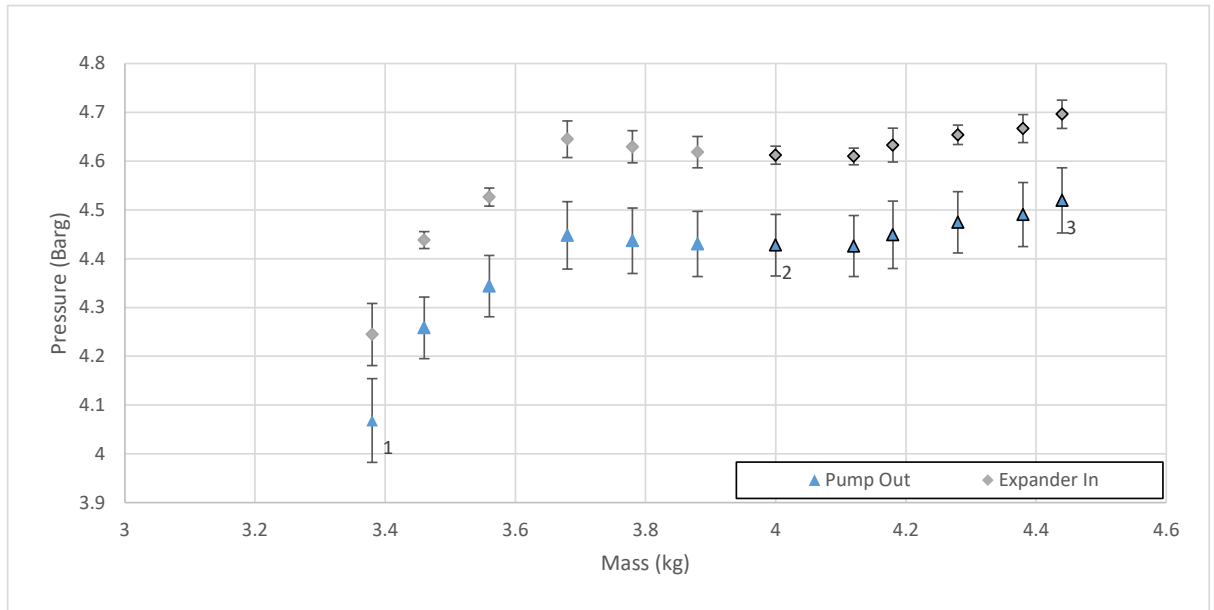
Figure 26: Averaged pump outlet and expander inlet pressure for various system charges at 800rpm pump speed. Increasing the system mass leads to an increase in ORC high side pressure up to approximately 3.8 kg of system mass.
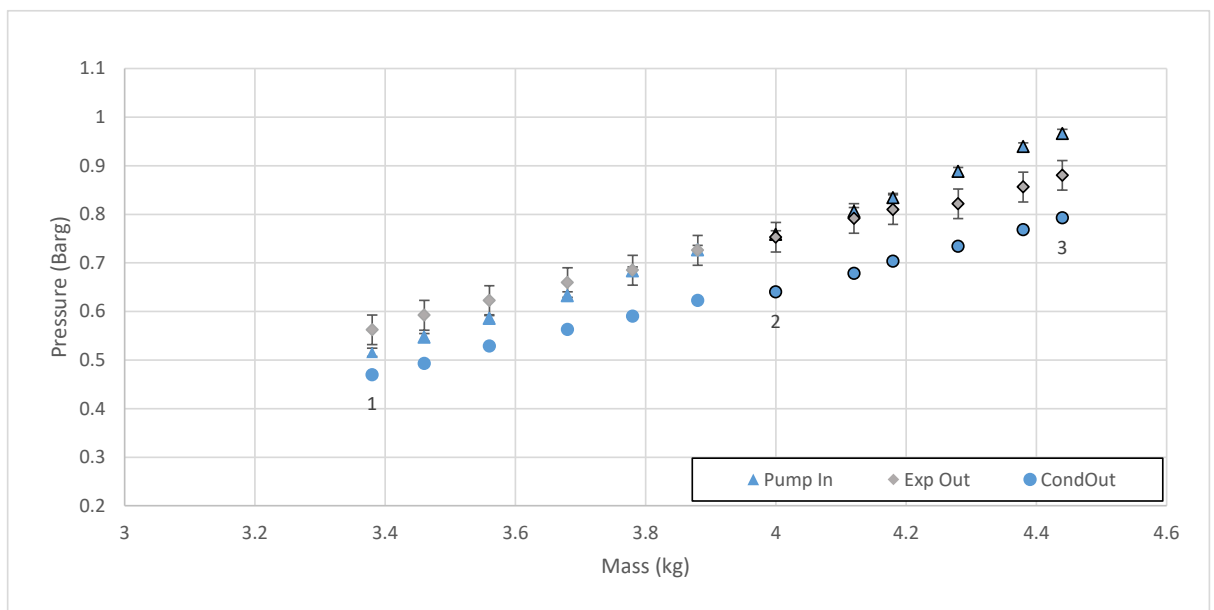
Figure 27: Averaged expander outlet and pump inlet pressure for various system charges at 800 rpm pump speed. Increasing the system mass results in a steady increase in cold side pressure at both the pump inlet and the expander outlet. A comparable small pressure differential exists between the pump inlet pressure and the expander outlet pressure up to 4.2kg of system charge. After this point these pressures begin to diverge significantly as the mass is increased.

The low pressure side, shown in Figure 27, of the system shows a gradual and sustained increase in pressure with increasing system charge. Albeit at different rates the pump inlet, expander outlet and condenser outlet increase in a fairly linear manner with system charge. There is an evident cross over in pressure between the pump inlet and expander outlet at

4kg of system charge, which equates to a liquid level column height in line with sight glass (S5) (1.6m).

Temperature:

During the experimental testing the system temperatures in general show no significant changes. The cold water feed temperature and condenser outlet temperature, shown in Figure 28, remain at effectively the same temperature across the testing range of 15.3±<0.1°C and 15.2±<0.1°C. Likewise after a slight increase in temperature over the first three data points (related to increasing performance of the system), the temperature of the cold return remains consistent at 22.8±<0.1°C for the remainder of the data points.
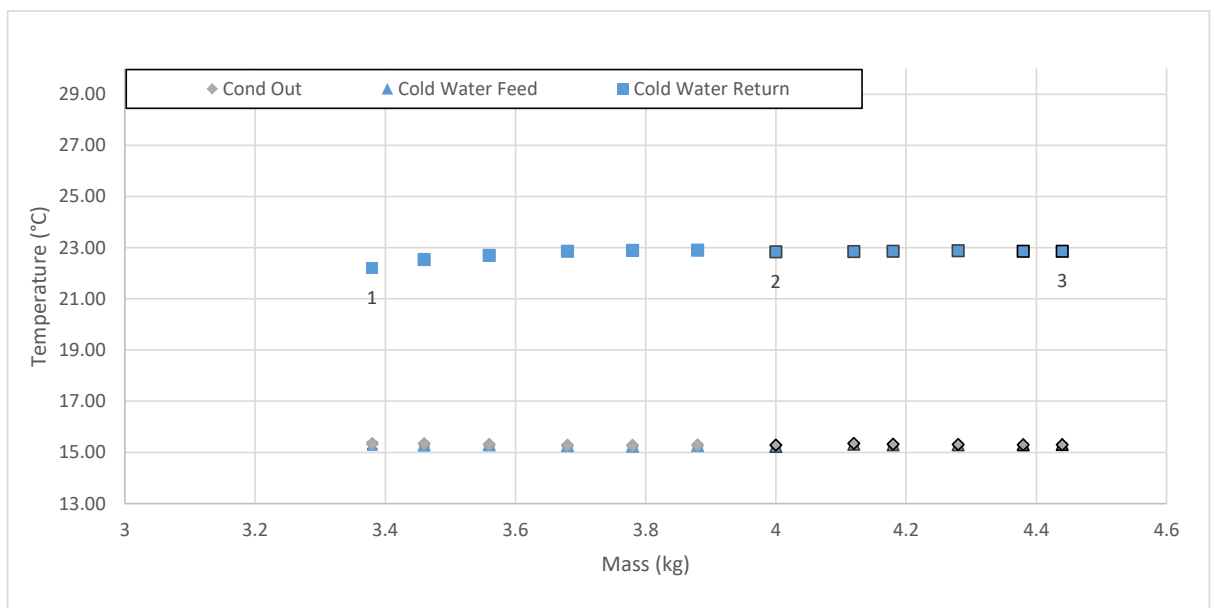
Figure 28: Average condenser outlet, cold water feed and cold water return temperature for various system charges at 800 rpm pump speed. The cold water feed and condenser outlet temperature show a close temperature match, with no significant change in temperature with system charge. The cold water return temperature on the other hand shows a gradual increase in temperature up to 4.2 kg system charge after which the temperature levels off with a potential slight decline.
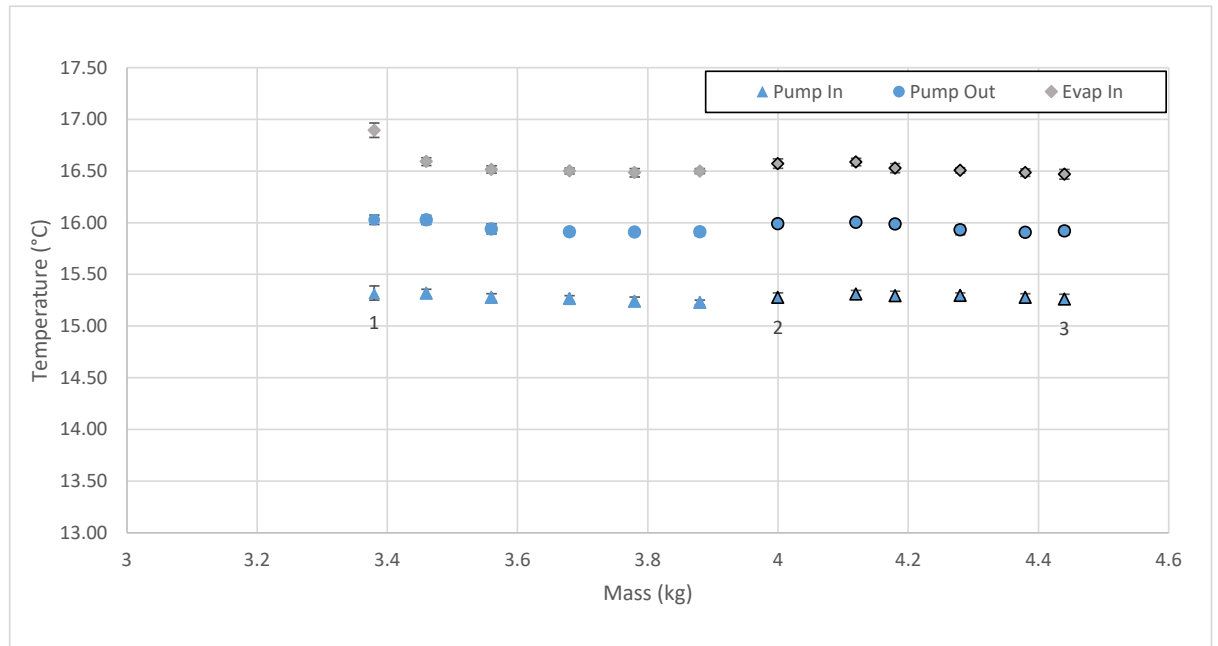
*Figure 29: Average pump inlet, pump outlet and evaporator inlet temperatures for various system charges at 800rpm pump speed. The pump inlet and outlet, and evaporator inlet temperatures remain reasonable constant with increasing mass. **Note: These initially high temperatures at the evaporator inlet are a result of thermocouple location.***

The pump inlet and pump outlet temperatures, shown in Figure 29, remain consistent across the test range, with the pump inlet temperature maintaining an average of 15.3±<0.1°C and the pump outlet similarly maintaining an average of 16±<0.1°C. After an initial elevated value, as a result of sensor location, the evaporator inlet temperature settles around an average of 16.5±<0.1°C. After an initial 2°C increase in temperature in the first two system charges, the expander inlet, hot water feed and hot water return temperatures, shown in Figure 30, stabilise out and maintain values of 83.9±<0.2°C, 86.7°C±<0.2°C and 85.1±<0.4°C respectively.
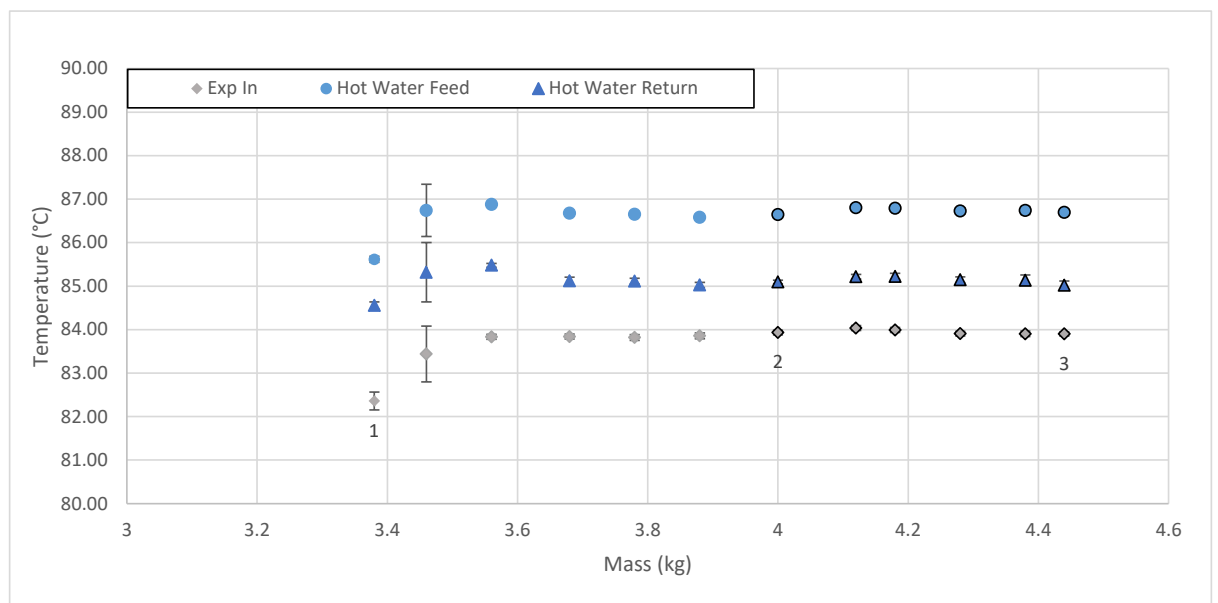
Figure 30: Average expander inlet, hot water feed and hot water return for various system charges at 800 rpm pump speed. After an initial increase in all three cases over the first two data points, the temperatures remain reasonable consistent for the remainder of the mass increments.
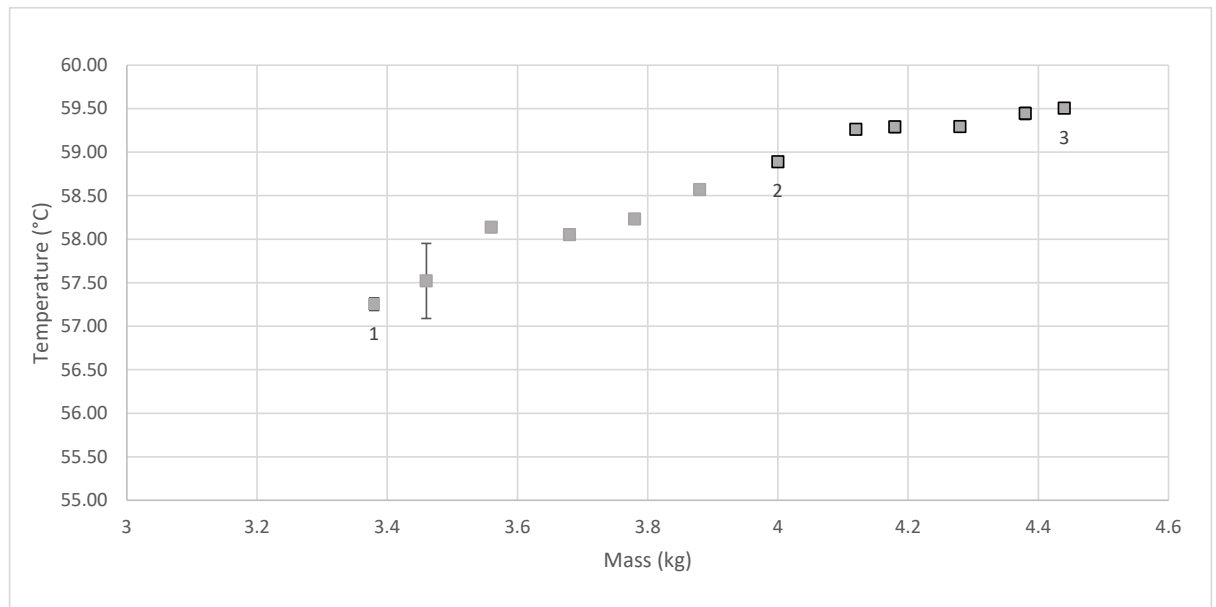
Figure 31: Average expander outlet temperature for various system charges at 800rpm pump speed. The expander outlet temperatures shows a steady and sustained increase in temperature with increasing system charge.

The expander outlet temperature of the system is the only measured temperature that shows significant change in temperature over the test range as presented in Figure 31. From an initial system temperature of 57°C, the expander outlet temperature shows a reasonably linear increase in temperature with system charge, up to approximately 60 degrees at 4.44kg of mass.

4.1.2. Discussion

The effect of increasing system mass results in a peak in system performance. Since the temperatures in the system shows no significant change over the tested charge range then the change in performance is as a results of the changes in system pressure. The low pressure side of the system shows a steady and linear increase in pressure whereas the high pressure side of the system shows a significantly steep increase in pressure followed by a plateau with increasing charge levels. Since the output of the expander is a function of the pressure differential across the expander and the low side pressure of the system continually increases with charge, the peak in system output coincides with the initial plateau in high side pressure. Increasing system charge and in effect system liquid column height improves the cycle performance as the pump output increases with reducing cavitation. Once the gains of this benefit begin to dwindle, the continual increasing low side pressure results in the decline in the overall performance. However, when calculating the NPSH based on the available NPSH from the measured data at the pump inlet and

required NPSH from the manufacture data. We get no indication of potential cavitation with a significant net positive suction head across the entire test range as shown in Figure 32.
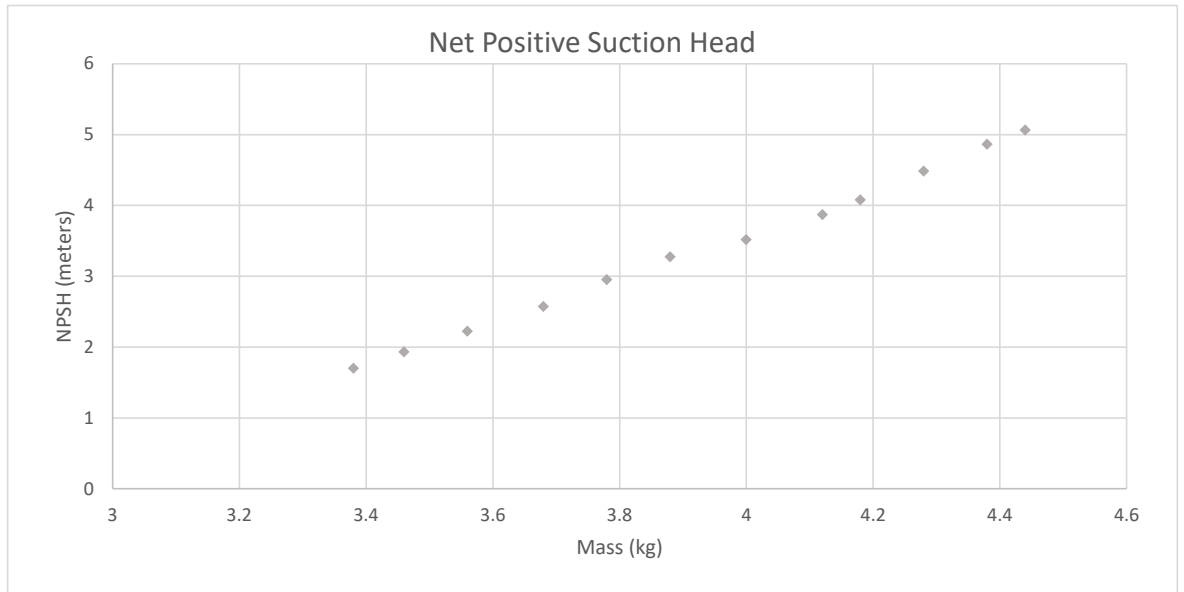
Figure 32: Net Positive Suction head for various system charges at 800rpm pump speed.

4.2. System Charge effect/Liquid column height on single set of ORC operational conditions at various pump speeds

In the last section it is evident that the increase in mass and associated increase in stored liquid column height has a significant impact on system performance. Since the NPSHr for the pump varies with pump speed, the same test was carried out at three additional pump speeds: 600, 1000 and 1200rpm. The results of these three cases and the previous 800 rpm case have been compared in this section.

4.2.1. Experimental results: Pump Speed Comparison

Pump Speed Comparison Experimental Observation Summary:

For the tested pump speeds below 1000rpm - The peak overall performance for the ORC system at different pump speeds varies with system mass and liquid column height. The high side pressure shows an initial steeper increase with increasing mass before leveling off with only a slight increase in pressure. The low side pressure increases in a linear manner with increasing mass. For the most part the system temperatures remain stable, with the most significant change occurring at the expander outlet which shows a reasonably linear increase in temperature with mass.

For the 1200 rpm case- The data fluctuates significantly throughout, in complete contrast to the previous test points. .

Overall performance:

The overall performance of the ORC system is evaluated from the expander rotational speed, expander output power and consumed pump power. The combined effect of pump speed and mass are compared in Figure 33, Figure 34 and Figure 35 respectively. Since the expander rotational speed and electrical output are directly linked the overall trends of Figure 33 and Figure 34 are similar. For the 600, 800 and 1000 rpm pump speed cases the system output initially increases with increasing mass to a peak, plateaus and then begins to decline. The maximum rotational expander speed occurs at: 1000rpm – 3247rpm, 5.14kg of system charge with the liquid height visible at sight glass S6. 800rpm- 2977rpm, 3.78kg and liquid height between sight glass S6 and S5. 600rpm- 2765rpm, 3.74kg with liquid height located below sight glass S6. As would be expected a higher pump speed results in a higher peak expander rotational speed for these three cases. However, as is evident from Figure 33 the increase to the highest pump speed results in a peak rotational speed of 2990, which is on par with the 800rpm pump speed case.

Figure 33: Expander rotational speed for various system charges at pump speeds of 600, 800, 1000 and 1200 rpm. For the 600, 800 and 1000 rpm pump speed cases: the rotational speed initially increases with mass to a peak value before reducing, an increasing pump speed results in an increase in the peak expander rotational speed. The 1200 rpm case does not conform to either of these trends
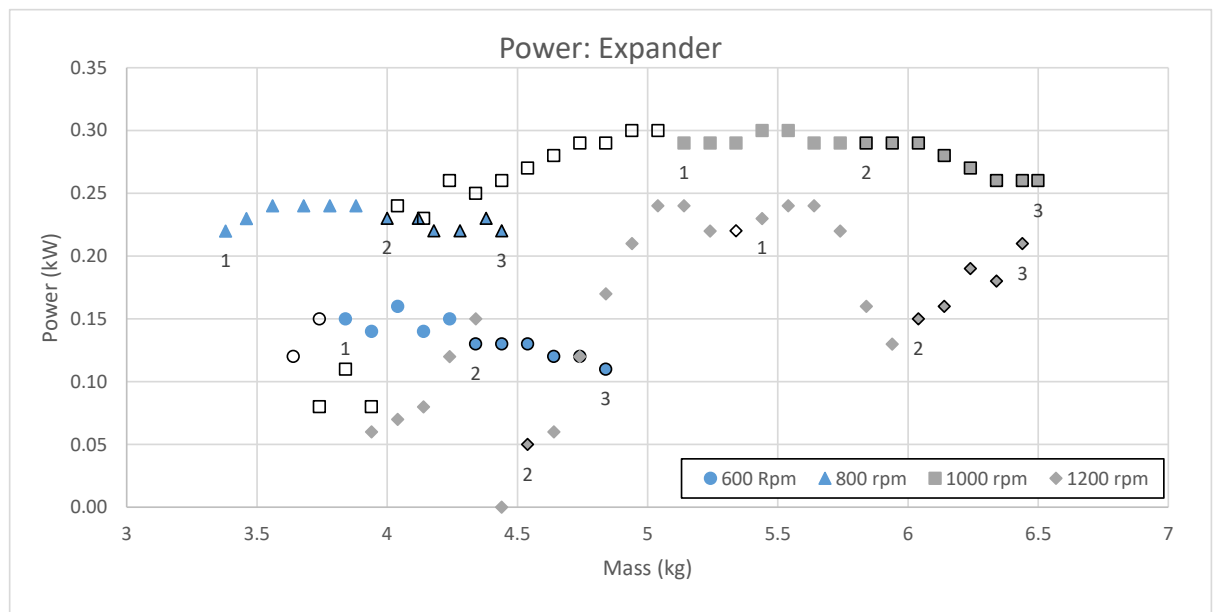
Figure 34: Expander power output for various system charges at pump speeds of 600, 800, 1000 and 1200 rpm. The trend of the electrical power output follows a very similar trend to the expander rotational speed. There is a peak in power, with increasing mass and overall increase in output with increasing pump speed for the 600, 800 and 1000 rpm cases. The 1200 rpm case does not follow either of these trends.

The expander electrical power output (Figure 34) follows a similar trend to expander rotational speed, with a slight difference in peak points: 1000rpm- 0.3 kW, 800rpm- 0.24kW, 600rpm- 0.16kW and 1200rpm- 0.24kW. The maximum power consumed by the pump as would be expected generally increases with increasing pump speed as shown in Figure 35. 600rpm- 0.07kW, 800rpm – 0.09kW, 1000rpm- 0.11kW and 1200rpm- 0.11kW.
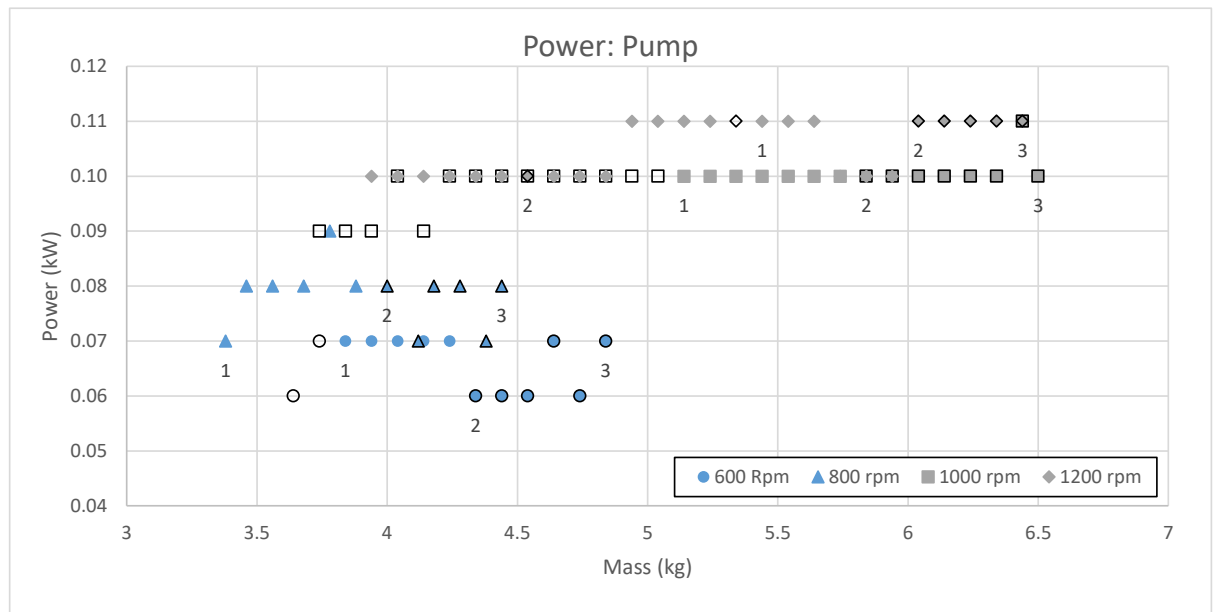
Figure 35: Pump power consumed for various system charges at pump speeds of 600, 800, 1000 and 1200 rpm. The pump power consumed shows a general increase for all four cases with increasing pump speed.

Pressure:

Both the pump outlet (Figure 36) and expander inlet (Figure 37) follow the same trend in pattern with differing pressure values. For the majority of data points in the 600, 800 and 1000rpm case, there is an initial steeper increase in pressure and a levelling off to a more gradual increase in pressure. Like most aspects of the 1200rpm case, the high side pressure doesn't follow this trend. The maximum pressure in the high side is on par with the slower pump speed case of 800rpm and well below that of the 1000 rpm case. Overall, the increase in pump speed leads to an increase in high side pressure, with the exception of the 1200rpm case.
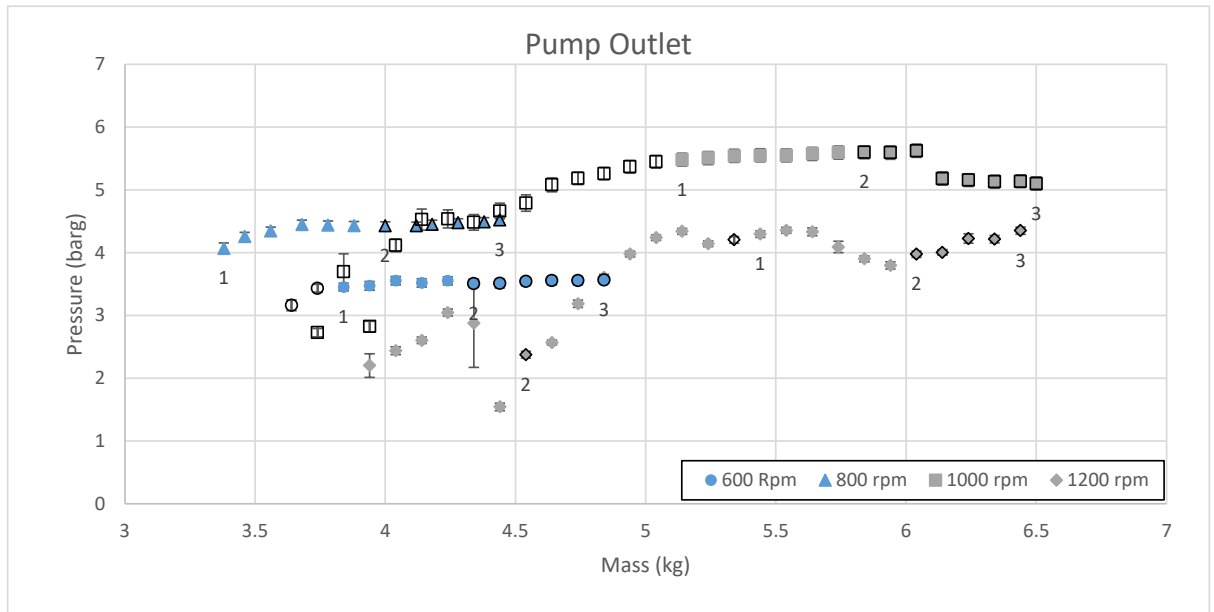
Figure 36: Pump outlet pressure for various system charges at pump speeds of 600, 800, 1000 and 1200 rpm. The general trend for the individual cases is an initially steeper increase in pressure with increasing charge, followed by a levelling off to a slight increase in pressure. Overall for these cases, an increase in pump speed for a fixed expander load results in an increase in pump outlet pressure. The 1200 rpm case does not conform to either of these trends.
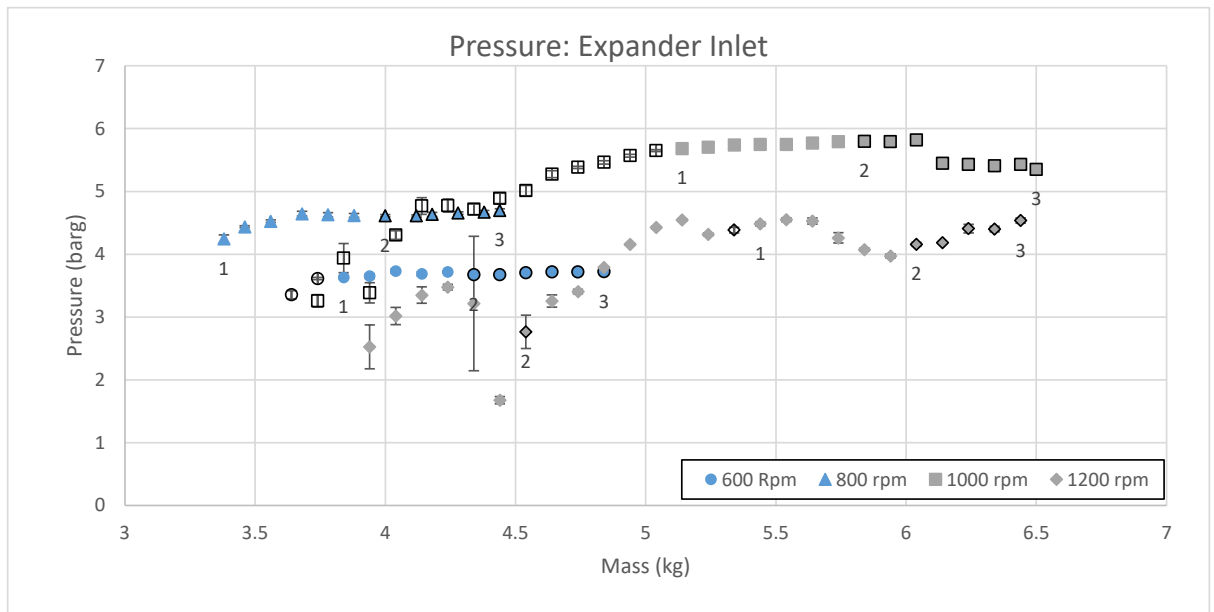
Figure 37: Expander inlet pressure for various system charges at pump speeds of 600, 800, 1000 and 1200 rpm. The expander inlet follows the same trend as the pump outlet pressure.

The expander outlet pressure (Figure 38) in all four cases rises linearly with increasing mass. The average rate of pressure increase with mass for the four pump speeds is: 600rpm- 0.27 barg/kg, 800rpm- 0.31barg/kg, 1000rpm-0.33 barg/kg and 1200rpm- 0.30 barg/kg. These rates are all fairly similar and are comparable with the condenser outlet, shown in Figure 39.
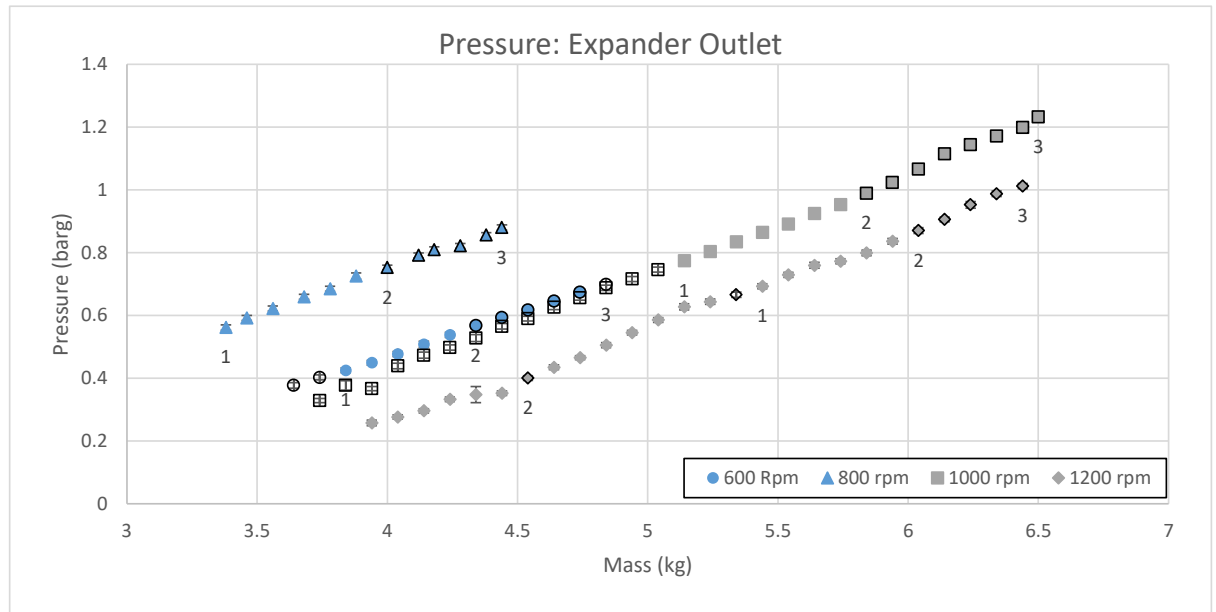
Figure 38: Expander outlet pressure for various system charges at pump speeds of 600, 800, 1000 and 1200 rpm. In all four pump speed cases the expander outlet pressure increases in a linear manner, with increasing system charge. The rate of increase in all fours cases is very similar.
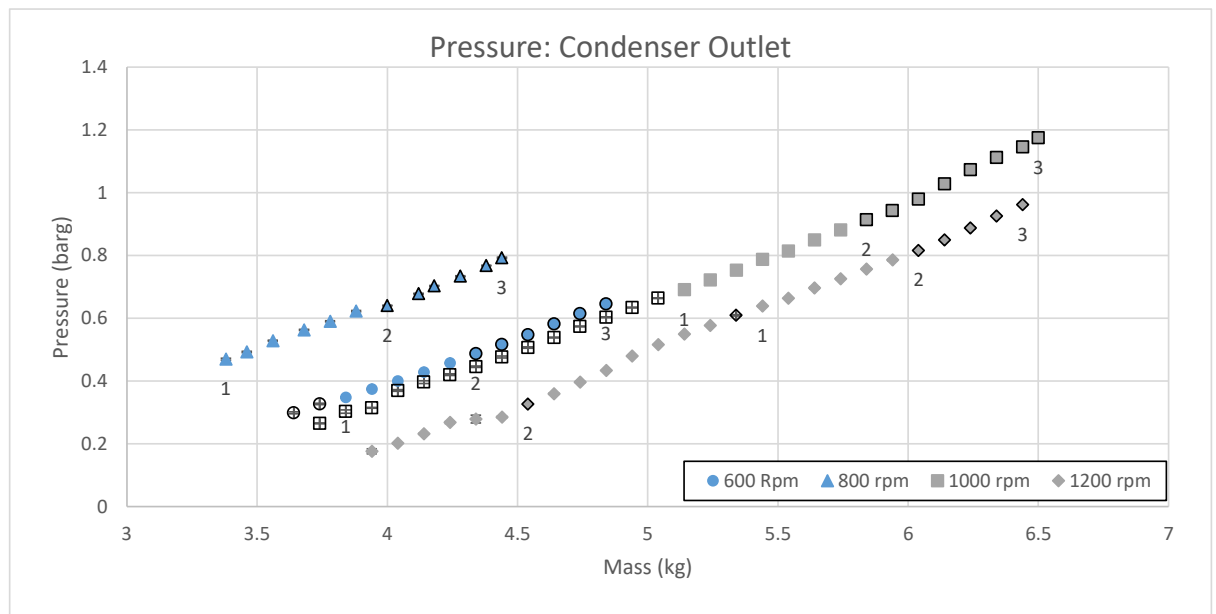
Figure 39: Condenser outlet pressure for various system charges at pump speeds of 600, 800, 1000 and 1200 rpm. In all four cases the condenser outlet pressure increases in a reasonable linear manner.

The average rate of pump inlet pressure increase with increasing mass for the four pump speeds is 0.29, 0.32, 0.33, and 0.31 barg/kg for 600, 800, 1000 and 1200 rpm respectively. The pump inlet pressure shown in Figure 40, also shows this increasing trend with mass. However, the rates of increase are more varied than those recorded at the expander outlet and condenser outlet. The average rate of increase with mass is 0.40, 0.43, 0.39 and 0.31 barg/kg.
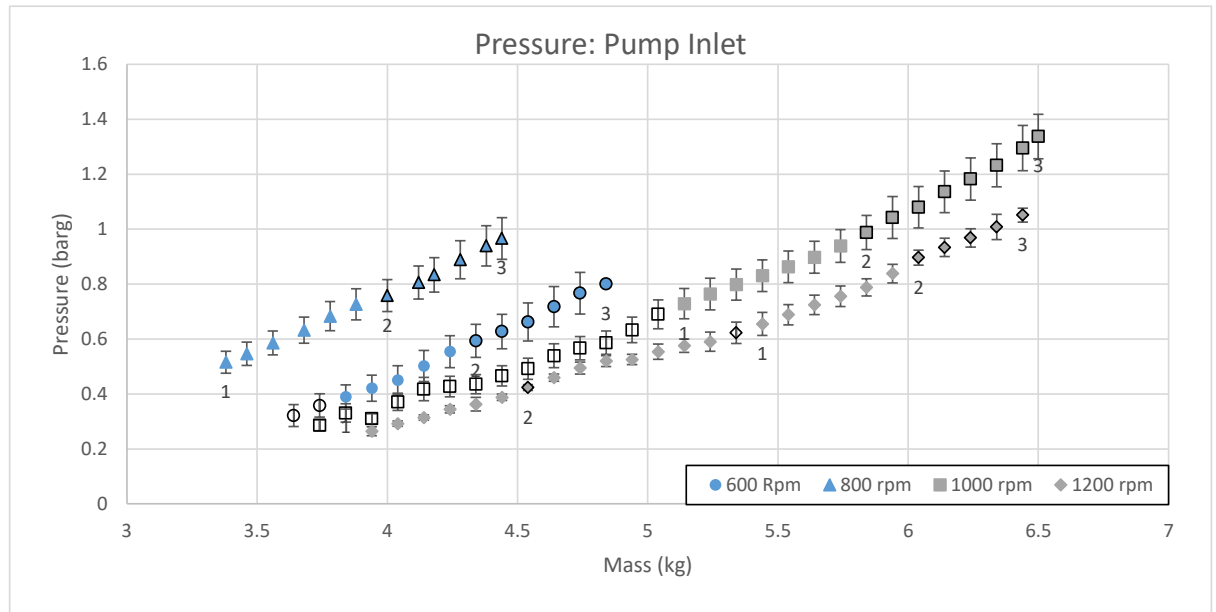
Figure 40: Pump inlet pressure for various system charges at pump speeds of 600, 800, 1000 and 1200 rpm. In all four cases the pressure at the pump inlet increases with increasing mass in a linear manner.

Temperature:

The temperature of the cold water feed (Figure 41) is externally controlled and shows no significant changes or patterns with ORC system operation. All the recorded data points for the four pump speeds lie between 15.1 and 15.4°C.
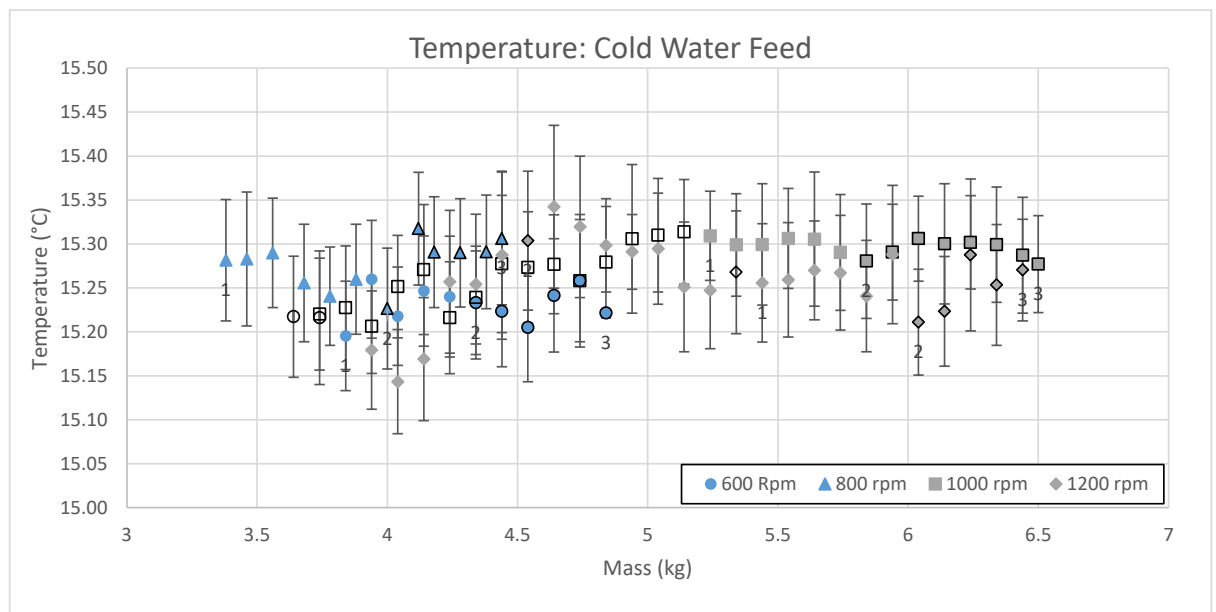
Figure 41: Cold water feed temperature for various system charges at pump speeds of 600, 800, 1000 and 1200 rpm. The controlled cold feed inlet temperature which is independent of the ORC operational conditions for all test data point lies between 15.10 and 15.35°C.

The cold water return temperature (Figure 42) for the 600, 800 and 1000rpm all show an initial increase with mass before flattening off and maintaining average temperatures of 21, 23 and 24°C respectively. The 1200rpm case does not stabilise at a consistent value.

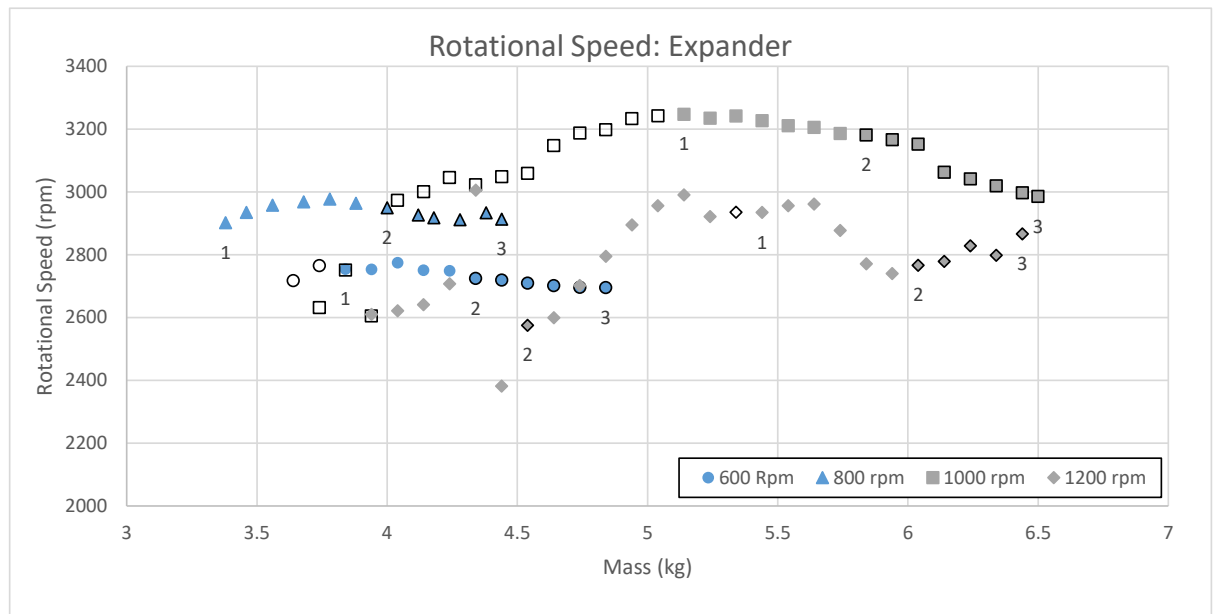*Figure 42: Cold water return temperature for various system charges at pump speeds of 600, 800, 1000 and 1200 rpm. For the 600, 800 and 1000 rpm pump speed cases the return temperature shows an initial increase in temperature with increasing mass before levelling off and maintaining a consistent value for the remainder of the test range. The 1200 rpm case varies significantly with increasing mass and follows a similar trend to the expander rotational speed and high side pressure.*
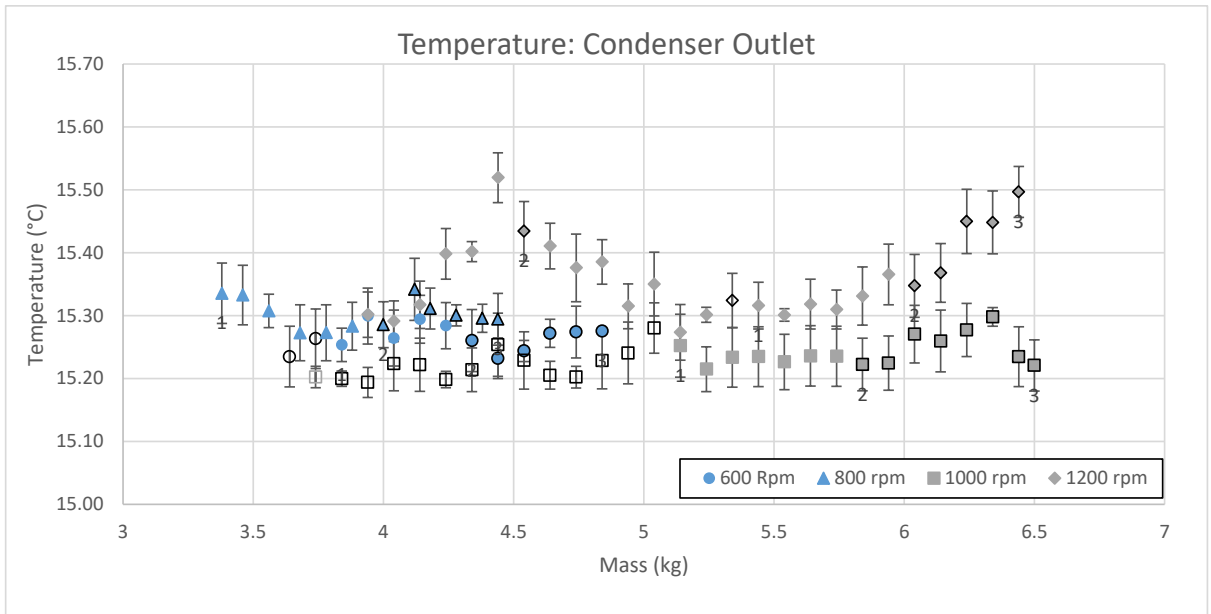
Figure 43: Condenser outlet temperature for various system charges at pump speeds of 600, 800, 1000 and 1200 rpm. With the exception of the 1200 rpm case, the remaining average recorded data points lie comfortably between 15.1 and 15.4°C. In the 1200 rpm case, the outlet temperature decreases towards 5.5kg of charge before increasing for the remainder of the test range.

The vast majority of condenser outlet temperature data points shown in Figure 43 lie between 15.1 and 15.4°C. The 1200rpm pump speed is the only case in which the data lies out with this range. The pump inlet temperatures (Figure 44) follows a similar trend with the majority of data points lying between 15.1 and 15.4°C. Likewise the 1200rpm pump speed is the only case which falls out with this range.
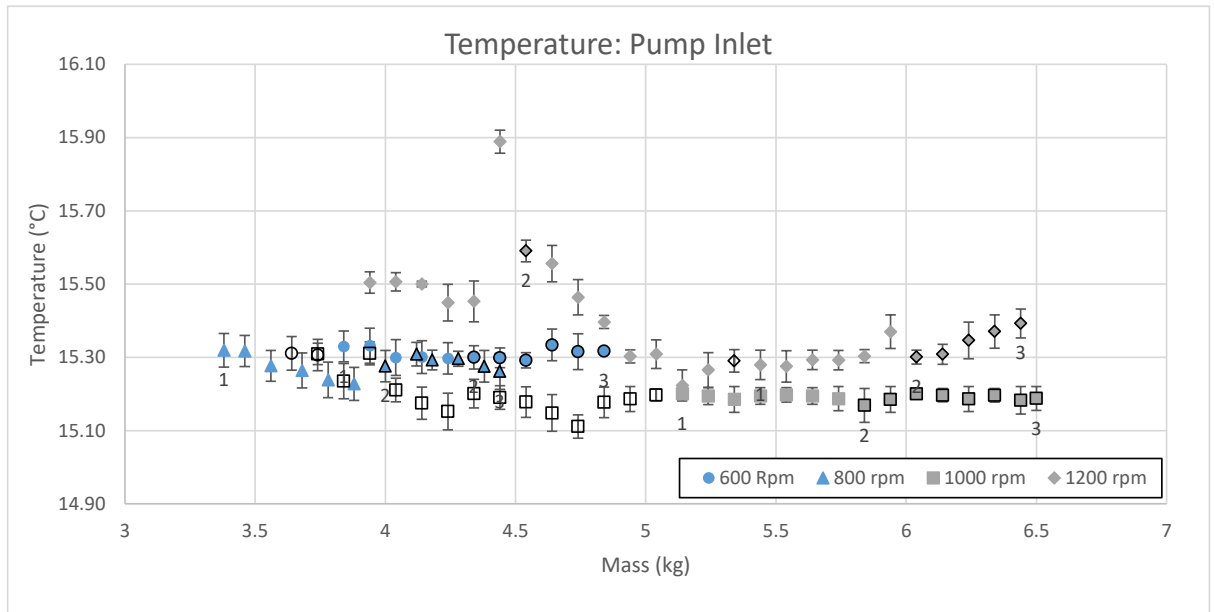
Figure 44: Pump inlet temperature for various system charges at pump speeds of 600, 800, 1000 and 1200 rpm. With the exception of the 1200 rpm case, the remaining test data points fall between 15.1 and 15.4°C. In the 1200 rpm case the initial test results up to around 5 kg of charge sit slightly higher than the bulk of the data points.

Again the pump outlet temperature (Figure 45) data points in the vast majority of cases fall between 15.8 and 16.3°C. The 1200rpm pump speed case starts with some initially high values but becomes more consistent with increasing mass.
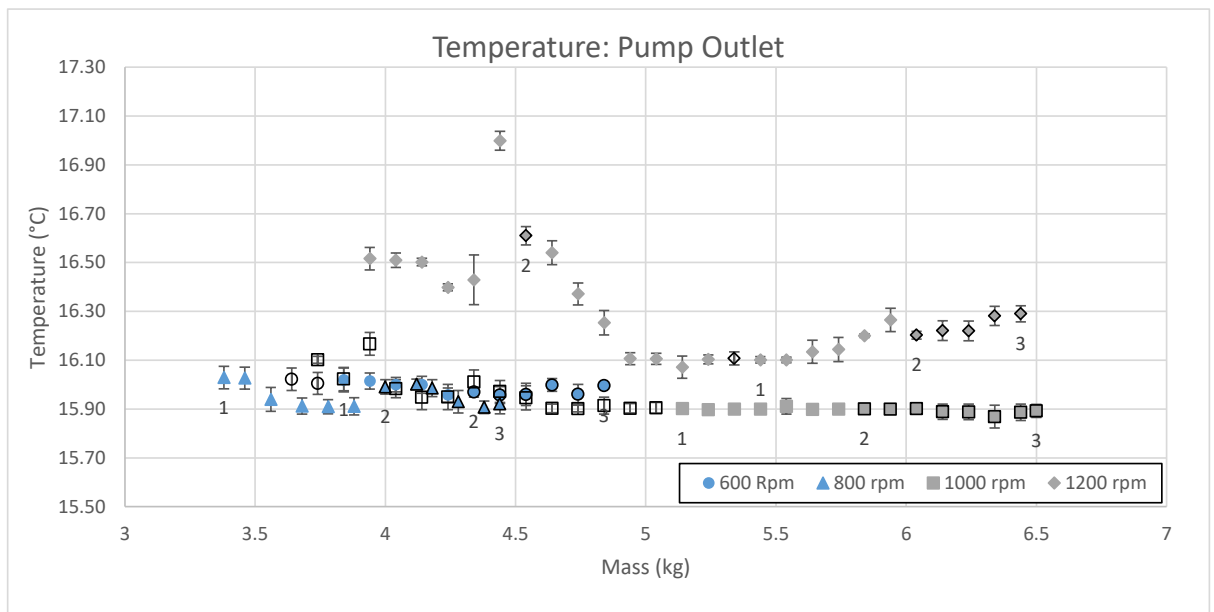
Figure 45: Pump outlet temperature for various system charges at pump speeds of 600, 800, 1000 and 1200 rpm. The majority of the three lower pump speed data points fall between 15.8 and 16.1°C. The 1200rpm case initially starts with a scattering of higher temperature data points with reduce towards 5kg of system charge. The temperature remains reasonably constant for an additional 0.5kg before steadily increasing at the end of the test run.

For the lower system charges of 600, 800 and 1200rpm pump speeds, the evaporator inlet temperature (Figure 46) has initially high values. As the mass is increased the temperature reduces significantly and the temperature becomes more consistent. It has been noted

throughout that these initially high temperature values are a result of the sensor location, which results in a measurement that is sensitive to ORC system flow rate.
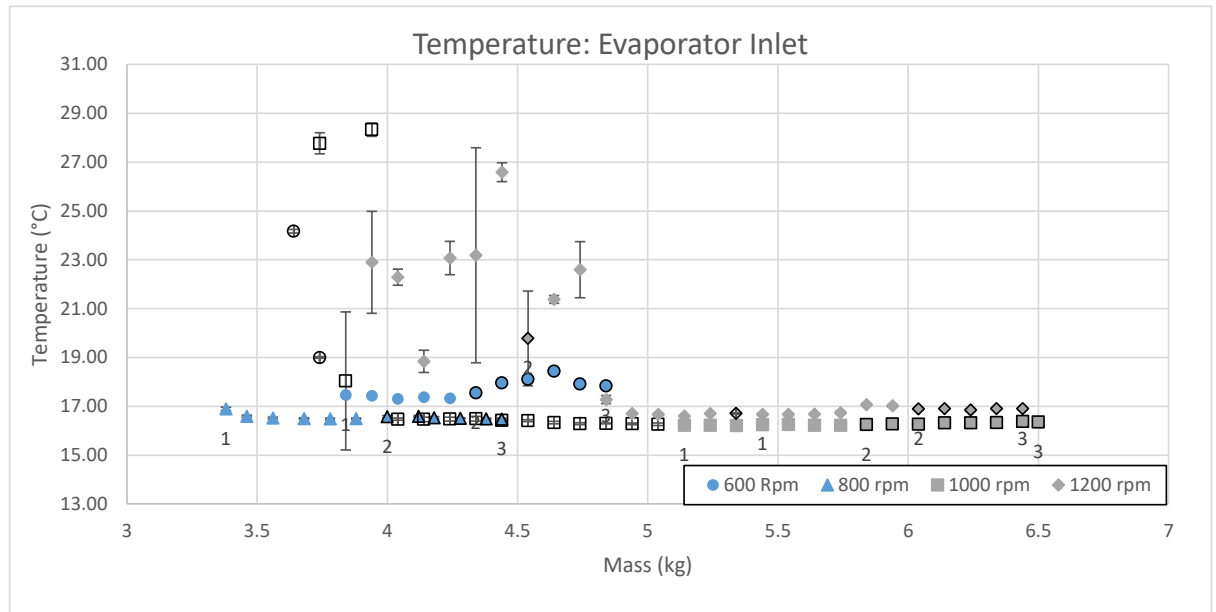
Figure 46: Evaporator inlet temperature for various system charges at pump speeds of 600, 800, 1000 and 1200 rpm. For the 800 rpm case there is no significant change in evaporator inlet temperature throughout the entire test run. In the 1000rpm case the majority of the test data, with the exception of three data points at low charge levels, coincides with the 800rpm data. At the slower pump speed of 600 rpm the temperature reduces significantly to a minimum point around 4.24kg of system charge. The temperature then gradually increases. The 1200 rpm case has significant variation in temperature as the charge level increases to 5kg before levelling off for the remainder of the test run. ***Note: The high initial temperatures are a result of sensor location and are sensitive the ORC system flow.***

Like the cold water feed temperature the hot water feed temperature is controllable, with the measured temperatures shown in Figure 47. The total range of the measured data is within 2.5°C, although the majority of the data points particular for the 600, 800 and 1000 rpm case fall between 86 and 87°C. It should be noted that the heating control system has a much slower response than the cold side feed system. When the ORC system is subjected to significant system changes during operation, the controller struggles to manage the supplied heat. The majority of outlying values are at the lower system charge levels or the 1200rpm case.
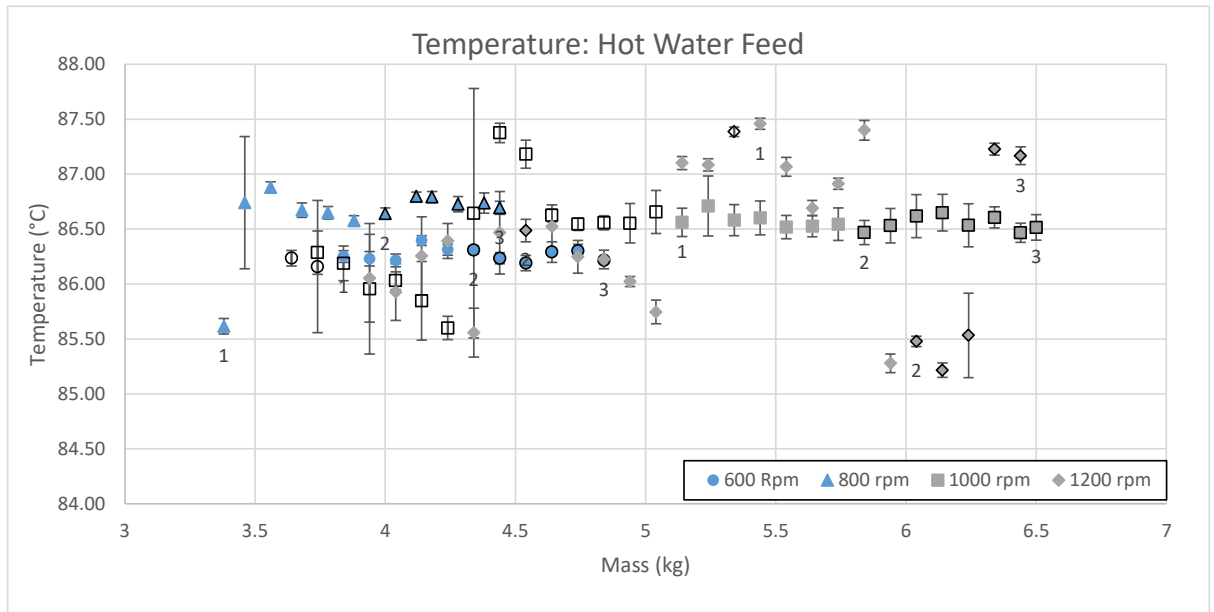
*Figure 47: Hot water feed temperature for various system charges at pump speeds of 600, 800, 1000 and 1200 rpm. For the vast majority of the data points of the 600, 800 and 1000 rpm pump speed cases, the recorded values fall between 86 and 87°C. The data that falls out with this range for the lower speed cases is at the lower end of the mass range. The feed temperature of the 1200 rpm cases varies significantly throughout the testing. **Note: When the system is significantly unstable the heater controller has issues maintaining consistent temperatures.**

The hot water return temperature shown in Figure 48 for the 600 and 1000 rpm case show an initial decrease in temperature before levelling off around 86°C and 83.5°C respectively. The 800rpm case shows an initial increase in temperature before levelling off at approximately 86°C. The 1200rpm case settles around no consistent value.
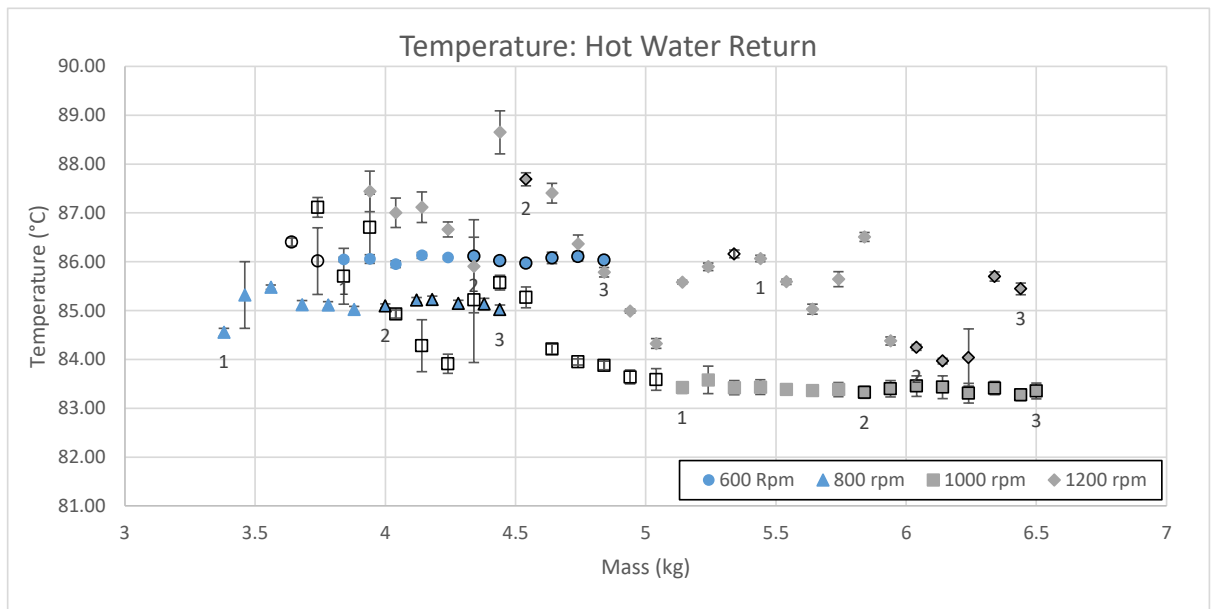
Figure 48: Hot water return temperature for various system charges at pump speeds of 600, 800, 1000 and 1200 rpm. In both the 600 and 1000 rpm case, the return temperature shows a reasonable decrease in temperature initially before levelling off. The 800 rpm case shows an initial increase in temperature before levelling off. The 1200 rpm case shows no consistent trend and varies significantly throughout testing.
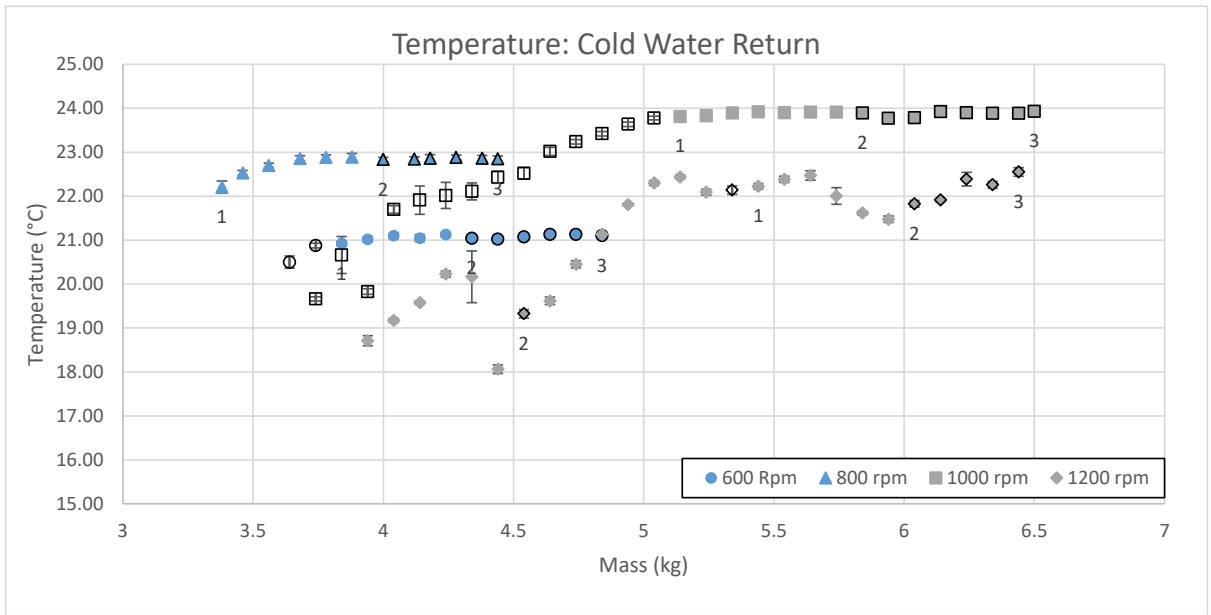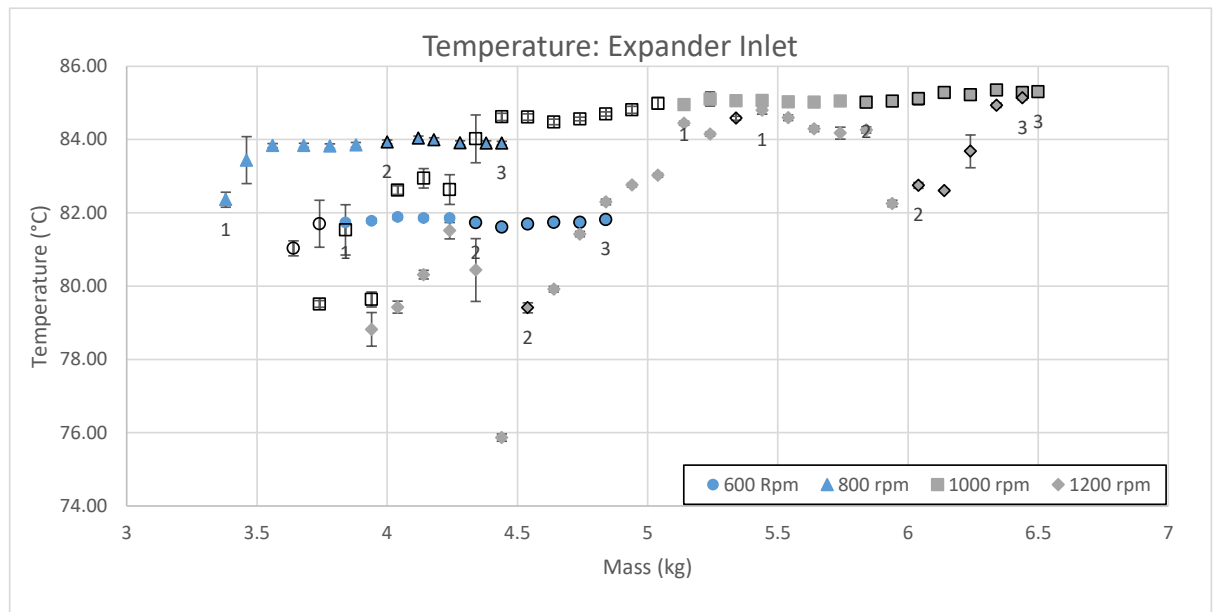
Figure 49: Expander inlet temperature for various system charges at pump speeds of 600, 800, 1000 and 1200 rpm. For the 600, 800 and 1000 rpm pump speed cases the expander inlet temperature shows an initial increase in temperature with increasing mass before levelling off and maintaining a consistent value for the remainder of the test range. The 1200 rpm case varies significantly with increasing mass and follows a similar trend to the expander rotational speed and high side pressure.

The expander inlet temperature shown in Figure 49 show an initially steep increase in temperature for the 600, 800 and 1000rpm cases, before levelling off at approximately 82, 84 and 85°C respectively. The 1200rpm case does not settle around a consistent value. The expander outlet temperature (Figure 50) for all four cases shows a general increase in temperature with increasing system charge. The increase for the 600 and 800 rpm cases is reasonable linear increasing at 1.12°C/kg and 3.1°C/kg respectively. The 1000 rpm case shows a section consistent linear increase between 4.5 and 6 kg of system charge, however shows significant changes at each end of the test range. Although the overall trend is increasing, the 1200rpm case shows inconsistent change between individual test increments.
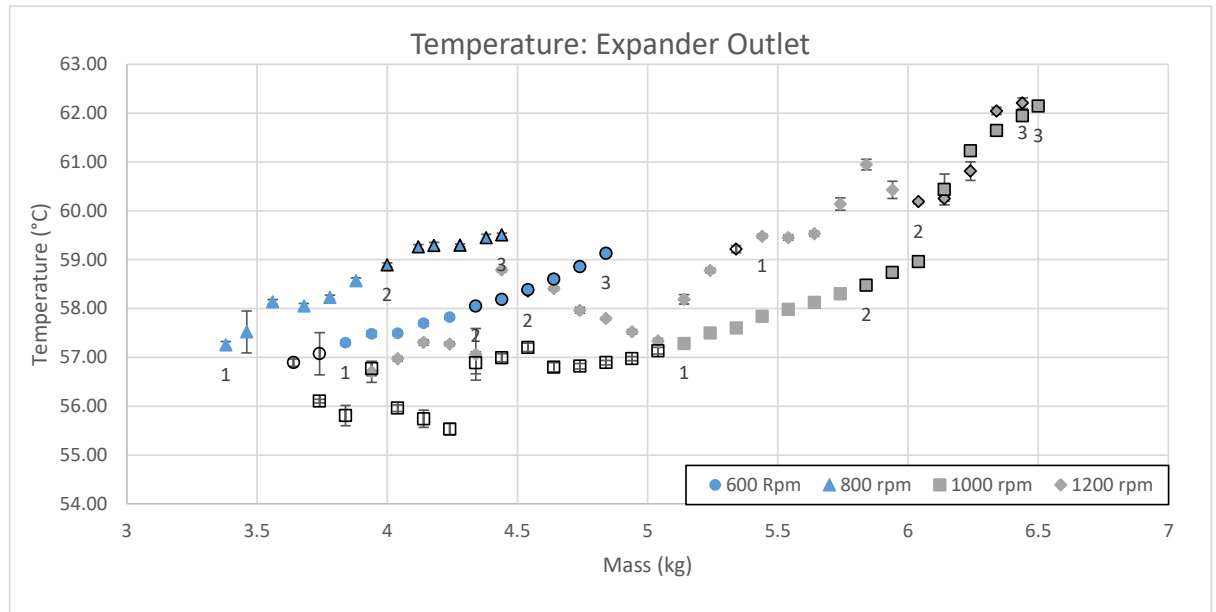
Figure 50: Expander outlet temperature for various system charges at pump speeds of 600, 800, 1000 and 1200 rpm. For both the 600rpm and 800rpm case the rate of increase with expander outlet temperature is similar with increasing charge level. Likewise a significant proportion of 1000rpm data points conform to a linear trend, where both the initial and end points show some significant changes. The 1200 rpm pump shows an overall increasing trend with mass but fluctuates significantly.

4.2.2. Analysis and discussion

It is evident across all the presented data in this section that the ORC system follows the same trends with increasing mass upto a pump speed of 1000rpm. There is an initial increase in performance as the increase in mass results in a reduction in pump cavitation. As the effects of cavitation become less prominent the continual increase in low side pressure with charge begins to reduce system output. At the highest pump speed of 1200 rpm the increasing system charge, resulting in an increase in liquid column height, is insufficient to fully satisfy the pump operational requirement and results in system performance far from what would be expected. However, based on the calculation of NPSH as shown in Figure 51, even for the 1200rpm pump speed case there is no indication from the calculation that pump cavitation is an issue. There is therefore a significant discrepancy between the experimental findings and the NPSH calculation.
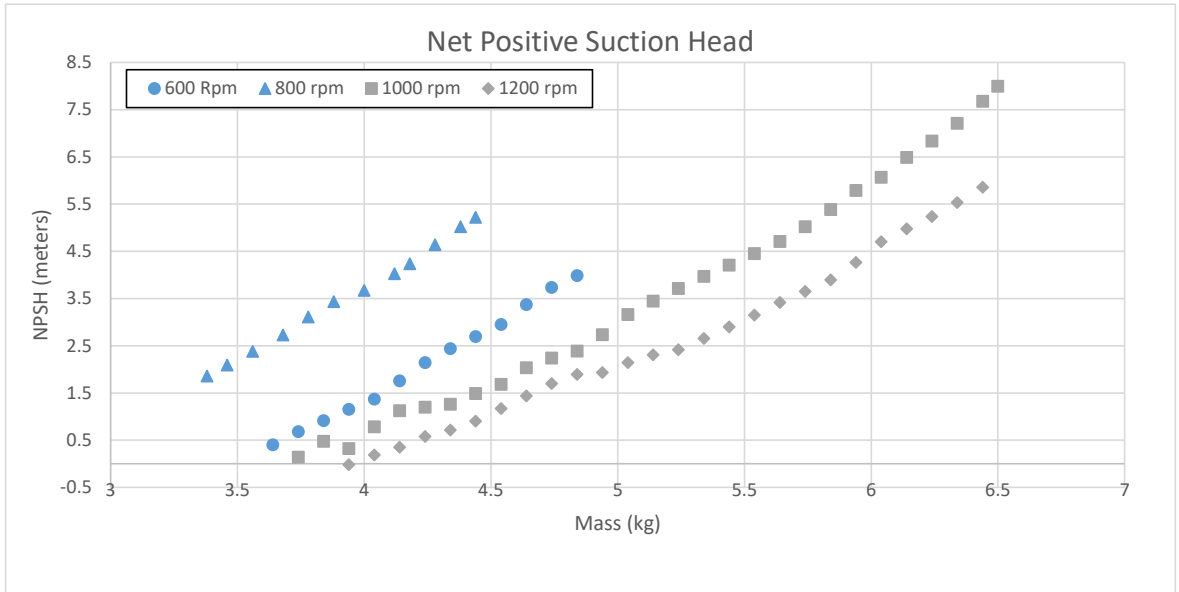
Figure 51: Net positive suction head at pump speeds of 600, 800, 1000 and 1200 rpm. With the exception of the very first 1200rpm case the Net positive suction head is positive across the entire test range indicating no cavitation would occur.

This point is further emphasised when the maximum output power case is taken from each of the three pump speeds and the measured available NPSH plotted against the manufactures data, shown in Figure 52.
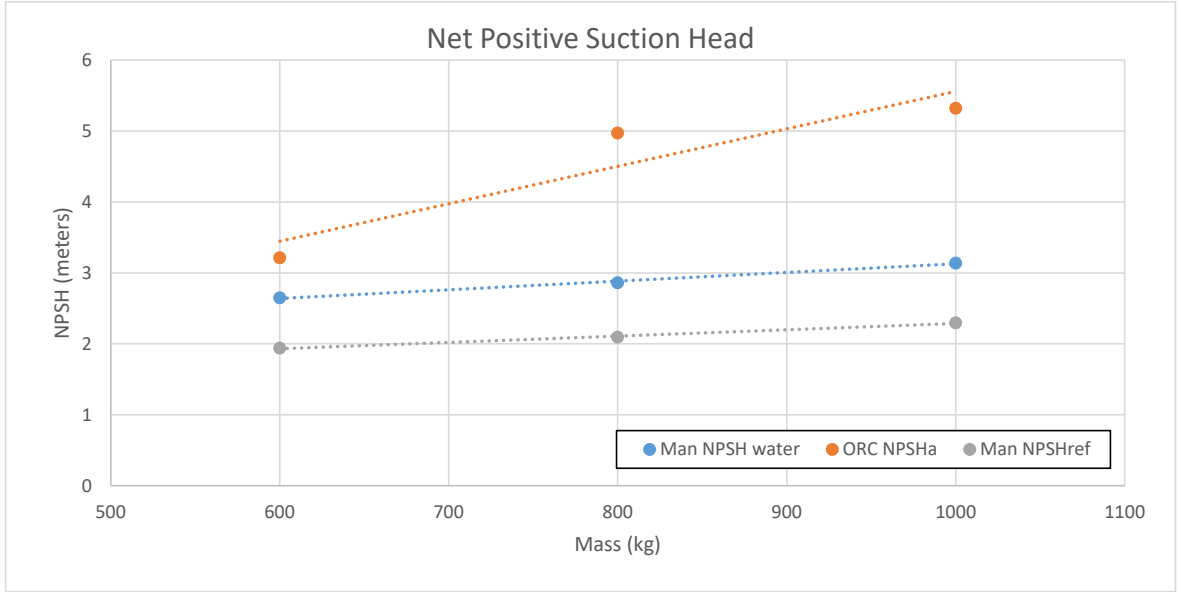
Figure 52: NPSH comparison: measured available NPSH from ORC at 600, 1000, 1200rpm. Compared against supplied manufacturer data for required NPSH based on water and R245fa.

4.4. **System Charge effect/liquid height on three cold side temperatures at fixed pump speed on ORC operational conditions**

In the previous two sections the effects of mass on a single set of operational conditions with varying pump speeds was considered. In order to assess if the effects of other system parameters affected the stored liquid column height. Three cold side temperatures and three expander loads for a single pump speed were conducted in a single mass fill run, which produced six individual data sets. There is significant amount of repetition in the data, therefore only the three light load results are presented in this section. Additionally, for these tests the overall tested mass range was reduced to cover the peak system performance up to a liquid column height of 1.6m.

4.4.1. Experimental results

Experimental observation summary: Reducing the cold side temperature has no effect on the stored liquid column height of the system. The overall performance of the system increases with reducing cold sink temperature. Both the high side and low side system pressures reduce with reducing cold sink temperature. The reduction in cold stream temperature results in a corresponding reduction in temperature from the condenser outlet to the evaporator inlet. There is no effect on the expander inlet temperature, however, there is a notably observable change in expander outlet temperature.

Overall performance:

Reducing the cold side temperature from 20 to 10°C results in a general increase in the rotational speed of the expander as shown in Figure 53. The maximum recorded rotational speed for the three cases is 2745, 2819 and 2893rpm for 20, 15 and 10°C respectively. Although, the value recorded at 20°C is significantly different from its surrounding data points. The second highest recorded value for the 10°C is 2876rpm. The most significant observation is that changing the cold sink temperature had negligible effect on the liquid column height over this temperature range and receiver volume with the level remaining visible at both sight glasses.

Figure 53: Expander rotational speed for various system charges: 800rpm pump speed and three cold sink set temperatures; 10, 15 and 20℃. Overall the expander rotational speed increases with reducing cold side temperature, changing the cold side temperature had negligible effect on the liquid column height.

The expander outlet power and consumed power for the three temperature cases at 800rpm pump speed are presented in Figure 54 and Figure 55. As with the expander rotational speed, the output power generally increases with decreasing cold sink temperature. The maximum recorded output power for the three cases is 0.13, 0.18 and 0.2 for 20, 15 and 10°C. It is worth noting that the peak expander rotational speed for the 20°C case does not match with a corresponding peak output power.

Figure 54: Expander output power for various system charges: 800rpm pump speed and three cold sink set temperatures; 10, 15 and 20℃. There is a general increase in electrical output power with decreasing temperature.

The recorded pump power for all three cases varies between 0.07 and 0.1kW with an average of 0.08kW for the 20 and 15°C, and 0.09kW for the 10°C case across the mass test range.

Figure 55: Pump power consumed for various system charges: 800rpm pump speed and three cold sink set temperatures; 10, 15 and 20°C. All the recorded data points for all three cases vary between 0.07 and 0.1 kW of consumed pump power

Pressure:

Reducing the cold side temperature of the system results in a decrease in high side pressure as shown in the recorded pump outlet and expander inlet pressure, Figure 56 and Figure 57. The average pressure for each of the three cases is 4.83 (20°C), 4.68 (15°C) and 4.49 barg (10°C) at the pump outlet and 4.97 (20°C), 4.84 (15°C) and 4.68 barg at the expander inlet.

Figure 56: Pump outlet pressure for various system charges: 800rpm pump speed and three cold sink set temperatures; 10, 15 and 20℃. Decreasing the cold sink temperature results in a decrease in pump outlet pressure.

Figure 57: Expander inlet pressure for various system charges: 800rpm pump speed and three cold sink set temperatures; 10, 15 and 20℃. Decreasing the cold sink temperature results in a decrease in expander inlet pressure.

In a similar manner decreasing the cold side temperature results in a decrease in low side pressure at the expander outlet (Figure 58), condenser outlet (Figure 59) and pump inlet (Figure 60). Similar to previously presented results the cold side pressure increases in a linear manner with increasing mass. The average rate of pressure increase with mass is: 0.40 (20°C), 0.36 (15°C) and 0.39 (10°C) barg/kg for the expander outlet, 0.40 (20°C), 0.47 (15°C) and 0.47 (10°C) at the condenser outlet, and 0.52 (20°C), 0.43 (15°C) and 0.35 (10°C) at the pump inlet.

Figure 58: Expander outlet pressure for various system charges: 800rpm pump speed and three cold sink set temperatures; 10, 15 and 20℃. The expander outlet pressure increases in a linear manner with mass and shows an overall decrease with decreasing temperature.

Figure 59: Condenser outlet pressure for various system charges: 800rpm pump speed and three cold sink set temperatures; 10, 15 and 20℃. The condenser outlet temperature increases with increasing mass and decreases with decreasing cold sink temperature.
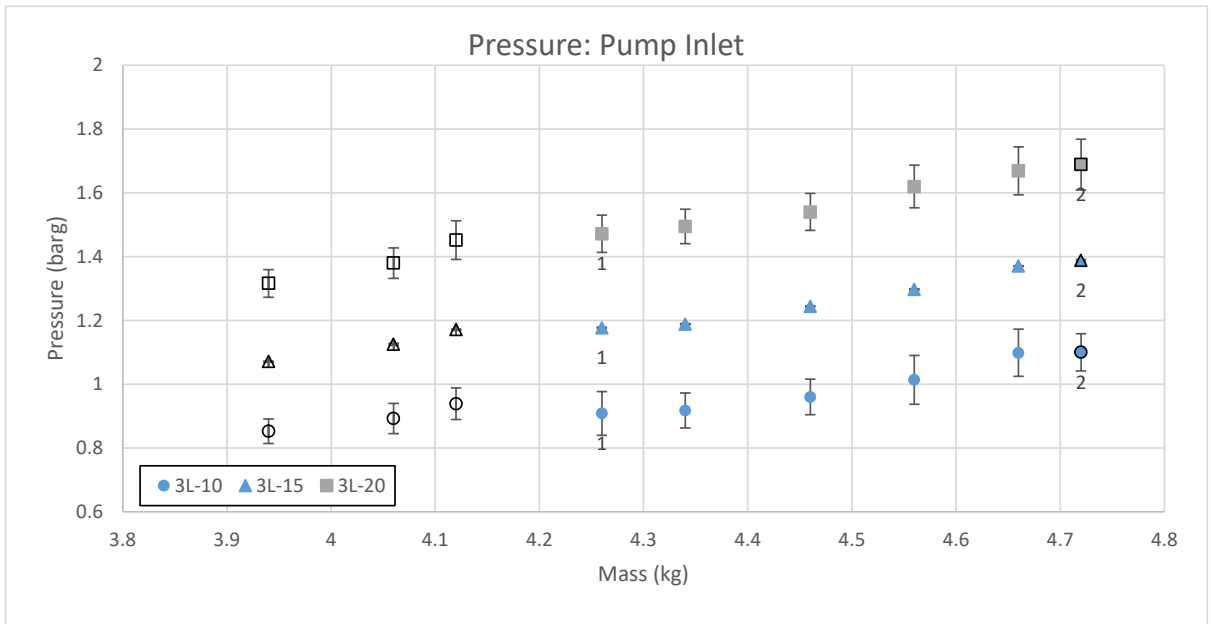
Figure 60: Pump inlet pressure for various system charges: 800rpm pump speed and three cold sink set temperatures; 10, 15 and 20°C. The pump inlet temperature increases with increasing mass and decreases with decreasing cold sink temperature.

Temperature:

Decreasing the cold sink set point temperature unsurprisingly reduces the cold water feed temperature as shown in Figure 61. The resulting measured cold water feed water temperature is 20±0.5°C, 14.8±0.5°C and 9.7±0.5°C.
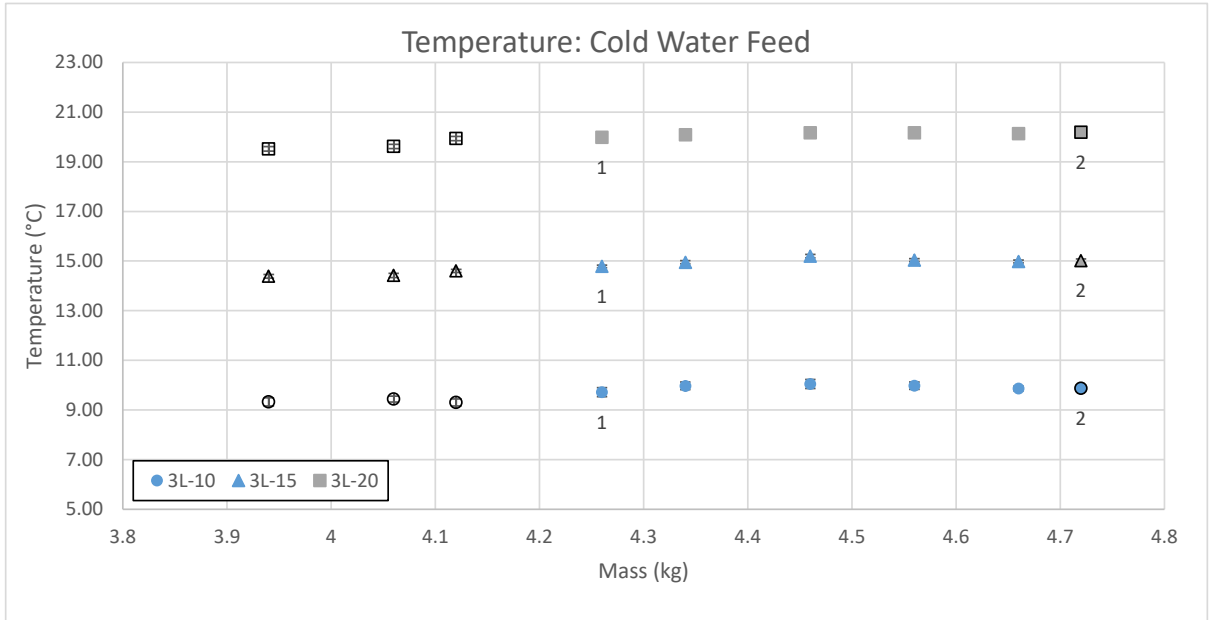
Figure 61: Cold water feed temperature for various system charges: 800rpm pump speed and three cold sink set temperatures; 10, 15 and 20°C. Reducing the cold sink set point temperature results in a reduction in cold water feed temperature.

The most significant change in temperature of the cold water return temperature (Figure 62) is as a result of the incremental change in feed temperature. There is a slight variation

with changing mass as has been noted to be a factor in previous sections, however this comparably small in relation to the 5°C feed changes. The average temperature across the entire tested charge range is 27±1°C, 22.2±1°C and 17.4±1°C.
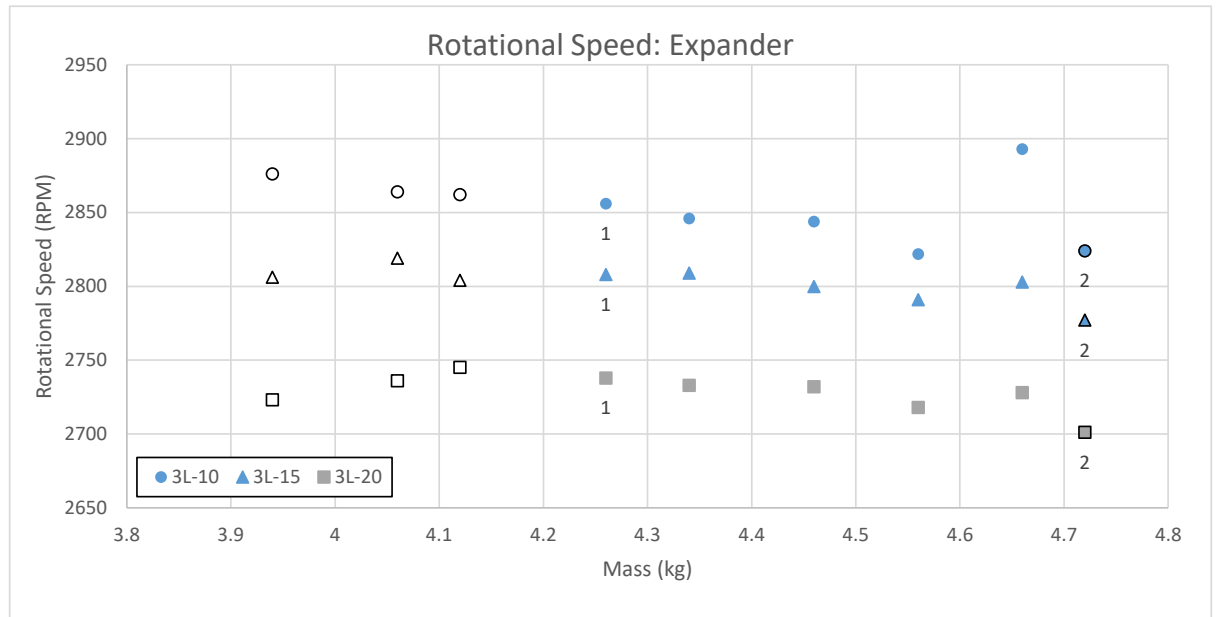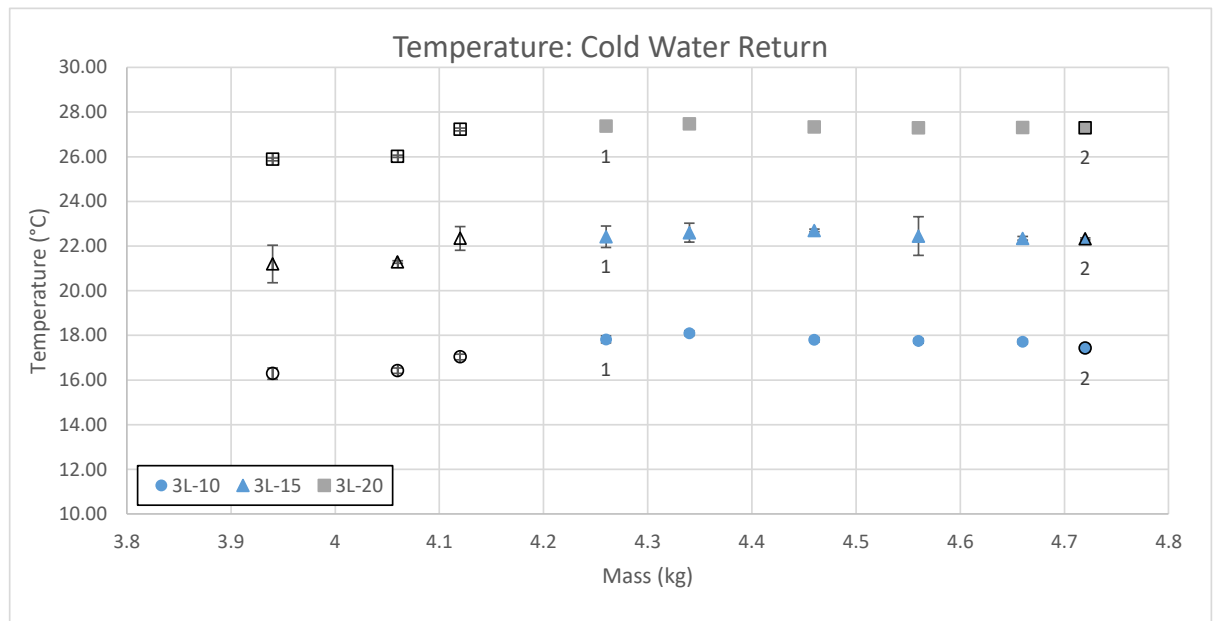

Figure 62: Cold water return temperature for various system charges: 800rpm pump speed and three cold sink set temperatures; 10, 15 and 20°C. Reducing the cold water feed temperature results in a reduction in cold water return temperature.

In a similar manner the 5°C change in feed temperature dominates any smaller fluctuations in temperature between changes in mass intervals. Since the change in cold sink temperature has negligible effect on liquid height the overall results trend for the condenser outlet (Figure 63), pump inlet (Figure 64), pump outlet (Figure 65) and evaporator inlet (Figure 66) are very similar. Therefore, in all four cases reducing the cold sink temperature results in a reduction in measured temperature in all four cases with the average temperatures across the tested mass range summarized in Table 6.

Table 6: Averaged temperatures at several ORC locations, for the three cold sink set point temperatures

Temperature location	Cold sink set point temperature		
	20°C	15°C	10°C
Condenser Outlet	19.6±0.9°C	14.9±0.9°C	10.1±0.9°C
Pump Inlet	19.7±0.8°C	14.9±0.9°C	10.1±0.9°C
Pump Outlet	20.1±1.1°C	15.5±1.1°C	10.9±1.2°C
Evaporator Inlet	20.4±1.3°C	16.1±1.4°C	11.8±1.5°C
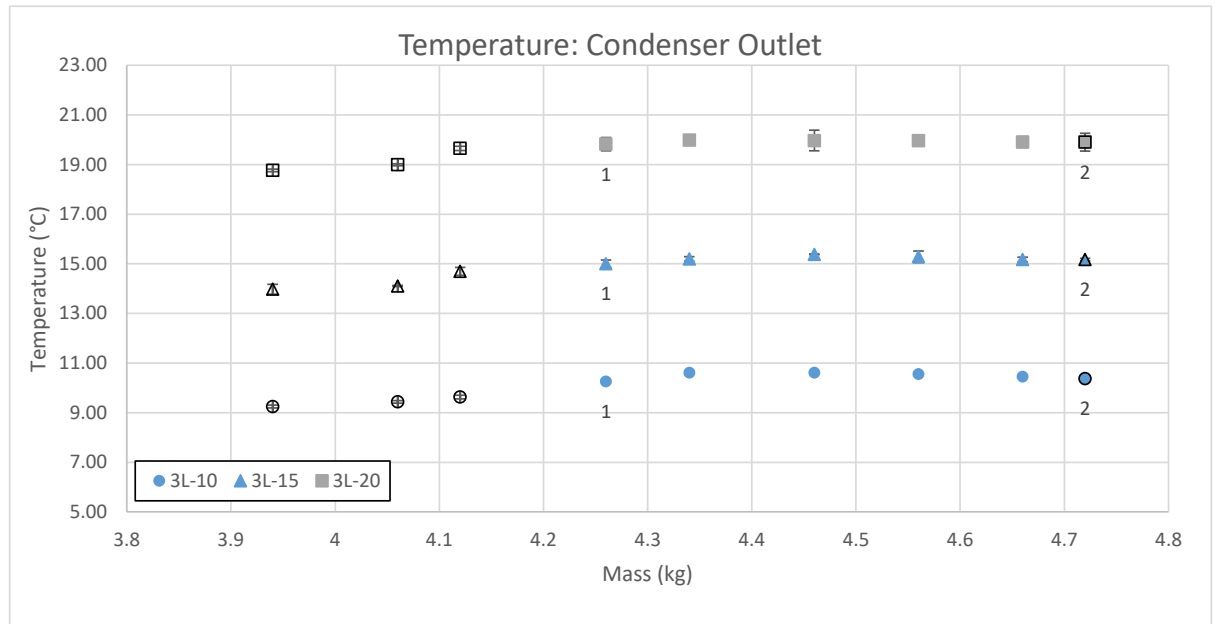
Figure 63: Condenser outlet temperature for various system charges: 800rpm pump speed and three cold sink set temperatures; 10, 15 and 20°C. Reducing the cold water feed temperature results in a reduction in condenser outlet temperature.
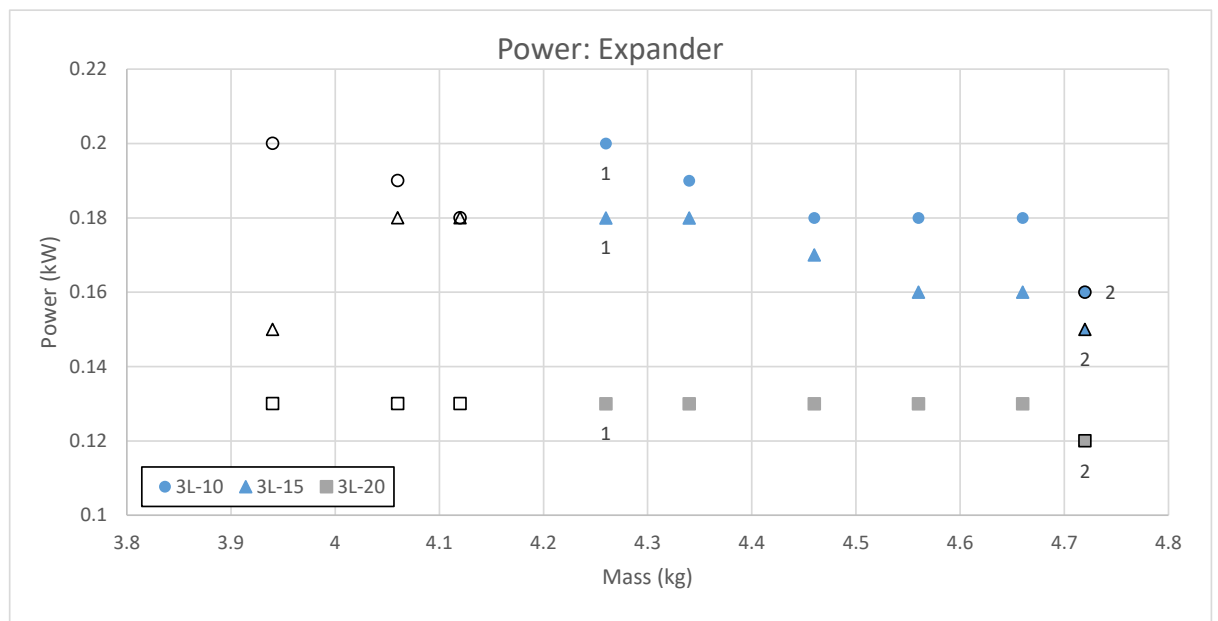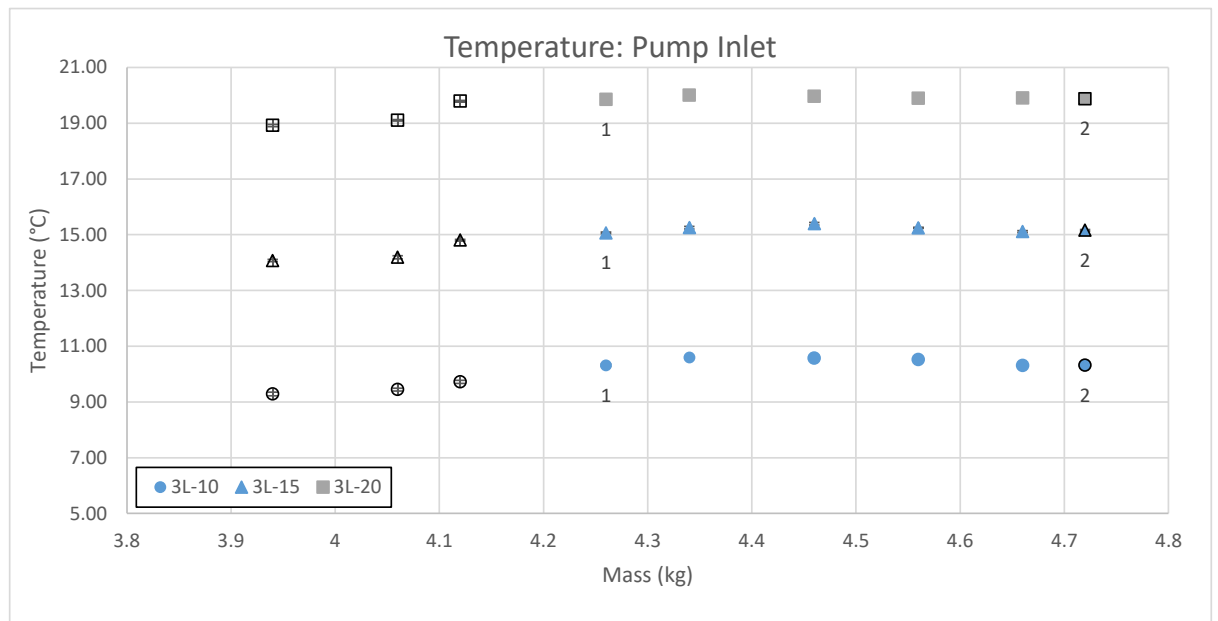

Figure 64: Pump inlet temperature for various system charges: 800rpm pump speed and three cold sink set temperatures; 10, 15 and 20°C. Reducing the cold water feed temperature results in a reduction in pump inlet temperature.
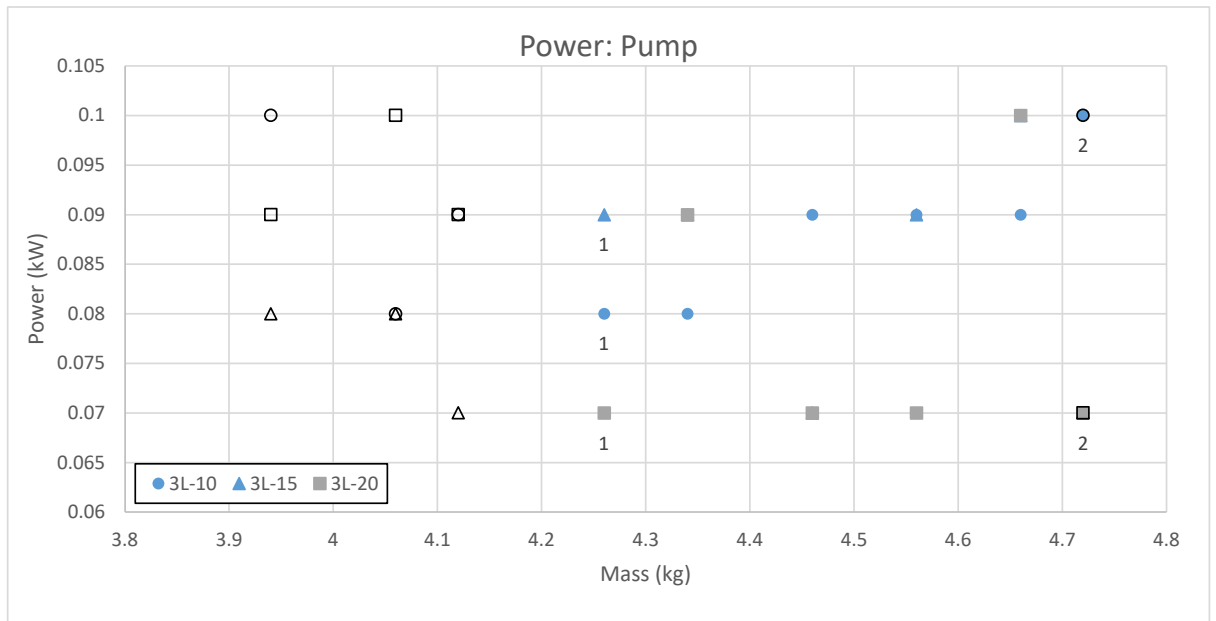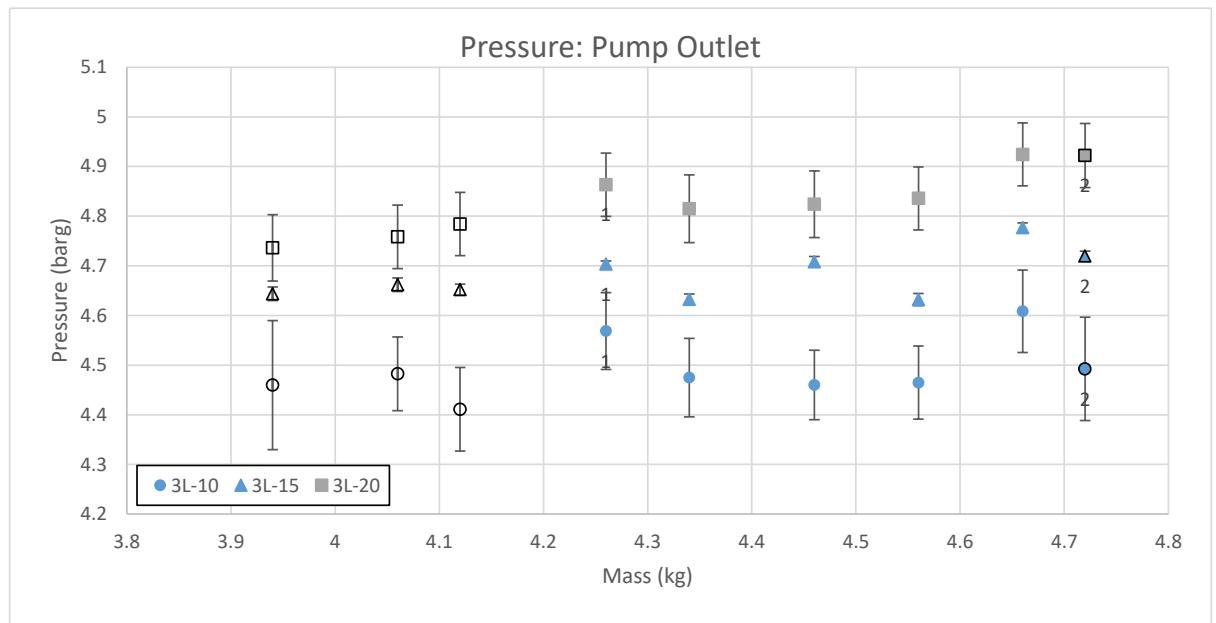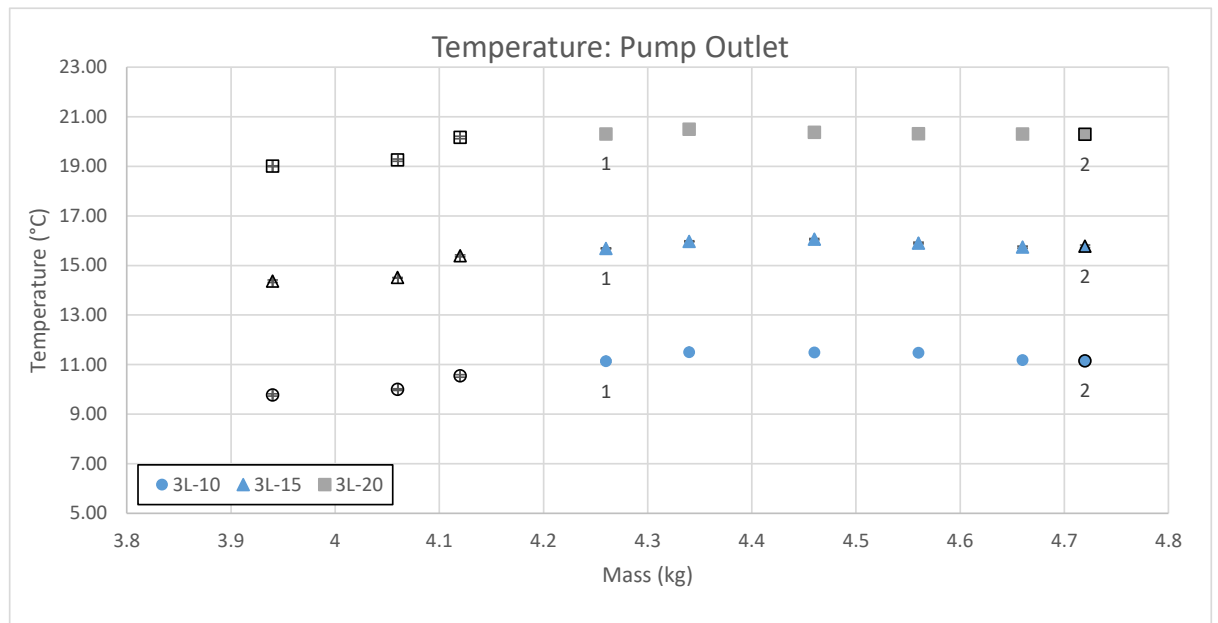
Figure 65: Pump outlet temperature for various system charges: 800rpm pump speed and three cold sink set temperatures; 10, 15 and 20°C. Reducing the cold sink temperature results in a reduction in pump outlet temperature.
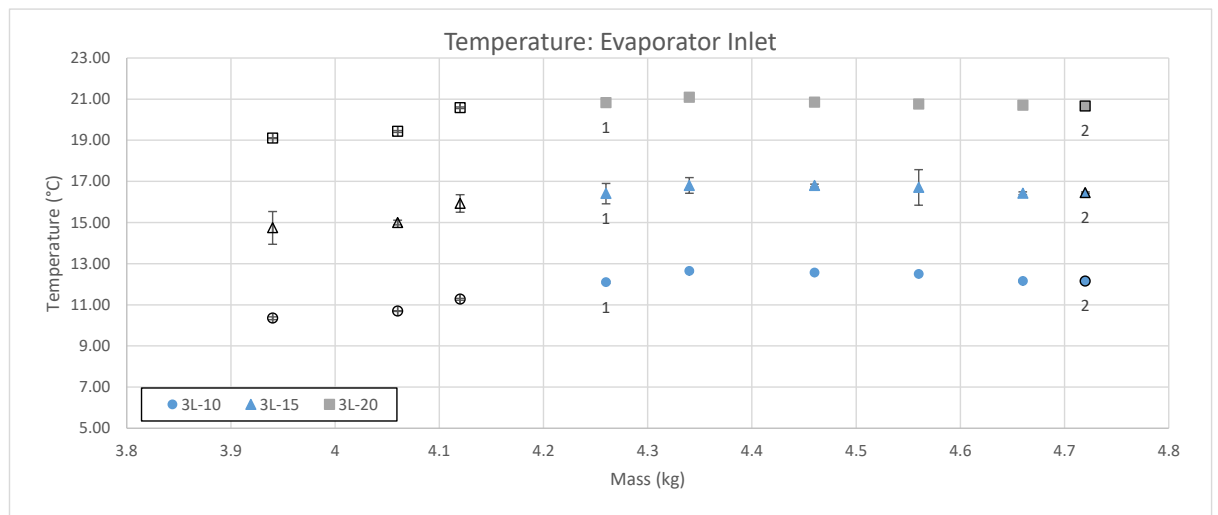
Figure 66: Evaporator inlet temperature for various system charges: 800rpm pump speed and three cold sink set temperatures; 10, 15 and 20°C. Reducing the cold sink temperature results in a reduction in the evaporator inlet temperature.

Although the hot water feed temperature is externally controlled, there is a three degree range in temperature across all the data points as shown in Figure 67. The average temperatures for the three cold sink temperature cases are 86.5±1.3°C (20°C), 86.7±1.3°C (15°C) and 86.5±1.4°C (10°C). The same three degree range is present at the hot water return and the expander inlet shown in Figure 68 and Figure 69. The average hot water return temperatures for the three cases is 85.4±1.3°C (20°C), 85.6±1.3°C (15°C) and 85.3±1.3°C. The average expander inlet temperature for the three cases is 20.4±1.3°C (20°C), 87.7±1.2°C (15°C) and 84.3±1.6°C (10°C).
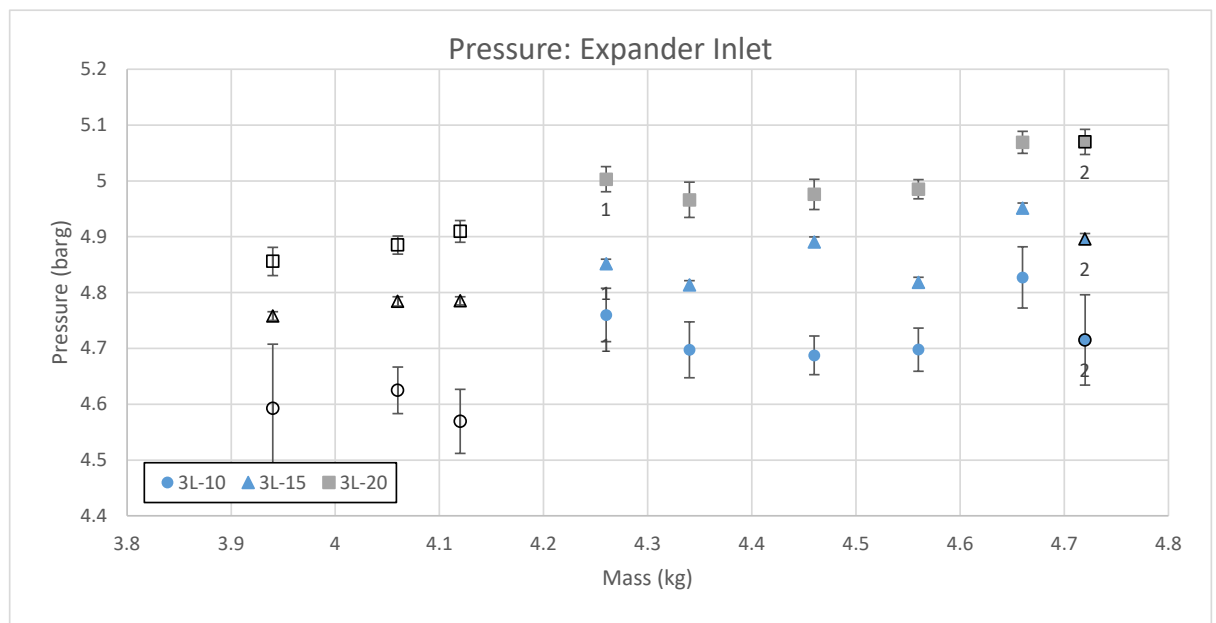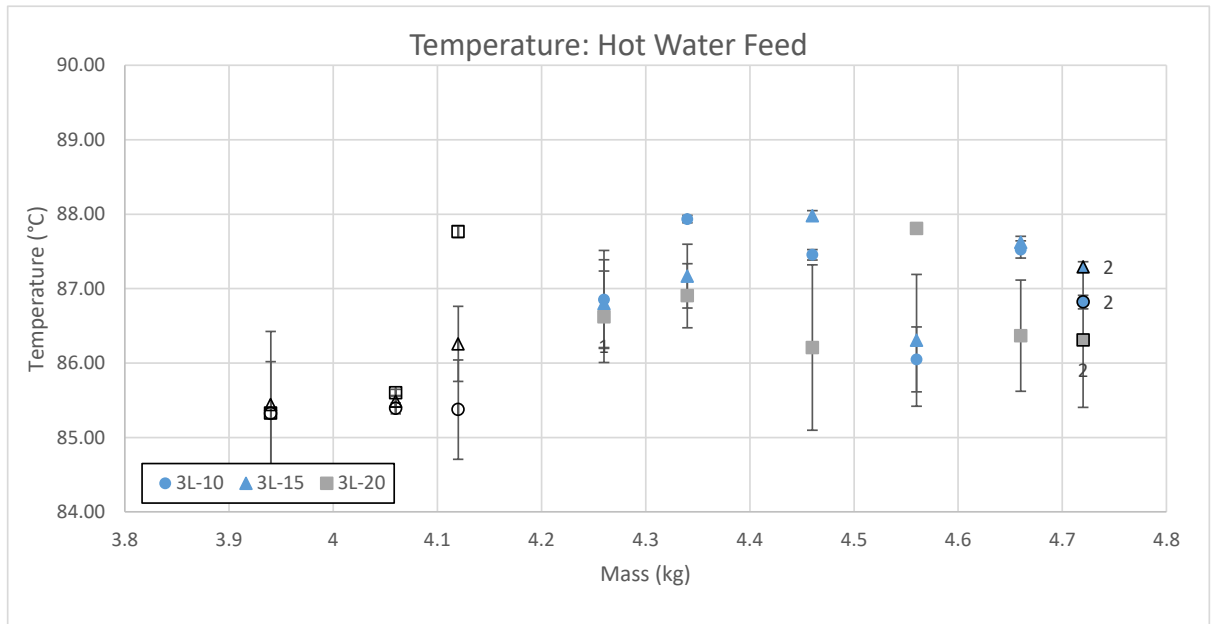
Figure 67: Hot water feed temperature for various system charges: 800rpm pump speed and three cold sink set temperatures; 10, 15 and 20°C. The recorded data points for all three cases lie within 85 and 88°C.
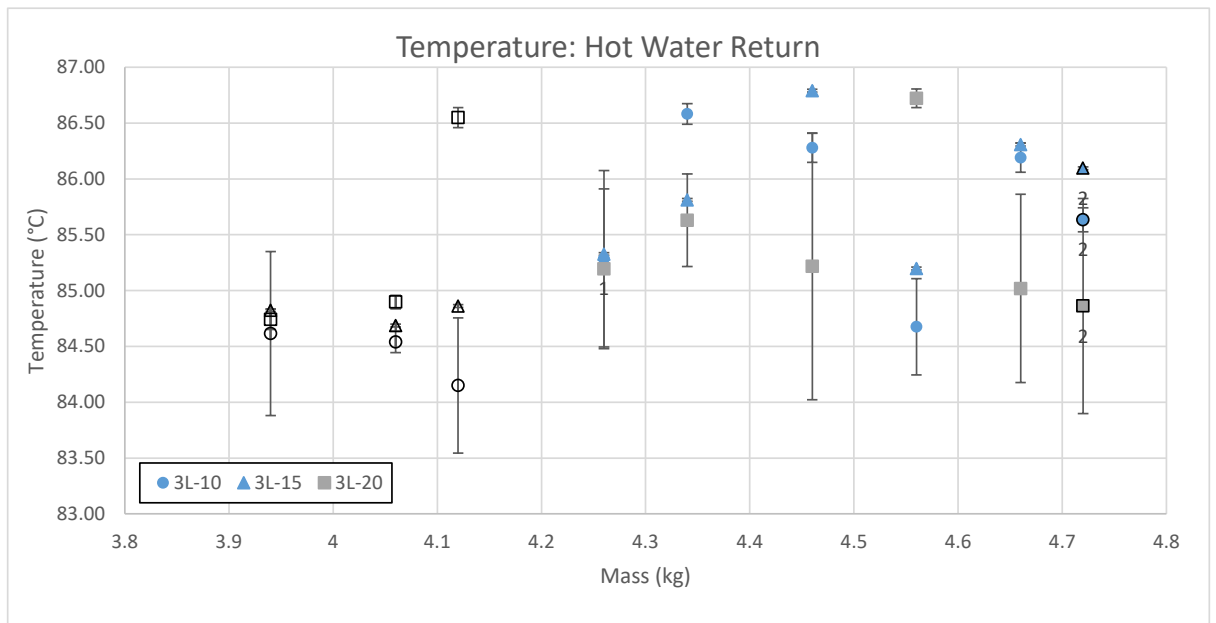
Figure 68: Hot water return temperature for various system charges: 800rpm pump speed and three cold sink set temperatures; 10, 15 and 20°C. The data points for all three cases lie within 84 and 87°C.
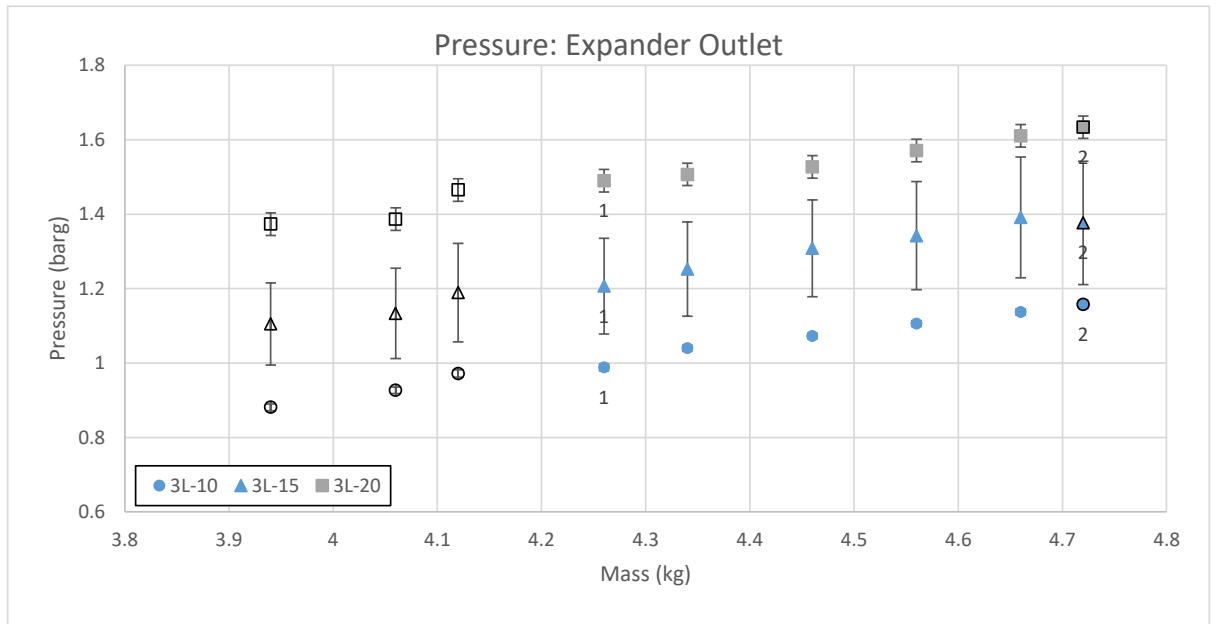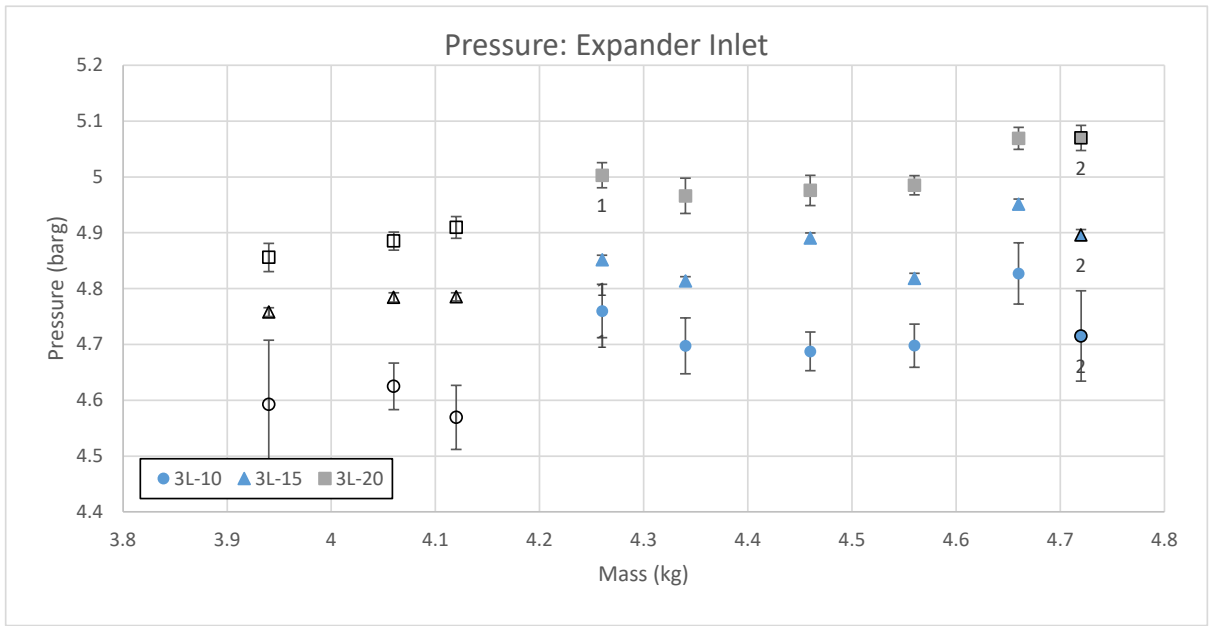
Figure 69: Expander inlet temperature for various system charges: 800rpm pump speed and three cold sink set temperatures; 10, 15 and 20°C. The data points for all three cases lie within 82.5 and 86°C.

Of all the high temperature data recorded the only location that shows any indicative change with respect to the reduction in cold side temperature is the expander outlet shown in Figure 70. Overall, the generally observed increasing temperature with increasing mass is evident in all three cases. Albeit less consistent compared with previously presented data as a results of the larger variation in feed temperature. There is also however a reduction in expander outlet temperature as a result of decreasing cold sink temperature with the degree of change showing some variation between each mass set.
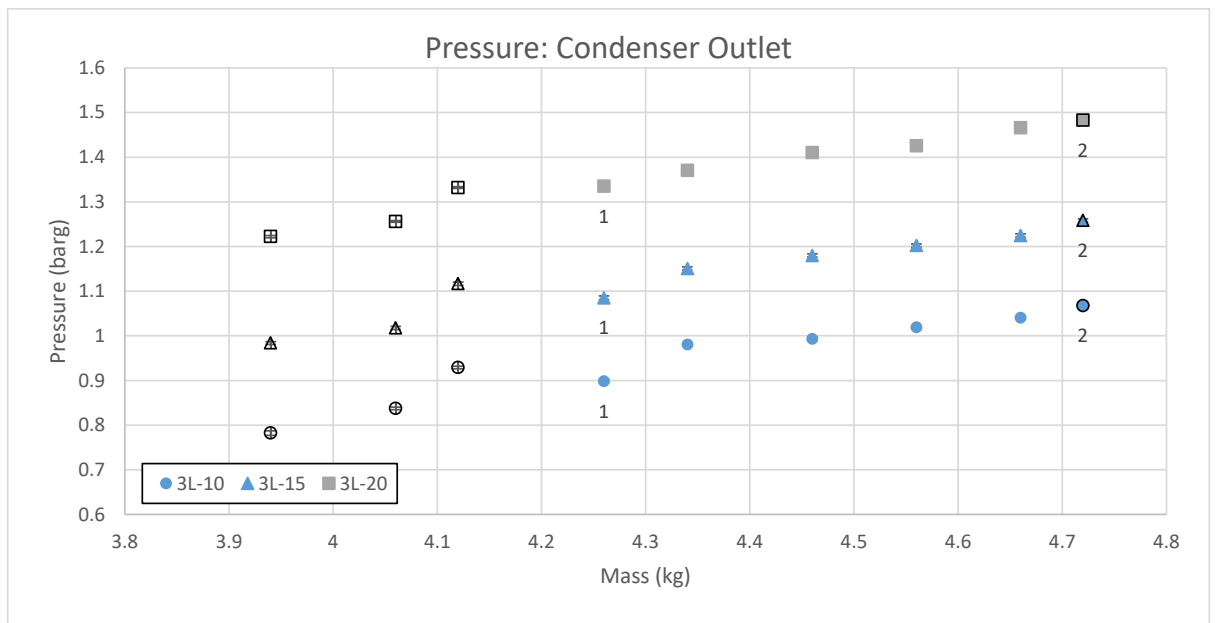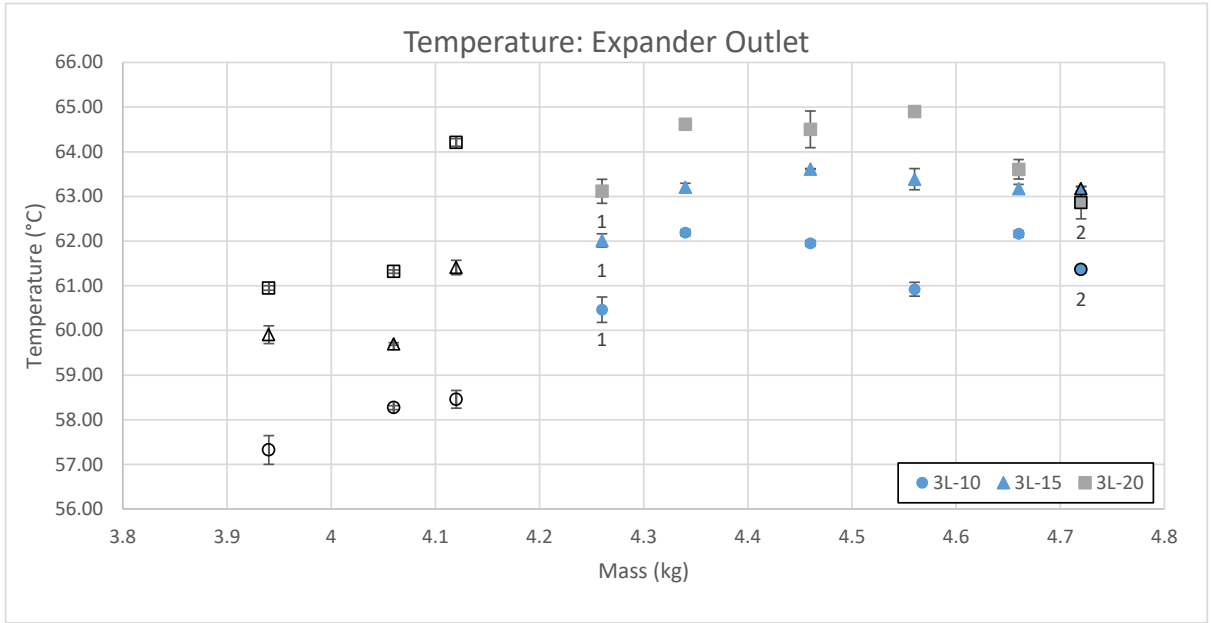

Figure 70: Expander outlet temperature for various system charges: 800rpm pump speed and three cold sink set temperatures; 10, 15 and 20°C. In general the expander outlet temperature increases with increasing mass and decreases with reducing cold sink temperature.

4.4.2. Discussion

The reduction in cold feed temperature results in no significant change in liquid column height but does result in a reduction in both the low and high side system pressure. The reduction in temperature however, results in a more significant change to the low pressure side than the high leading to an increase in pressure ratio across the expander as the condenser temperature reduces. For the 800rpm case the reduction in pressure at the pump inlet as the temperature decreases, doesn't appear to have a significant influence on pump cavitation. The calculated net positive suction head for this case is shown in Figure 71, although there is no change in the column height with varying condenser temperature there is slight variation in NPSH. Over the tested range the NPSH was well above the calculated threshold for cavitation.
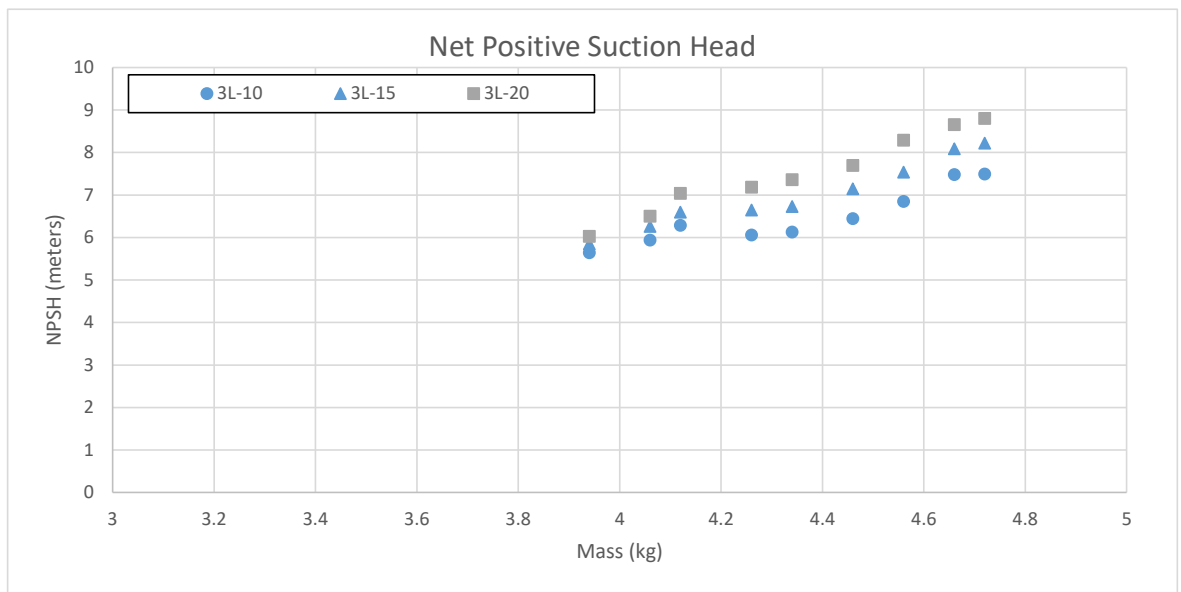
Figure 71: Net Positive Suction head for 800rpm pump speed and three cold sink set temperatures; 10, 15 and 20°C. Slight increase in measured NPSH with increasing condenser temperature.

4.5. **System Charge/liquid height effect at three expander loads at fixed pump speed on ORC operational conditions**

In the previous sections the effects of mass on a single set of operational conditions with varying pump speeds was considered. In order to assess if the effects of other system parameters affected the stored liquid column height. Three cold side temperatures and three expander loads for a single pump speed were conducted in a single mass fill run, which produced six individual data sets. There is significant amount of repetition in the data, therefore only the 15°C cold sink temperature results are presented in this section. Additionally, for these tests the overall tested mass range was reduced to cover the peak system performance up to a liquid column height of 1.6m.

4.5.1. Experimental results

Overall Performance: The overall performance of the system decreases with increased expander load, the increase in load takes the electrical generator further way from its design speed of 3600 rpm. Increasing load results in an increase in high side pressure and has negligible effect on the low pressure side of the system. Increasing expander load has no significant effect on the system temperatures. The increase in expander load also has no effect on the liquid column height of the system.

The overall performance of the ORC system with increasing system charge at three different electrical loads of 3, 4 and 5 resistive lights is shown in Figure 72, Figure 73 and Figure 75, the expander rotational speed, electrical power output and the pump power consumed. Increasing the resistive load on the expander reduces the expander rotational speed. The average rotational speed for the three cases is 2801 (3L), 2659 (4L) and 2547 rpm (5L).
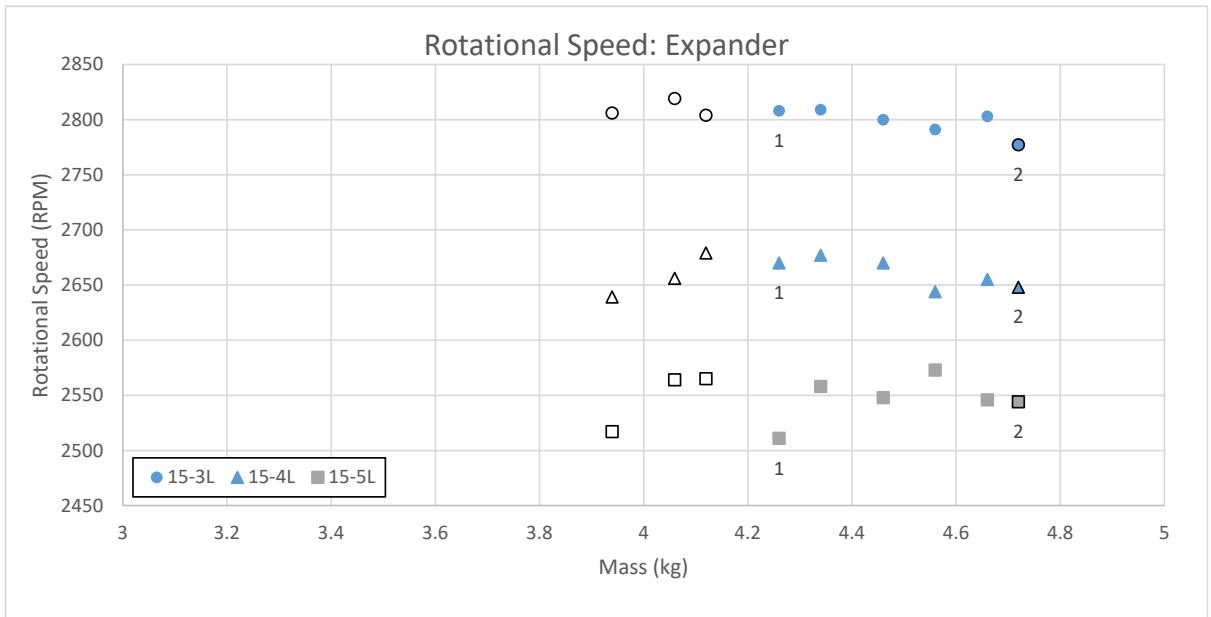
Figure 72: Expander rotational speed for various system charges: 800rpm pump speed at varying electrical loads of 3, 4 and 5 lights. Increasing the resistive load on the expander reduces the expander rotational speed. There was negligible change in the liquid column height with the level remaining within the visible limits of the sight glass.

The decrease in expander rotational speed results in a corresponding reduction in real electrical power output with average power outputs of 0.17 (3L), 0.15 (4L) and 0.13 kW(5L). However, it is worth considering that the reduction in rotational speed takes the electrical generator away from its design speed of 3600rpm. The reactive electrical power has been included in this example and is shown in Figure 74.
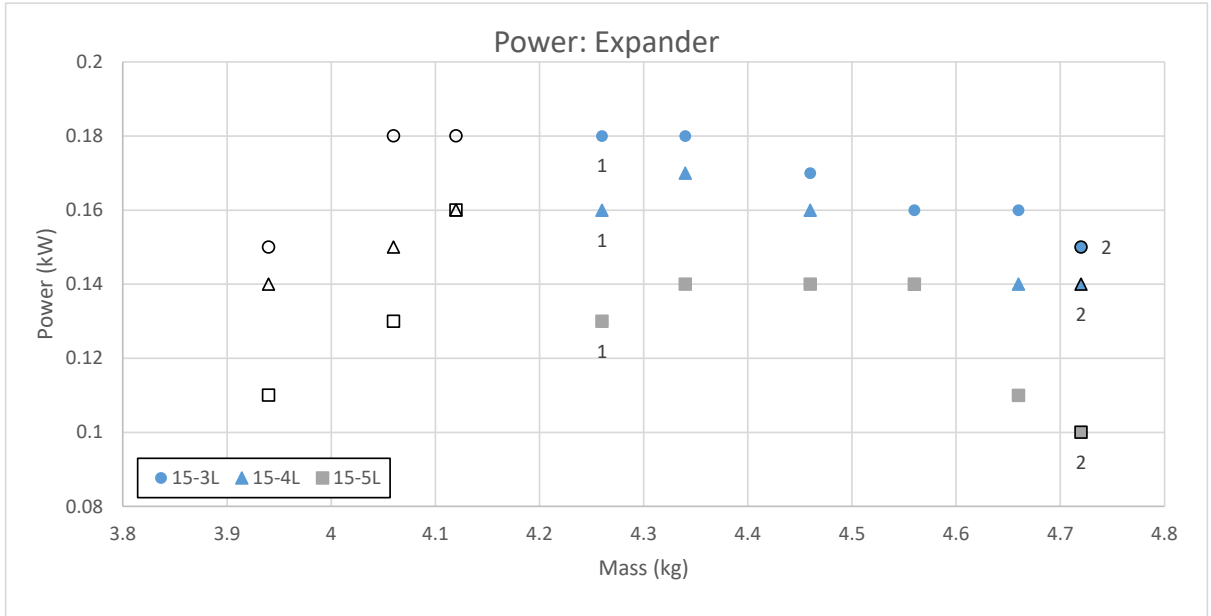
Figure 73: Real electrical expander output power for various system charges: 800rpm pump speed at varying electrical loads of 3, 4 and 5 lights. Increasing electrical resistance on the expander reduces the real electrical power output.
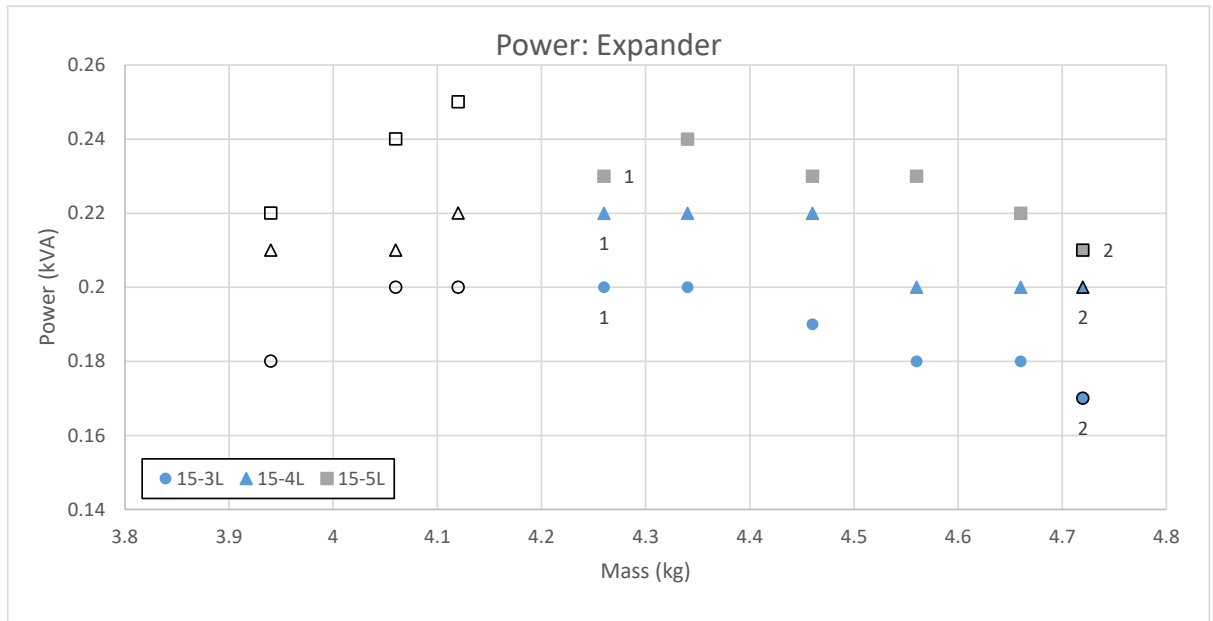
Figure 74: Reactive electrical expander output power for various system charges: 800rpm pump speed at varying electrical loads of 3, 4 and 5 lights. Increasing the expander rotational speed increases the reactive electrical power output.

The trend of the reactive power is the opposite of the real power trend, with increasing electrical resistance resulting in an increase in reactive power. The average reactive power for the three cases is 0.19 (3L), 0.21 (4L) and 0.23 kVA (5L). The power consumed by the pump for the three resistive loads is shown in Figure 75. The average consumed pump power for the three cases is 0.08 (3L), 0.08 (4L) and 0.08 kW (5L).
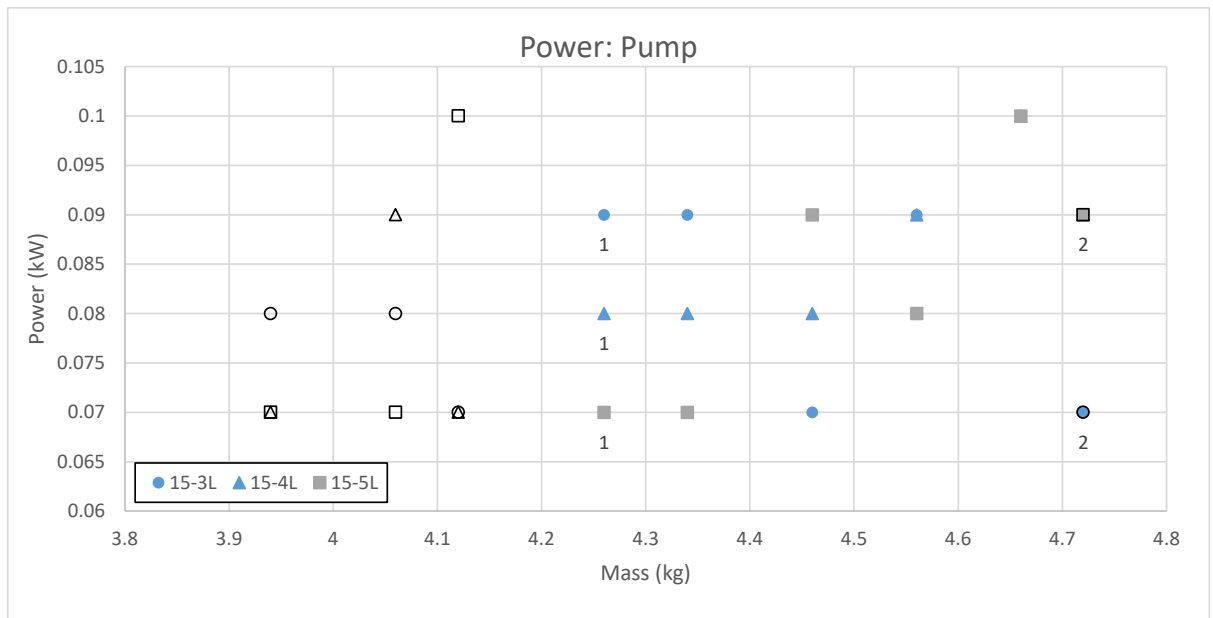
Figure 75: Pump power consumed for various system charges: 800rpm pump speed at varying electrical loads of 3, 4 and 5 lights. The electrical power consumed by the pump fluctuates between 0.07 and 0.1 for all electrical resistive loads.

Pressure:

Increasing the electrical resistance increases the high side pressure of the system as shown at the expander inlet and pump outlet, Figure 76 and Figure 77. The average pressure across the tested mass range is 4.68 (3L), 4.78 (4L) and 4.88 barg (5L) for the pump outlet and 4.84 (3L), 4.94 (4L) and 5.04 barg (5L) for the expander inlet.

Figure 76: Pump outlet pressure for various system charges: 800rpm pump speed at varying electrical loads of 3, 4 and 5 lights. Increasing the rotational resistance of the expander increases the pump outlet pressure.

Figure 77: Expander inlet pressure for various system charges: 800rpm pump speed at varying electrical loads of 3, 4 and 5 lights. Increasing the rotational resistance of the expander increasing the expander inlet pressure.

Although increasing the rotational speed of the expander increases the high side pressure of the system. It has negligible impact on the system low side pressure as shown at the expander outlet, condenser outlet and pump inlet: Figure 78, Figure 79 and Figure 80

respectively. In all three cases the low side pressure increase in a linear manner with increasing mass, but shows comparable insignificant change with changing load.
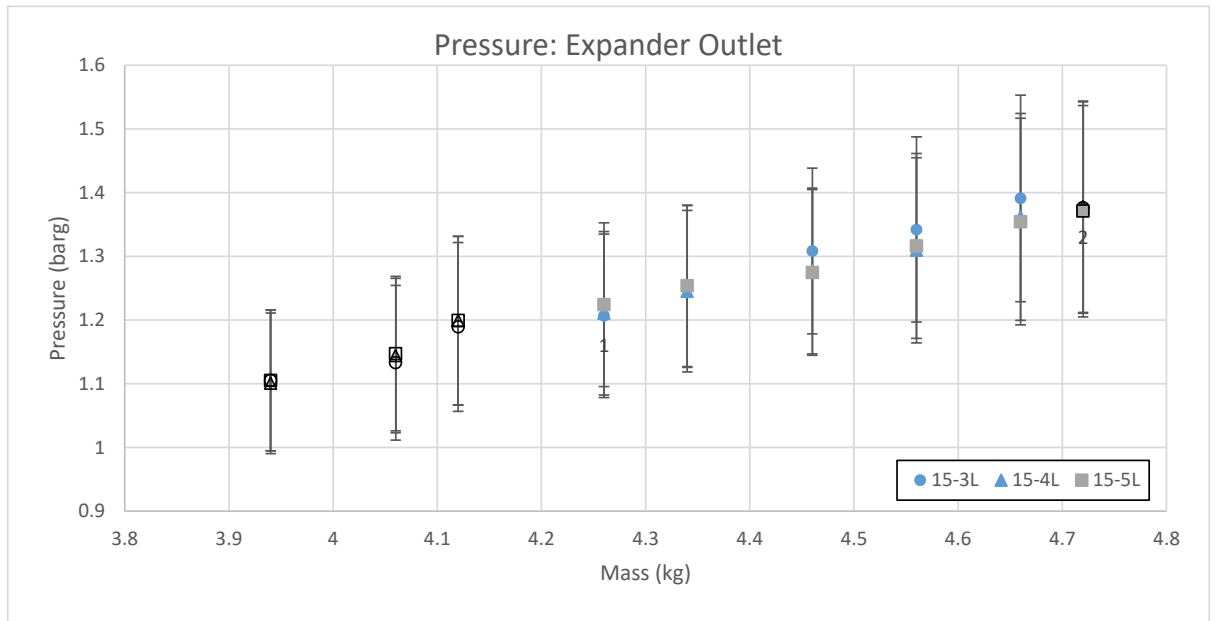
Figure 78: Expander outlet pressure for various system charges: 800rpm pump speed at varying electrical loads of 3, 4 and 5 lights. The expander outlet pressure increases with increasing mass but shows no significant change with respect to changes in rotational resistance.
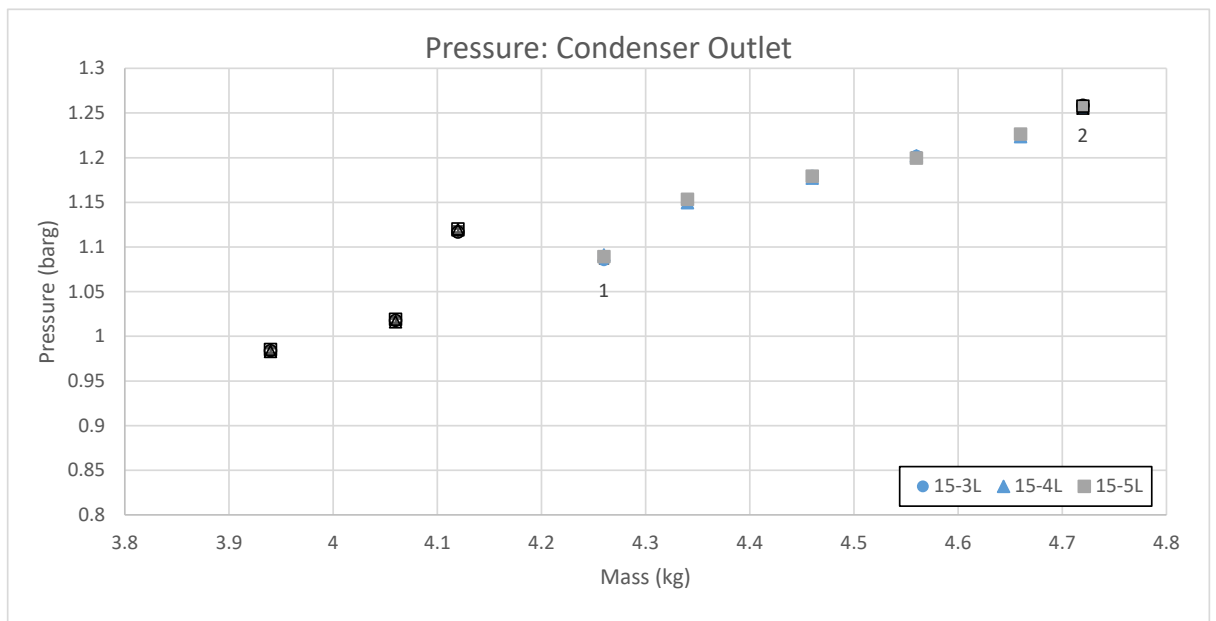
Figure 79: Condenser outlet pressure for various system charges: 800rpm pump speed at varying electrical loads of 3, 4 and 5 lights. The condenser outlet pressure increases with increasing mass but shows no significant change with increasing expander rotational resistance.
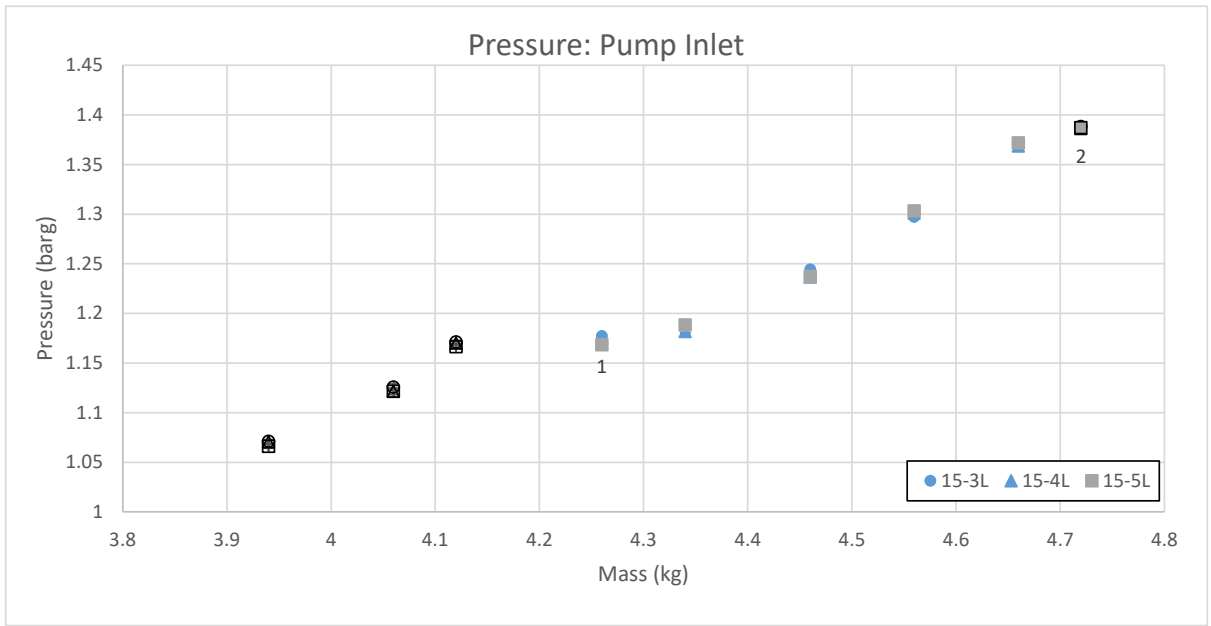
Figure 80: Pump inlet pressure for various system charges: 800rpm pump speed at varying electrical loads of 3, 4 and 5 lights. The pump inlet pressure increases with increasing mass but shows no significant change with increasing expander rotational speed.

Temperature:

Similar with no significant change in low side pressure the cold side of the system at the: cold water feed (Figure 81), cold water return (Figure 82), condenser outlet (Figure 83), pump inlet (Figure 84), pump outlet (Figure 85) and evaporator inlet (Figure 86) show no significant changes in temperature with changing rotational resistance. All six locations follow the same variation trend in temperature as the cold water feed.
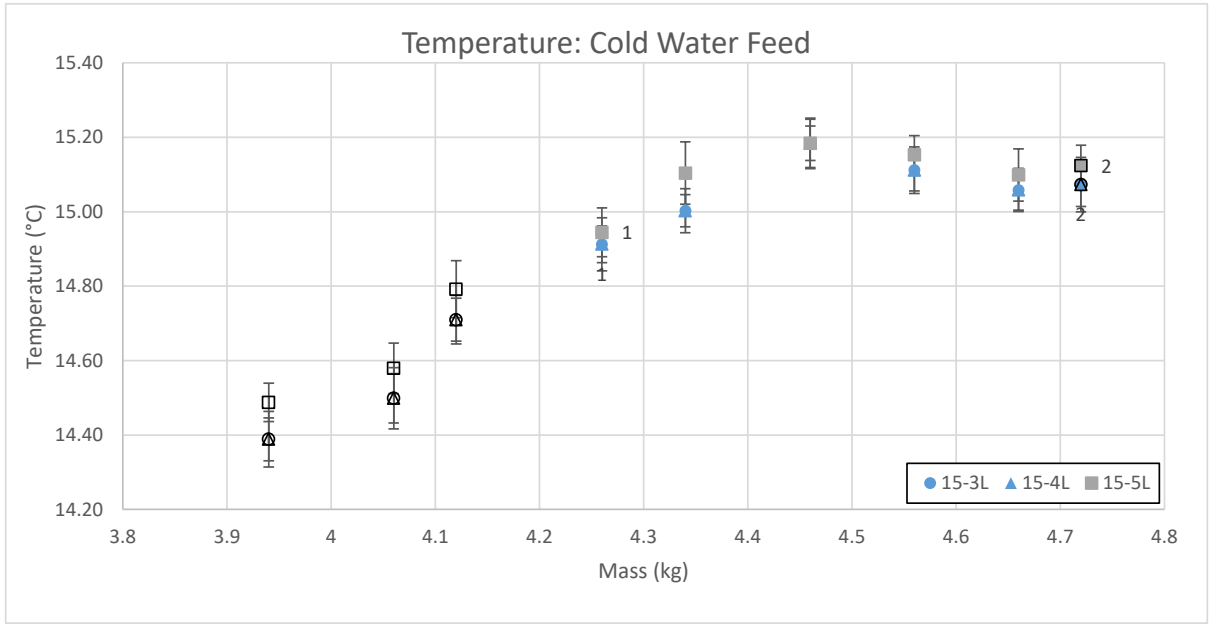
Figure 81: Cold water feed temperature for various system charges: 800rpm pump speed at varying electrical loads of 3, 4 and 5 lights. The cold water feed temperature is controlled externally and has a slight variation in temperature from slightly lower initial temperatures of 14.4 to 15.1°C.
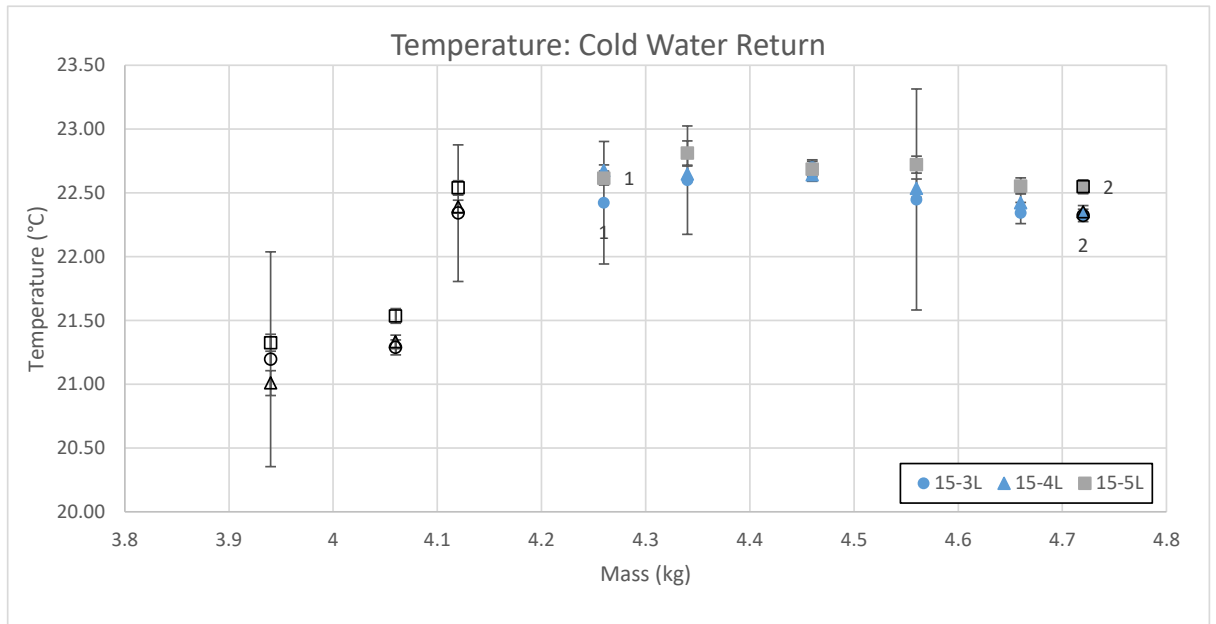
Figure 82: Cold water return temperature for various system charges: 800rpm pump speed at varying electrical loads of 3, 4 and 5 lights. The cold water return temperature shows no significant changes in temperature as a result of changes in expander resistive load. Some variation exists as a result of feed temperature fluctuation.
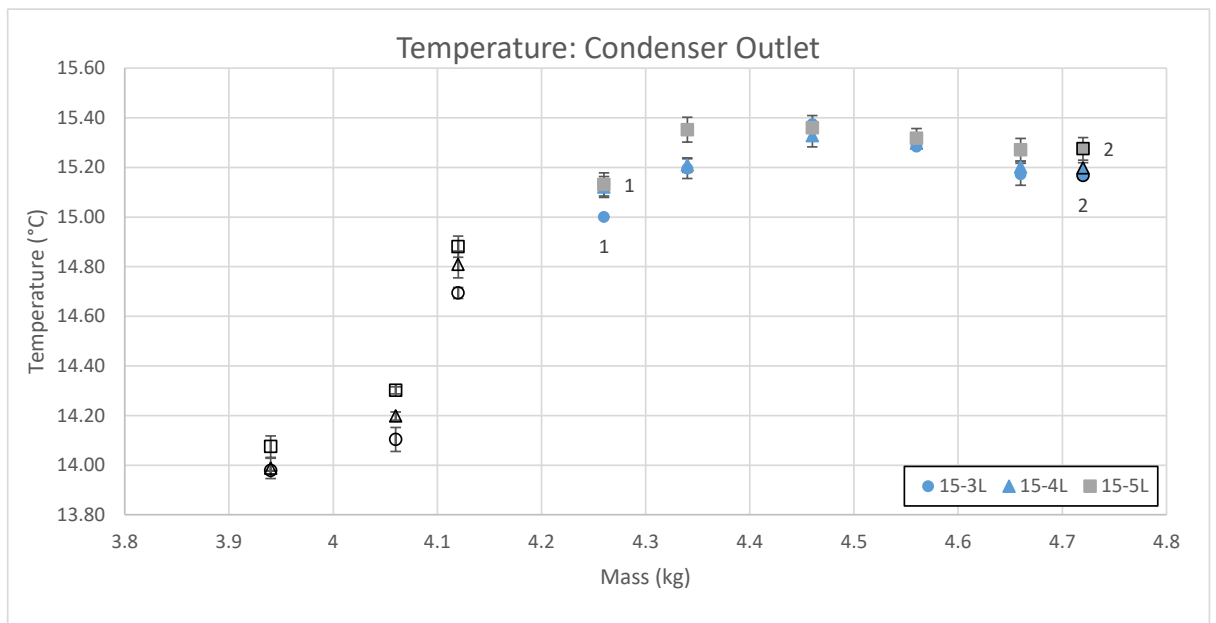
Figure 83: Condenser outlet temperature for various system charges: 800rpm pump speed at varying electrical loads of 3, 4 and 5 lights. The condenser outlet temperature shows no significant changes in temperature as a result of changes in expander resistive load. Some variation exists as a result of feed temperature fluctuation.
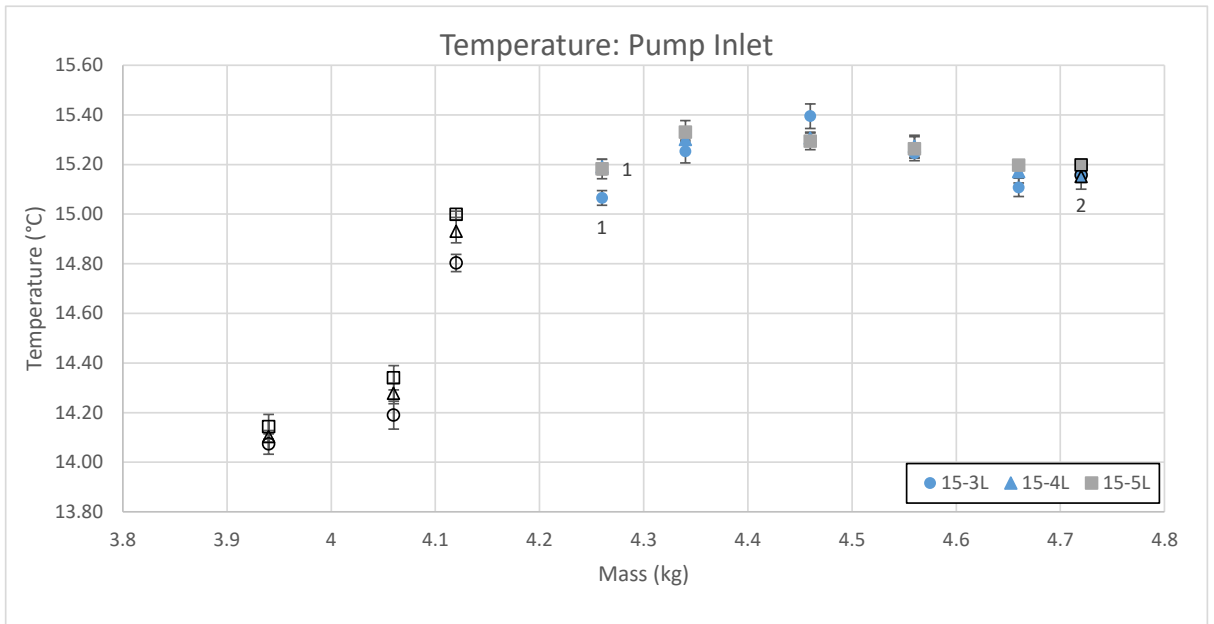
Figure 84: Pump inlet temperature for various system charges: 800rpm pump speed at varying electrical loads of 3, 4 and 5 lights. The pump inlet temperature shows no significant changes in temperature as a result of changes in expander resistive load. Some variation exists as a result of feed temperature fluctuation.
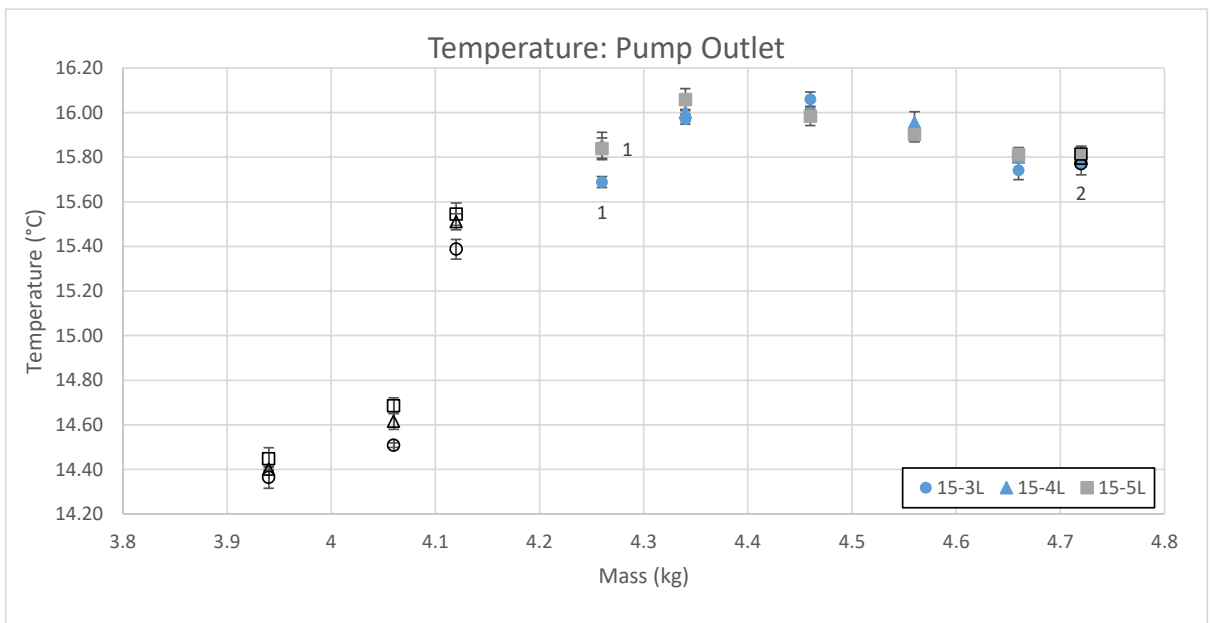
Figure 85: Pump outlet temperature for various system charges: 800rpm pump speed at varying electrical loads of 3, 4 and 5 lights. The pump outlet temperature shows no significant changes in temperature as a result of changes in expander resistive load. Some variation exists as a result of feed temperature fluctuation.
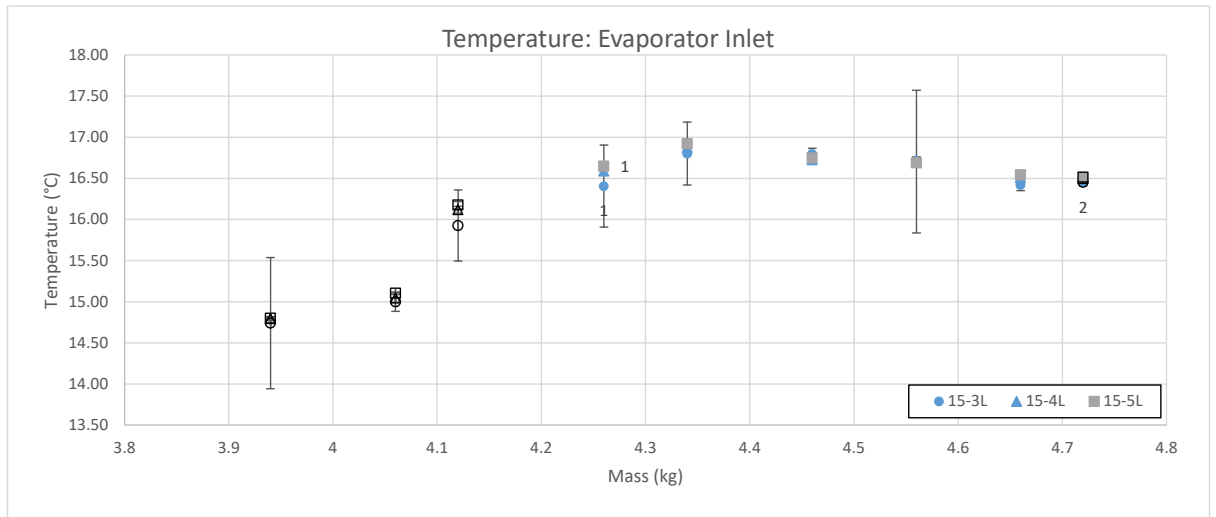
Figure 86: Evaporator inlet temperature for various system charges: 800rpm pump speed at varying electrical loads of 3, 4 and 5 lights. The evaporator inlet temperature shows no significant changes in temperature as a result of changes in expander resistive load. Some variation exists as a result of feed temperature fluctuation.

The externally controlled hot water feed temperature is subjected to a three degrees variation in temperature across the testing range as shown in Figure 87 as a results there is no observable changes in temperature at the hot water return, expander inlet and expander outlet (Figure 88, Figure 89 and Figure 89) as a result of changes in increasing expander rotational resistance.
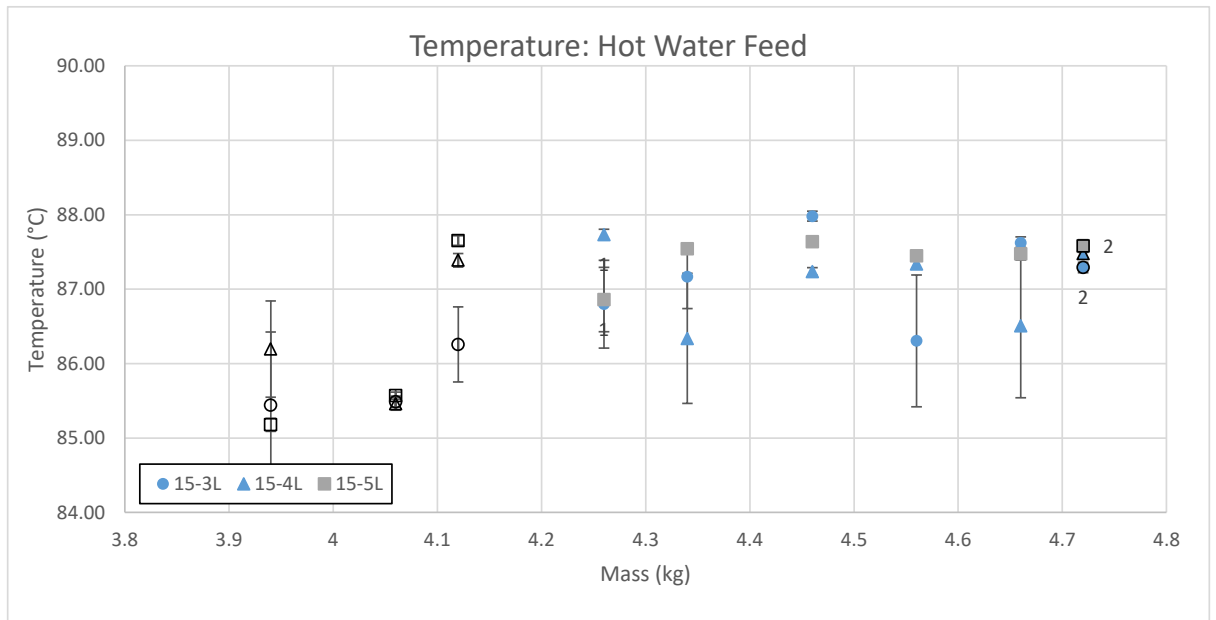
Figure 87: Hot water feed for various system charges: 800rpm pump speed at varying electrical loads of 3, 4 and 5 lights. The hot water feed temperature is subject to a 3°C variation in temperature across the test range, with recorded temperatures between 85 and 88°C.
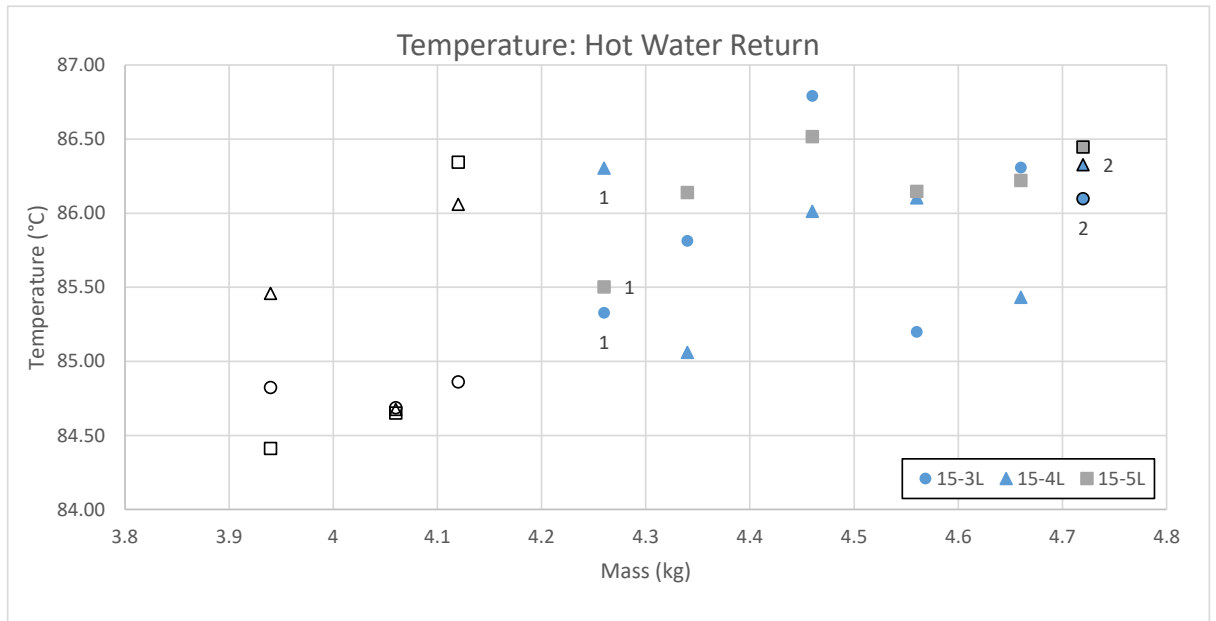
Figure 88: Hot water return for various system charges: 800rpm pump speed at varying electrical loads of 3, 4 and 5 lights. There is no observably significant change in hot water return temperature as a result of changes in expander rotational resistance.
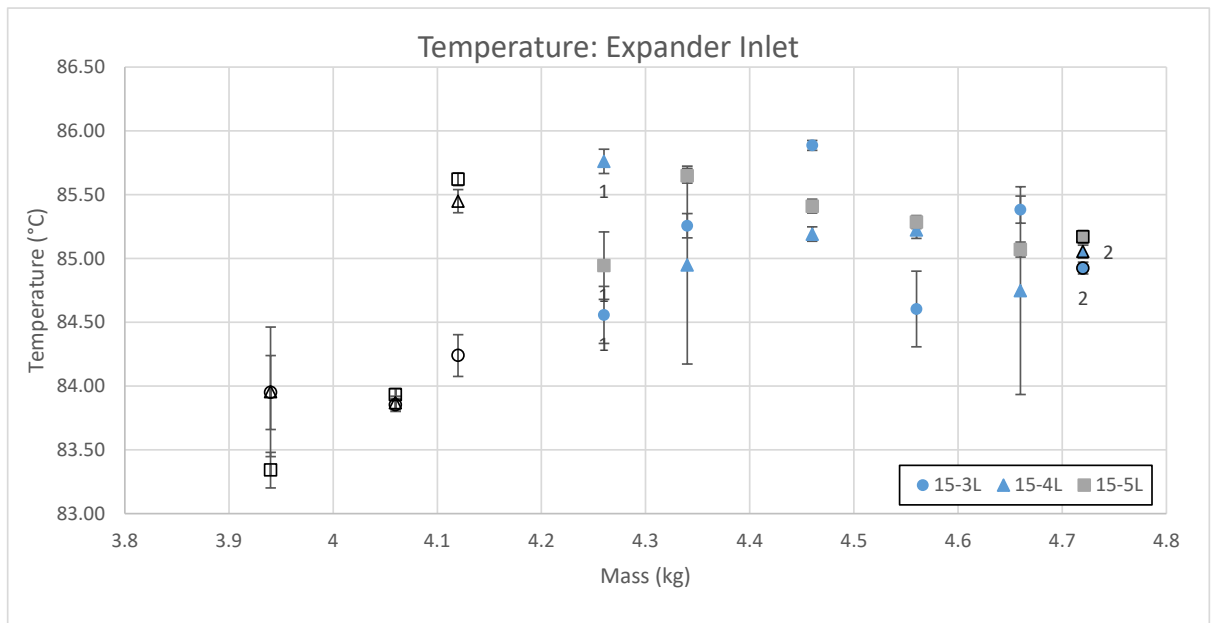
Figure 89: Expander inlet temperature for various system charges: 800rpm pump speed at varying electrical loads of 3, 4 and 5 lights. There is no observably significant change in expander inlet temperature as a result of changes in expander rotational resistance.
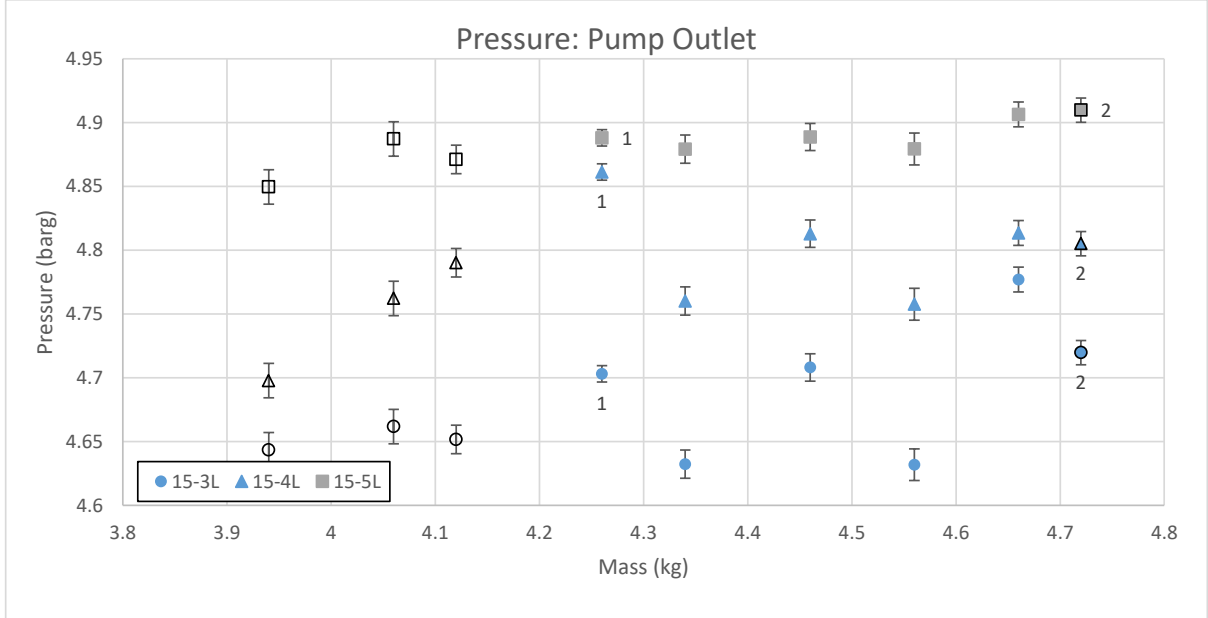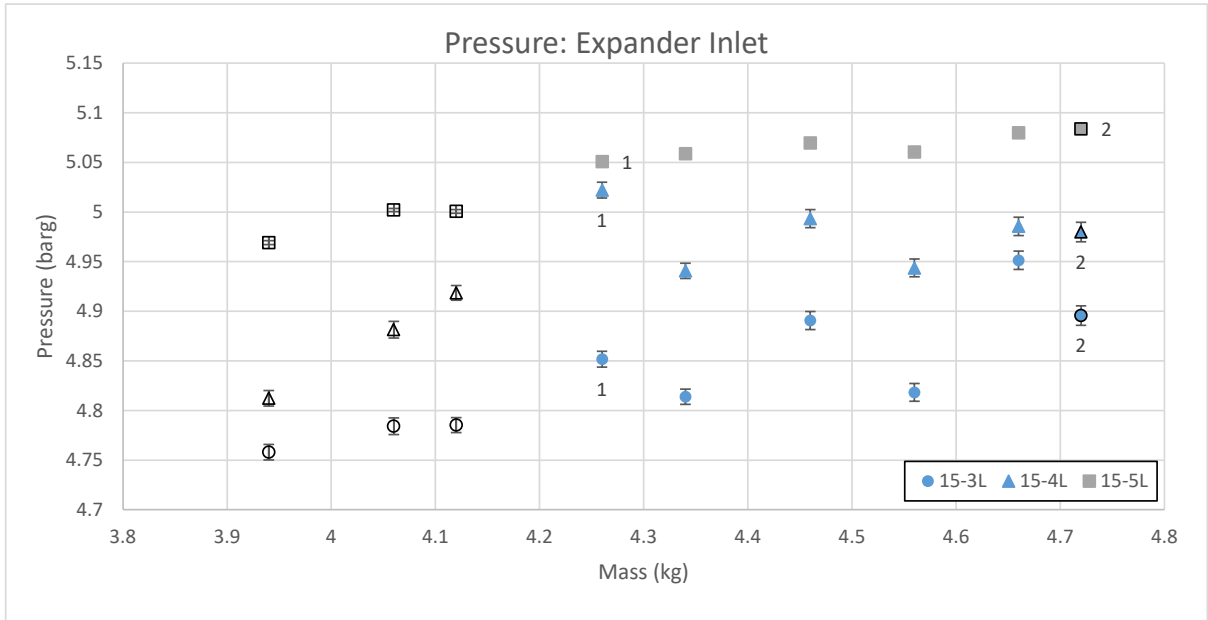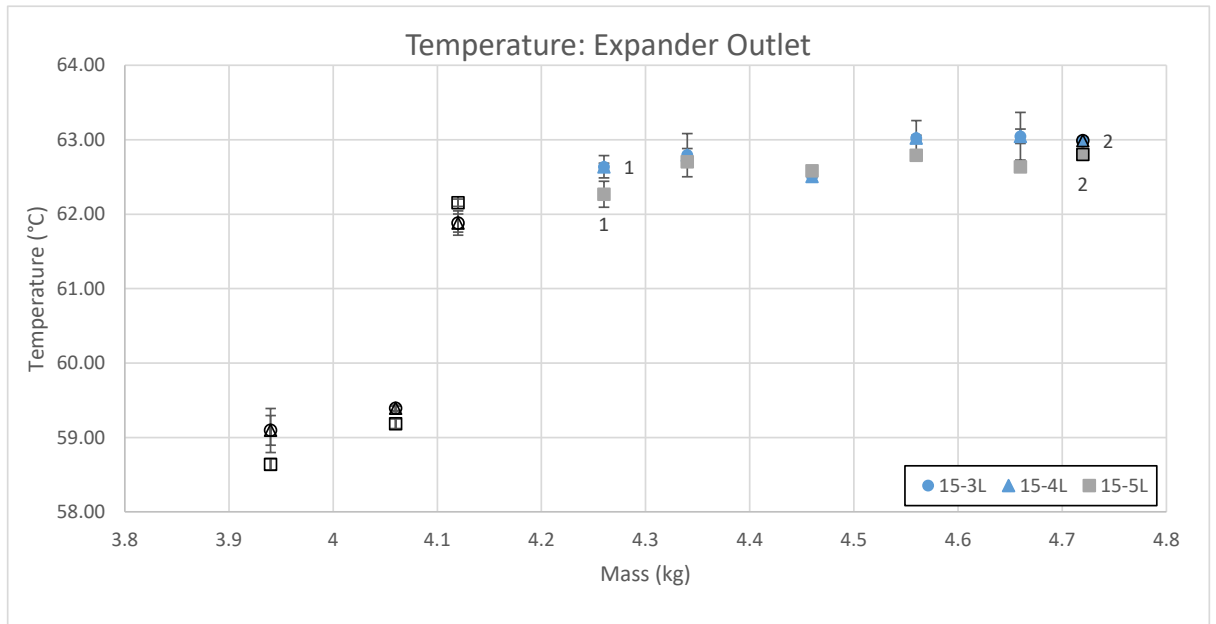
Figure 90: Expander outlet temperature for various system charges: 800rpm pump speed at varying electrical loads of 3, 4 and 5 lights. There is no observably significant change in expander outlet temperature as a result of changes in expander rotational resistance.

4.5.2. Discussion

Since the load on the expander has negligible effect on the liquid column height and the pump inlet pressure, it has no significant effect on the cavitation performance of the pump. The increase in mass in this case has a more dominant effect on the overall system performance. The calculated NPSH for this case is shown in Figure 91, and shows no significant effect on the low pressure side of the system as a result of changing load.
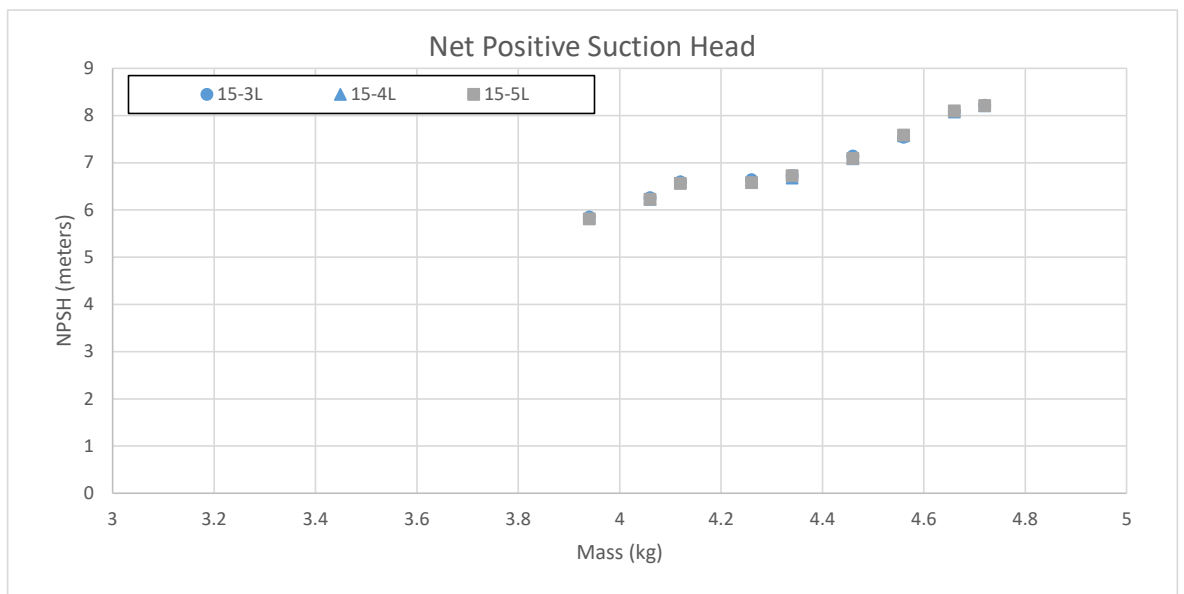
Figure 91: Net Positive suction head at 800rpm pump speed at varying electrical loads of 3, 4 and 5 lights. The expander load has no significant effect on cavitation performance of the ORC system.

4.6. **Summary**

For a single set of ORC conditions, increasing the mass results in an increase in overall system performance to a peak value. Further increase in charge results in a decrease in performance. This same trend was repeated at different pump speeds with the exception of the 1200rpm case where the system performance showed significant instability. Calculation of the net positive suction head indicated that there should be no pump cavitation occurring which directly contradicts the experimental findings.

For the 800 rpm case both a reduction in cold side temperature and increase in expander load had no effect on liquid column height. Although a small change in NPSH occurred with increasing condenser temperature. Decreasing the cold sink temperature resulted in a decrease in both the high and low side pressure. The overall performance of the system increased as a result of the increase in pressure ratio across the expander. The reduction in pressure at the pump outlet as a result appeared to have adverse effects on the system. The expander load had negligible effect on the liquid column height and the low pressure side of the system. The overall reduction in performance is as a result of a drop in rotational speed pushing the generator further way from its design speed.

Although the NPSH calculation based off of the experimental data indicated that the layout and operation of Test system 1 was sufficient to overcome pump cavitation. The pump failed to operate in a stable manner at the higher tested pump speed of 1200 rpm. Based on the current system layout no further operational changes can be made to enable the pump to operate in the higher range. Further investigation is required both in terms of experimental testing of cavitation mitigation techniques and required NPSH model.

Chapter 5 – Effect of Subcooling and Liquid Column Height on ORC System performance

In the previous chapter the effect of system mass and liquid column height was investigated to determine its impact on the performance of the ORC system and in particular its effect on pump cavitation. The increase in system mass significantly improved the ORC performance, however, operation at the highest pump speed was still subjected to flow problems. The 2.3m liquid column height was itself insufficient to cover the full pump operational range. A further increase in column height could be adopted, however 2.3m is already impractical in real world applications of small scale ORC. Therefore, in order to try and reach the full potential of the pump and thus maximise the performance of the ORC system, the two other cavitation mitigation techniques, subcooling and pump bypass, have been investigated. The combined effects of subcooling and liquid column height in this chapter and combined effects of pump bypass and liquid column height in the subsequent. The experimental test rig was therefore adapted to include a subcooler and pump bypass valve (Test system 2).

In order to assess the combined effects of subcooling and liquid column height the cold water feed temperature was reduced from 14°C to 6°C in 2°C increments, with the remaining ORC parameters held constant. This test was then repeated for increasing mass increments of 200g. The resulting data set has been presented for the three pump speeds of 800, 1000 and 1200 rpm.

Key: The observed liquid height at and between the system sight glasses has been included in the graphs as data symbol changes. The data in this chapter follows

Table 7: Experimental Liquid level Indication: Subcooling data

Symbol style	Liquid level (m)	Sight glass number
△	< 0.6	< S9
▲	0.6-0.85	S9-S8
◮	0.85-1.1	S8-S6
▲	1.1-1.6	S6-S5
△	1.6-2.1	S5-S4
⬚	> 2.1	>S4

5.1. **Experimental results: 800 Rpm pump speed**

Experimental results observation summary: At a pump speed of 800rpm the decreasing subcooler temperature has no observably effect on the overall system performance. The high pressure side of the system shows a general decrease in pressure with decreasing subcooler temperature at the lower levels of system charge. The low pressure side of the system shows no change in pressure with decreasing subcooler temperature. The ORC temperature from the subcooler to evaporator inlet reduces accordingly and the temperature at the expander inlet and outlet showing no obvious trend with decreasing subcooler temperature.

Overall performance:

The overall performance of the ORC system at 800rpm pump speed is shown in Figure 92, Figure 93 and Figure 94 the expander rotational speed and output power, and consumed pump power respectively. In terms of the expander rotational speed, electrical output power and consumed pump power, decreasing the subcooler temperature shows no clearly observable change to the overall performance. In addition both the expander speed and the expander output power decrease with increasing levels of system charge. The maximum output occurs at the lowest level of system charge 4.38kg and one degree of system subcooling. The consumed pump power shows no significant change with either increasing mass or increasing levels of subcooling.
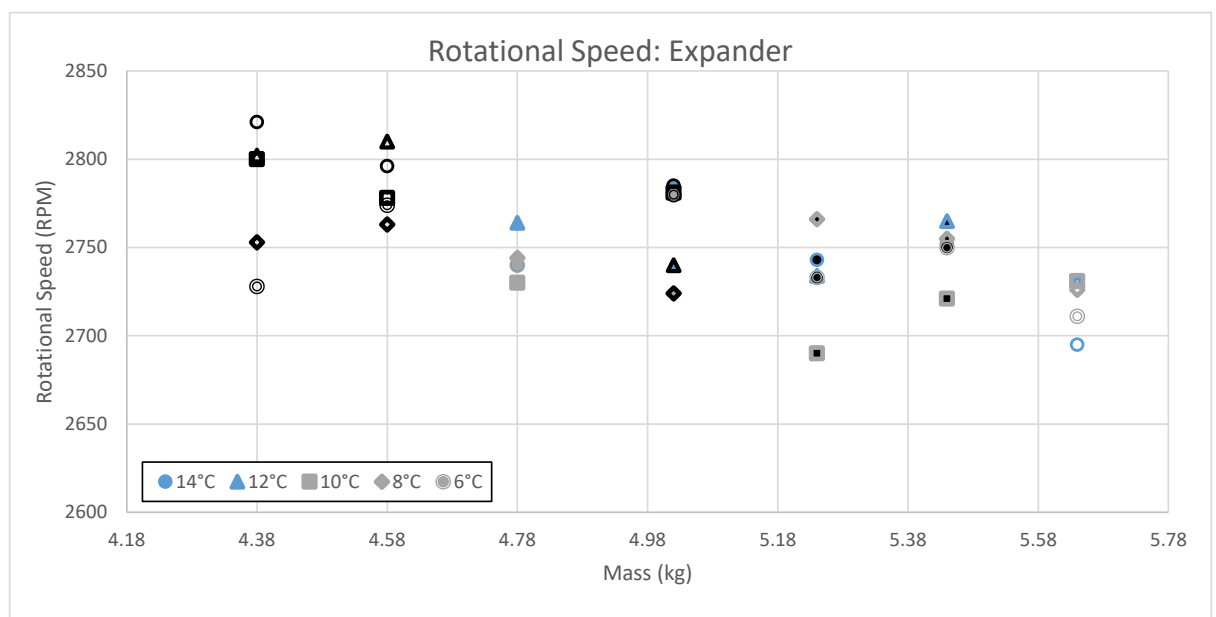
Figure 92: Expander Rotational speed for various system charges and multiple subcooler inlet temperatures at 800rpm pump speed. The stored liquid height level between the sight glasses is indicated by marker changes. Overall the expnder rotational speed decreases with increaseing mass (which would indicate the system is past the point of caviation). There is no clearly observable trend between expander rotational speed and decreaseing subcooler temperature.
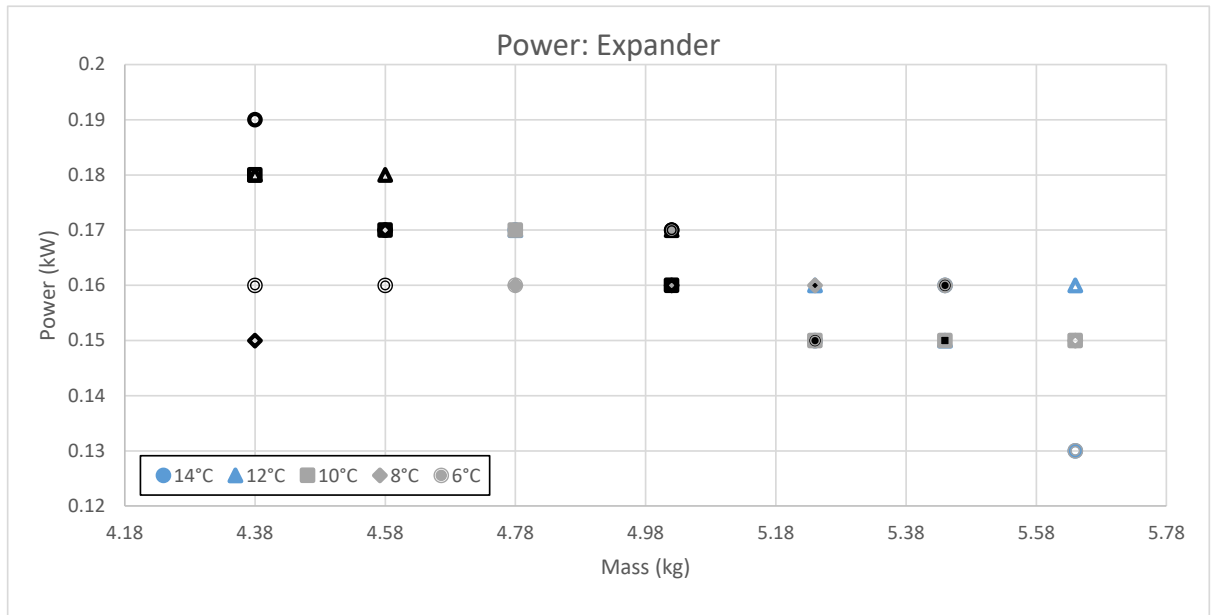
Figure 93: Expander power output for various system charges and multiple subcooler inlet temperatures at 800rpm pump speed. There is a general decrease in expander output power with increaseing mass. The decreasing subcooler temperature shows no decernable positive benefit on the expander output power.
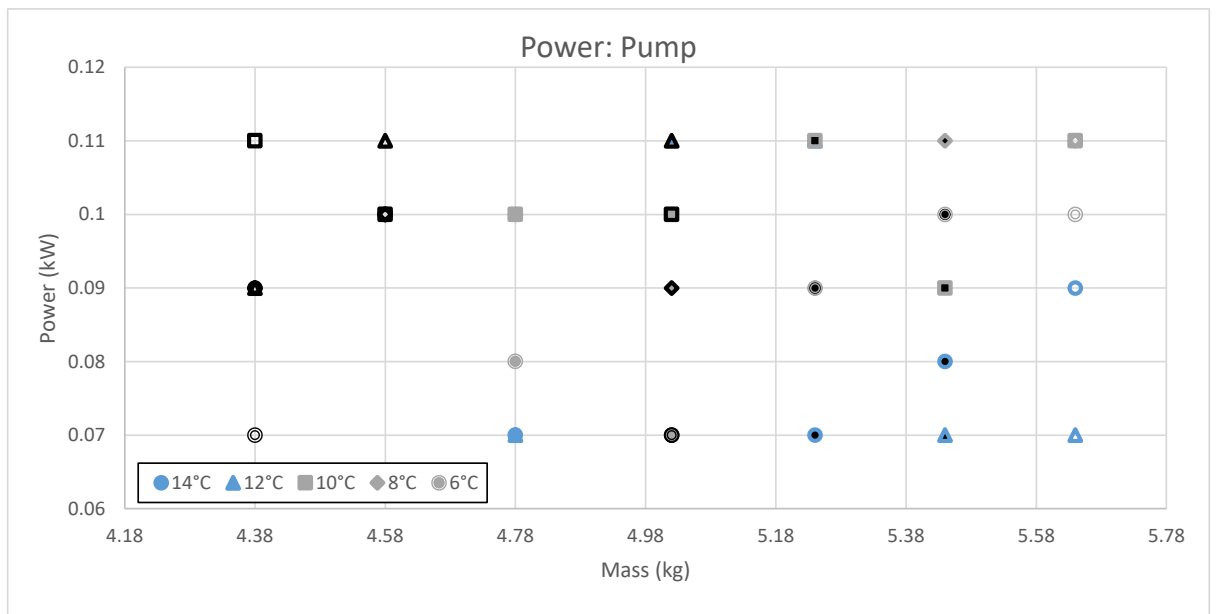
Figure 94: Consumed pump power for various system charges and multiple subcooler inlet temperatures at 800rpm pump speed. There is no significant change in pump power with increasing mass of decreasing subcooler temperature.

Pressure:

The high pressure side of the system is shown in Figure 95 and Figure 96, the pump outlet and expander inlet respectively. The recorded trend at both the pump outlet and expander inlet are the same, with a general reduction in pump outlet pressure with decreasing subcooler temperature. The effect is more prominent at the lower end of tested system charge. Increasing the system mass results in an increase in high side pressure shown at both the expander inlet and the pump outlet. The maximum high side pressure occurs at

5.48kg of system charge, which doesn't correlate with the maximum output power case of 4.48kg.

Figure 95: Pump outlet pressure for various system charges and multiple subcooler inlet temperatures at 800rpm pump speed. In general across the entire test range a reduction in subcooler temperature tends to result in a decrease pump outlet pressure, this effect is more prominent at lower system charge levels.

Figure 96: Expander inlet pressure for various system charges and multiple subcooler inlet temperatures at 800rpm pump speed. In general across the entire test range a reduction in subcooler temperature tends to result in a decrease in pump outlet pressure, this effect is more prominent at lower system charge levels.

The low pressure side of the system is shown in Figure 97, Figure 98, Figure 99 and Figure 100, the expander outlet, condenser outlet, sub cooler inlet and pump inlet respectively. Reducing the sub cooler temperature has no effect on the low pressure side of the system in comparison to system charge which has a significant effect. In all four cases the pressure follows the same consistent trend with increasing levels of system charge resulting in

increasing pressure. The lowest low side pressure of approximately 1.04 barg at the expander outlet corresponds with the maximum output power case of 4.38kg of system charge. Due to the liquid column height the resulting pressure at the pump inlet is 1.09 barg.

Figure 97: Expander outlet pressure for various system charges and multiple subcooler inlet temperatures at 800rpm pump speed. Decreaseing subcooler temperautre has negligable effect on the expander outlet pressure.

Figure 98: Condenser outlet pressure for various system charges and multiple subcooler inlet temperatures at 800rpm pump speed. Decreasing the subcooler temperature has negliable effect on the condenser outlet pressure.

Figure 99: Subcooler inlet pressure for various system charges and multiple subcooler inlet temperatures at 800rpm pump speed. Decreasing the subcooler temperature has negligable effect on the subcooler inlet pressure.

Figure 100: Pump inlet pressure for various system charges and multiple subcooler inlet temperatures at 800rpm pump speed. Decreasing the subcooler temperature has negligable effect on the pump inlet pressure

Temperature:

The cold water feed, cold water return and condenser outlet temperature are shown in Figure 101, Figure 102 and Figure 103 respectively. The cold water feed temperature and condenser outlet temperature have a variation of less than 1°C across the entire test range and follows a very similar pattern, with fluctuations in controlled cold water feed temperature. Since these temperatures are controlled parameters the close match in temperature helps to improve the reliability of the data.

Figure 101: Cold water feed temperature for various system charges and multiple subcooler inlet temperatures at 800rpm pump speed. The controlled cold water feed temperature has a variation of approximetly 1°C over the entire test range.

Figure 102: Cold water return temperature for various system charges and multiple subcooler inlet temperatures at 800rpm pump speed. The cold water return temperature shows no observably consistant trend with decreasing subcooler temperature.
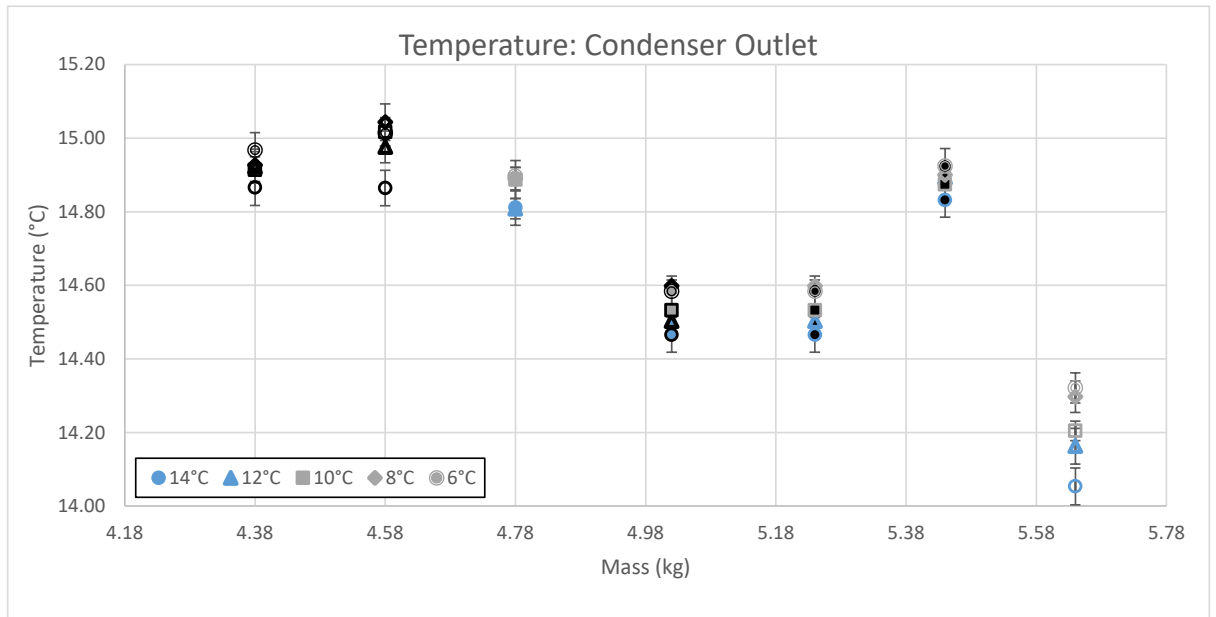
Figure 103: Condenser outlet temperature for various system charges and multiple subcooler inlet temperatures at 800rpm pump speed. The condenser outlet temperature has an overall variation of approximently 1°C and follows a similar pattern to the cold water feed temperature.

The pump inlet, pump outlet and evaporator inlet temperatures are shown in Figure 104, Figure 105 and Figure 106. The temperatures in all three cases has a corresponding reduction in temperature with reducing subcooler temperature. Similar to the cold water feed temperature the very close match in subcooling temperature between each test run indicates good repeatability in the experimental testing.
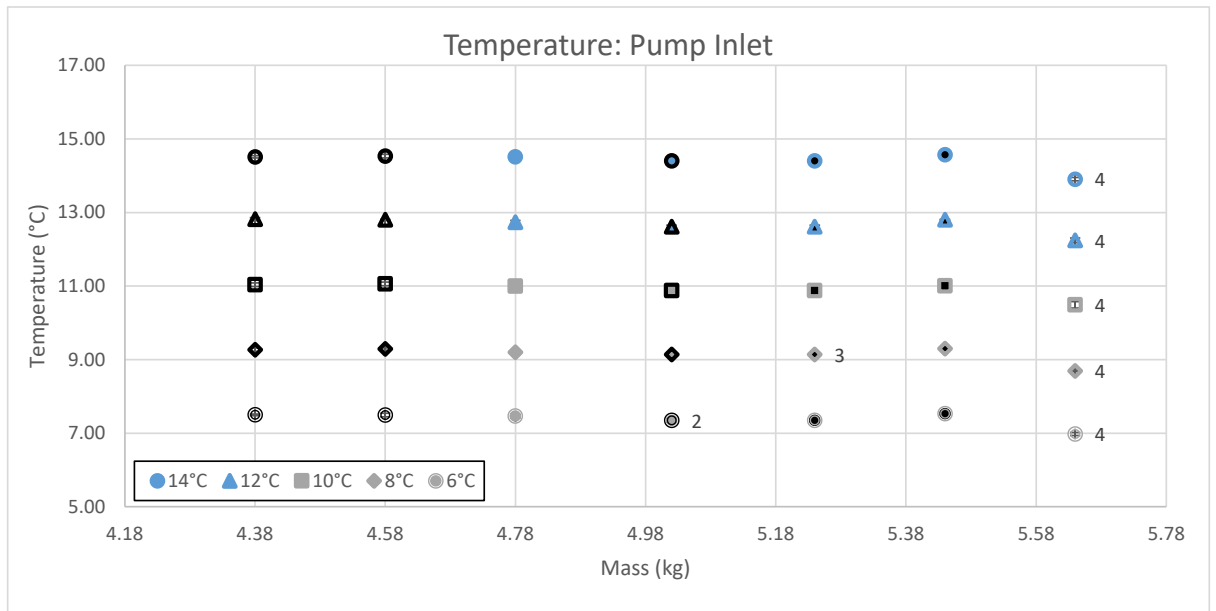
Figure 104: Pump inlet temperature for various system charges and multiple subcooler inlet temperatures at 800rpm pump speed. Decreasing the subcooler temperature results in a reduction in pump inlet temperature.

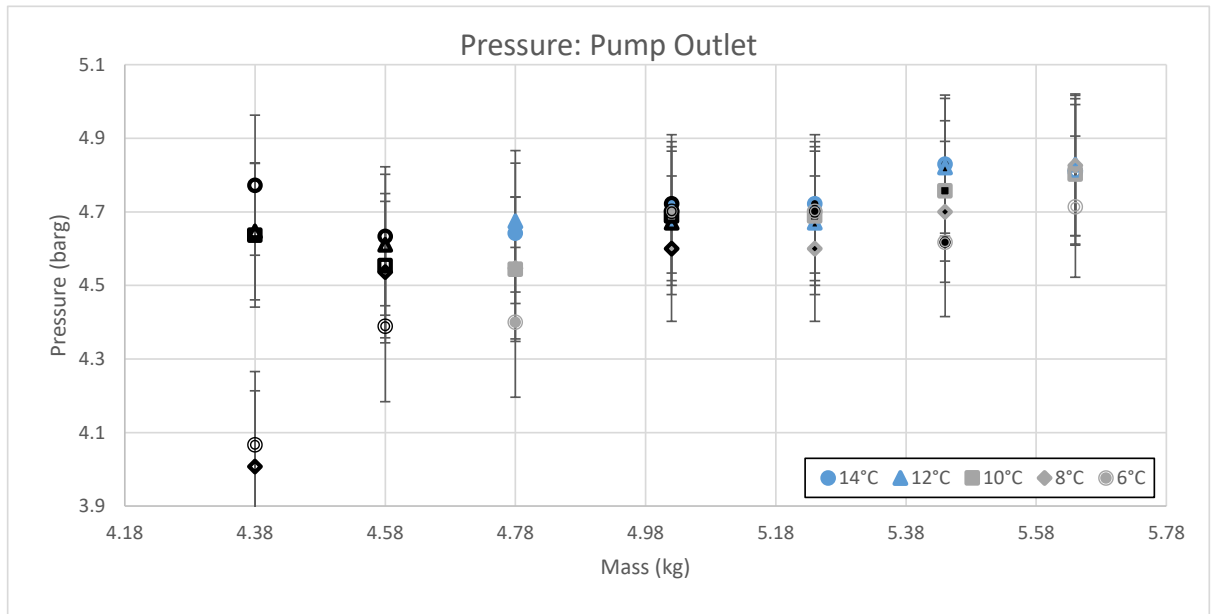*Figure 105: Pump outlet temperature for various system charges and multiple subcooler inlet temperatures at 800rpm pump speed. Decreasing the subcooler temperature results in a reduction in pump outlet temperature*

Figure 106: Evaporator inlet temperature for various system charges and multiple subcooler inlet temperatures at 800rpm pump speed. Decreasing the subcooler temperature results in a decrease in the evaporator inlet temperature.

The controlled hot water feed and return temperatures are shown in Figure 107 and Figure 108. The hot water feed temperature has a variation of over 3°C for the entire test range but less than 1°C variation for each individual mass run. The hot water return temperature shows a similar overall trend to the feed temperature with no clearly observable trend between return temperature and decreasing subcooler temperature.
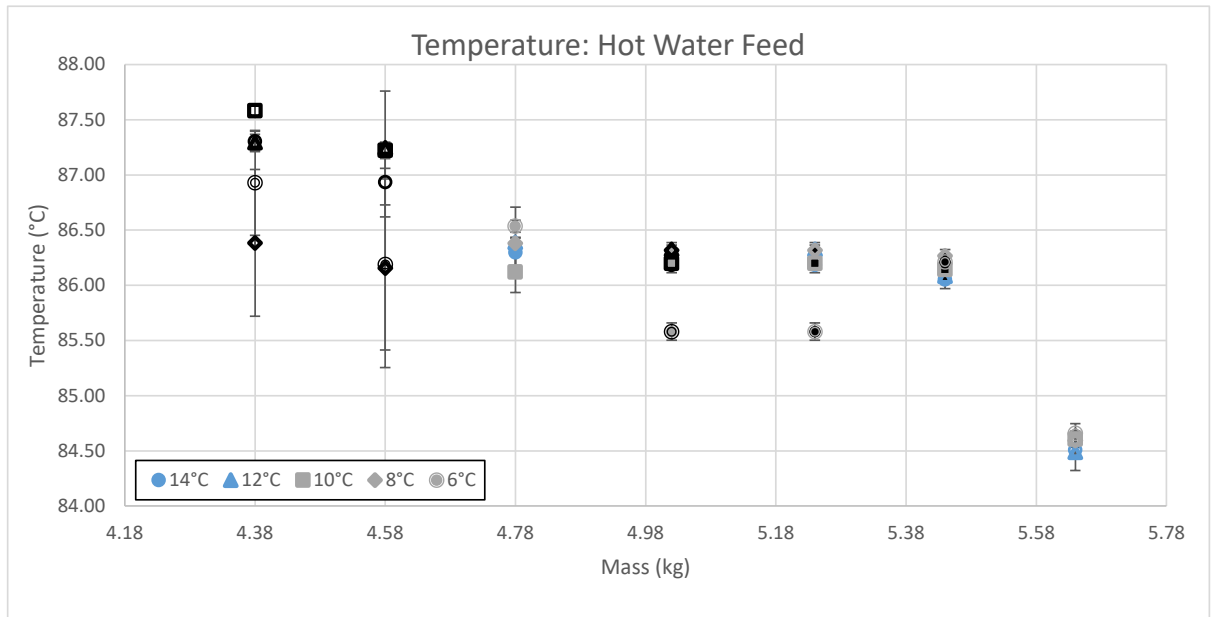
Figure 107: Hot water feed temperature for various system charges and multiple subcooler inlet temperatures at 800rpm pump speed. The controlled hot water feed temperature has a variation of approximitely 3°C over the entire test range. The variation for each individual mass increament is <1°C.
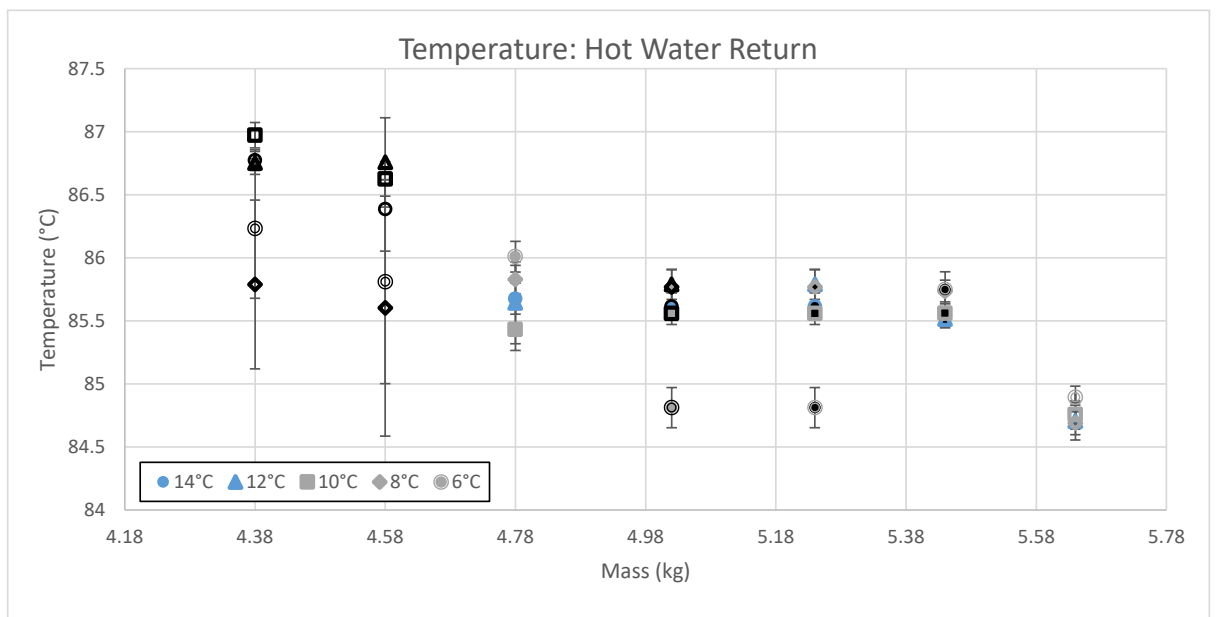
Figure 108: Hot water return temperature for various system charges and multiple subcooler inlet temperatures at 800rpm pump speed. The data shows no obvious trend between hot water return tempertautre and decreasing subcooler temperature.

The expander inlet and outlet temperature are shown in Figure 109 and Figure 110 respectively. The variation in expander inlet temperature is as a result of hot water feed variation, with no clearly observable trend between expander inlet temperature and subcooling temperature. Likewise the variation in expander inlet translates through to the outlet temperature with no clearly observable trend. In both cases the trend increases with increasing levels of system mass.
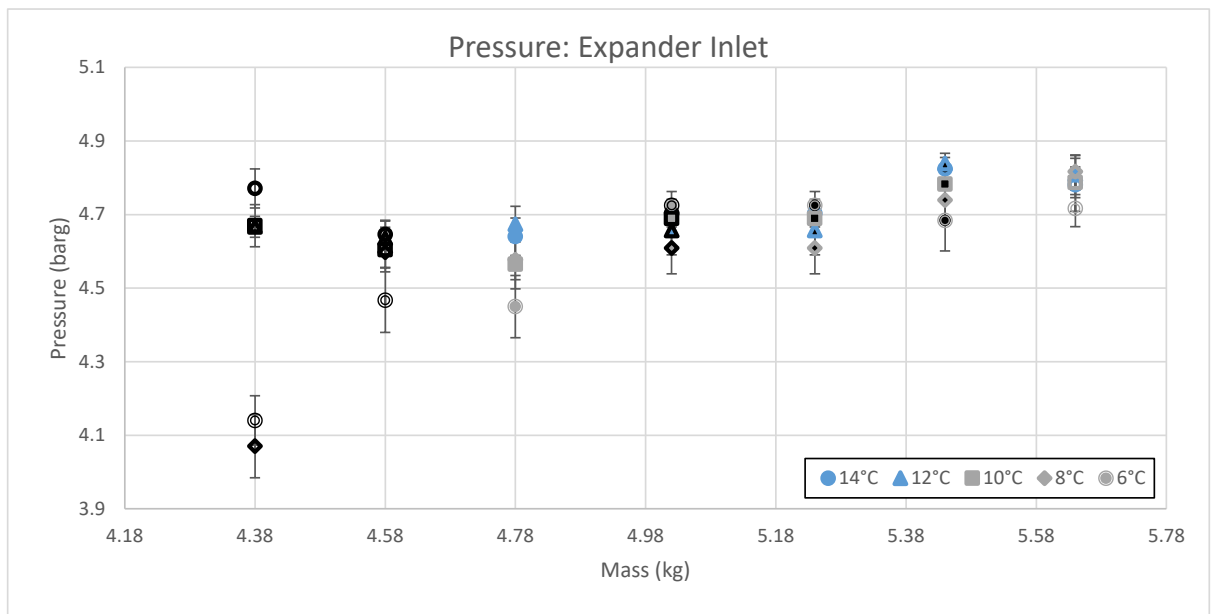
Figure 109: Expander inlet temperature for various system charges and multiple subcooler inlet temperatures at 800rpm pump speed. There is no obvious trend between expander inlet temperature and decreasing subcooler temperature.

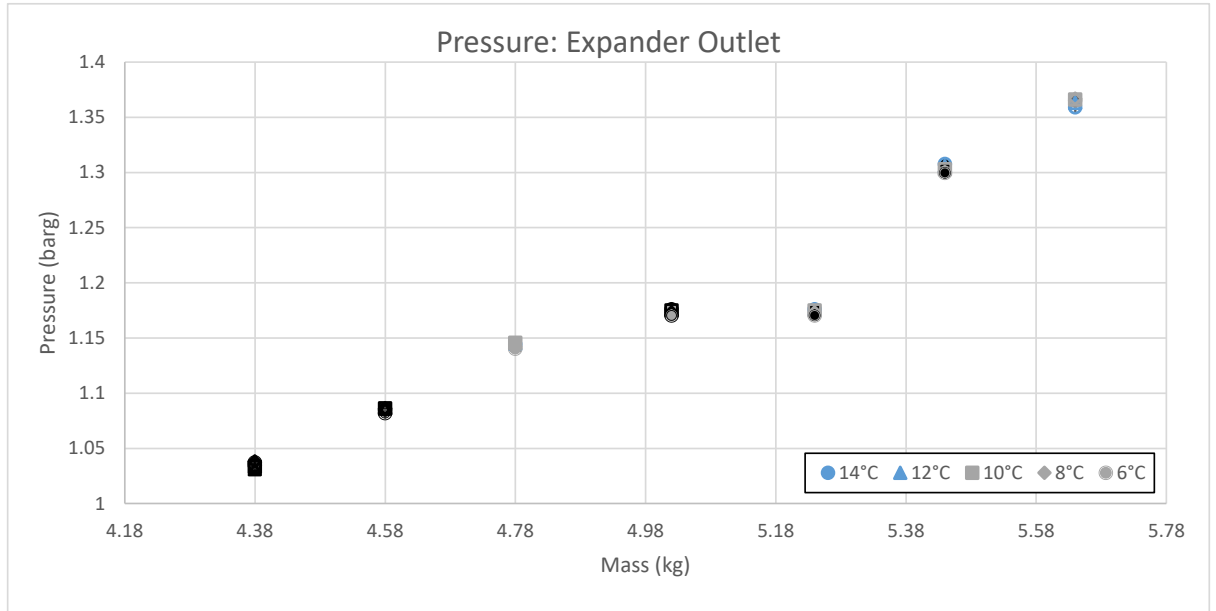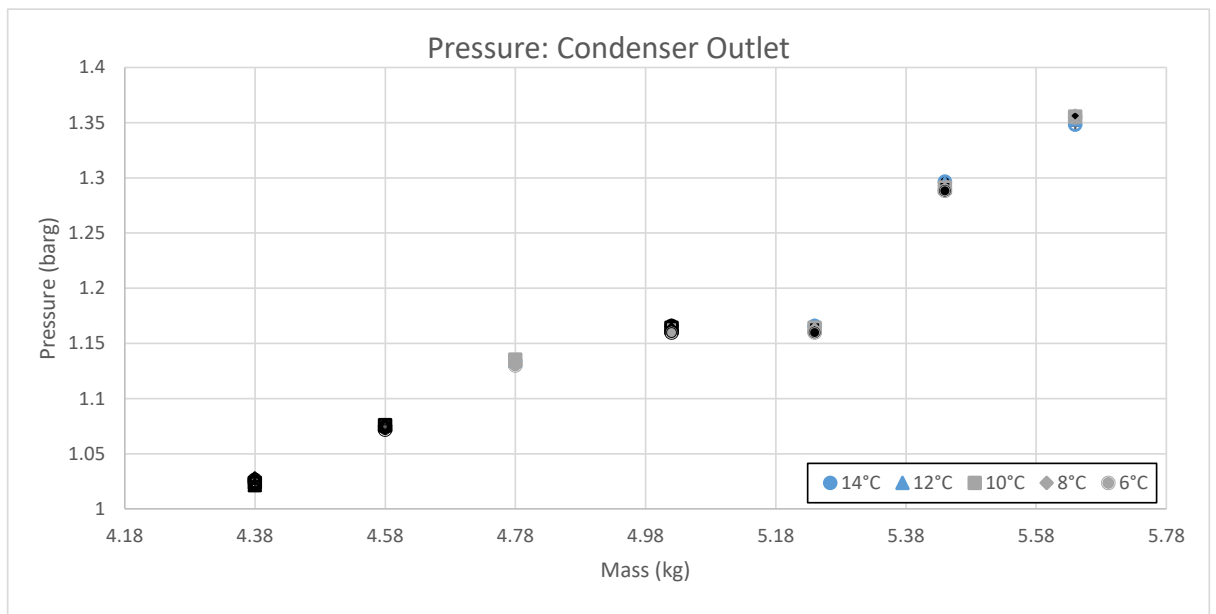*Figure 110: Expander outlet temperature for various system charges and multiple subcooler inlet temperatures at 800rpm pump speed. There is no obvious trend between expander outlet temperature and decreaseing subcooler tempeature.*

5.2. **Experimental results: 1000 Rpm pump speed**

Experimental results observation summary: At 1000rpm pump speed there is a clear increase in overall system performance with decreasing subcooler temperature. Likewise the pressure in the high side of the system shows a clear increase with decreasing increments of temperature, the degree of change decreases with increasing system mass. In comparison to increasing system charge decreasing subcooler temperature has negligible effect on the low pressure side of the system. The temperature at the pump inlet and outlet decrease according, along with the majority of evaporator inlet temperatures with the exception of the lower mass higher subcooler temperature results. The expander inlet temperature increases with decreasing subcooler temperature, indicating and increase in flow. The expander outlet temperature shows no observably consistent trend.

Overall performance:

The overall performance of the ORC system operating at 1000rpm pump speed with varying subcooler temperature is shown in Figure 111, Figure 112 and Figure 113, the expander rotational speed, electrical power output and the consumed pump power respectively. It is clear from both the expander rotational speed and the output power that decreasing subcooler temperature results in an increasing in ORC output. The degree of improvement reduces with increasing system charge. The consumed pump power shows no clear trend with varying subcooler temperature and fluctuates between 0.09 and 0.11 kW.
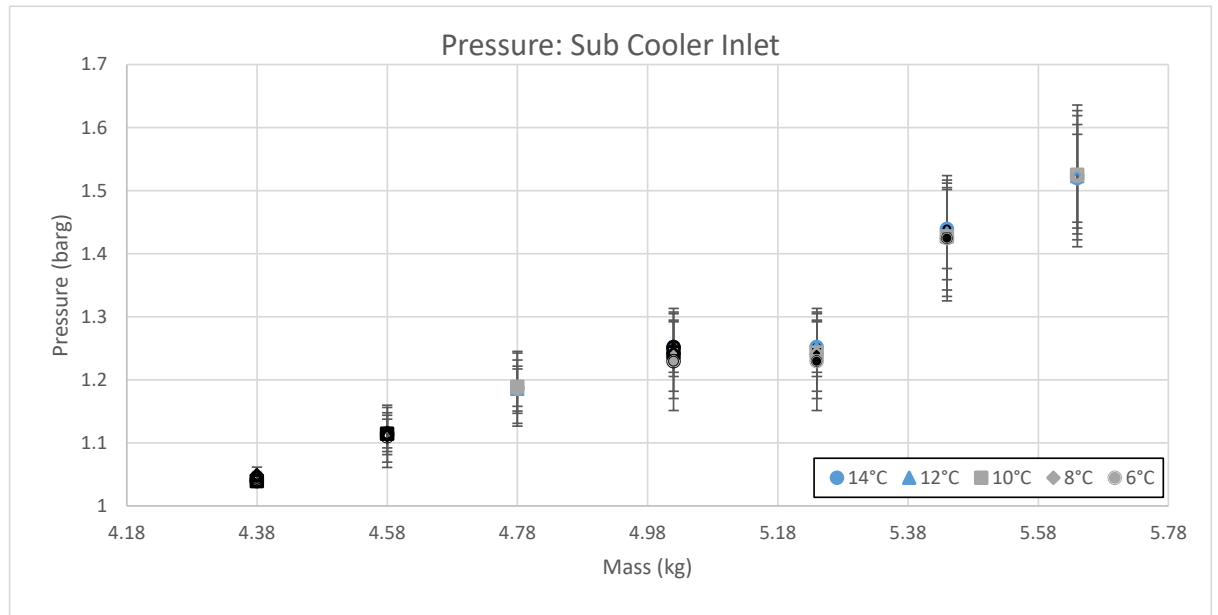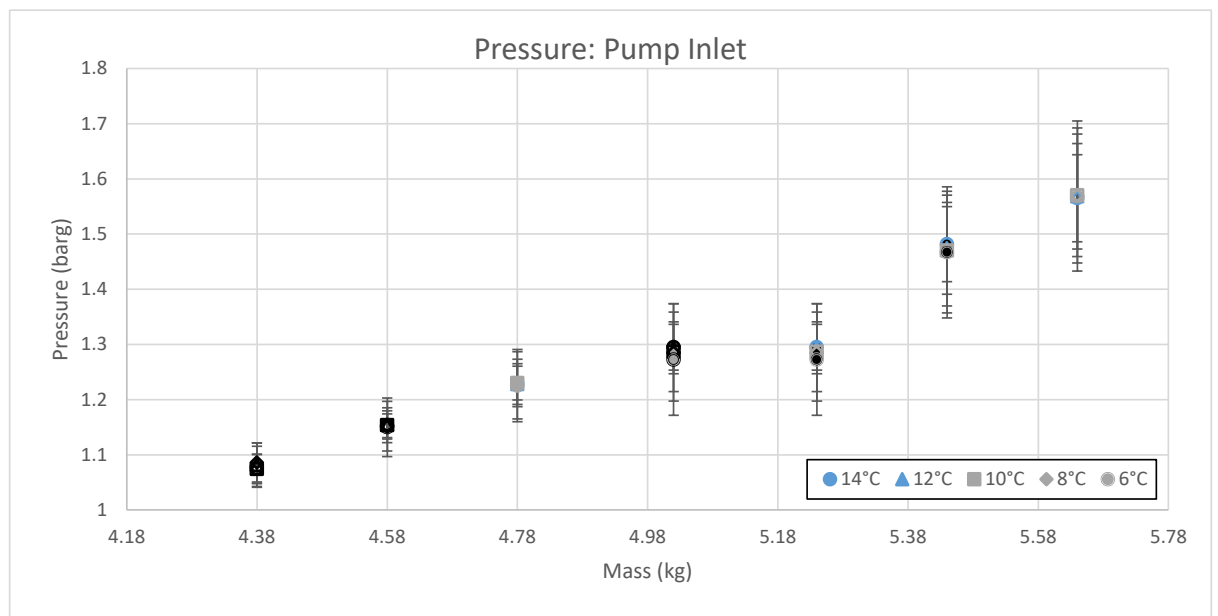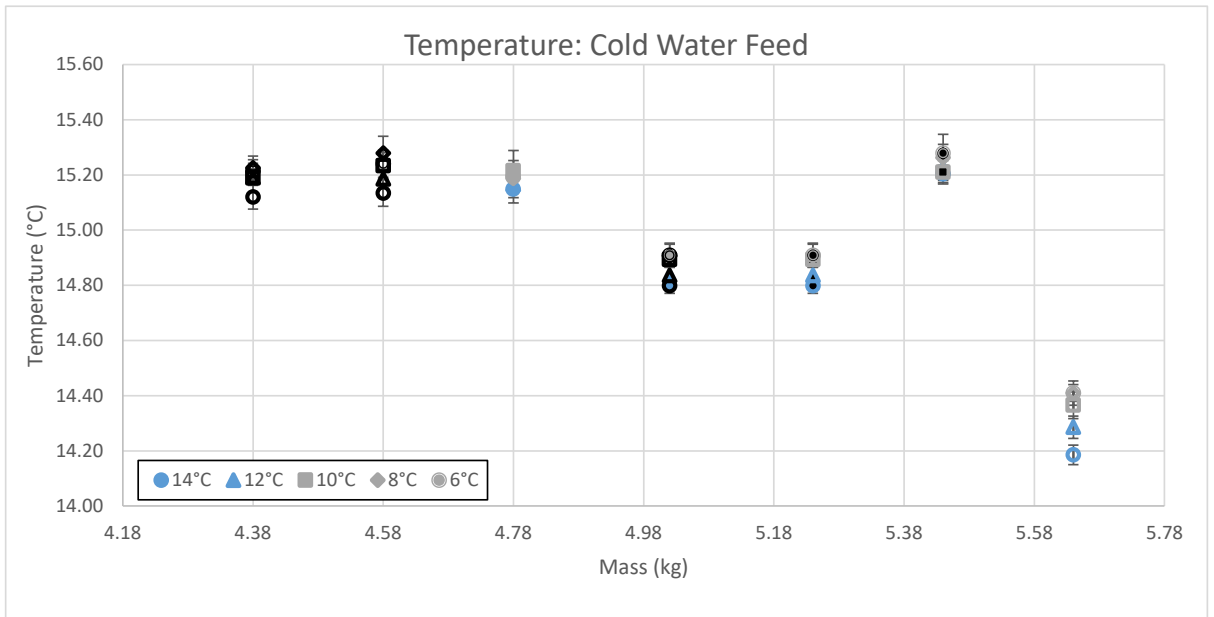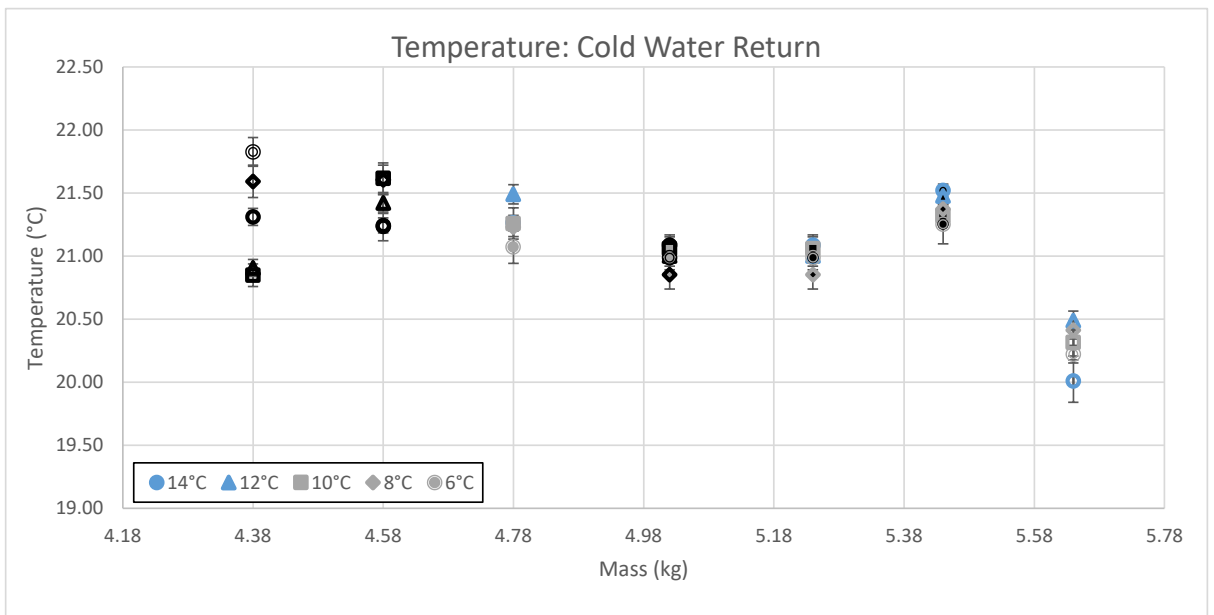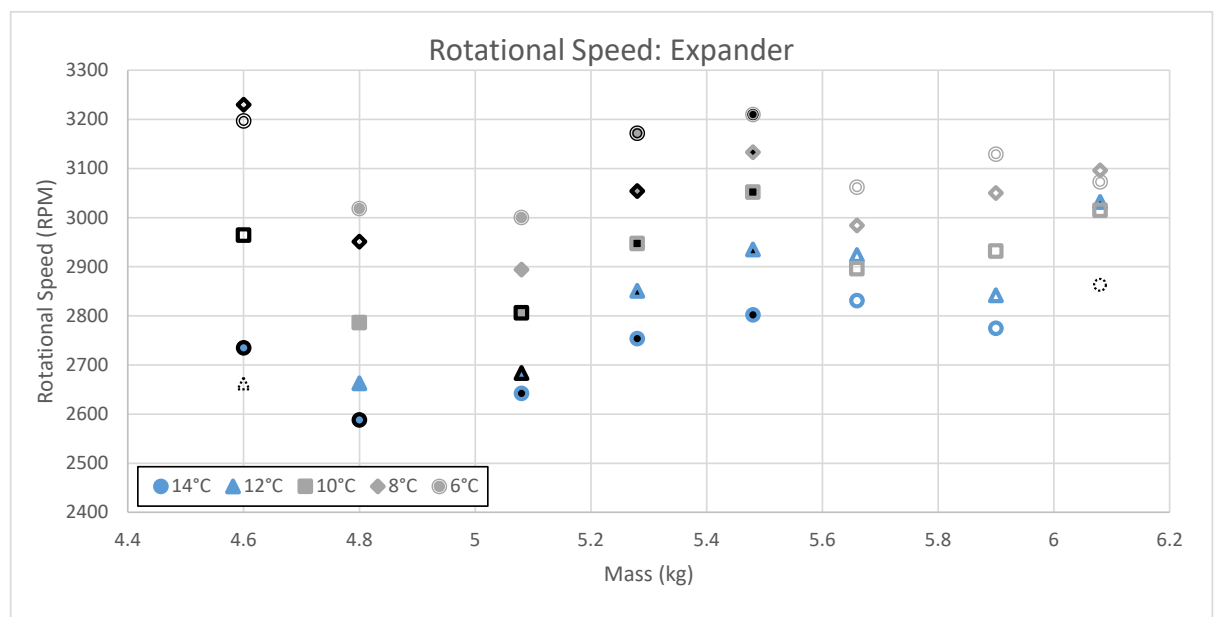

Figure 111: Expander rotational speed for various system charges and multiple subcooler inlet temperatures at 1000rpm pump speed. Decreasing subcooler temperature results in an incerase in expander rotational speed, the degree of change reduces with increasing system charge.
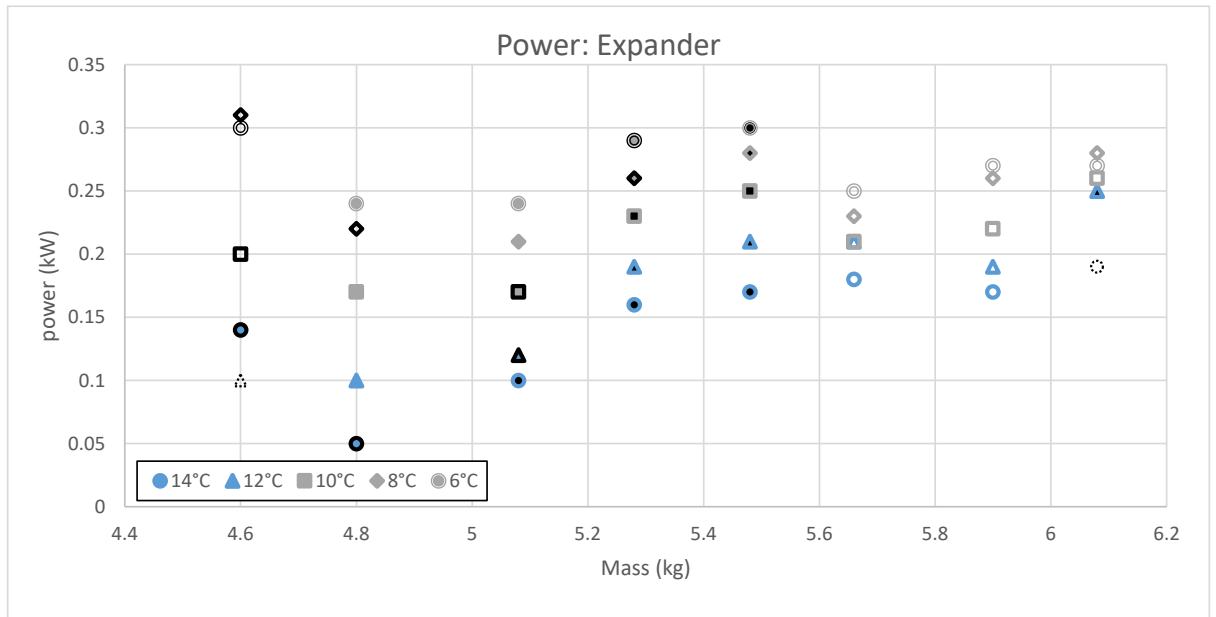
Figure 112: Expander power output for various system charges and multiple subcooler inlet temperatures at 1000rpm pump speed. Expander output power increases with decreasing subcooler temperature, the degree of change reduces with increasing charge.
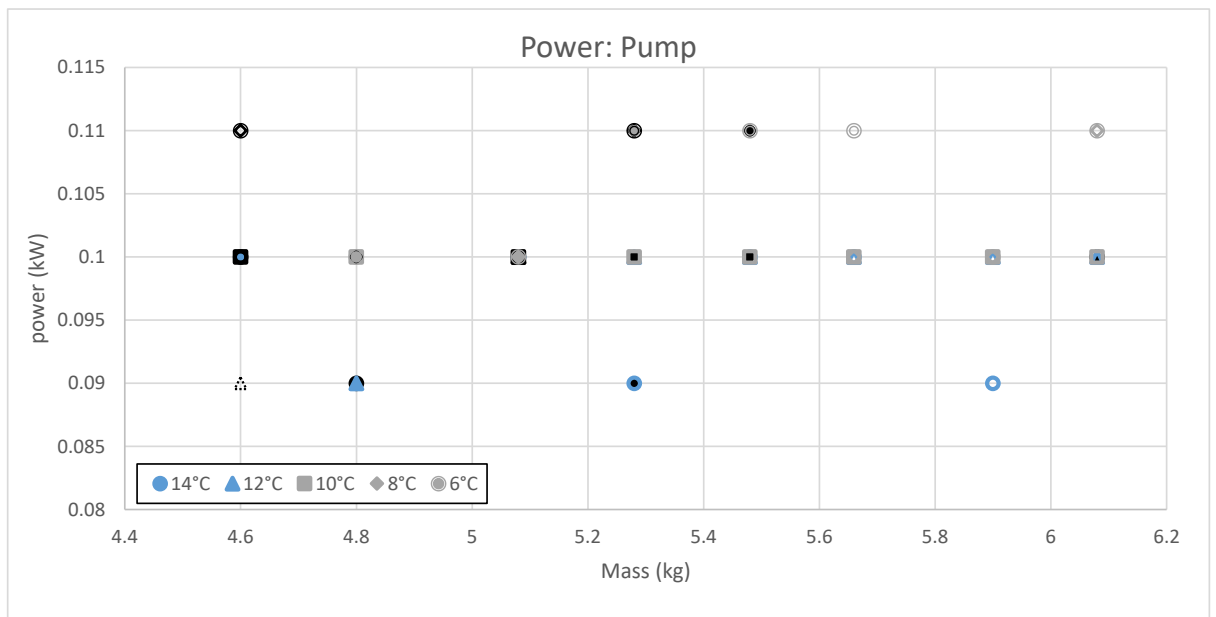
Figure 113: Pump power consumed for various system charges and multiple subcooler inlet temperatures at 1000rpm pump speed. There is no distinct trend between pump power consumption and decreasing sub cooler temperature.

Pressure:

The pressure on the high side of the system at the pump outlet and expander inlet is shown in Figure 114 and Figure 115. Both graphs show the same trend with reducing sub cooler temperature resulting in an increase in high side pressure, the degree of change reduces with increasing system mass. The pressure at the expander inlet reaches 5.1barg at 5.48kg of system charge and 6°C of sub cooler inlet temperature. For the same level of system

charge the reduction in sub cooler inlet temperature from 14°C to 6°C results in an increase in approximately 1.4 barg significantly improving the output of the system.
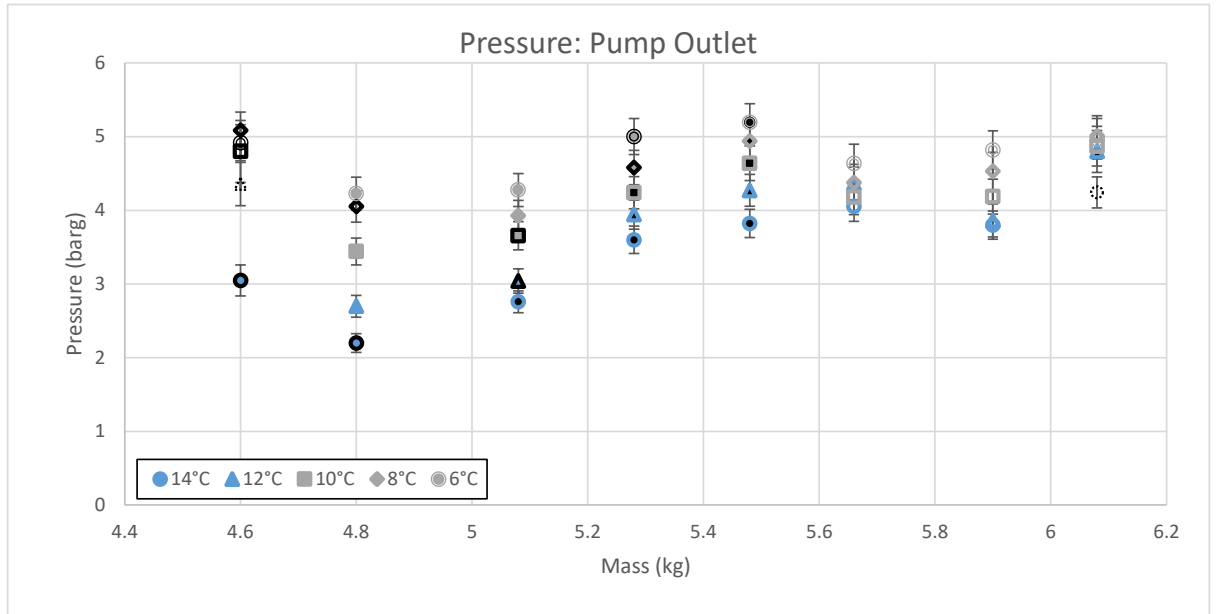
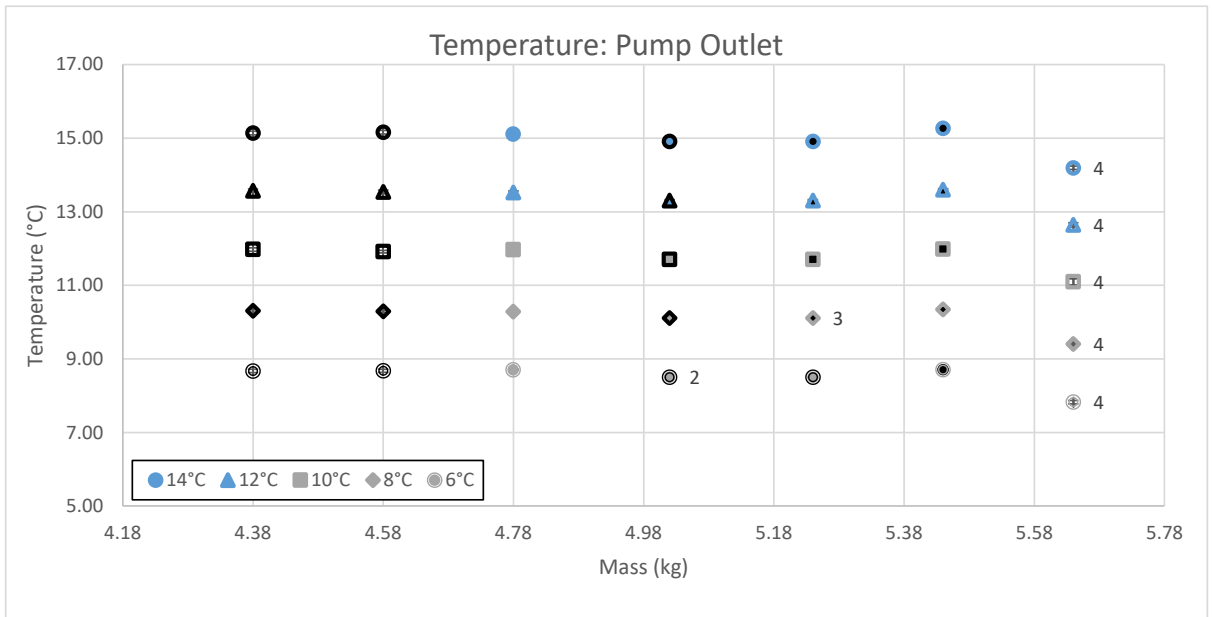*Figure 114: Pump outlet pressure for various system charges and multiple subcooler inlet temperatures at 1000rpm pump speed. Pump outlet pressure increases with decreasing subcooler temperature. The change is smaller with increasing system charge.*

Figure 115: Expander inlet pressure for various system charges and multiple subcooler inlet temperatures at 1000rpm pump speed. The expander inlet pressure increases with reducing subcooler temperature, The change is smaller with increasing system charge.
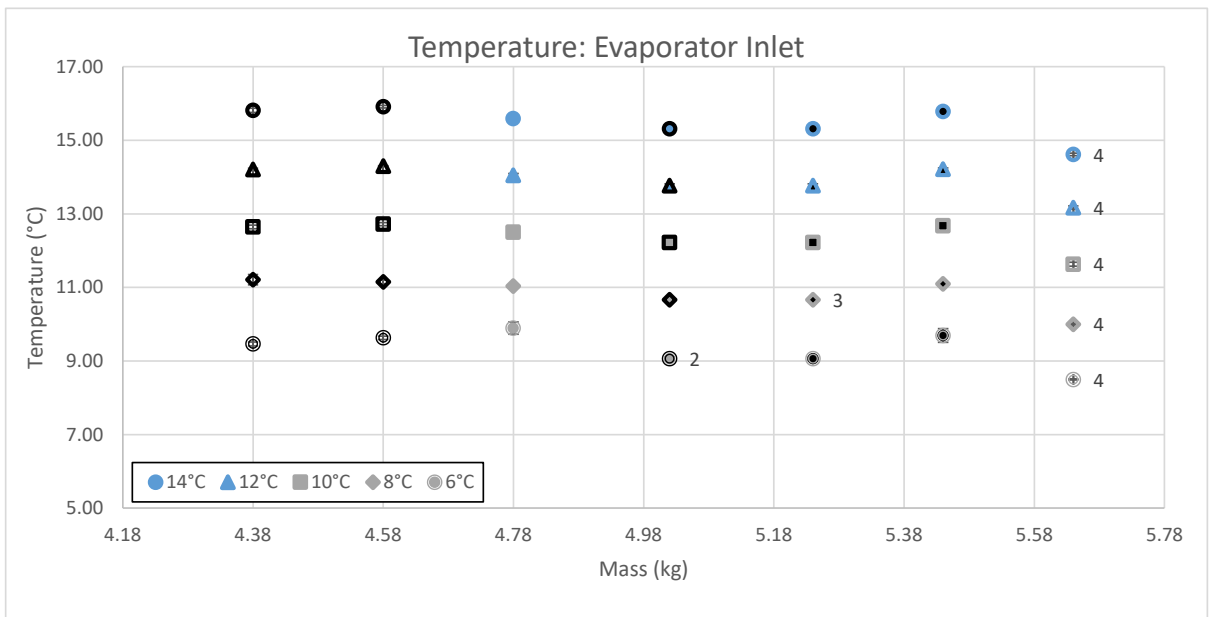
Figure 116: Expander outlet pressure for various system charges and multiple subcooler inlet temperatures at 1000rpm pump speed. Decreasing subcooler temperature has negligable effect on expander outlet pressure.

The low pressure side of the system is shown in Figure 117, Figure 118 and Figure 119 at the condenser outlet, sub cooler inlet and pump inlet. In all three cases the subcooler temperature has minimal effect on low side pressure in comparison to increasing system charge. Similar to the previous test cases, only the increase in system mass effects the low pressure side of the system with 200g of refrigerant resulting in an increase of approximately 0.6 barg. For the 5.48kg of system charge case the pressure at the pump inlet shows no change, as a result the increase in performance in due to the decreasing subcooler temperature alone.

Figure 117: Condenser outlet pressure for various system charges and multiple subcooler inlet temperatures at 1000rpm pump speed. Decreasing subcooler temperature has negligable effect on condenser outlet pressure
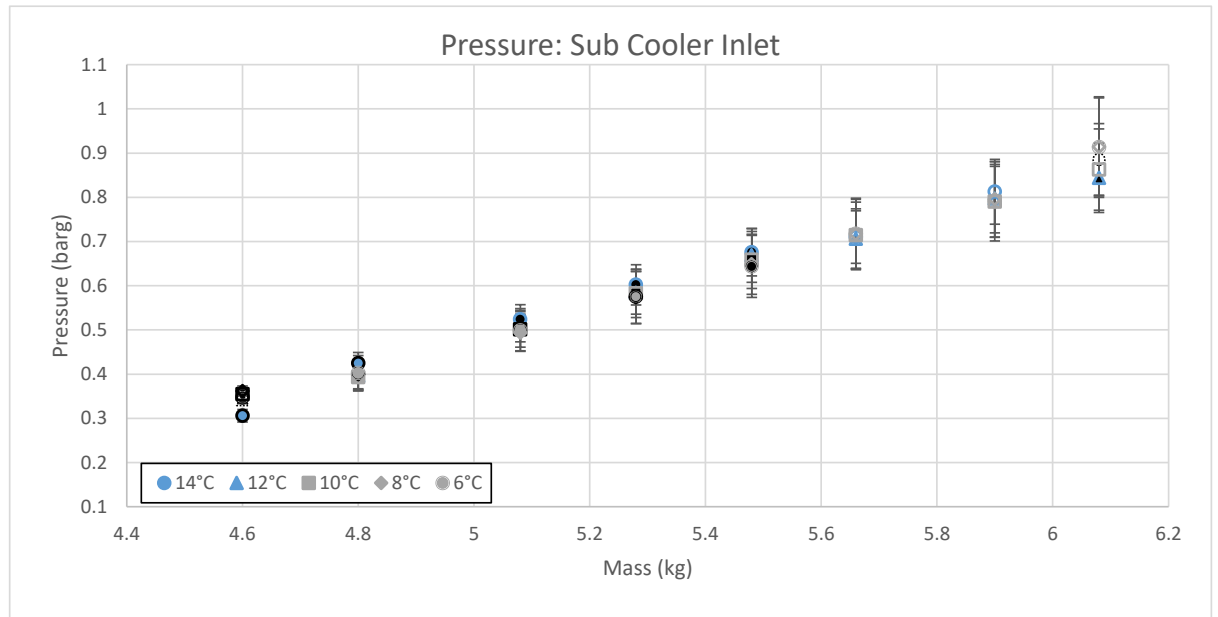
Figure 118: Sub cooler inlet pressure for various system charges and multiple subcooler inlet temperatures at 1000rpm pump speed. Decreasing subcooler temperature has negligable effect on subcooler inlet pressure.
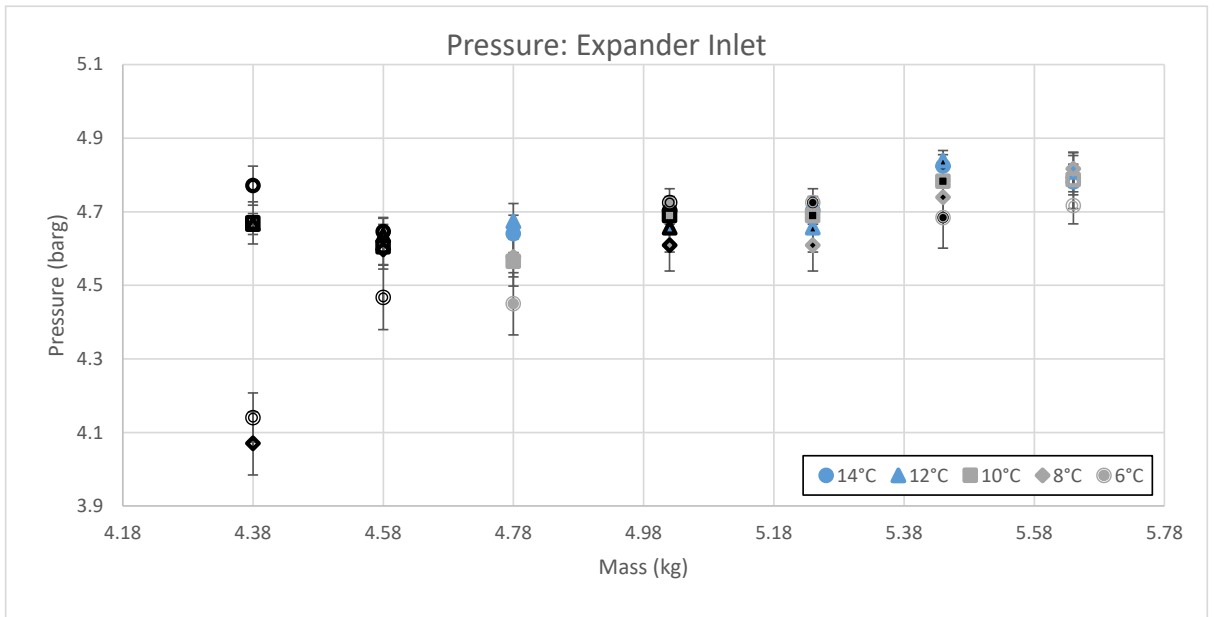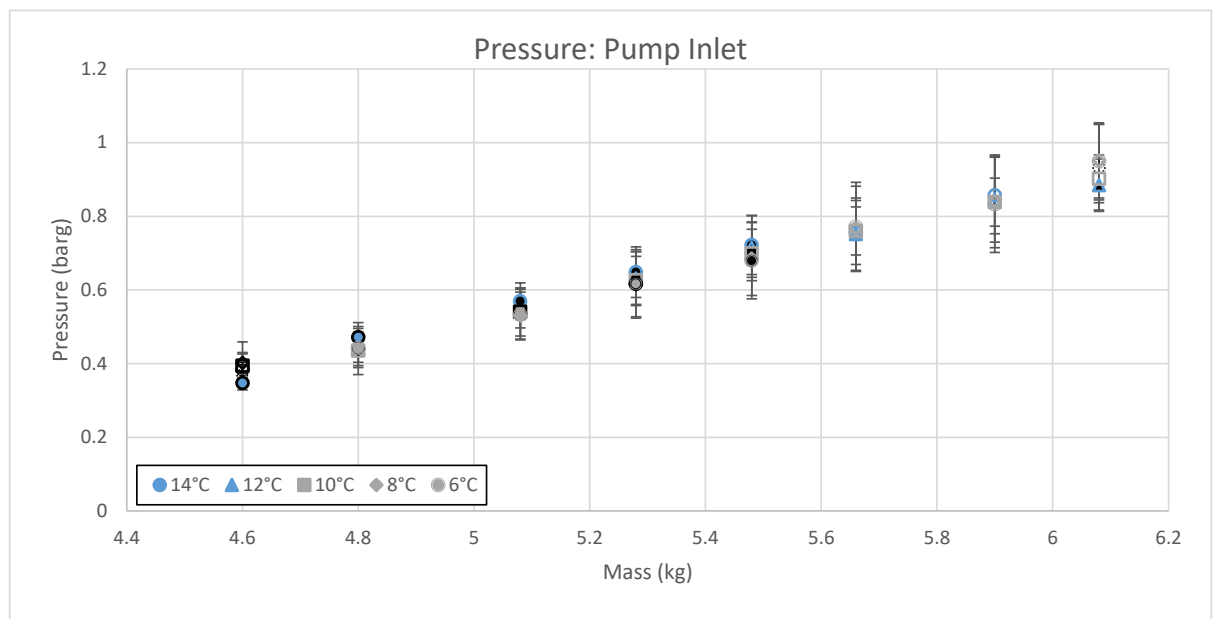

Figure 119: Pump inlet pressure for various system charges and multiple subcooler inlet temperatures at 1000rpm pump speed. Varying subcooler temperature has minor effect on the pump inlet pressure in comparision to increasing levels of system charge.

Temperature:

The controlled cold water feed is shown in Figure 120 there is an overall temperature variation of less than 0.6°C over the entire test range. The variation for each mass increment is considerably less. The cold water return temperature is shown in Figure 121. Reducing subcooler temperature results in an increase in cold water return temperature with an increase in temperature indicative of higher system heat removal.
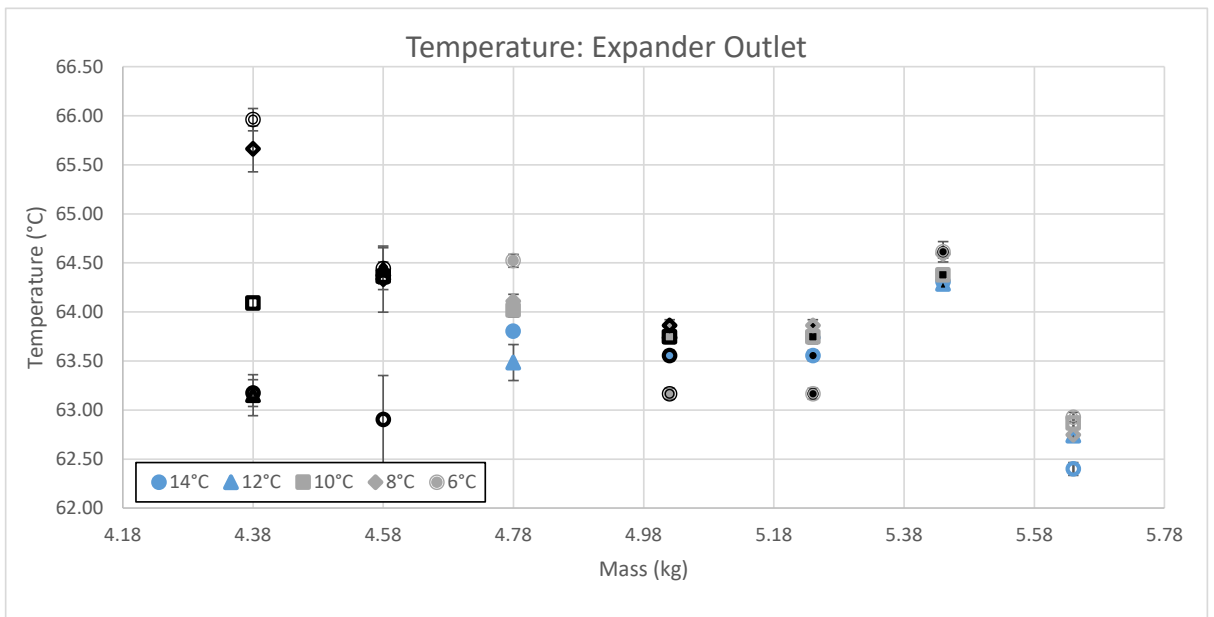
Figure 120: Cold water feed temperature for various system charges and multiple subcooler inlet temperatures at 1000rpm pump speed. The controlled cold water feed temperature has a variation of <0.6°C acorss the entire test range and <0.3°C or each individual mass increment.
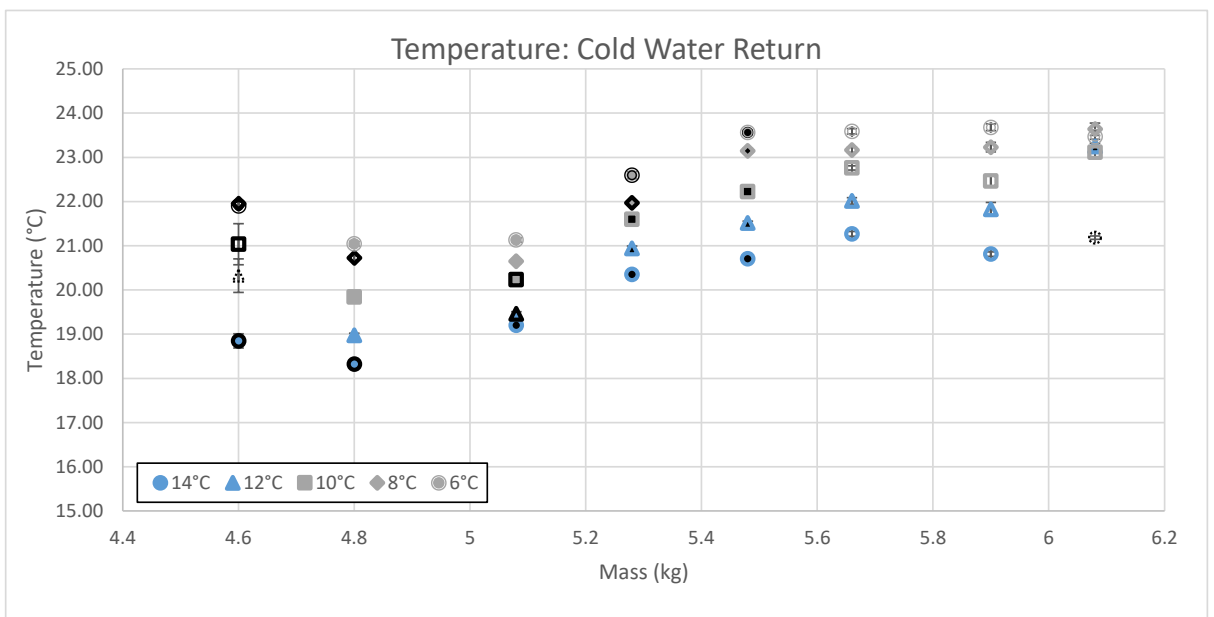
Figure 121: Cold water return temperature for various system charges and multiple subcooler inlet temperatures at 1000rpm pump speed. The cold water return temperature increases with decreasing subcooler temperature.

The condenser outlet temperature is shown in Figure 122. The trend in data is very similar to the cold water feed temperature and has a variation of less than 0.4°C, over the entire test range and significantly less for the majority of individual mass increments.
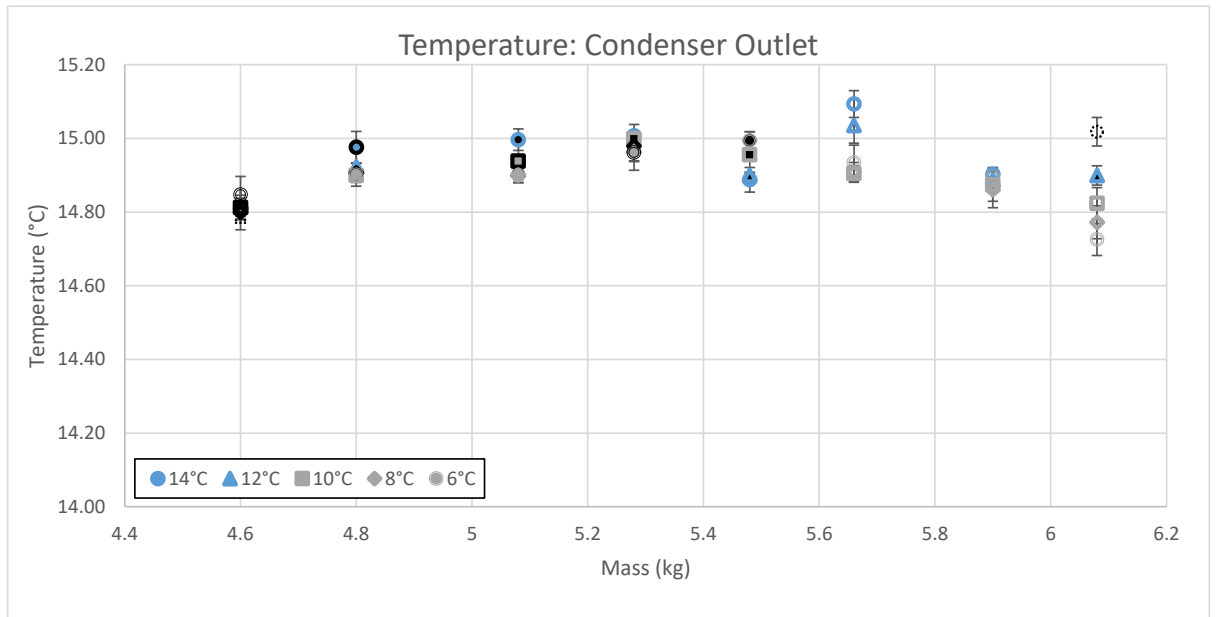
Figure 122: Condenser outlet temperature for various system charges and multiple subcooler inlet temperatures at 1000rpm pump speed. The condenser outlet temperature has a variation of <0.3°C across the entire test range.

The pump inlet and outlet temperature are shown in Figure 123 and Figure 124 in both cases the reduction in subcooler temperature results in a corresponding reduction in temperature. The consistence between each data point is indicative of strong repeatability in the experimental testing.

Figure 123: Pump inlet temperature for various system charges and multiple subcooler inlet temperatures at 1000rpm pump speed. The pump inlet temperature decreases accordingly with decreasing subcooler temperature.

Figure 124: Pump outlet temperature for various system charges and multiple subcooler inlet temperatures at 1000rpm pump speed. The pump outlet temperature decreases accordingly with decreasing subcooler temperature.

The evaporator inlet temperature is shown in Figure 125, the reduction in sub cooler temperature also results in a reduction in evaporator inlet temperature. The unexpectedly high evaporator inlet values upto 5.4kg of system charge are as a result of temperature sensor location and are normal an indication of low working fluid flow.
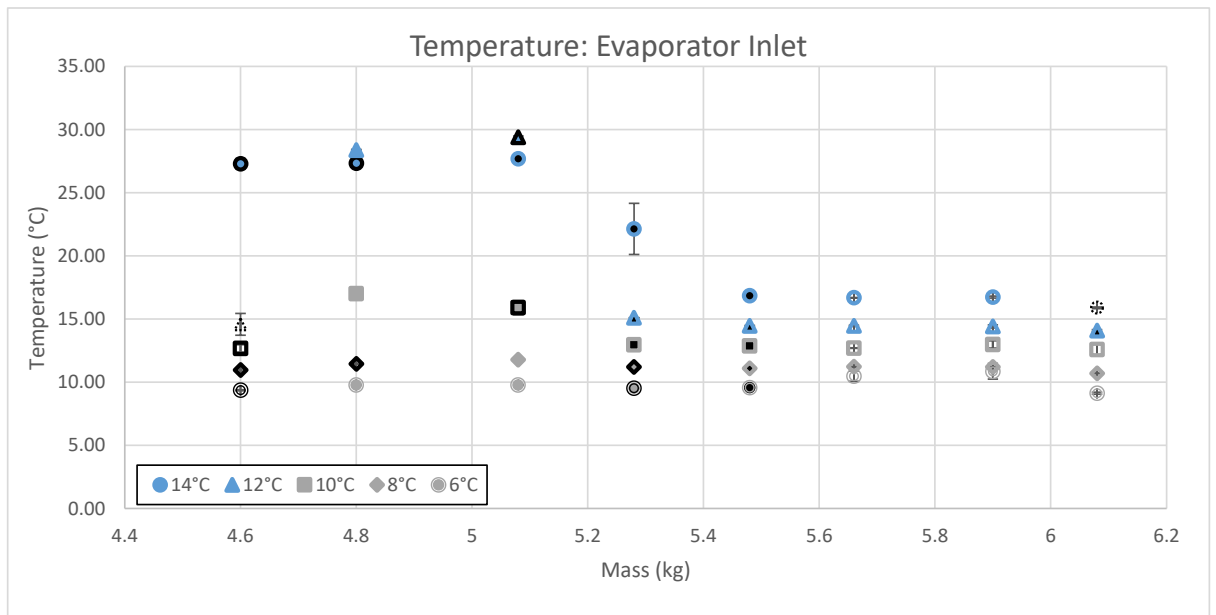
*Figure 125: Evaporator inlet temperature for various system charges and multiple subcooler inlet temperatures at 1000rpm pump speed. The evaporator inlet temperature decreases with decreasing subcooler temperature. **Note: The location of the temperature sensor results in the unexpectedly high values over the initial masss increaments***

The controlled hot water feed temperature is shown in Figure 126, the feed temperature has a variation of less than 3°C. The hot water return temperature is shown in Figure 127 , the hot water return temperature decreases with decreasing subcooler temperature.

Figure 126: Hot water feed temperature for various system charges and multiple subcooler inlet temperatures at 1000rpm pump speed. The controlled hot water feed temperature has a varation of approximetly 2°C over the entire test range.

Figure 127: Hot water return temperature for various system charges and multiple subcooler inlet temperatures at 1000rpm pump speed. The hot water return temperature decreases with decreasing subccoler temperature. The incremental change decreases with increasing system charge.

The expander inlet and outlet temperatures are shown in Figure 128 and Figure 129 respectively. The expander inlet temperature shows an overall increase with decreasing subcooler temperature. The expander outlet generally indicates an opposite trend with a reduction in subcooler temperature resulting in a reduction in expander outlet temperature.
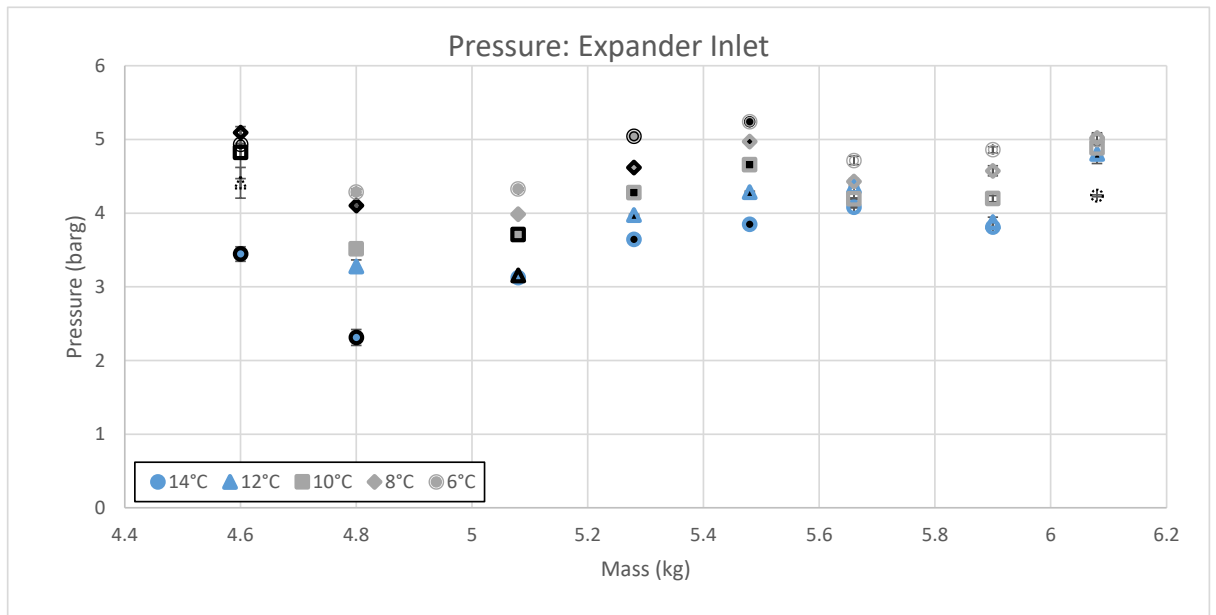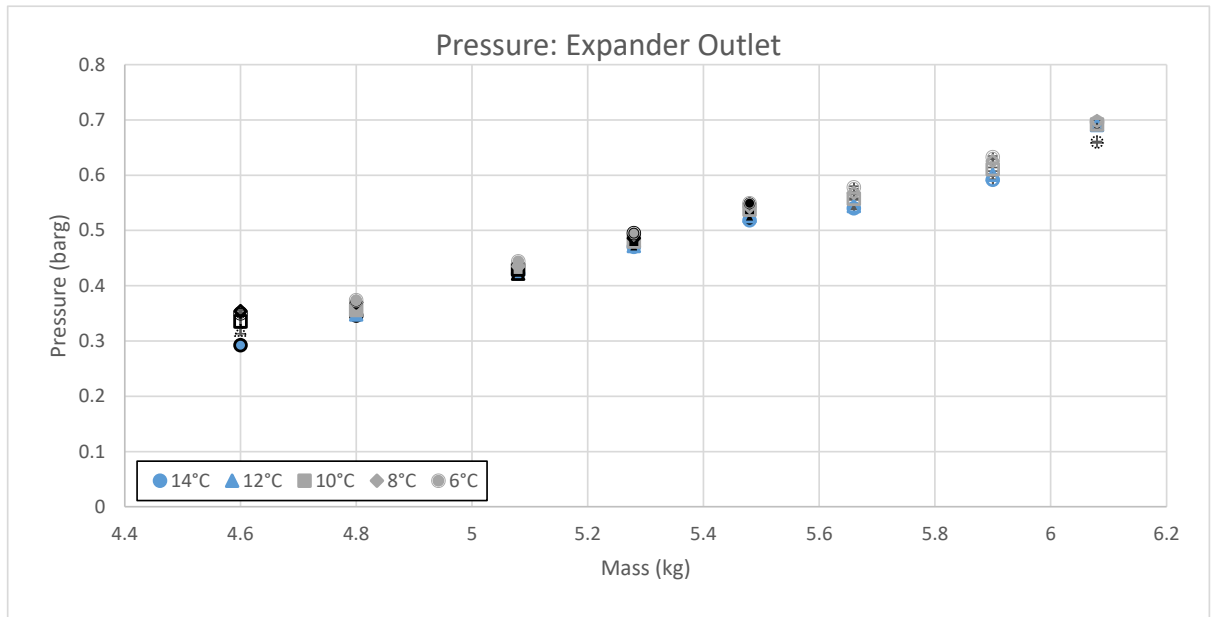
Figure 128: Expander inlet temperature for various system charges and multiple subcooler inlet temperatures at 1000rpm pump speed. The expander inlet temperature increases with decreaseing subcooler temperature.
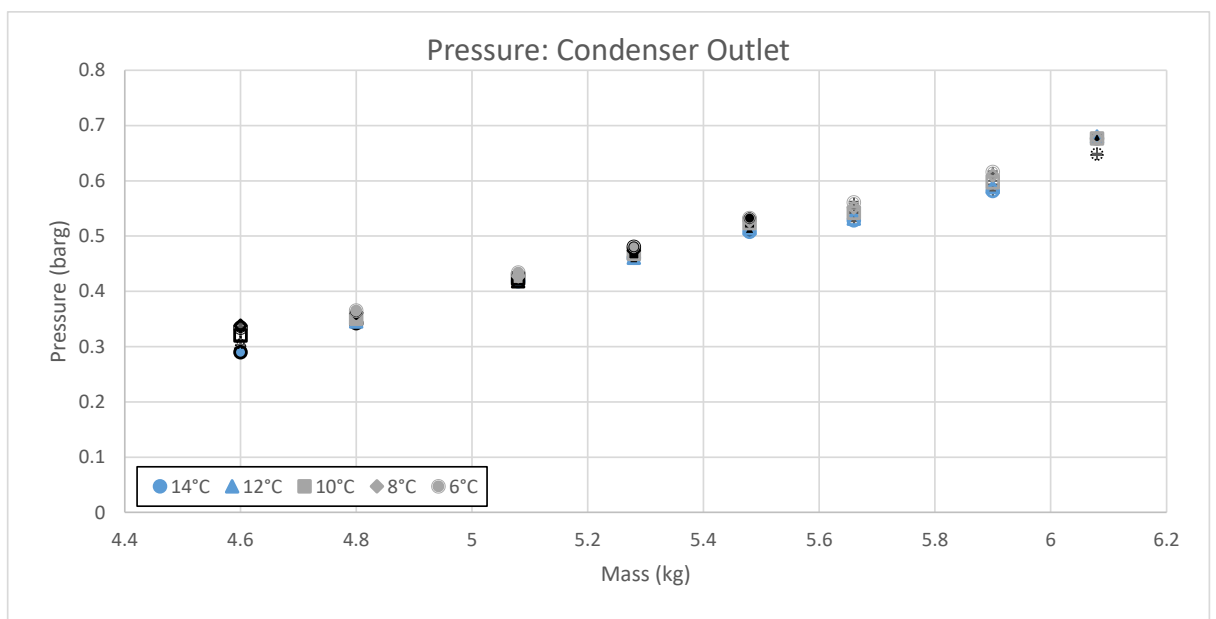

Figure 129: Expander outlet temperature for various system charges and multiple subcooler inlet temperatures at 1000rpm pump speed. There is no observably consistant trend between decreasing subcooler temperature and expander outlet temperature.

5.3. **Experimental results: 1200 Rpm pump speed**

Experimental results observation summary: The overall performance of the ORC system increases with decreasing subcooler temperature, the benefit decreases with increasing system mass. The high side system pressure increases with decreasing subcooler temperature, the incremental increase in pressure decreases with increasing system charge. The low pressure side of the system shows no significant change in pressure with decreasing subcooler temperature. The pump inlet and outlet temperature decrease accordingly, with a significant variation in evaporator inlet temperature over the entire test range. The expander inlet temperature increases with decreasing subcooler temperature, the effect of which decreases with increasing mass. The expander outlet temperature shows no observably consistent trend with temperature.

Overall Performance:

In a similar trend to the 1000rpm case the overall system performance of the ORC system increases with decreasing subcooler temperature. The increase in performance decreases with increasing system charge. The expander rotational speed and generated electrical output are shown in Figure 130 and Figure 131 respectively. In both cases the output of the ORC system increases with decreasing subcooler temperature, the degree of improvement decreases with increasing system charge. The maximum expander rotational speed and output power occur at 6.3kg of system charge generating 370W of power.
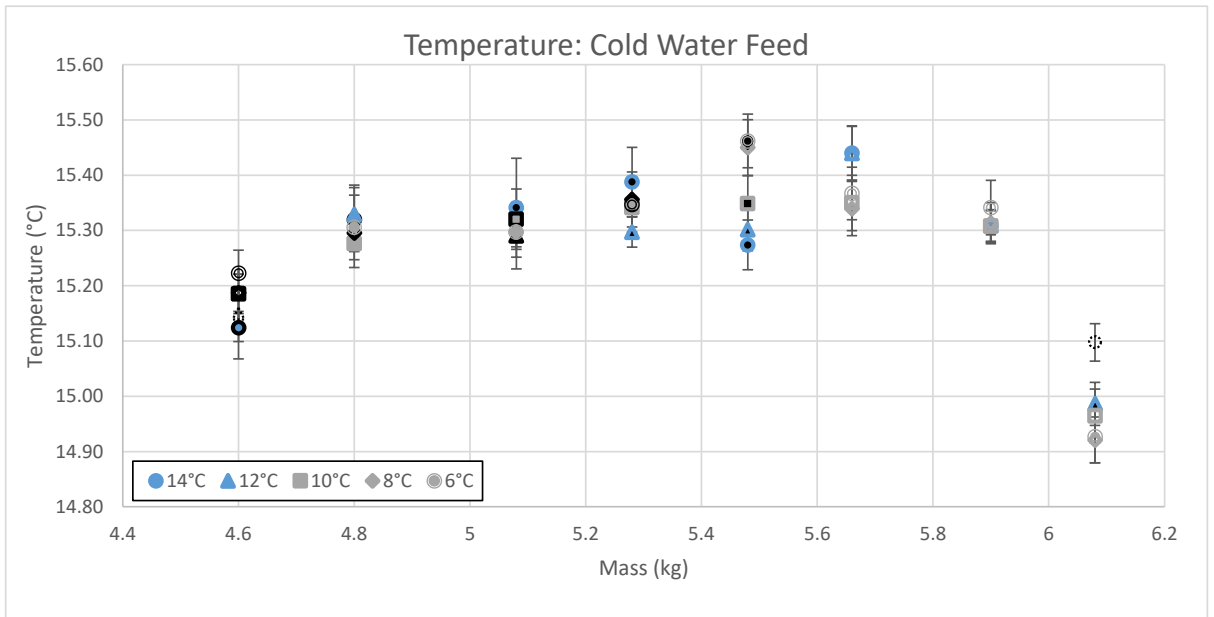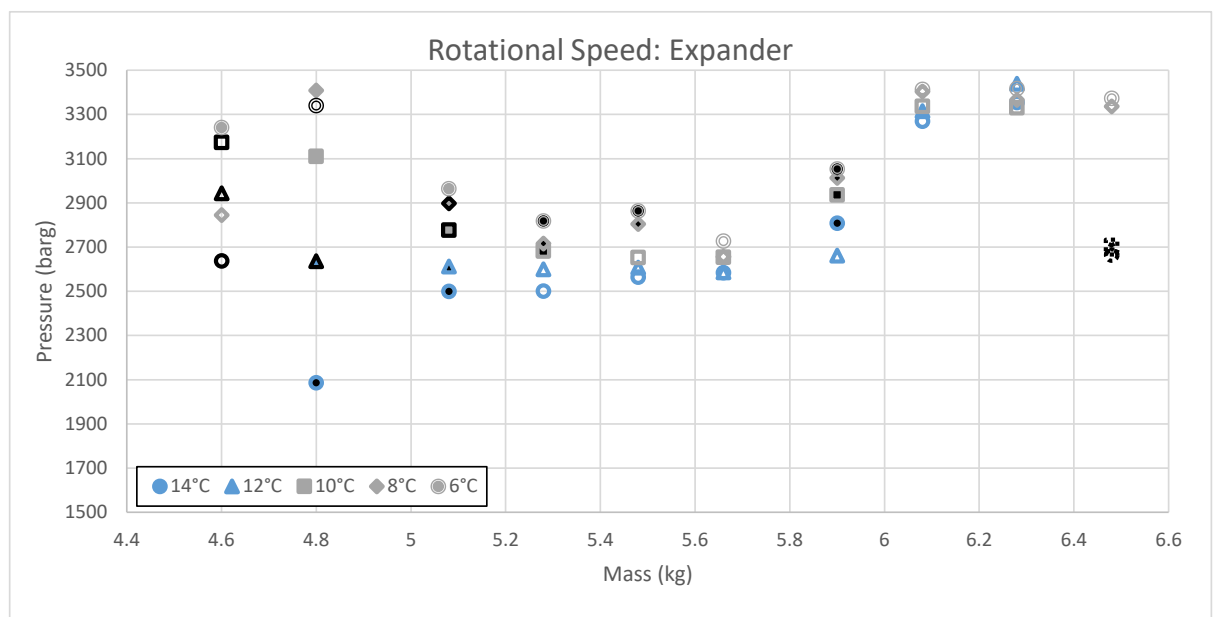

Figure 130: Expander rotational speed for various system charges and multiple subcooler inlet temperatures at 1200rpm pump speed. The expander rotatational speed increases with decreasing subcooler temperature. The degree of change decreases with increasing system charge.
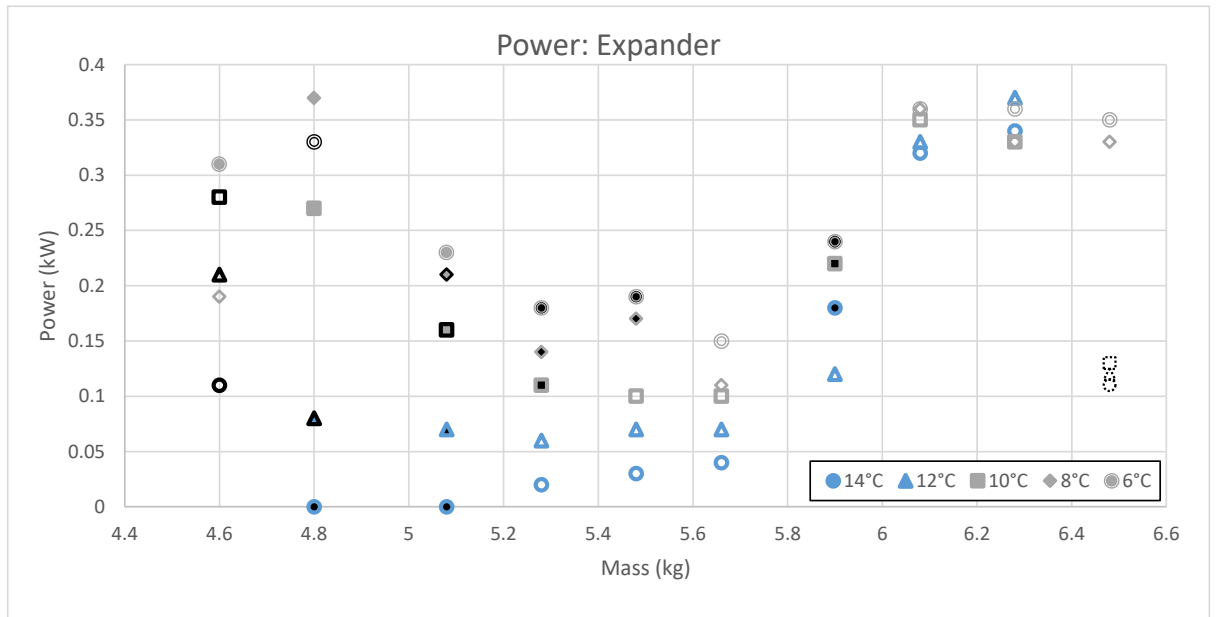
Figure 131: Expander power output for various system charges and multiple subcooler inlet temperatures at 1200rpm pump speed. The expander outlet power increases with decreasing subcooler temperature. The degree of change decreases with increasing system charge.

The consumed pump power is shown in Figure 132 the consumed pump power fluctuates between 0.1 and 0.13 kW with no obvious trend with decreasing subcooler temperature.
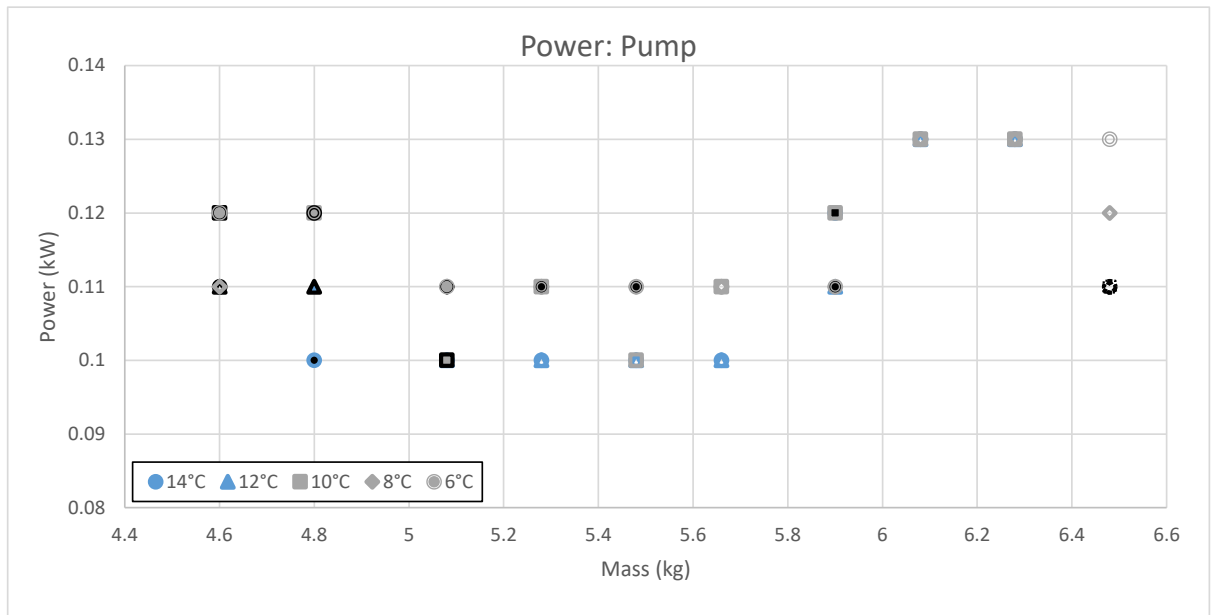
Figure 132: Consumed pump power for various system charges and multiple subcooler inlet temperatures at 1200rpm pump speed. The consumed pump power shows no observable trend with decreasing subcooler temperature.

Pressure:

The high pressure side of the system shown in Figure 133 and Figure 134 follows a very similar trend with an increase in pressure with decreasing subcooler temperature. The degree of increase reduces with increasing system charge. The maximum high side

pressure corresponds with 6.3kg of system charge and results in 6 barg in pressure at the expander inlet.
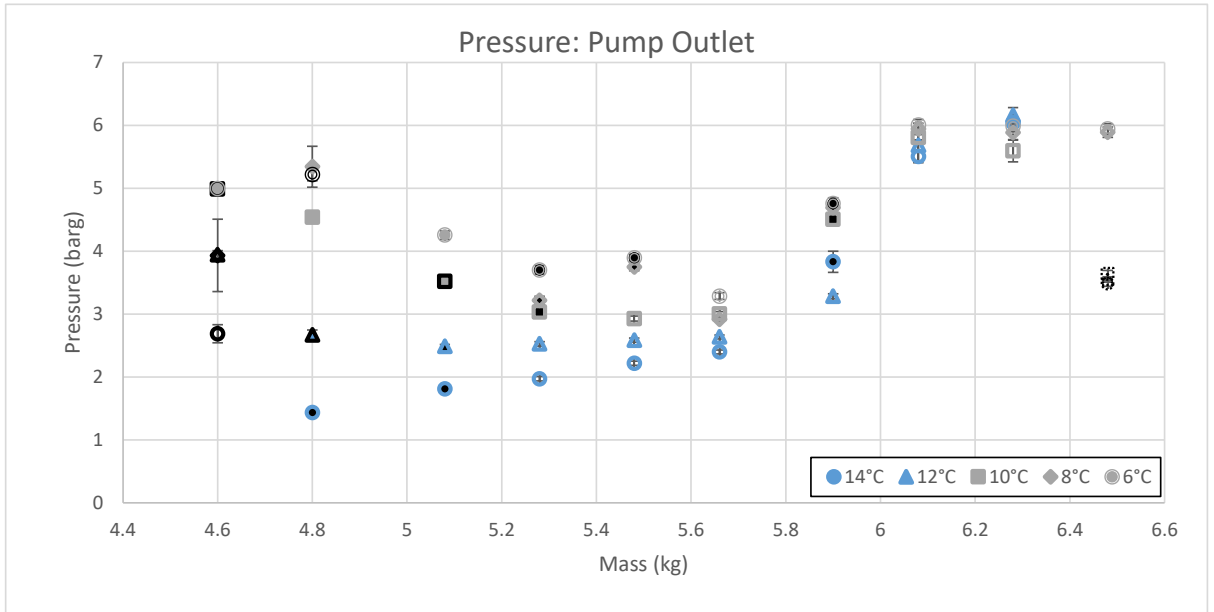
Figure 133: Pump output pressure for various system charges and multiple subcooler inlet temperatures at 1200rpm pump speed. The pump outlet pressure increases with decreasing subcooler temperature, the degree of change reduces with increasing system charge.
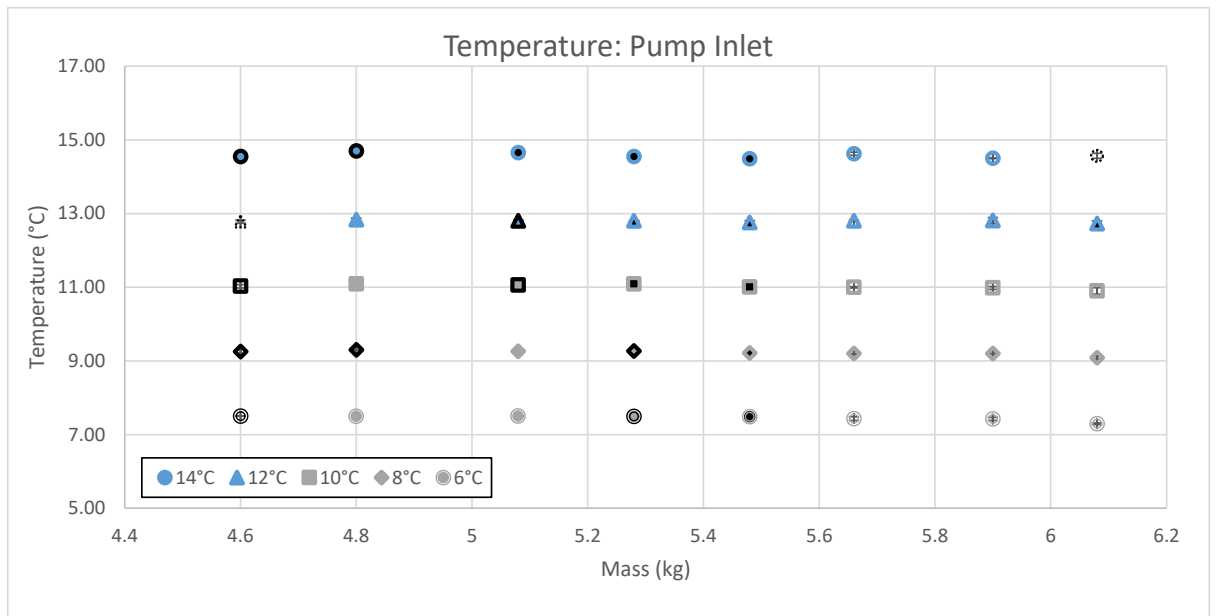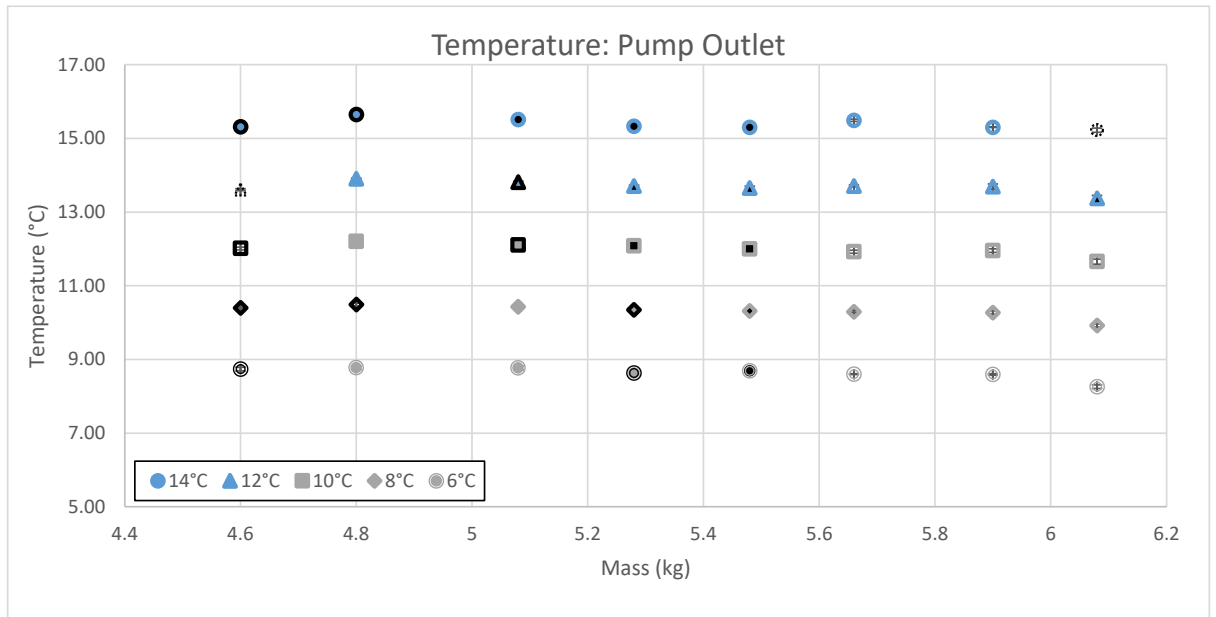

Figure 134: Expander inlet pressure for various system charges and multiple subcooler inlet temperatures at 1200rpm pump speed. The expander inlet pressure increases with decreasing subcooler temperature, the degree of change reduces with increasing system charge.

The low pressure side of the system is shown in Figure 135, Figure 136, Figure 137 and Figure 138, the expander outlet, condenser outlet, sub cooler inlet and pump inlet respectively. In all four cases there is no significant change in pressure with decreasing subcooler temperature in comparison to an increase in system charge.

Figure 135: Expander outlet pressure for various system charges and multiple subcooler inlet temperatures at 1200rpm pump speed. There is no significant change in expander outlet pressure with decreasing subcooler temperature.
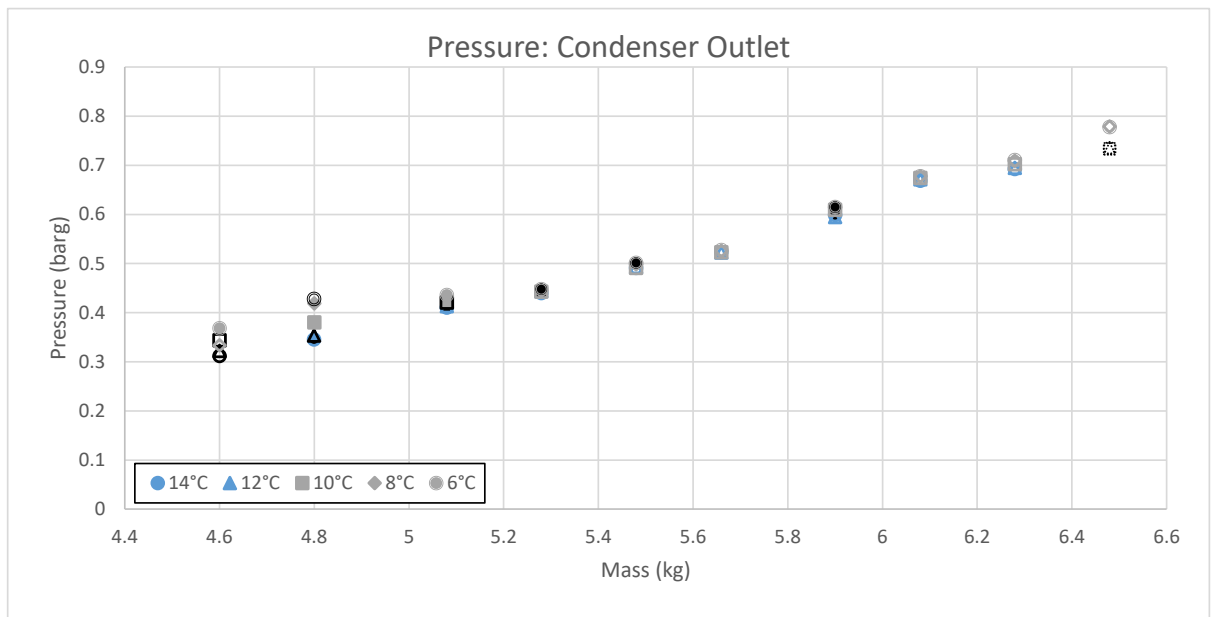
Figure 136: Condenser outlet pressure for various system charges and multiple subcooler inlet temperatures at 1200rpm pump speed. There is no significant change in condenser outlet pressure with decreasing subcooler temperature.
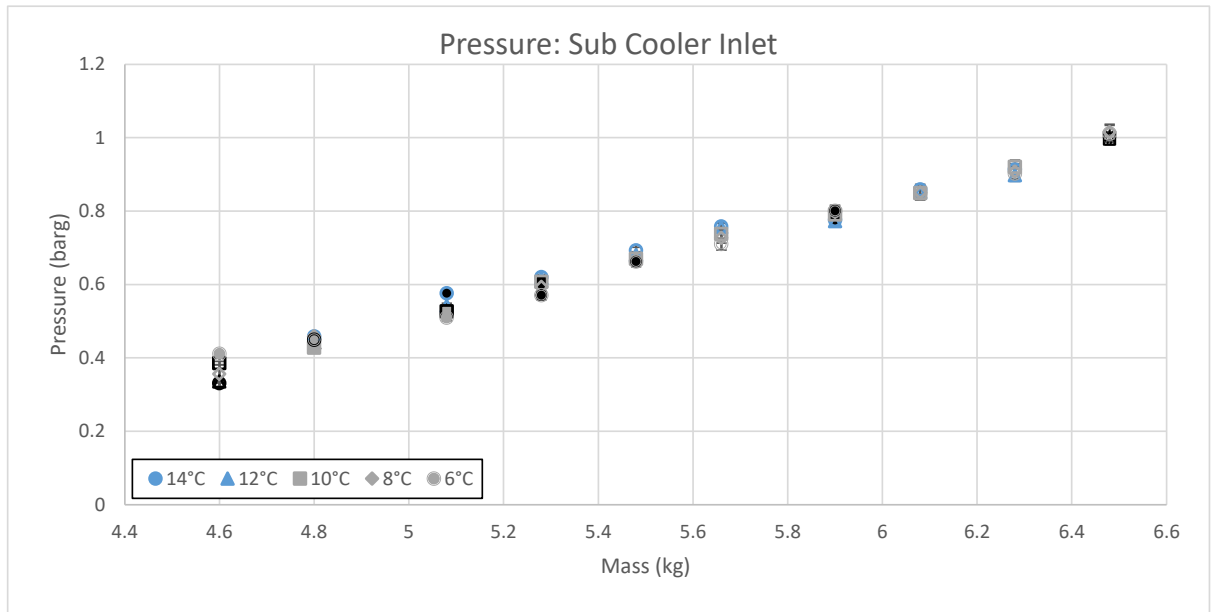
Figure 137: Sub cooler inlet pressure for various system charges and multiple subcooler inlet temperatures at 1200rpm pump speed. There is no significant change in subcooler inlet pressure with decreasing subcooler temperature.
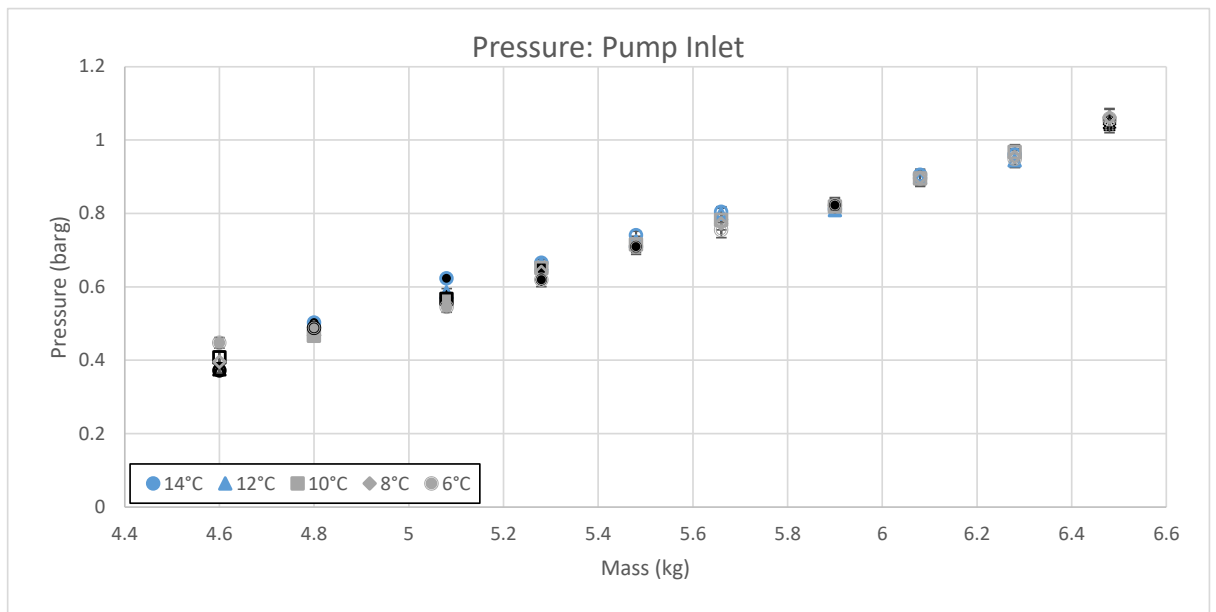
Figure 138: Pump inlet pressure for various system charges and multiple subcooler inlet temperatures at 1200rpm pump speed. There is no significant change in pump inlet pressure with decreasing subcooler temperature.

Temperature:

The cold water feed temperature is shown in Figure 139 with the return temperature shown in Figure 140. There is less than 1°C variation in temperature across the entire test range with a significantly small variation for each individual mass increment. The cold water return temperature shows an increase in temperature with a reduction in subcooler temperature.
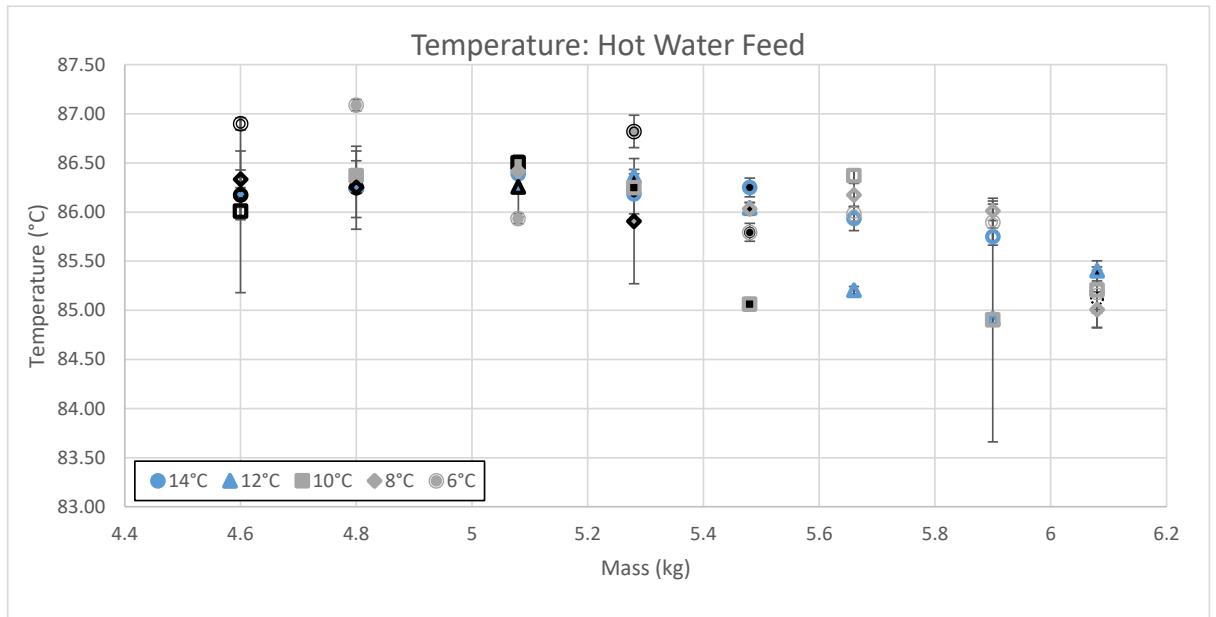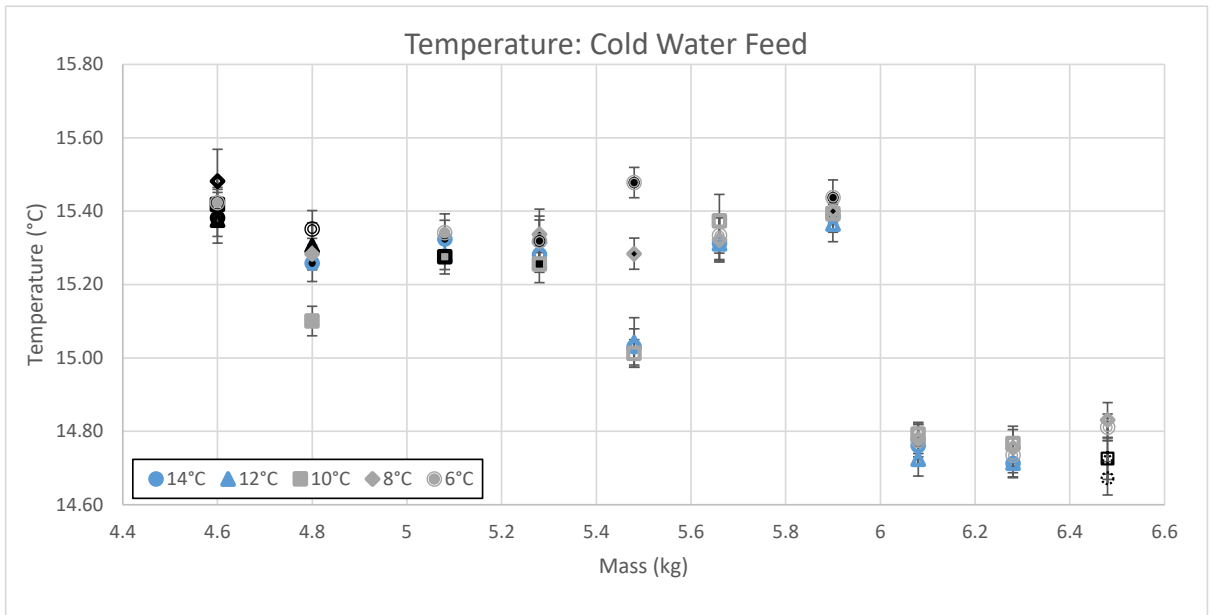
Figure 139: Cold water feed temperature for various system charges and multiple subcooler inlet temperatures at 1200rpm pump speed. The controlled cold water feed temperature has a variation of <1°C over the entire test range.
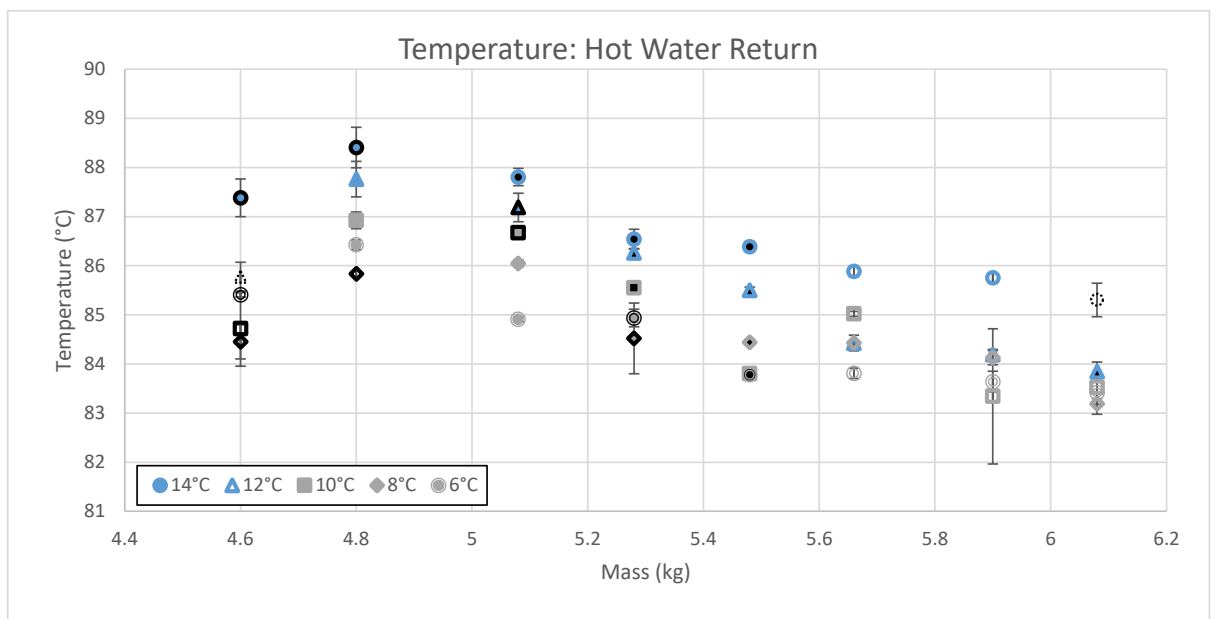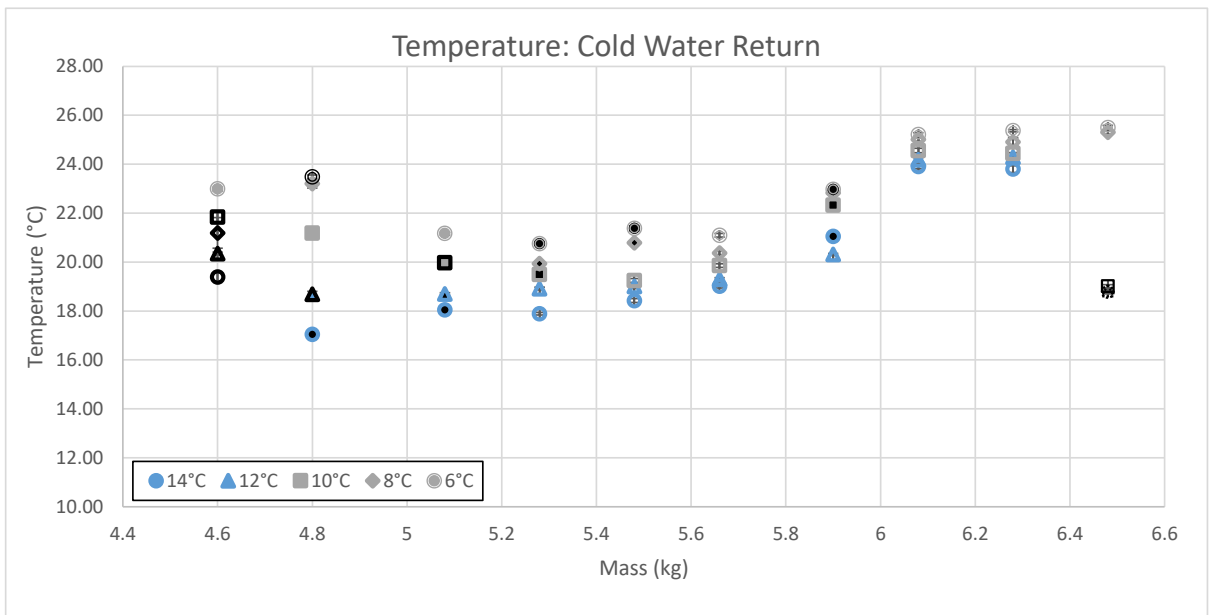

Figure 140: Cold water return temperature for various system charges and multiple subcooler inlet temperatures at 1200rpm pump speed. The cold water return temperature increases with decreasing subccoler temperature, the degree of change decreases with increasing mass

The condenser outlet temperature is shown in Figure 141 and it follows a similar trend to the cold water feed temperature with a variation of less than 1°C over the entire test range. There is no obvious or significant trend with decreasing sub cooler temperature.
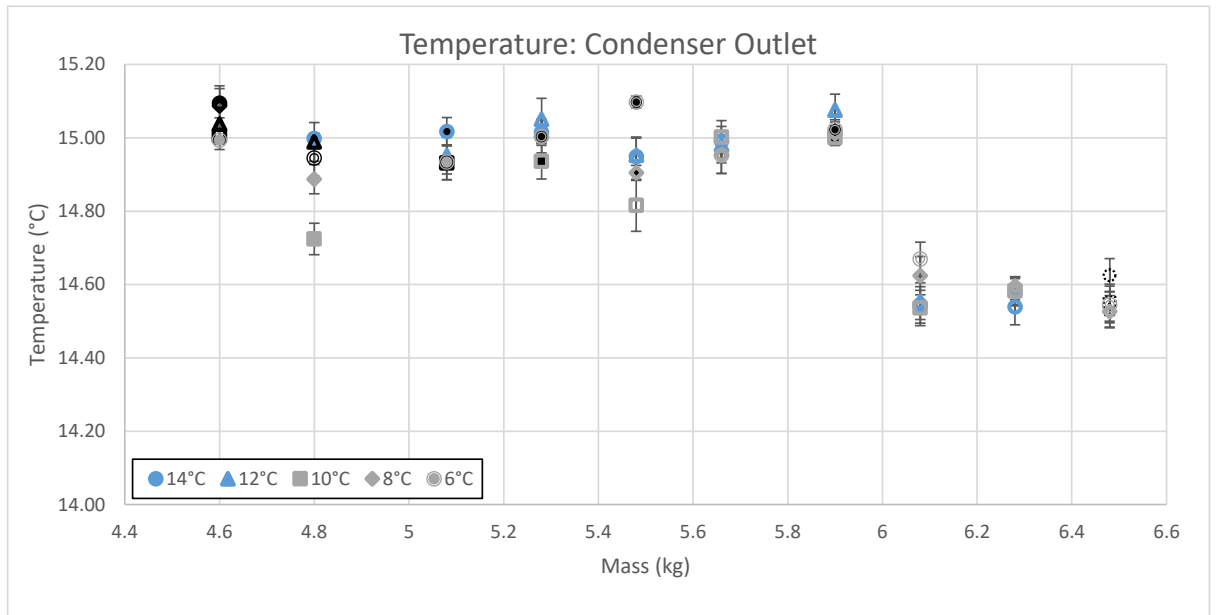
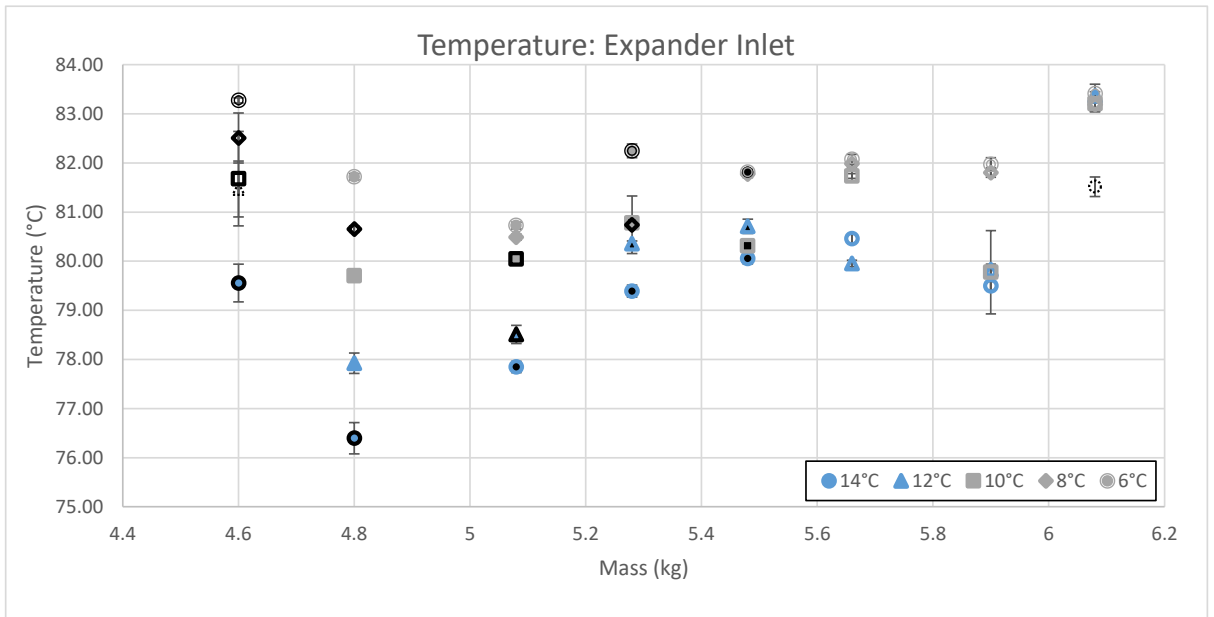*Figure 141: Condenser outlet temperature for various system charges and multiple subcooler inlet temperatures at 1200rpm pump speed. The condenser outlet temperature shows no observable trend with decreasing subccoler temperature. The values follow a similar pattern to the variation in cold water feed.*

The pump inlet and outlet temperature are shown in Figure 142 and Figure 143 respectively. The reduction in sub cooler temperature results in a corresponding reduction in both the pump inlet and outlet temperature.
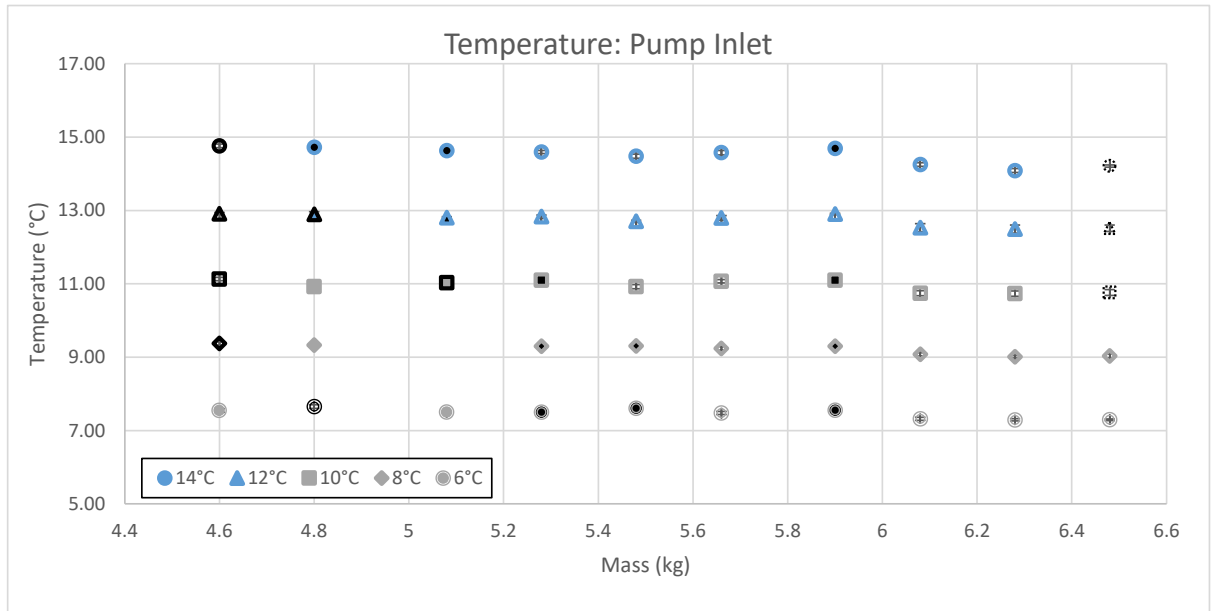
Figure 142: Pump inlet temperature for various system charges and multiple subcooler inlet temperatures at 1200rpm pump speed. The pump inlet temperature decreases with decreasing subcooler temperature
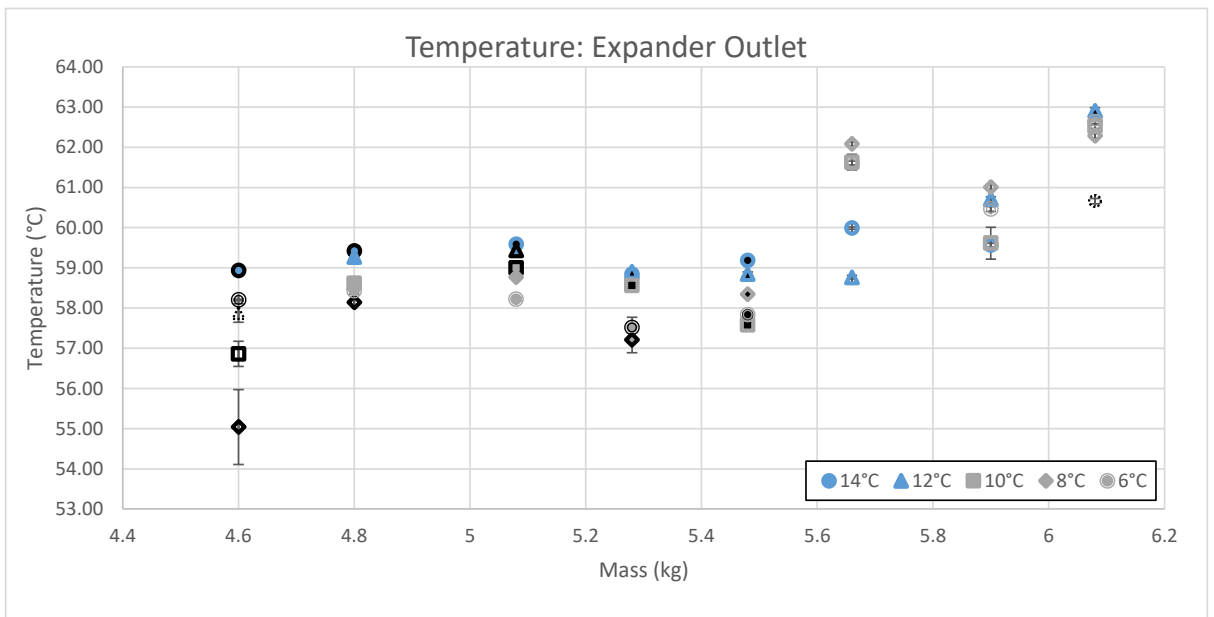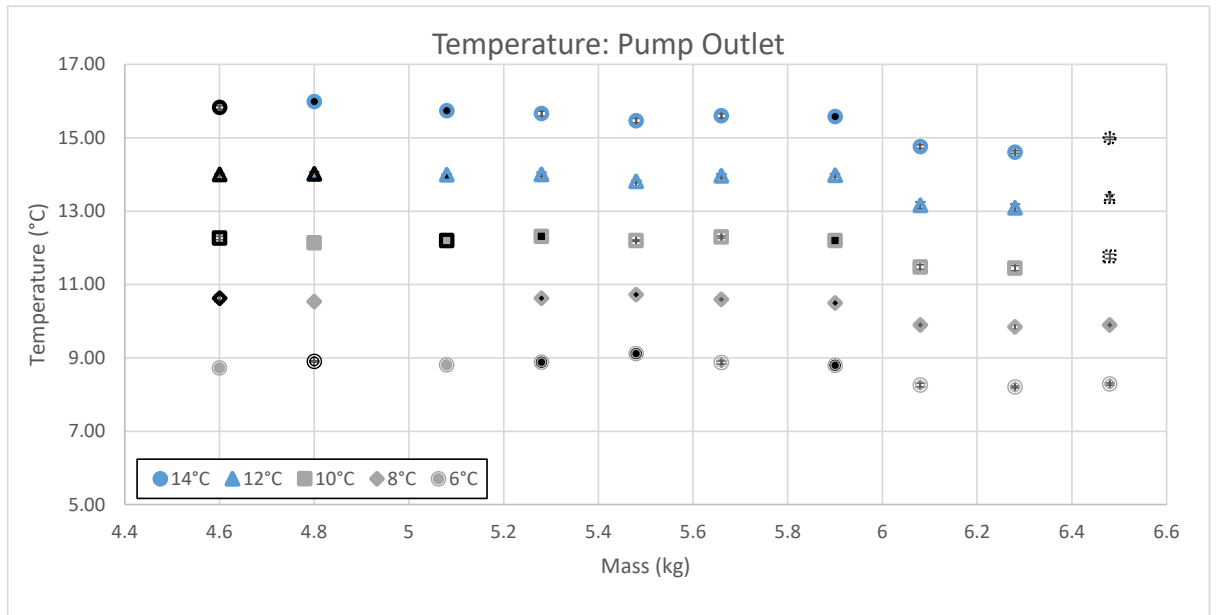
Figure 143: Pump outlet temperature for various system charges and multiple subcooler inlet temperatures at 1200rpm pump speed. The pump outlet temperature decreases with decreasing subcooler temperature.

The evaporator inlet temperature is shown in Figure 144, the reduction in subcooler temperature results in reduction in evaporator inlet temperature. The unexpectedly high temperature readings are a result of the temperature sensor location, which indirectly gives an indication of low ORC system flow.
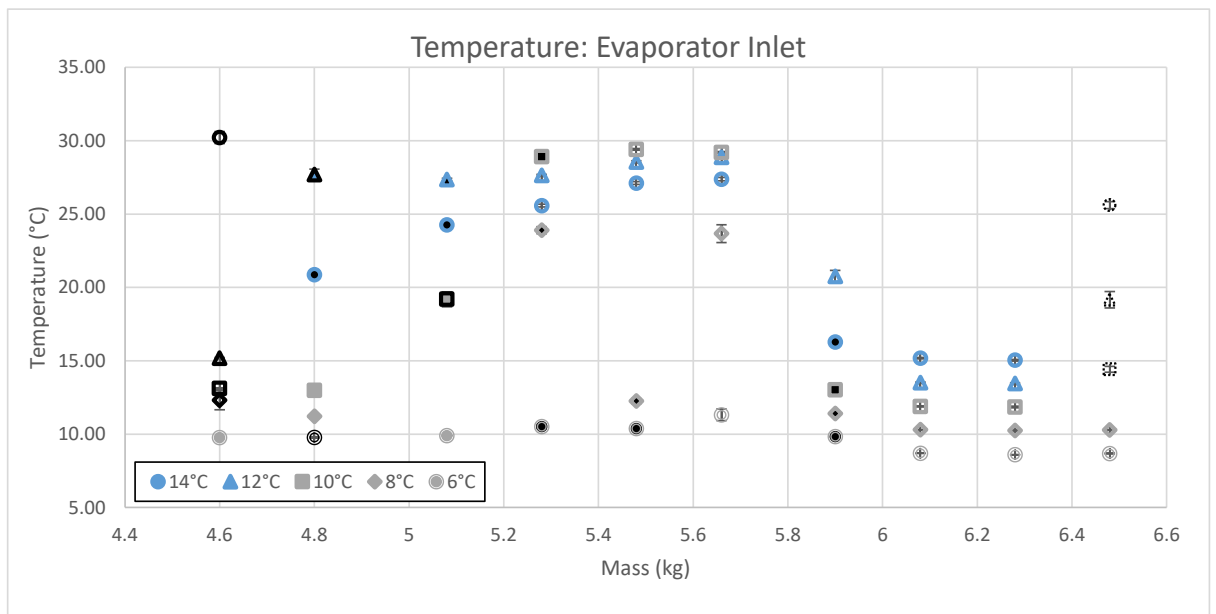
*Figure 144: Evaporator inlet temperature for various system charges and multiple subcooler inlet temperatures at 1200rpm pump speed. In general the evaportor inlet temperature decreases with decreasing subcooler temperature, this is particulary clear above 5.8kg of system charge. **Note: The location of the temperature sensor results in the unexpectedly high values over the initial masss increaments.***

The hot water feed and return temperature is shown Figure 145 and Figure 146 respectively. The hot water feed temperature has an overall variation of less than 3°C over the entire test range. The variation is significantly less for the majority of individual mass

increments. The hot water return temperature reduces with decreasing subcooler temperature.
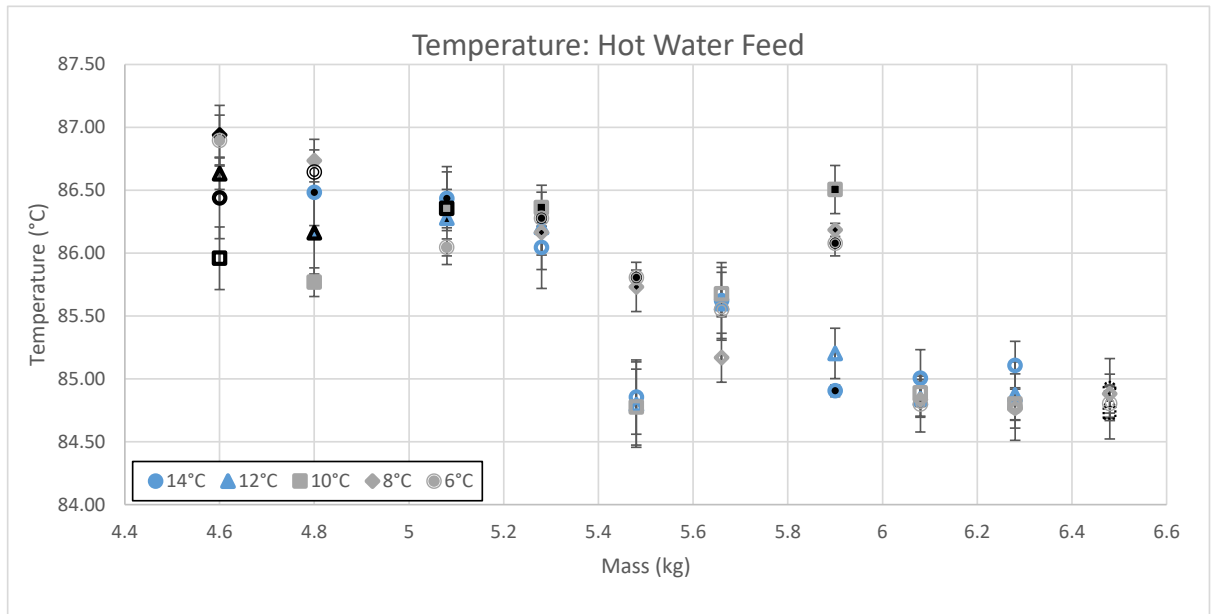
Figure 145: Hot water feed temperature for various system charges and multiple subcooler inlet temperatures at 1200rpm pump speed. The controlled hot water feed temperature has an overal variation of <2°C, for the most part the variation within each mass test is significantly less.
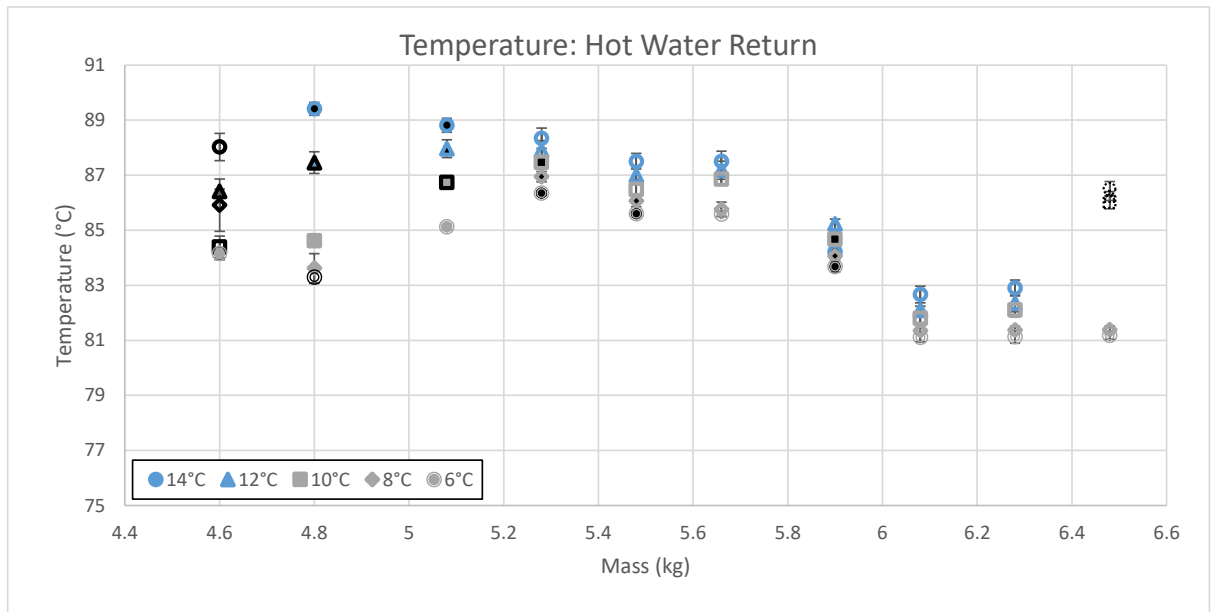
Figure 146: Hot water return temperature for various system charges and multiple subcooler inlet temperatures at 1200rpm pump speed. The hotwater return temperature decreases with decreasing subcooler temperature. The degreee of change reduces with increasing mass.

The expander inlet temperature is shown in Figure 147 with the expander outlet temperature shown in Figure 148. The expander inlet temperature increases with decreasing subcooler temperature, with a lesser degree of change with increasing system charge. The expander outlet temperature in this case shows clearly observable trend with decreasing subcooler temperature.
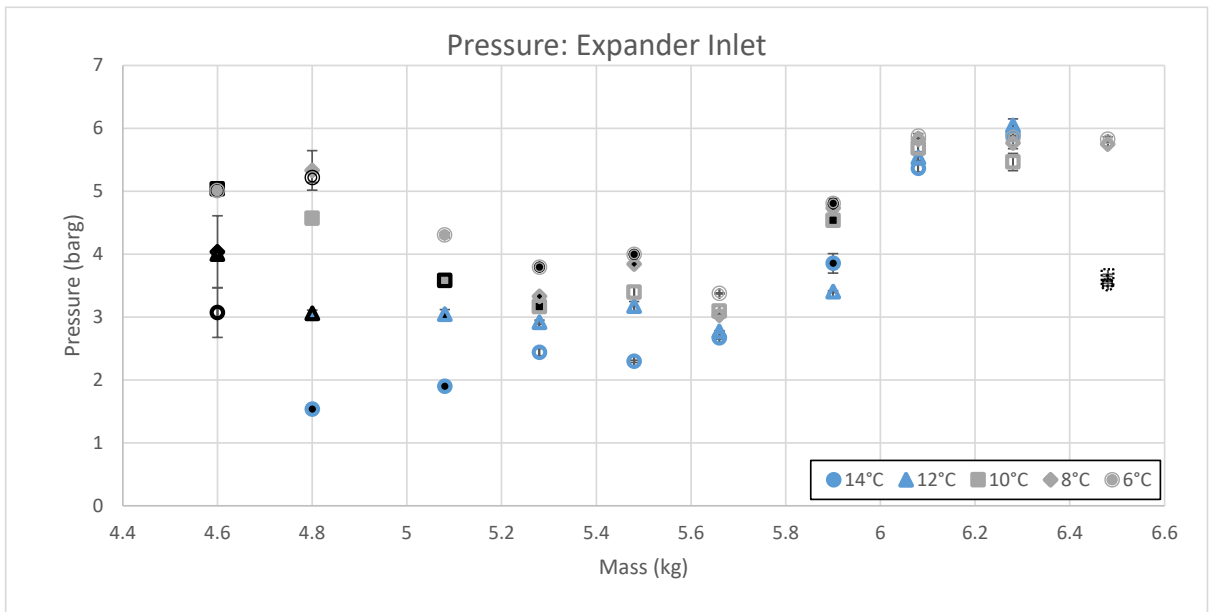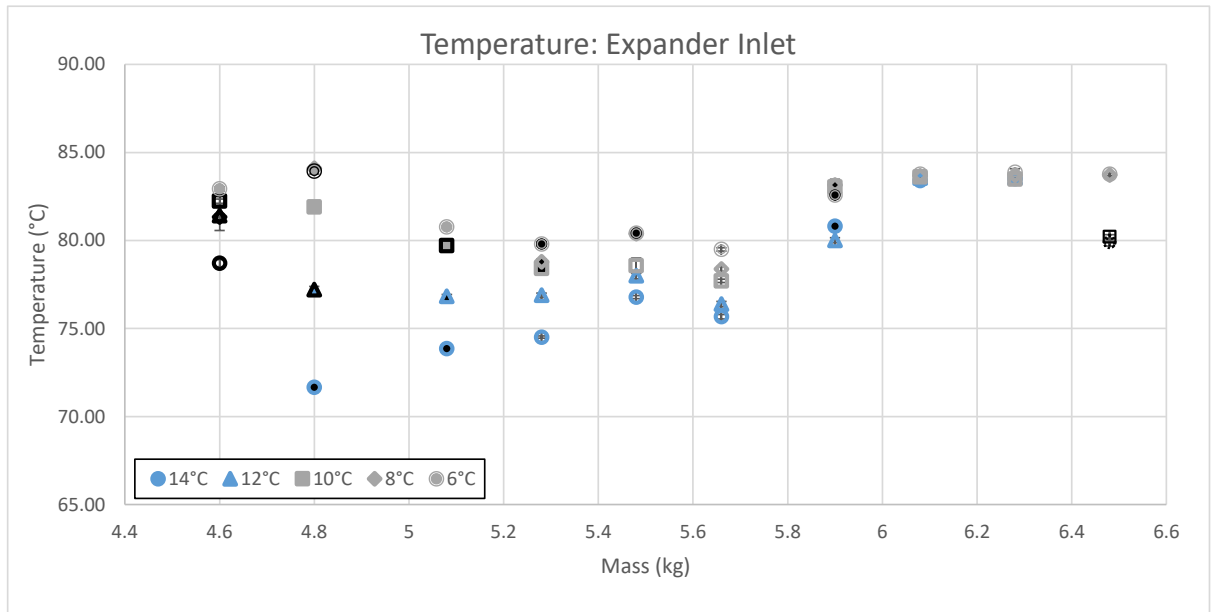
Figure 147: Expander inlet temperature for various system charges and multiple subcooler inlet temperatures at 1200rpm pump speed. The expander inlet temperature increases with decreasing subcooler temperature, the degree of change decreases with increasing mass increment.
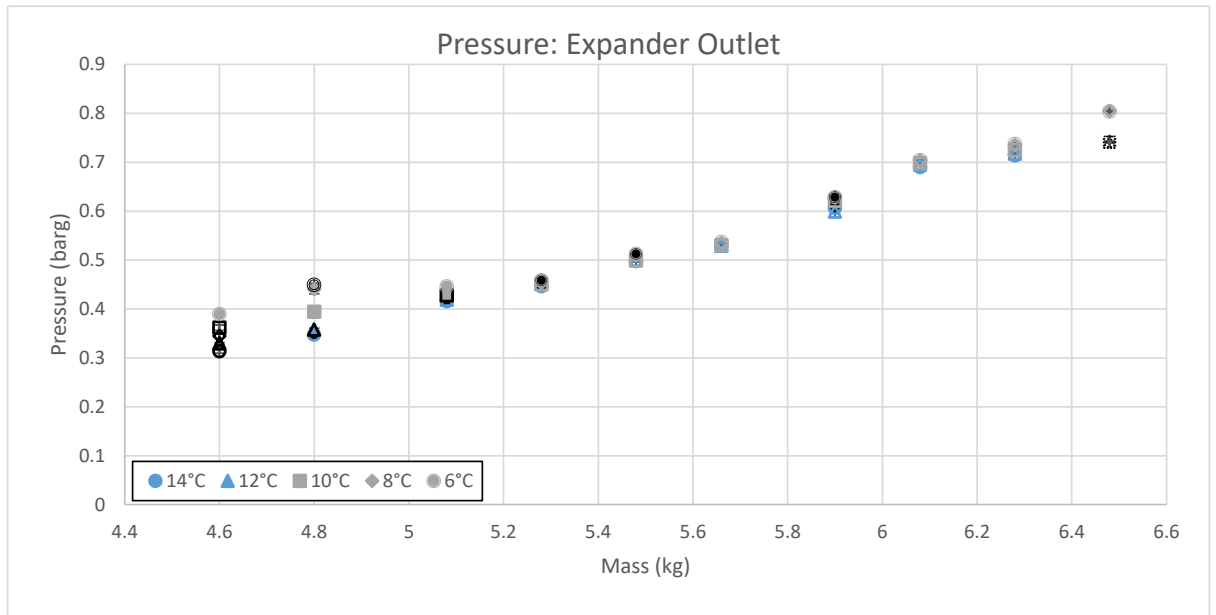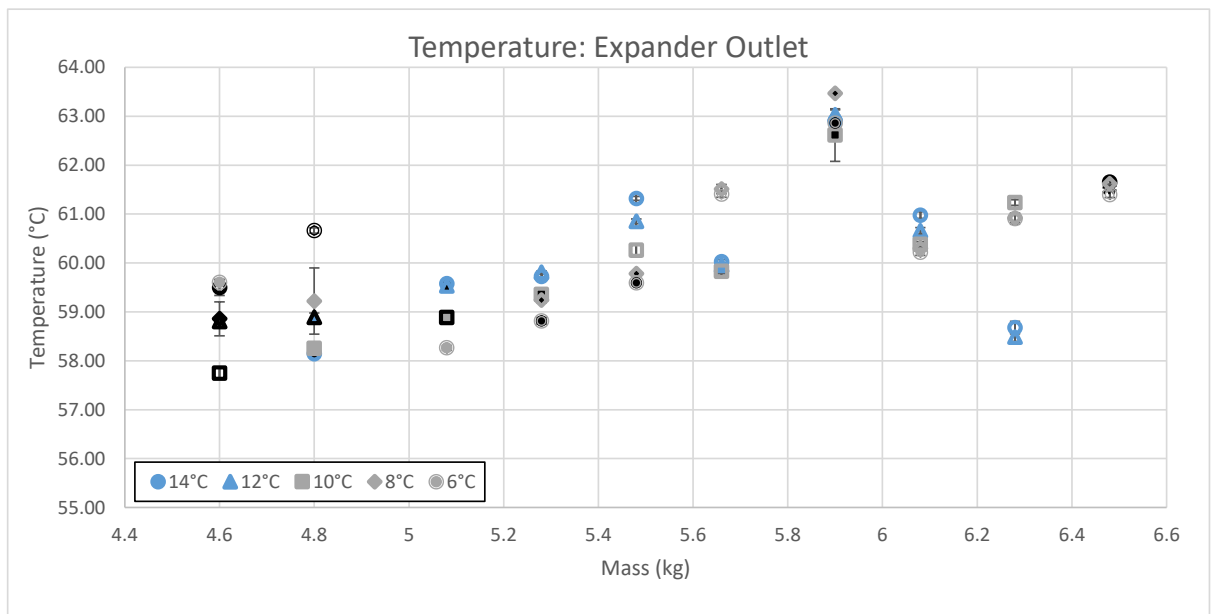

Figure 148: Expander outlet temperature for various system charges and multiple subcooler inlet temperatures at 1200rpm pump speed. The expander outlet temperature shows no observable trend with decreasing subcooler temperature.

5.4. **Analysis & Discussion**

The results of the 800 rpm test case indicate that the base test point already has sufficient subcooling in order to mitigate the impacts of cavitation. Therefore any increase in system subcooling has no significant effect on the expander output. The increase in system charge therefore only results in a deterioration in system performance.

The effect of sub-cooling on the performance of the ORC system is prominent in both the 1000 and 1200rpm pump test run. In both cases decreasing subcooler temperature

increases the overall performance of the system, the degree of improvement in both cases reduces with increasing system charge. The sub cooling has negligible effect on the low side pressure of the system, whereas the increasing mass continues to have a significant effect.

The interaction between the system charge and the system subcooling follows a fairly consistent trend for both the 1000 and 1200rpm case with the 1000rpm case shown in Figure 149.
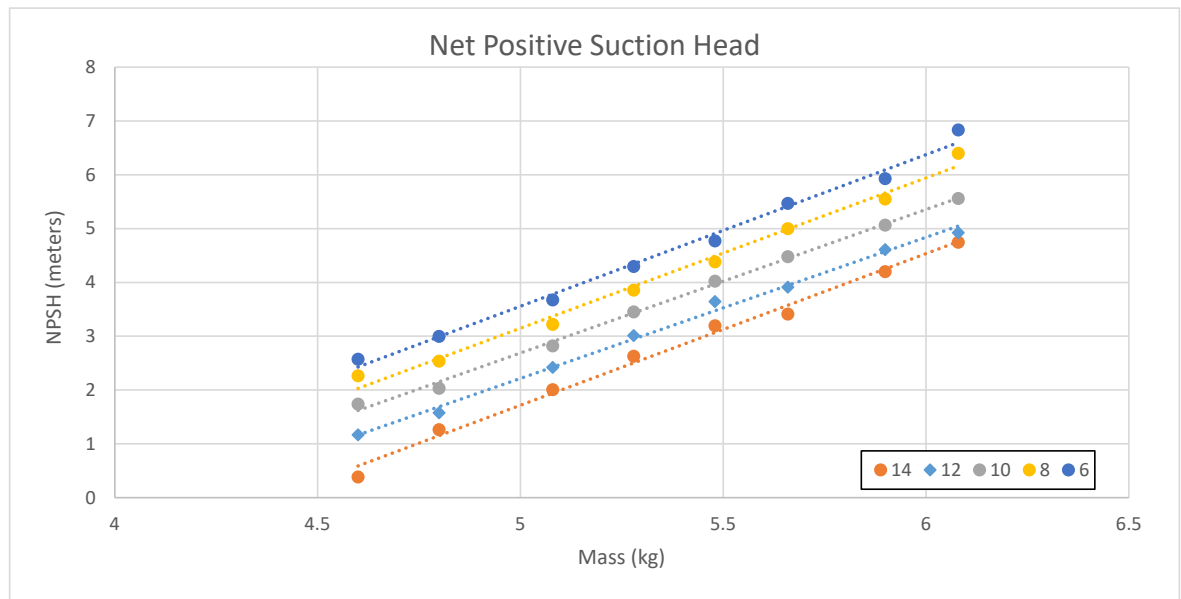
Figure 149: Effect of subcooling and increasing system charge on the NPSH at 1000rpm and 5 pump inlet temperatures.

In theory operational tests cases which have the same NPSH would result in similar output performances of the pump. This holds reasonably true for the 1000 rpm case particularly between 5 and 5.6 kg of system charge. However, below this range the system shows signs of instability and you would also expect the output of the system to converge with increasing NPSH. If you treat each subcooling case as separate increasing mass test run as was conducted in the last chapter then the output of each case increases to a maximum point (at 5.5kg) then begins to decline.

The 1200rpm case differs from the 1000 rpm case where a significant step up in system output occurs after 5.6kg of charge where by the output of the system increases significantly with system charge and the subcooling has minor effect in comparison. The output of the system then plateaus.

Tradeoff between system charge and subcooling

Various attempts have been made to numerically compare the trade offs between liquid column height and subcooling, using the collated data. However, neither data set conforms to the idea that the required NPSH can be meet by subcooling alone, liquid column height alone or a combination of the two. This issue can be illustrated from a comparison of the output power between the 5.9kg and 6.08 kg of system charge case at 1200rpm, as shown in Figure 150.
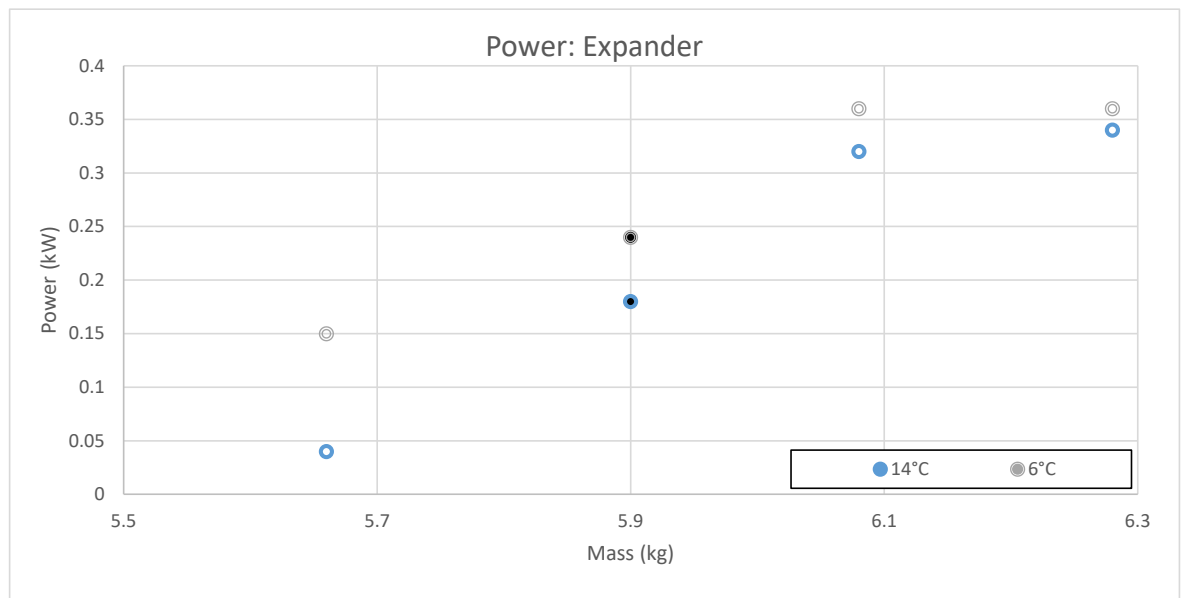
Figure 150: Shortened data set of the expander power output at 1200rpm.

Considering the 5.9kg of system charge at a subcooling temperature of 14°C (which is 1°C colder than the condenser temperature), a 200g increase in system charge resulted in an increase in approximately 120W of power. Compared to only a 50W gain for a reduction in subcooler temperature to 6°C. Assuming, 7/8" copper tubing, the 200g increase in system charge is equivalent to a liquid level height increase of approximate 350mm. In practice an increase is 350mm is significantly less system complexity and cost compared to the incorporation of a subcooler and sourcing a lower temperature source. However, when this liquid column idea only was applied to Test system 1 in Chapter 5 the system failed to operate in stable manner. Where the maximum output power reached 250W at 1200 rpm and 300 W for the 1000 rpm case, which is the same as the maximum output power for Test system 2 at 1000rpm.

Test system 1 and 2 comparison

The maximum output power of test system 1 reached 300W based on a 1000 rpm pump speed. The maximum output power of test system 2 of 370W occurred at 1200 rpm at a subcooler supply temperature of 12°C. Although, there is an increase in maximum output

power for Test system 2, the overall system efficiency is 3.6% compared to 3.7% for the 1000 rpm case. The back work ratio is also 2.8 compared with 3%. Based on these simple calculations it becomes evident that the increased complexity in order to reach the higher pump speed of Test system 2 provides no benefit based on the calculated results.

5.5. **Summary**

The effects of liquid column height and subcooling on the micro-scale ORC system show that decreasing subcooler temperature increases the overall performance of the system, if the pump is cavitating. However, if there is sufficient liquid column height in order for the pump to operate properly, decreasing subcooler temperature has a negative impact on the system performance. The increasing of mass with decreasing sub cooler temperature follows a fairly consistent trend. However, when compared against the liquid only case the additional complexity, capital cost and lower temperature cold sink only results in a 0.1% increase in overall system efficiency. It is therefore difficult to justify the addition of subcooling to increase the operational range of the pump, in this organic Rankine cycle test system.

Chapter 6 – Effect of bypass and Liquid Column Height on ORC System performance

In a previous chapter the effect of system mass and liquid column height was investigated to determine its impact on the performance of the ORC system and in particular its effect on pump cavitation. The increase in system mass significantly improved the ORC performance, however, operation at the highest pump speed was still subjected to flow problems. The 2.3m liquid column height was insufficient to cover the full pump operational range. In order to try and reach the full potential of the pump and thus maximise the performance of the ORC system, the two other commonly used cavitation mitigation techniques, subcooling and pump bypass, have been investigated. The combined effects of subcooling and liquid column height in the last chapter and combined effects of pump bypass and liquid column height in this chapter. The experimental test rig was therefore adapted to include a subcooler and pump bypass valve (Test System 2).

In order to assess the combined effects of pump bypass and liquid column height the pump bypass valve was opened from 0°C to 25°C in 5° increments, with the remaining ORC parameters held constant. This test was then repeated for increasing mass increments of 200g. The resulting data set has been presented for the three pump speeds of 800, 1000 and 1200 rpm.

Table 8: Experimental Liquid level Indication: Bypass

Symbol style	Liquid level (m)	Sight glass number
△	< 0.6	< S9
▲	0.6-0.85	S9-S8
◮	0.85-1.1	S8-S6
▲	1.1-1.6	S6-S5
△	1.6-2.1	S5-S4
⬮	> 2.1	>S4

6.1. **Experimental results: 800 rpm**

Experimental results observation summary: Up to 15° bypass angle the pump bypass had negligible effect on the overall performance of the ORC system. Further increase in bypass angle resulted in a deterioration in system performance. This was also observed in the high pressure side of the system. In the low pressure side of the system, up to 15° bypass angle had negligible effect on the pressure. Further increase in bypass angle results in an increase in pressure. The temperature from the pump inlet to the evaporator inlet showed no change up to 15°, past this point there was an increase in temperature.

Overall performance:

The overall performance of the bypass valve at varying levels of system charge is shown in Figure 151, Figure 152 and Figure 153, the expander rotational speed, output power and consumed pump power. Increasing degree of bypass opening angle has a negative effect on overall system performance. In terms of both the expander rotational speed and the generated expander output power, there is little change in output from 0 to 15° after which there is significant deterioration. The consumed pump power fluctuates between 0.07 and 0.11 kW with no observable change with increasing bypass angle.
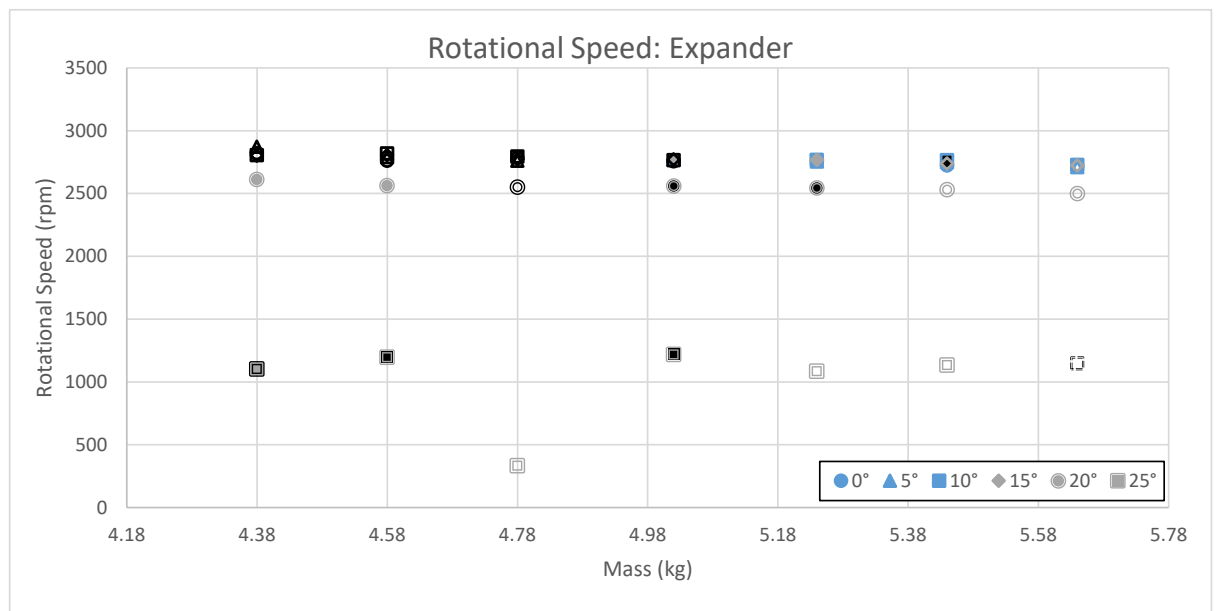
Figure 151: Expander Rotational speed for various system charges and multiple bypass valve postitions at 800rpm pump speed. Increasing the bypass opening angle has negligable effect upto 15° after which a further increase results in a significant reduction in expander rotational speed.
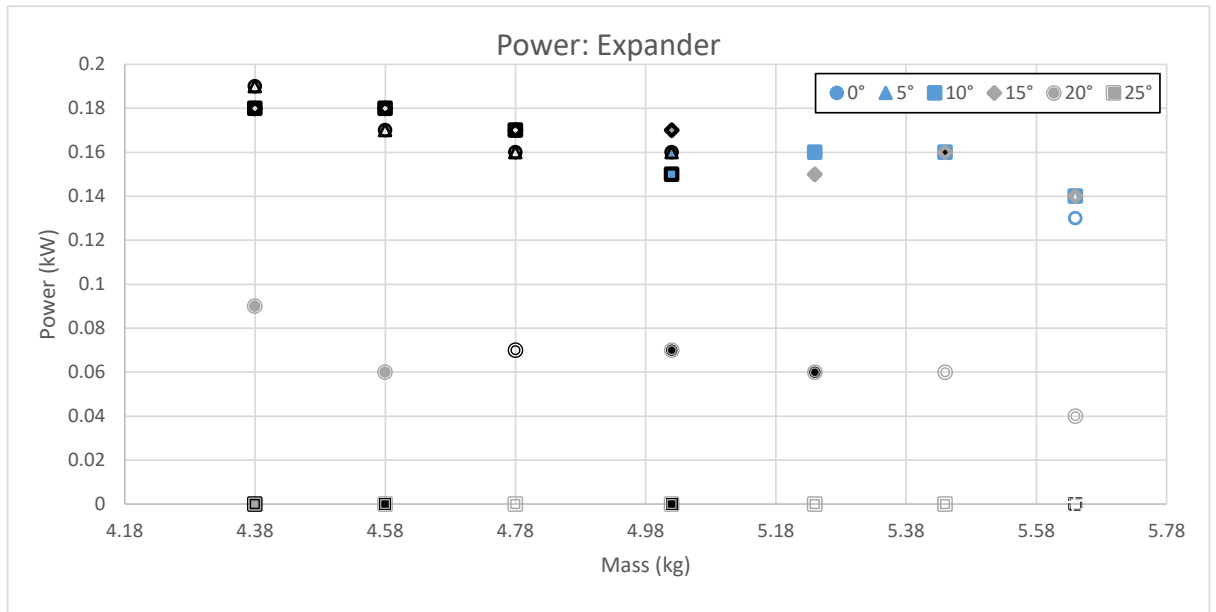
Figure 152: Expander power output for various system charges and multiple bypass valve postitions at 800rpm pump speed. Increasing the bypass opening angle past 15° results in a significant redution in expander output power.
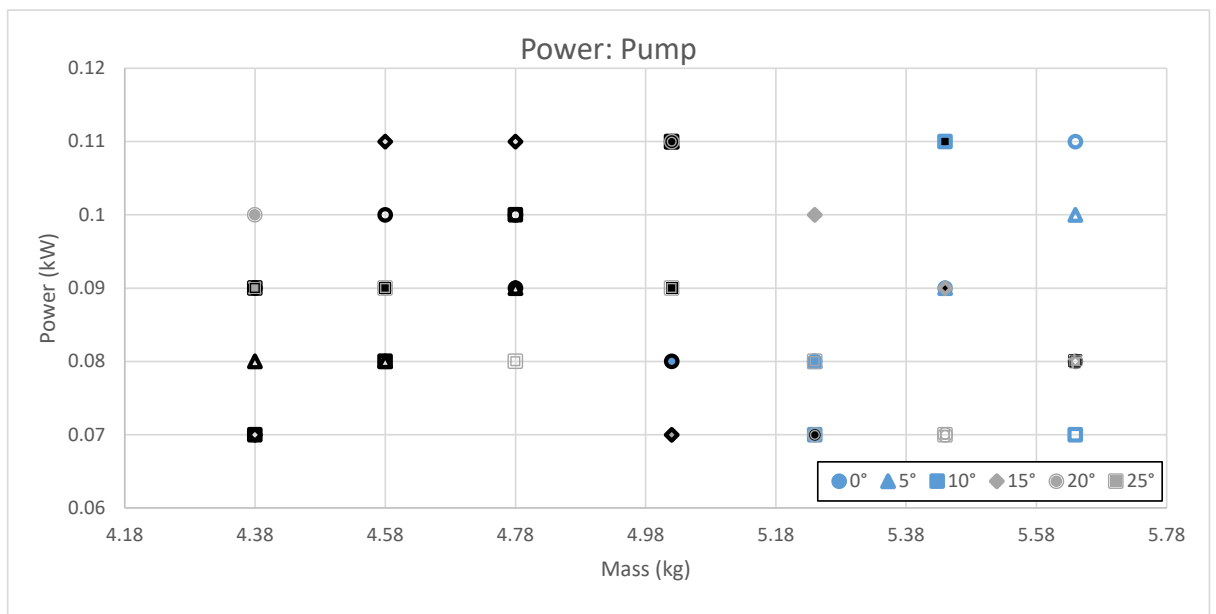
Figure 153: Expander consumed pump power for various system charges and multiple bypass valve postitions at 800rpm pump speed. The low resoultion of the power meter makes it diffiuclt to assess the effect of bypass angle with pump power consumption.

Pressure:

The high pressure side of the system is shown in Figure 154 and Figure 155 at the pump outlet and pump inlet. The trend at both the pump inlet and outlet is the same there is no significant change in pressure upto a bypass angle of 15°, further increase results is a significant reduction in high side system pressure.

Figure 154: Pump outlet pressure for various system charges and multiple bypass valve postitions at 800rpm pump speed. Upto 15° opening angle the is no significant changes in pressure with bypass valve angle. Further increase results in a significant drop off in pump outlet pressure.
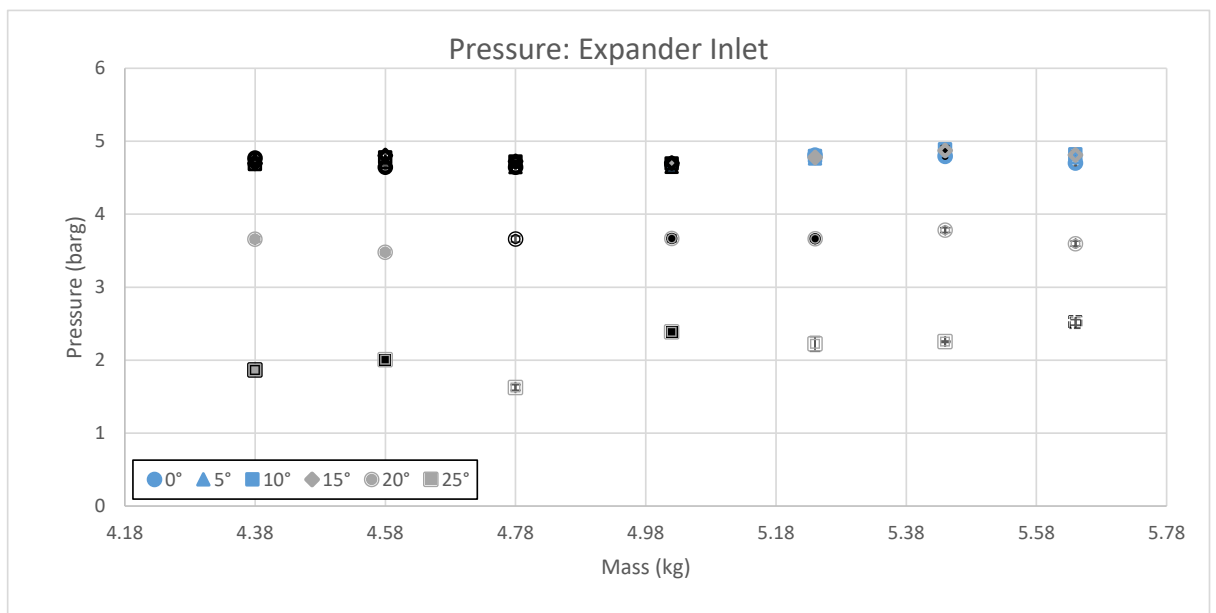
Figure 155: Expander inlet pressure for various system charges and multiple bypass valve postitions at 800rpm pump speed. Upto 15° there is no significant change in expander inlet pressure with bypass opening angle. Further increase results in a singificant reduction in expander inlet pressure.

The low pressure side of the system at the expander outlet and condenser outlet shown in Figure 156 and Figure 157, show no significant change in pressure with increasing bypass opening angle in comparison to increasing system charge.
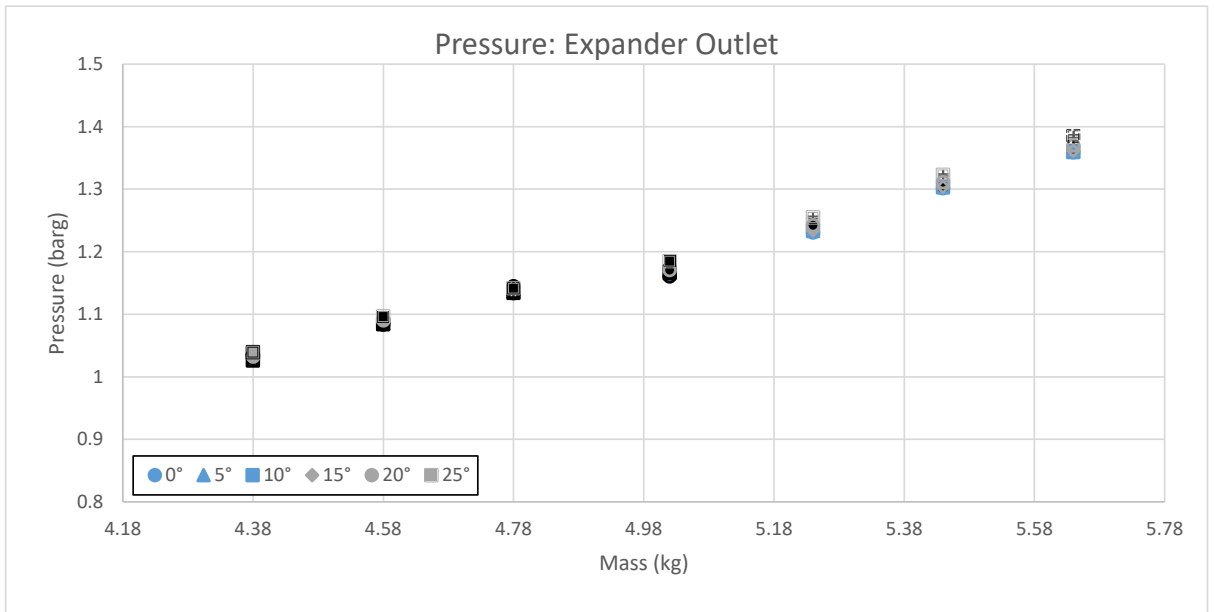
Figure 156: Expander outlet pressure for various system charges and multiple bypass valve postitions at 800rpm pump speed. The bypass opening angle has negliable effect on the expander outlet pressure incomparison to the system mass.
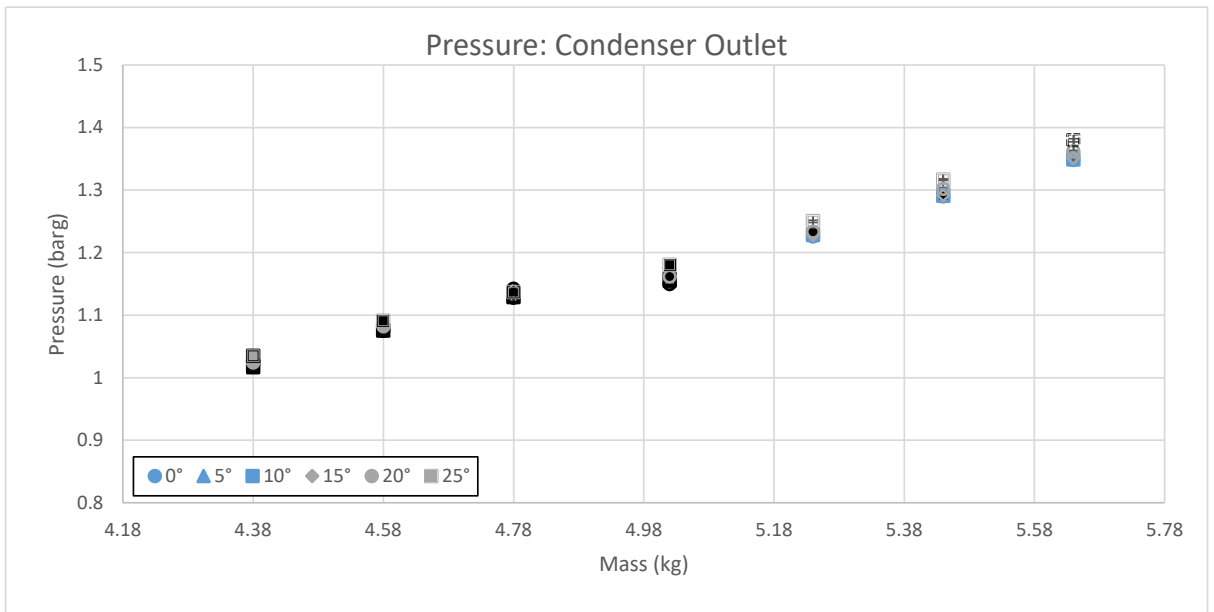
Figure 157: Condenser outlet pressure for various system charges and multiple bypass valve postitions at 800rpm pump speed. The bypass opening angle has negliable effect on condenser outlet pressure incomparision to the refigerant mass of the system.

The pressure at the sub cooler inlet and pump inlet, Figure 158 and Figure 159, on the other hand show a clear increase in pressure at a bypass opening angle of 20 and 25°. This pressure increase does not correlate with an improvement in system performance and is likely to be a results of increased stored liquid column height which is observable from the marker changes indicating liquid level height.

Figure 158: Sub cooler inlet pressure for various system charges and multiple bypass valve postitions at 800rpm pump speed. Upto 15° bypass opening angle there is negliable change in the subcooler inlet pressure further increase results in an increase in pressure at both 20 and 25° opening angles.

Figure 159: Pump inlet pressure for various system charges and multiple bypass valve postitions at 800rpm pump speed. Upto 15° bypass opening angle there is negliable change in the pump inlet pressure, further increase result in an increase in pump inlet pressure at 20 and 25°.

Temperature:

The controlled cold water feed temperature is shown in Figure 160 with the return temperature shown in Figure 161. There cold water feed temperature has an overall variation of less than 1°C over the entire test range and significantly less for each individual mass increment. The cold water return temperature shows no significant change upto an opening angle of 15° with further increase resulting in a reduction in temperature.

Figure 160: Cold water feed temperature for various system charges and multiple bypass valve postitions at 800rpm pump speed. There is a small variation in cold water feed temperature: approximetly 0.4°C variation for each individual mass test and approximetly 1°C over the entire test range.

Figure 161: Cold water return temperature for various system charges and multiple bypass valve postitions at 800rpm pump speed. The stored liquid height level between the sight glasses is indicated by marker changes. Generally, there is no significant change in return temperature up to 15° bypass opening angle, past this point there is a noticeable decline with increase opening angle.

The condenser outlet temperature is shown in Figure 162, the temperature follows a very similar trend to the cold water feed temperature, with the exception of the 25° case. In the majority of cases a 25° opening angle results in a significant increase in condenser outlet temperature.

Figure 162: Condenser outlet temperature for various system charges and multiple bypass valve postitions at 800rpm pump speed. There is approximetly 0.2°C variation in condenser outlet temperature for the majortiy of data points for each indvidual mass increament, with the excception of the 25° bypass opening angle which has a considerably higher temperature.

The pump inlet and pump outlet temperature are shown in Figure 163 and Figure 164. Both cases follow a very similar trend with no significant variation in temperature upto a 15° bypass angle opening. Above 15° there is a slight increase in temperature for the 20° case and a significant increase for the 25° case.
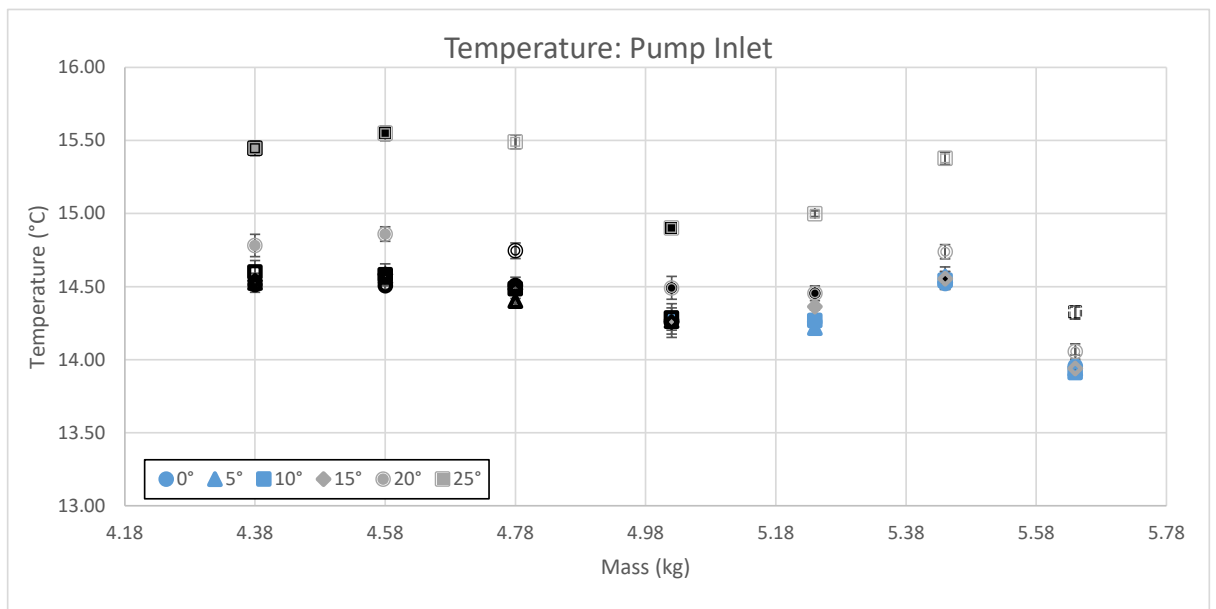
Figure 163: Pump inlet temperature for various system charges and multiple bypass valve postitions at 800rpm pump speed. There is negligable changes in pump inlet temperature upto 15° at which point the pump inlet temperature increases with increasing bypass opening angle.
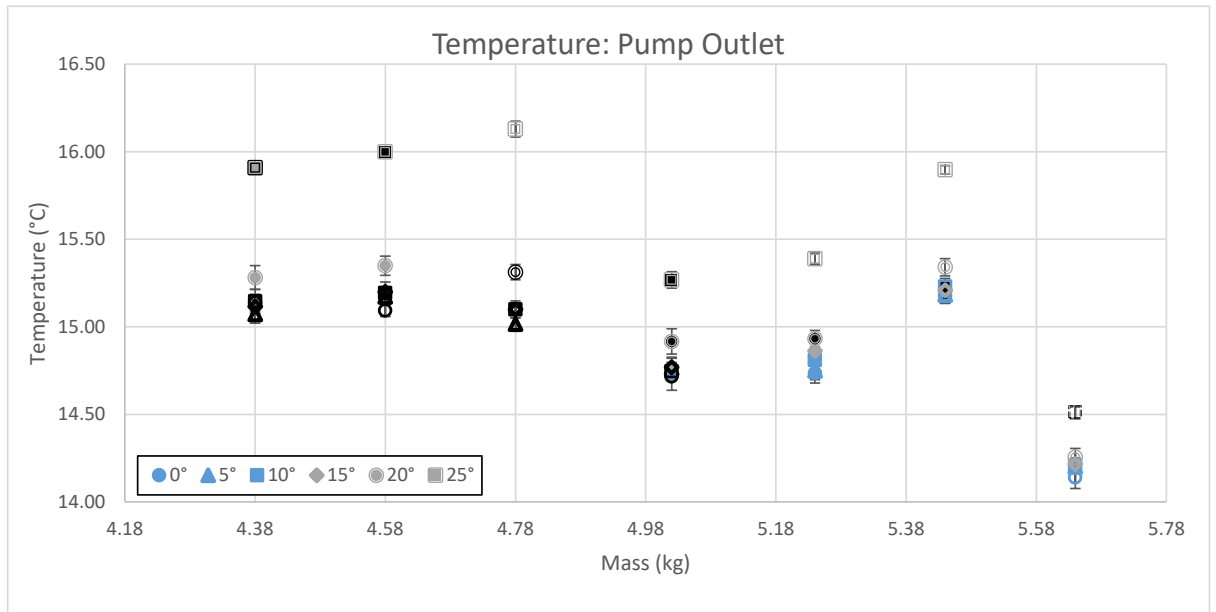
Figure 164: Pump outlet temperature for various system charges and multiple bypass valve postitions at 800rpm pump speed. Theres is negligable changes in pump outlet temperature upto a bypass opening angle of 15° after which the pump inlet temperature increases with increase valve opening angle.

The evaporator inlet temperature is shown in Figure 165 upto 15° opening angle there is no significant change in temperature. A further opening of the valve results in a significant increase in temperature.
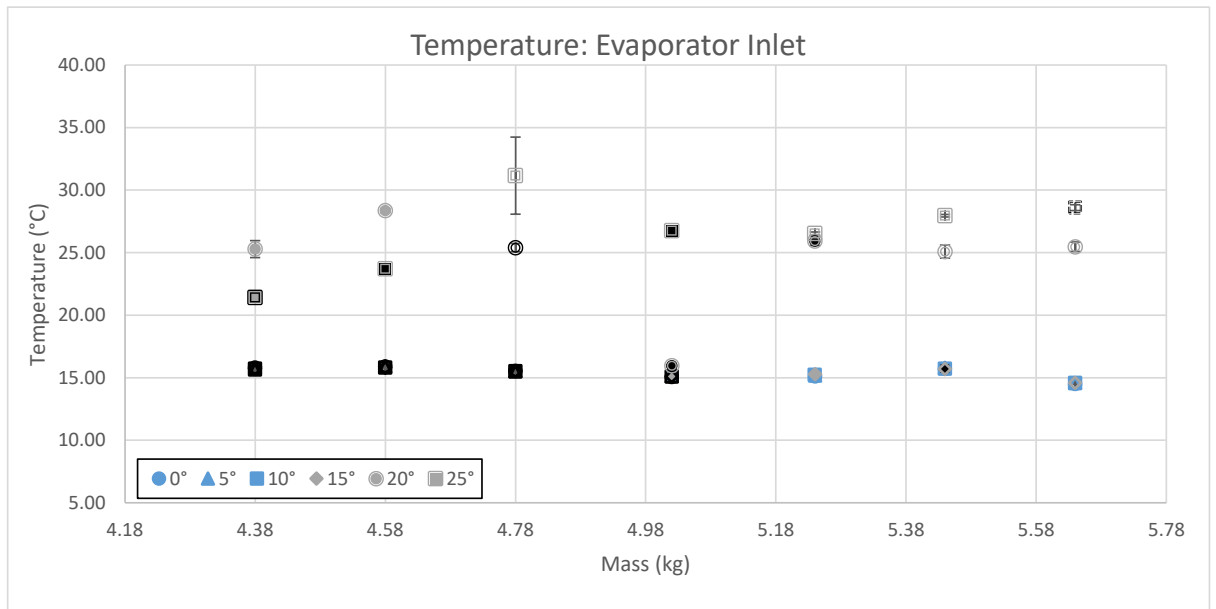
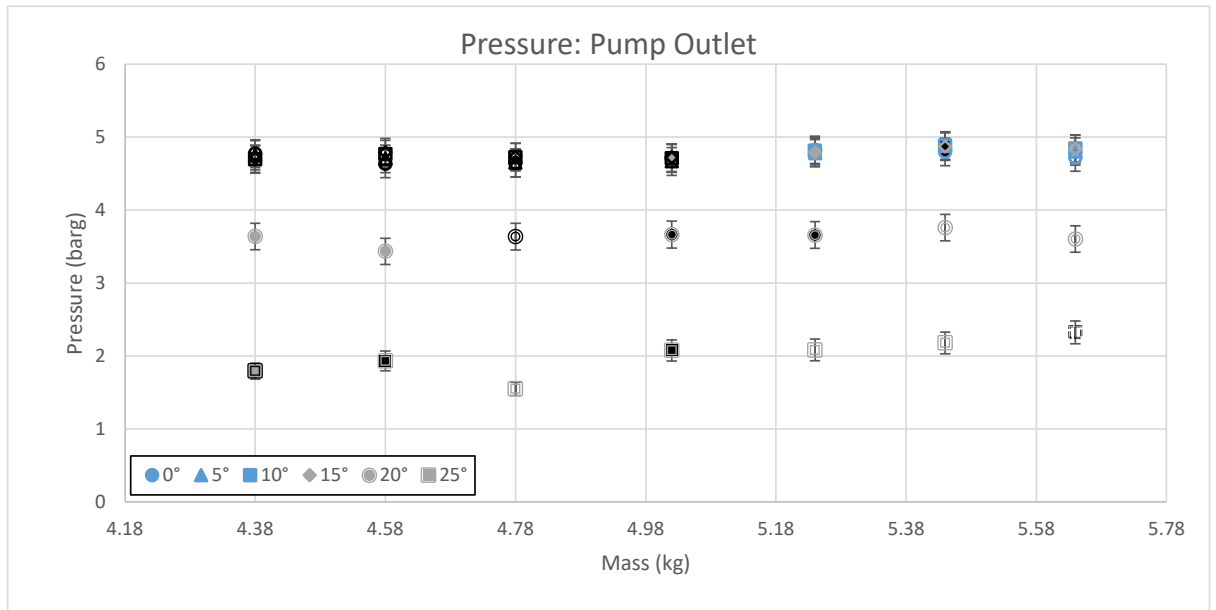*Figure 165: Evaporator inlet temperature for various system charges and multiple bypass valve postitions at 800rpm pump speed. Upto 15° opening angle there is negligable change in evaporator inlet temperature after which the evaporator inlet temperature increases with increasing opening angle*

The controlled hot water feed temperature is shown in Figure 166 with the hot water return temperature shown in Figure 167. The feed temperaure has an overall varation of around 3°C over the entire test range and significantly less for the majority of individual mass increments. There is no clearly observable trend between hot water return temperature and

upto 15° bypass opening angle. A further increase in valve opening leads to an increase in the hot water return temperature.
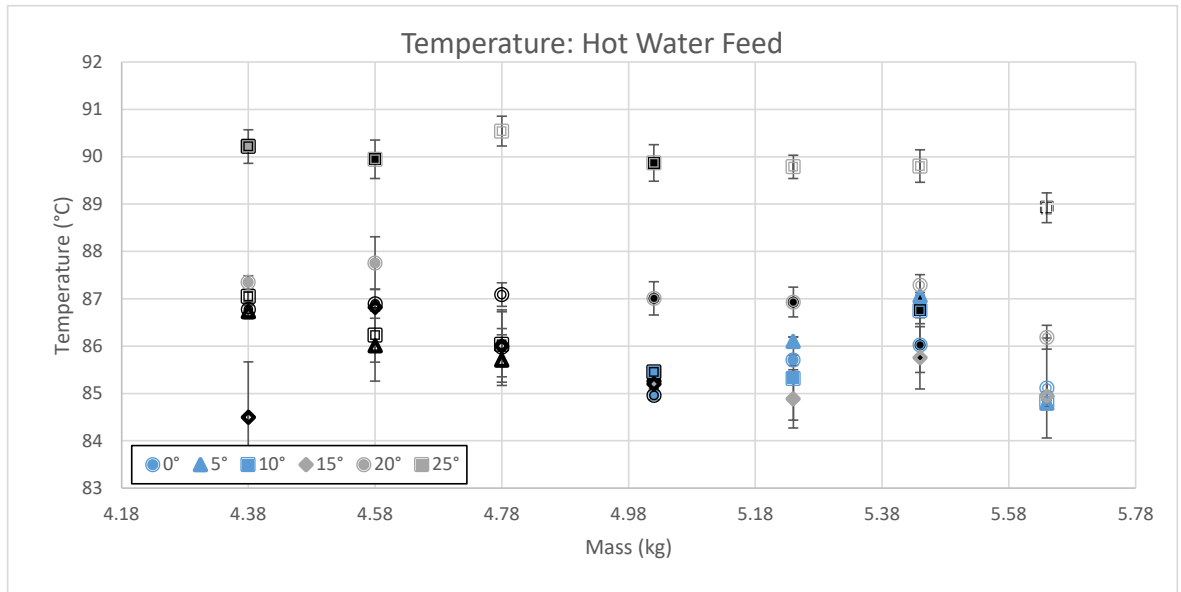
Figure 166: Hot water feed temperature for various system charges and multiple bypass valve postitions at 800rpm pump speed. The externally controlled hot water feed temperature lies with 1°C varation for the majoriy of indivual mass increment tests and has an overal variation of approximetly 3°C over the entire test range.
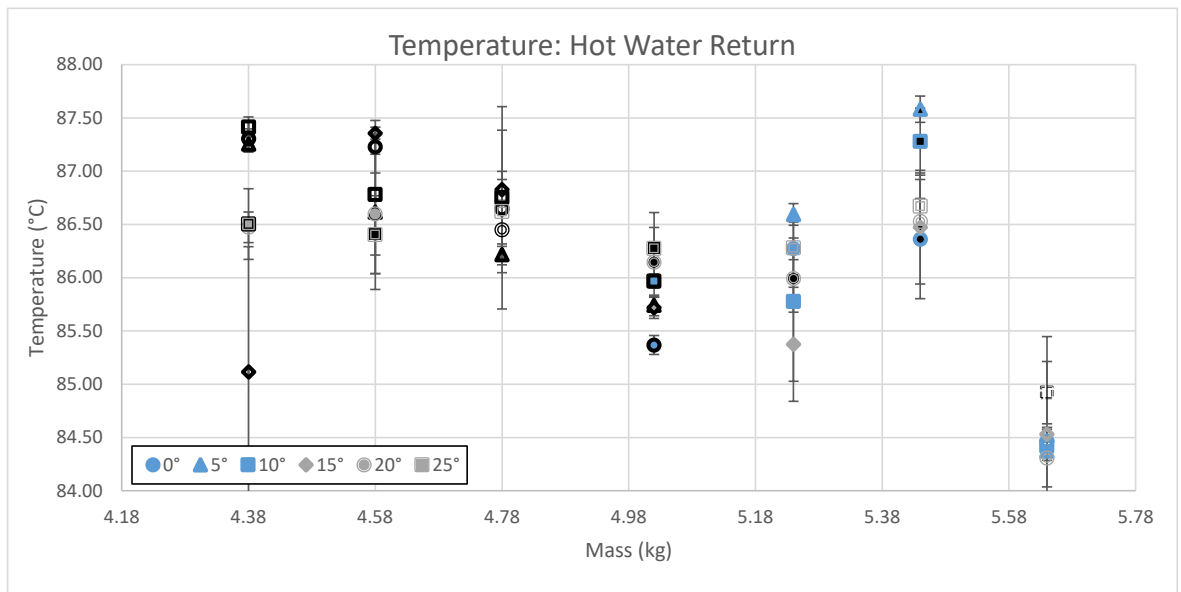
Figure 167: Hot water return temperature for various system charges and multiple bypass valve postitions at 800rpm pump speed. The hot water return temperature for the majority of data points upto 15° opening angle falls within an approximelty 1°C range. Further increase in opening angle results in a significant increase in hot water return temperature.

The expander inlet and outlet temperature are shown in Figure 168 and Figure 169. The expander inlet case upto 15° opening has no significant effect on temperature. Further increases in bypass results in a reduction in temperature. The expander outlet temperature on the other hand shows no observably clear change in temperature with bypass.
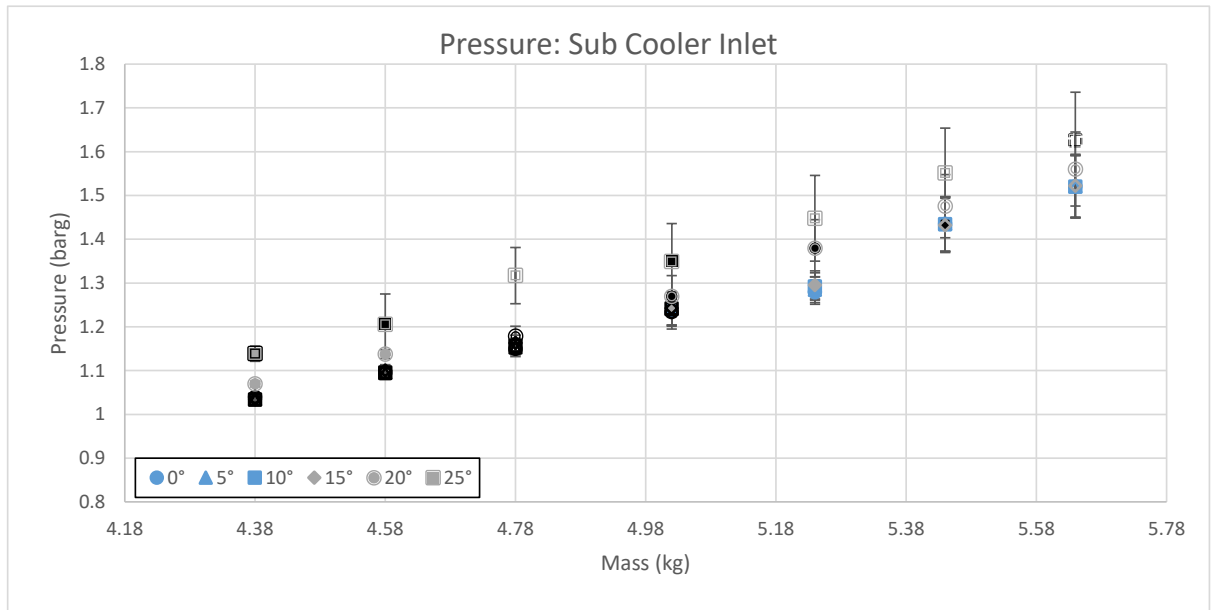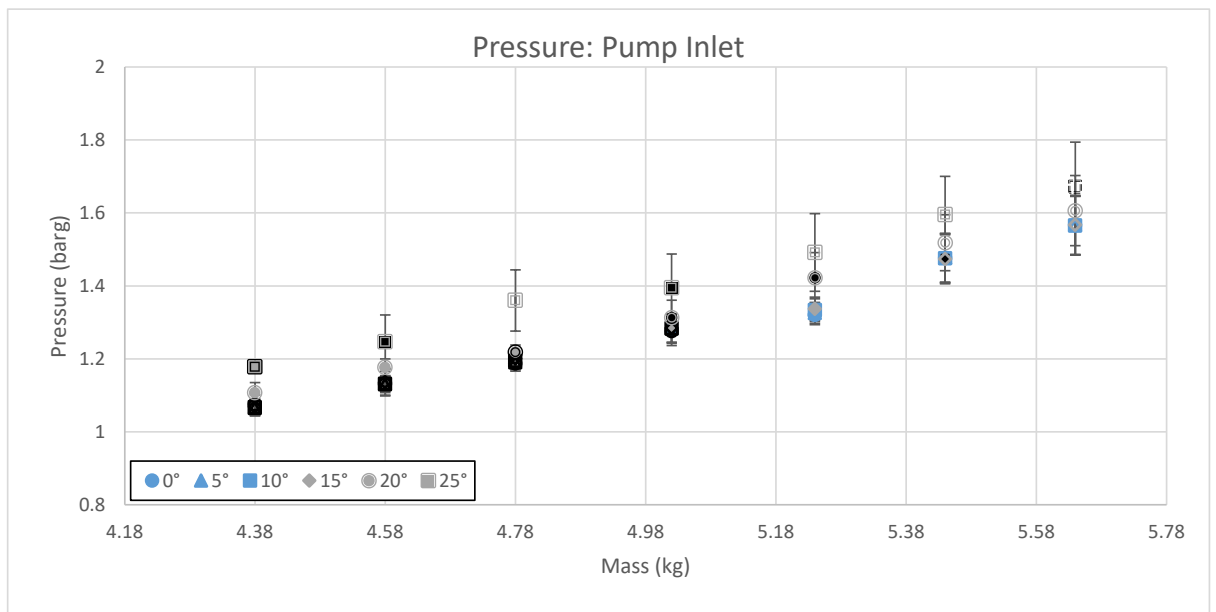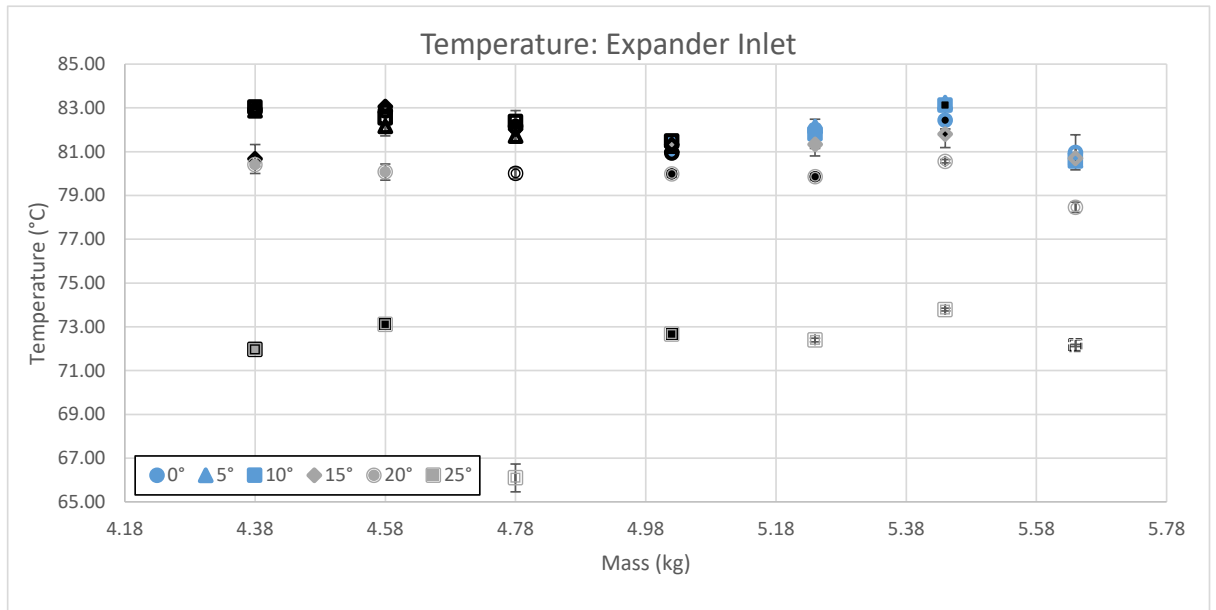
Figure 168: Expander inlet temperature for various system charges and multiple bypass valve postitions at 800rpm pump speed. Upto 15° opening angle the expander inlet tempeature remains within a 1°C variation in temperature. After which further increase in opening angle results in a significant reduction in expander inlet temperature.
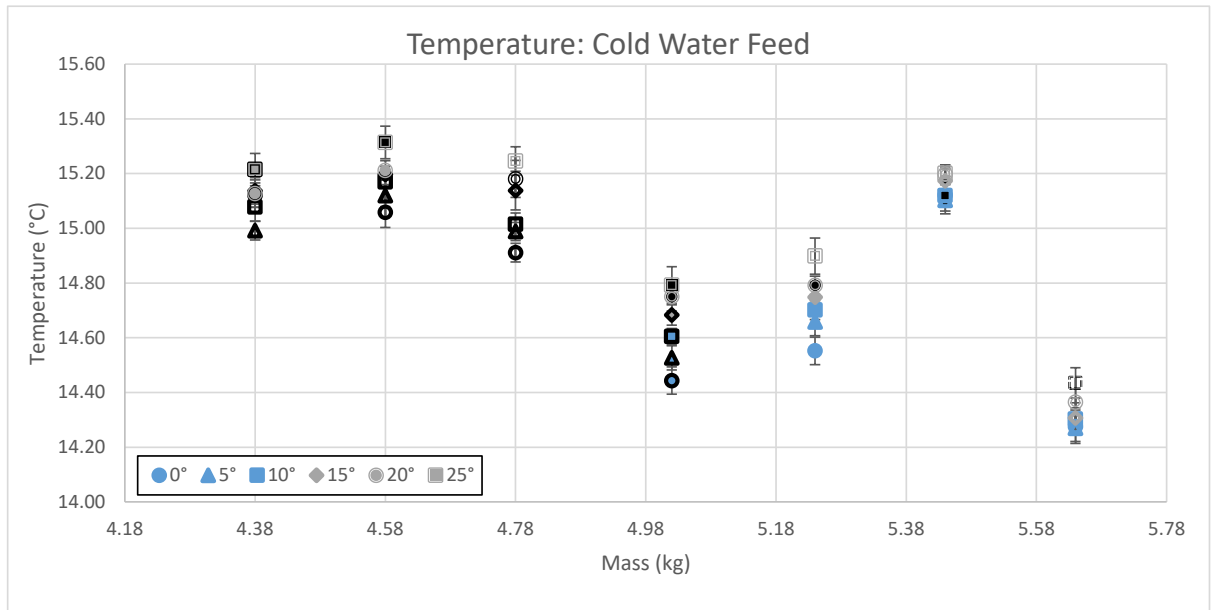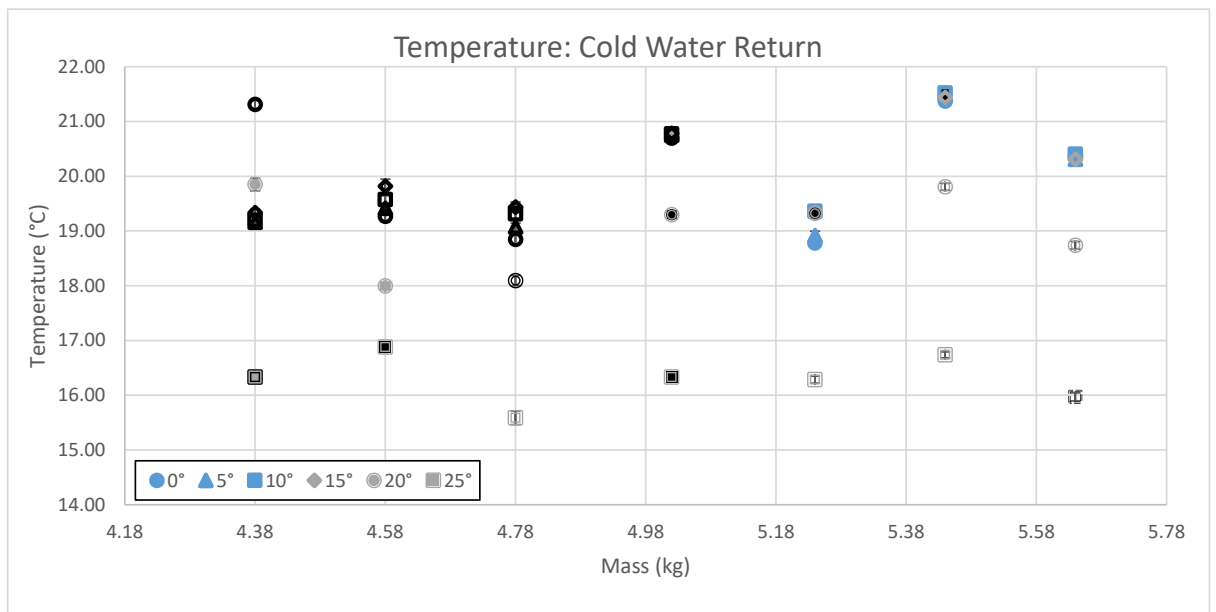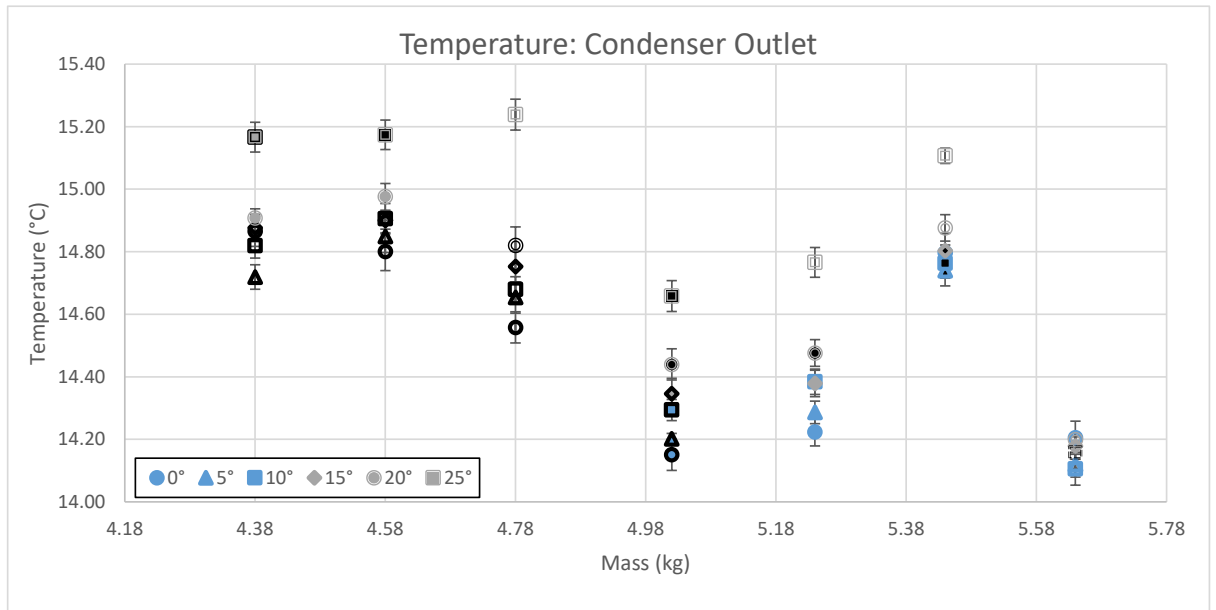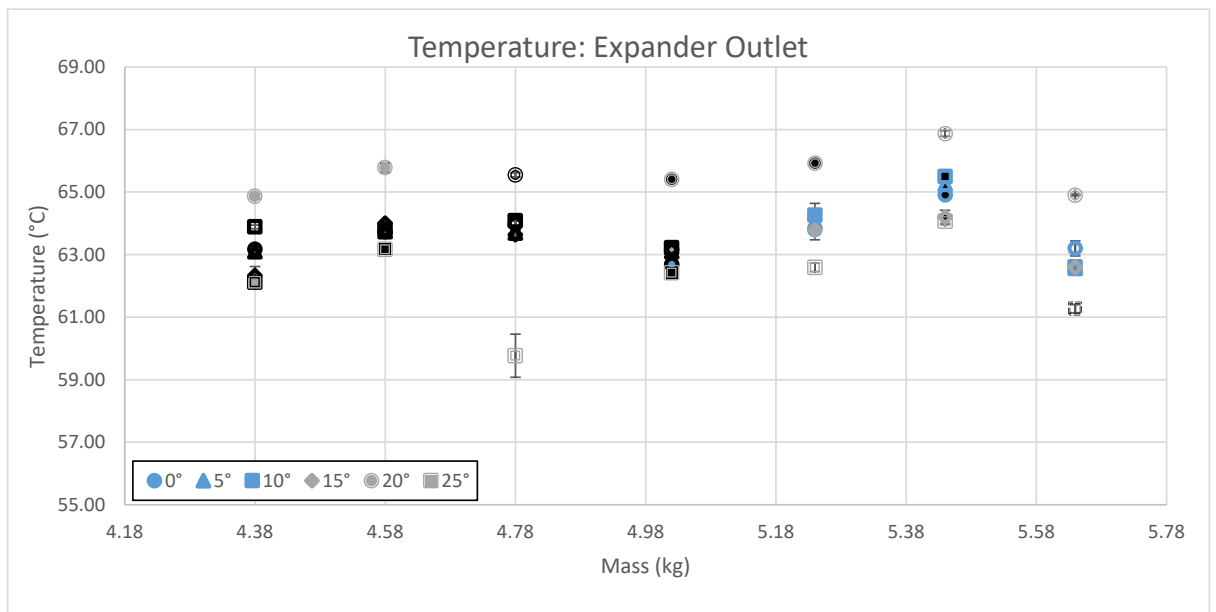

Figure 169: Expander outlet temperature for various system charges and multiple bypass valve postitions at 800rpm pump speed. The variation in expander outlet temperature shows no significant trend with opening angle with the exception of the 20° case which records consistently higher outlet temperatures across the test range.

6.2. **Experimental results: 1000 Rpm pump speed**

Experimental results observation summary: Above 5.08kg of system charge there is no significant variation upto 15° bypass angle for the overall system performance, the high and low side pressure and the majority of temperatures. Above 15° bypass angle there is a significant deterioration in the system with increasing opening angle. Below 5.08kg of system charge there is no observable system trend with increasing bypass angle.

Overall performance:

The overall performance of the ORC system at 1000rpm with varying bypass valve opening angles is shown in Figure 170, Figure 171 and Figure 172, the expander rotational speed, generated output power and consumed pump power respectively. The output of the ORC system with regards the expander rotational speed and output power show no significant variation upto 15° bypass opening angle and above 5.08kg of system charge. A further increase in bypass angle results in a reduction in system output. Below 5.08kg of system charge there is no consistent trend with increase degrees of bypass. In terms of consumed pump power there is no clearly observable trend between consumed pump power and bypass opening angle, with the consumed power fluctuating between 0.8 and 0.1 kW.
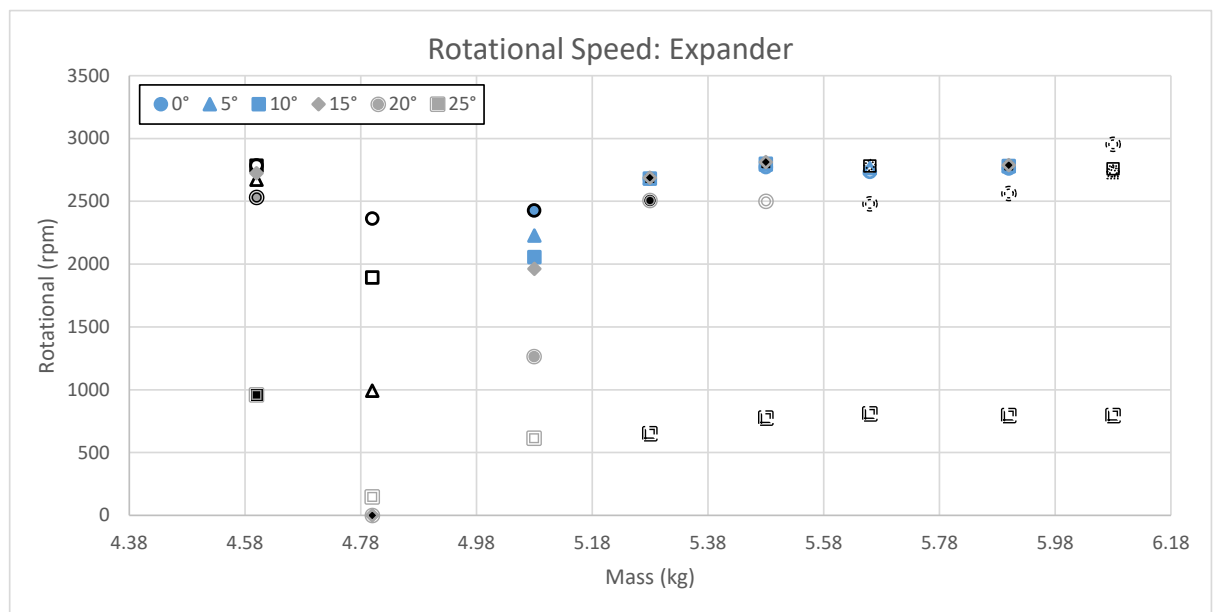
Figure 170: Expander rotational speed for various system charges and multiple bypass valve postitions at 1000 rpm pump speed. The expander roational speed above 5.08 kg of mass produces a reasonably consistant trend with increseing mass, with small comparable changes in roational speed upto 15° bypass valve opening. Further increases in valve opeinging results in a significant drop off in expander roational speed. Below 5.08kg of system charge there is no obserable correlation between bypass valve opening and expander rotational speed. At 5.08kg of system charge the expander roational speed decreases with increasing bypass valve opening.
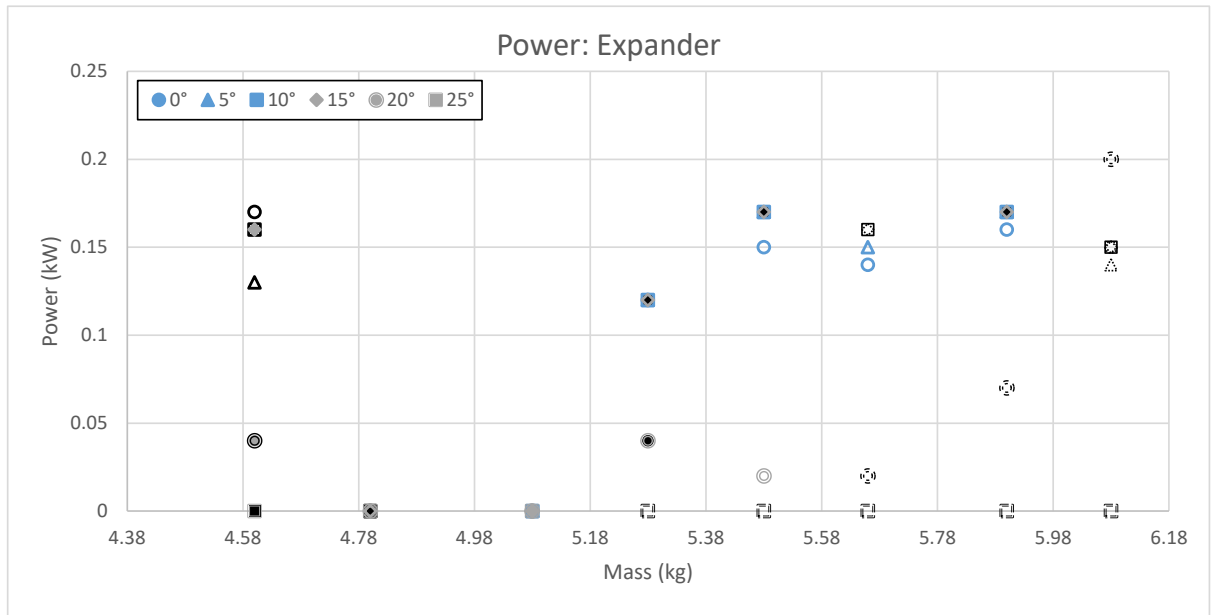
Figure 171: Expander output power for various system charges and multiple bypass valve postitions at 1000 rpm pump speed. At 5.08 and 4.8kg of charge the rotational speed of the expander is below the synconisation speed of the generator resulting in the recoreded output power of 0W. Above 5.08 kg of mass there is no significant change with increaseing bypass angle upto 15° after which there is a significant drop off in expander output power with increase bypass angle.
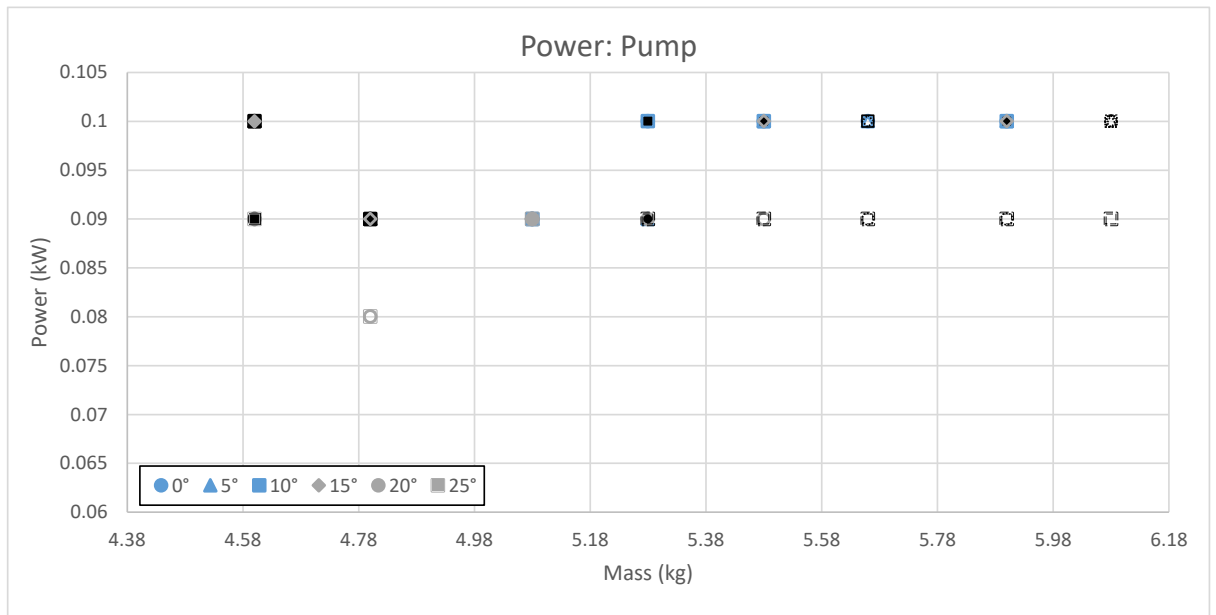
Figure 172: Consumed pump power for various system charges and multiple bypass valve postitions at 1000 rpm pump speed. There is an oversable dip in pump power between 4.8kg ang 5.08 kg. Above 5.08 the pump power shows no significant change with bypass opening angle with the exception of the 25° case which is consistantly lower.

Pressure:

The pressure in the high side of the system at the pump outlet and expander inlet are shown in Figure 173 and Figure 174, with the trend in both cases is being very similar. Above 5.08kg of system charge there is no significant change in pressure with increasing bypass angle upto 15°. Any further increase results in a deterioration in high side system pressure.

Below 5.08kg of system charge there is no obvious trend between increasing bypass angle and high side system pressure.

Figure 173: Pump outlet pressure for various system charges and multiple bypass valve postitions at 1000 rpm pump speed. Above 5.08kg upto 15° opening angle there is no signficant change in pressure with increaseing bypass angle. Further increase in opening angle results in a significant decrease in pump outlet pressure.
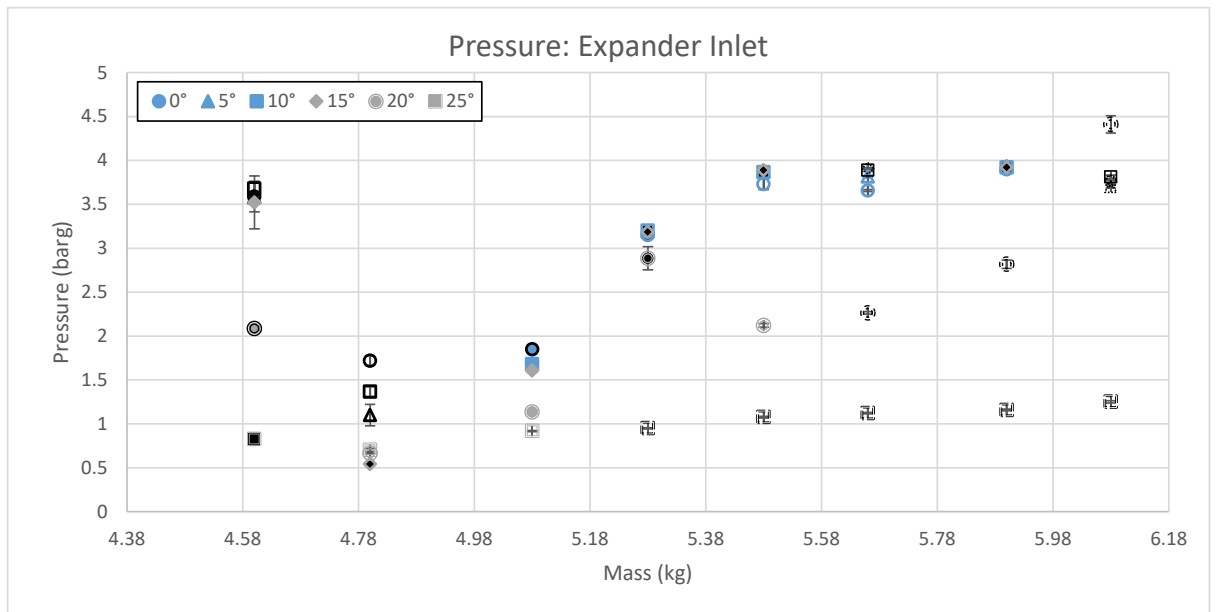
Figure 174: Expander inlet pressure for various system charges and multiple bypass valve postitions at 1000 rpm pump speed. Above 5.08kg and upto 15° opening angle there is no significant change in expander inlet pressure with increasing opening angle. Further increase in angle results in a decrease in expander inlet pressure.

The low pressure side of the ORC system is shown in Figure 175, Figure 176, Figure 177 and Figure 178. Both the expander and condenser outlet pressure show no significant variation with changing bypass angle when compared with increasing system charge. The

subcooler inlet and pump inlet pressure show a similar trend with the exception of the 25°
bypass angle which shows an increase in pressure on both cases.
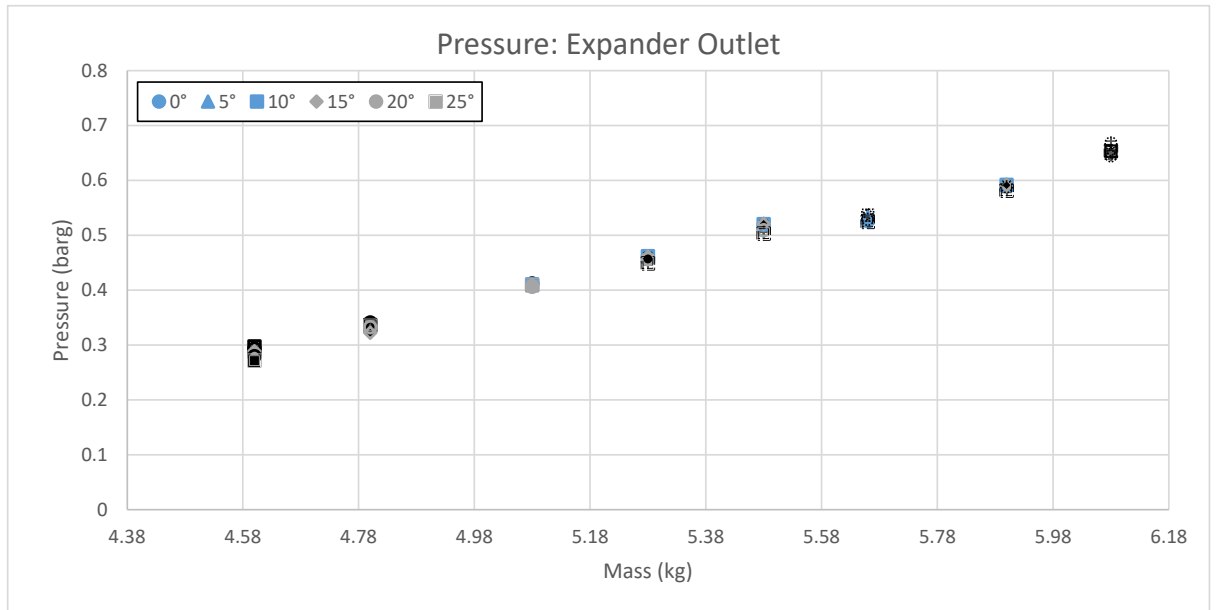
Figure 175: Expander outlet pressure for various system charges and multiple bypass valve postitions at 1000 rpm pump speed. There is negligable change in expander outlet pressure with increasing bypass opening angle.
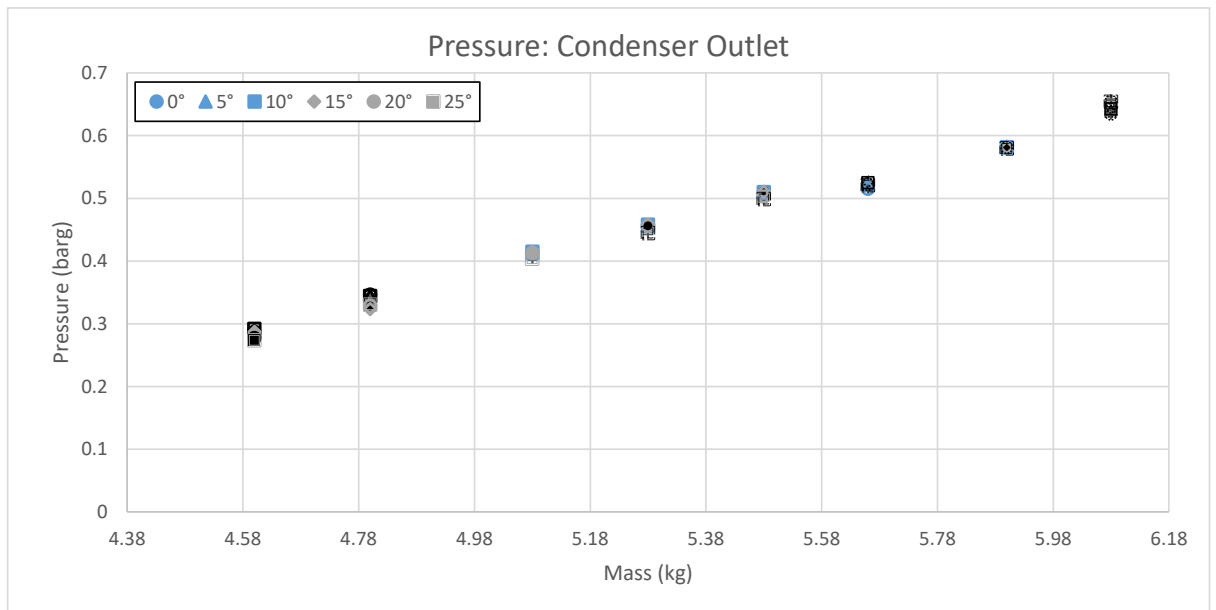
Figure 176: Condenser outlet pressure for various system charges and multiple bypass valve postitions at 1000 rpm pump speed. There is negligable change in condenser outlet pressure with increasining bypass angle.
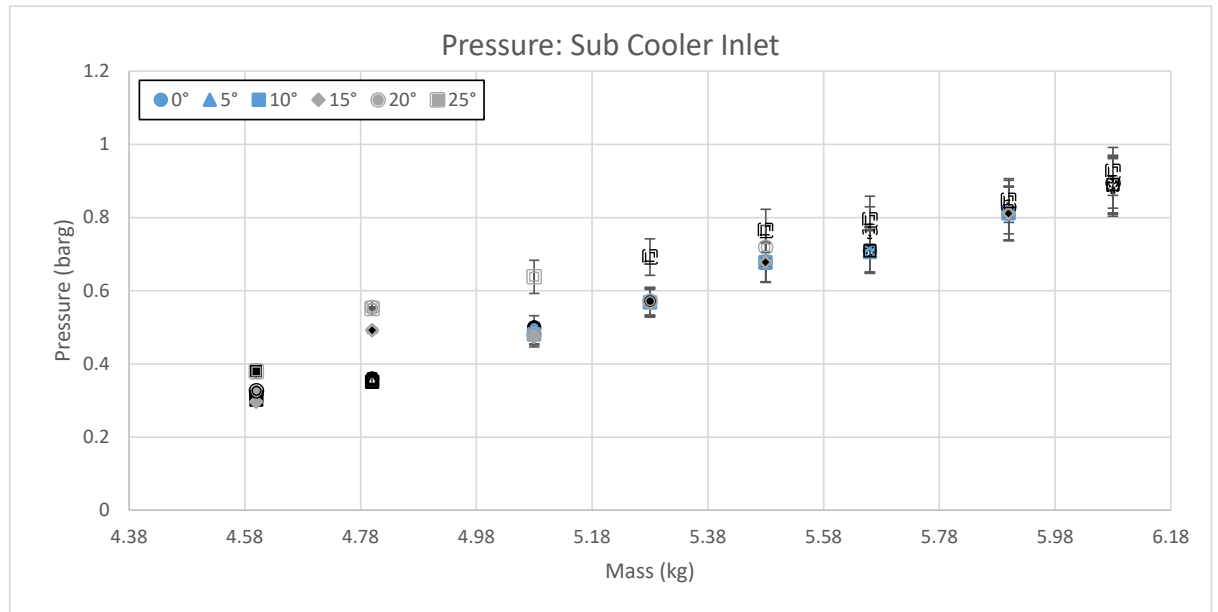
Figure 177: Sub cooler inlet pressure for various system charges and multiple bypass valve postitions at 1000 rpm pump speed. Upto 15° there is negligable change in subcooler inlet pressure with increasing bypass angle. Above 15° there is an increase in subcooler inlet pressure particulary for the 25° case.
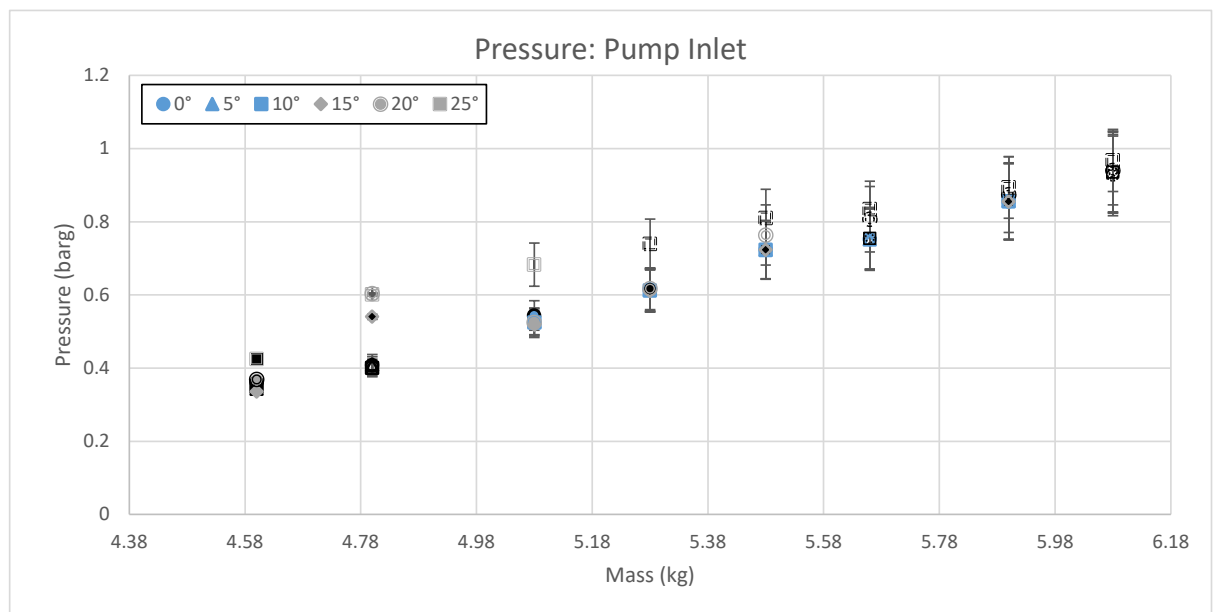

Figure 178: Pump inlet pressure for various system charges and multiple bypass valve postitions at 1000 rpm pump speed. Upto 15° there is negligable change in pump inlet pressure with increasing opeing angle. The 25° case shows in considerable increase in pump inlet pressure.

Temperature:

The cold water feed and return temperature are shown Figure 179 and Figure 180 respectively. The controlled water feed temperature has a variation of less than 0.6°C across the entire test range with significantly less variation for each individual mass increment. The cold water return temperature above 5.08kg of system charge shows no significant variation with increasing bypass angle upto 15°. A further increase results in a

reduction in return temperature. Below 5.08kg of system charge there is no observable trend between cold water return temperature and increasing bypass angle.
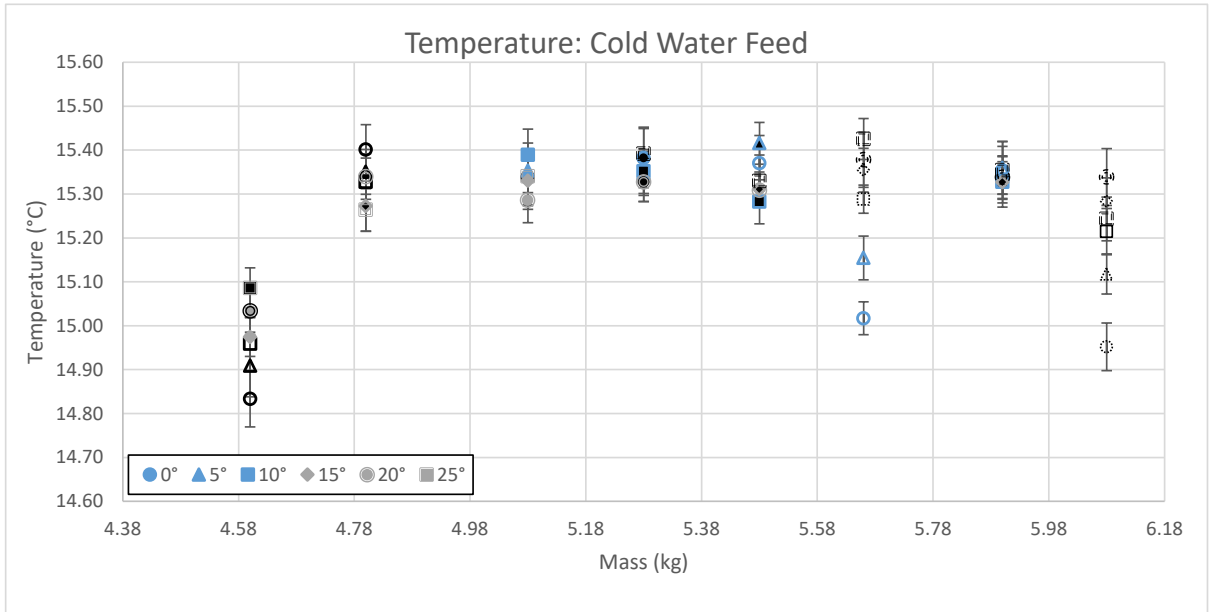
Figure 179: Cold water feed temperature: for various system charges and multiple bypass valve postitions at 1000 rpm pump speed. The controlled cold water feed temperature has a varation of 0.7°C across the whole test range.

Figure 180: Cold water return temperature for various system charges and multiple bypass valve postitions at 1000 rpm pump speed. Upto 5.08kg of system charge there is no obvious trend between bypass opening angle and cold water return temperature. Above 5.08kg of system charge and upto 15°C opening angle there is no signficant change accosciated with increaseing bypass valve angle. Further increase in opening angle resutls in a decline in cold water return temperature.

The condenser outlet temperature is shown in Figure 181 which follows a similar trend to the cold water feed temperature with an overall variation of less than 1°C over the entire test range and significantly less for each individual mass increments.

Figure 181: Condenser outlet temperature for various system charges and multiple bypass valve postitions at 1000 rpm pump speed. The overall variation across the test range is less than 1°C with no obvious significant trend increaseing bypass angle.

The pump inlet and pump outlet temperatures are shown in Figure 182 and Figure 183 respectively. In both cases there is no significant change in temperature upto 15° bypass opening angle, any further increase in both cases results in an increase in temperature.
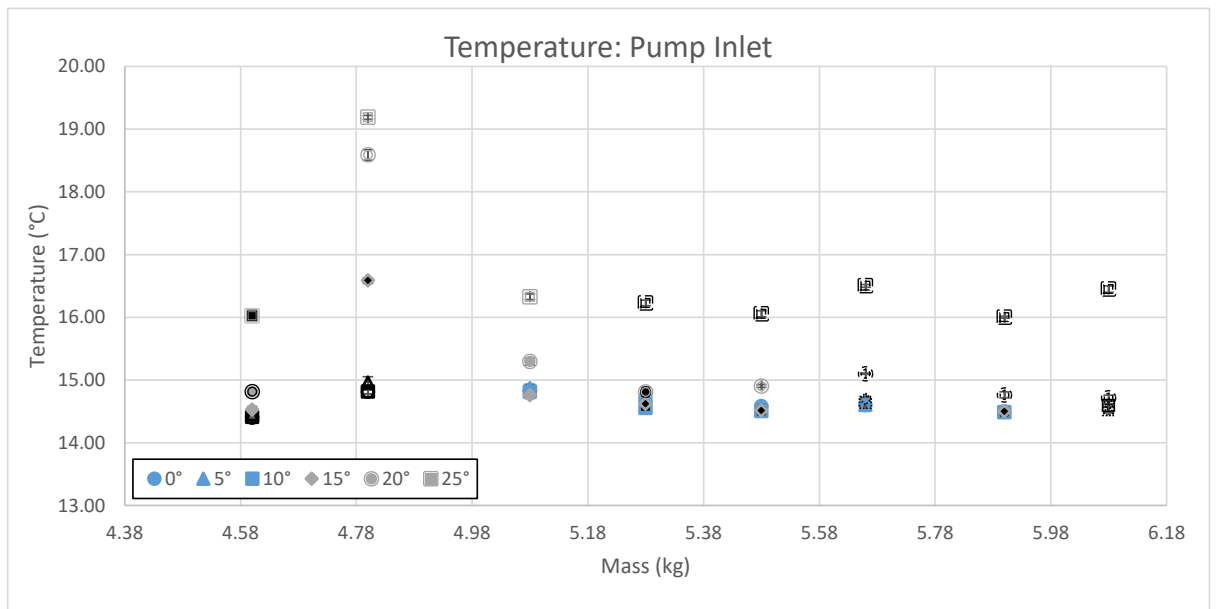
Figure 182: Pump inlet temperature for various system charges and multiple bypass valve postitions at 1000 rpm pump speed. The pump inlet temperature upto 15° opening angle shows no significant change with varying bypass angle. Further increase results in an increase in pump inlet temperature.
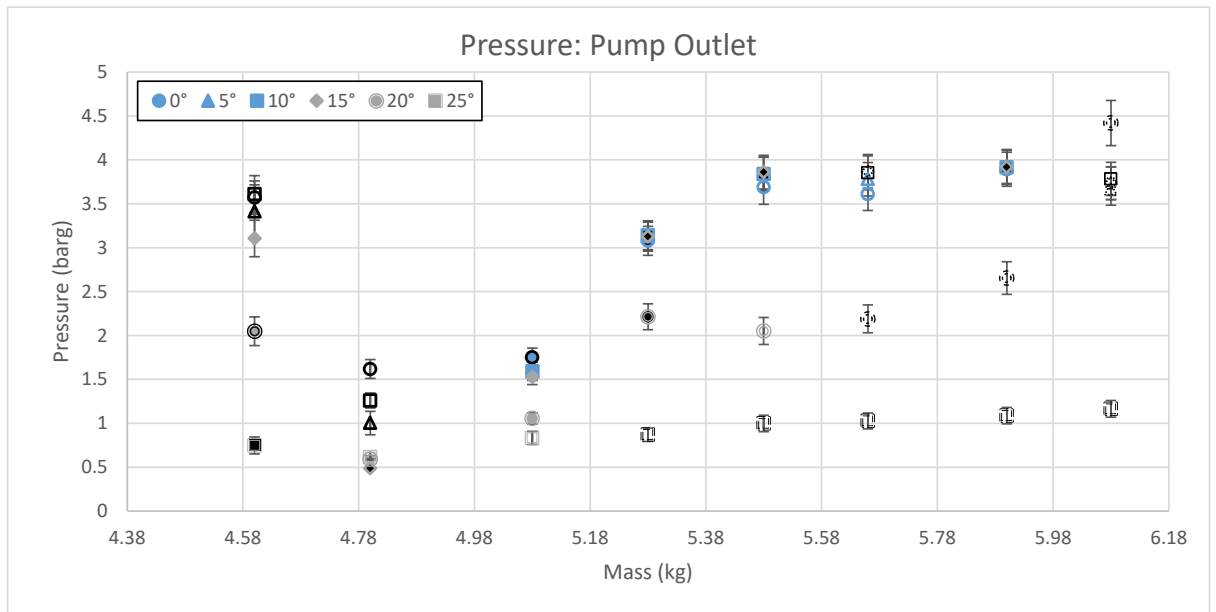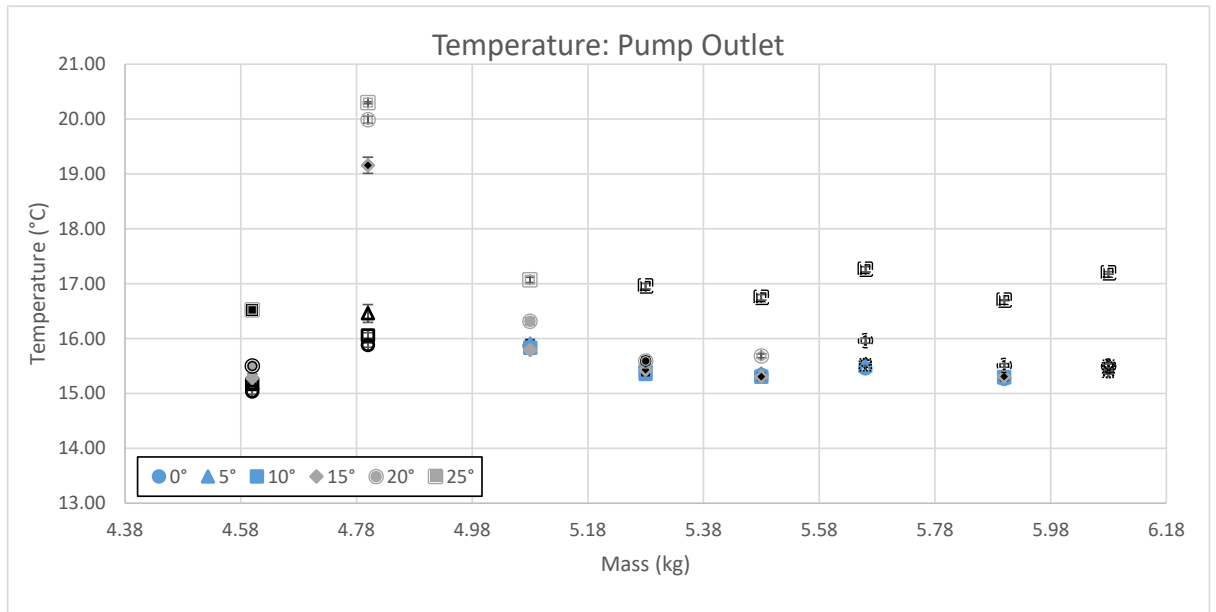
Figure 183: Pump outlet temperature for various system charges and multiple bypass valve postitions at 1000 rpm pump speed. The pump outlet temperature upto 15° opening angle shows no significant change with varying bypass angle. Further increase resultsin in an increase in pump outlet temperature.

The evaporator inlet temperature is shown in Figure 184 above 5.08kg of system charge upto 15° bypass angle there is no significant change in pressure with increasing bypass angle, further increases results in an increase is temperature. Below 5.08kg of system charge there is no consistent trend between bypass angle and evaporator inlet temperature. It is again worth nothing that the unexpectedly high temperature reading are as a results of the temperature sensor location. It readings give an indication of ORC system flow.
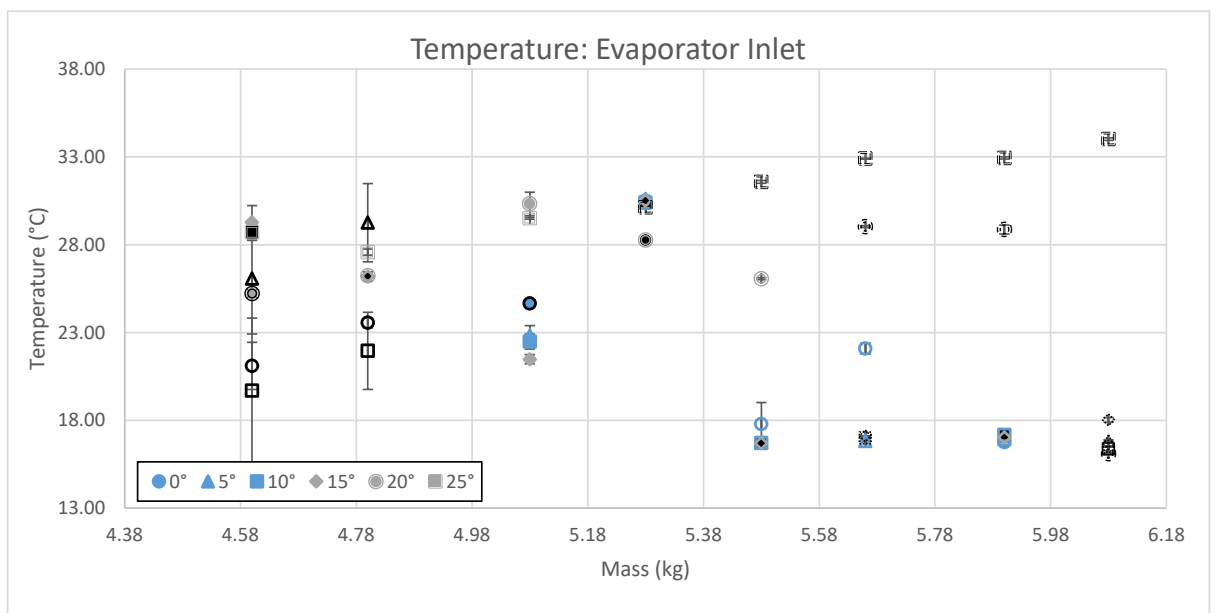
*Figure 184: Evaporator inlet temperature for various system charges and multiple bypass valve postitions at 1000 rpm pump speed. **Note: the location of the temperature sensor effects the measurement at the evaporator inlet and gives an indication of system flow**. Above 5.08kg of system charge and upto 15° bypass angle there is no substantial change in the majority of the data points with bypasss angle. Further increase in opening angle results in an increase in evaporator inlet tempeature. Below 5.08kg of charge there is no obvious trend with increasing bypass angle.*

The hot water feed and return temperatures are shown in Figure 185 and Figure 186 respectively. The controlled hot water feed temperature has a variation of less than 2°C with a significantly smaller variation for each individual mass increment. Above 5.08kg of system charge and upto 15° bypass angle there is no significant change in hot water return temperature with increasing bypass angle. Below 5.08kg of system charge there is no observably consistent trend between return temperature and increasing bypass angle.
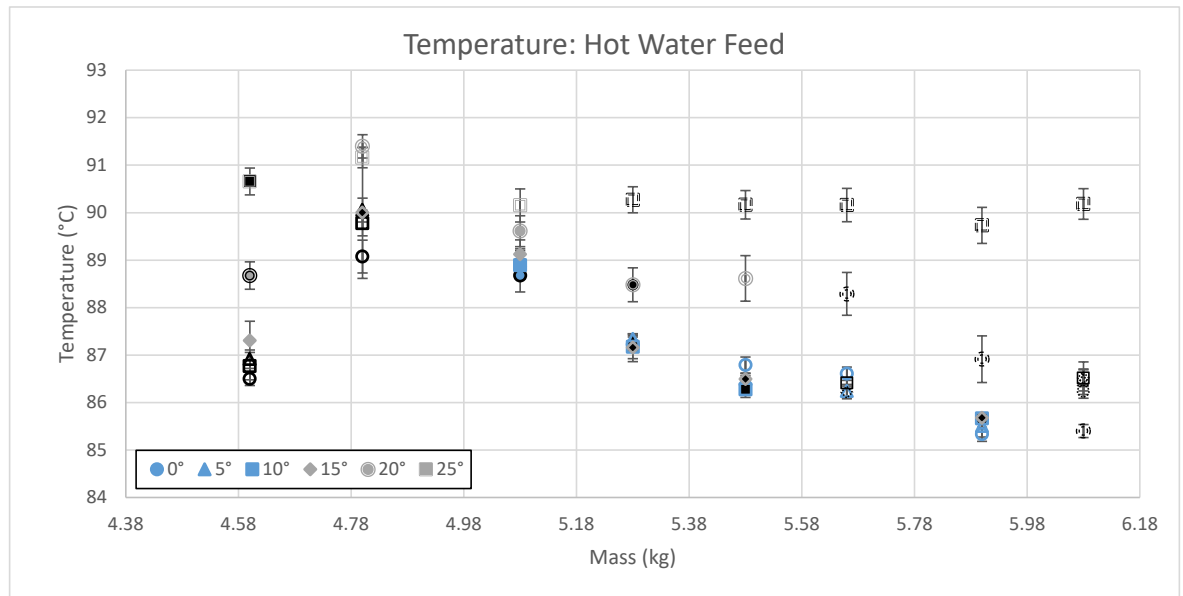
Figure 185: Hot water feed temperature for various system charges and multiple bypass valve postitions at 1000 rpm pump speed. The controlled hot water feed temperature has a 1.5°C variation in temperature across the entire test range.
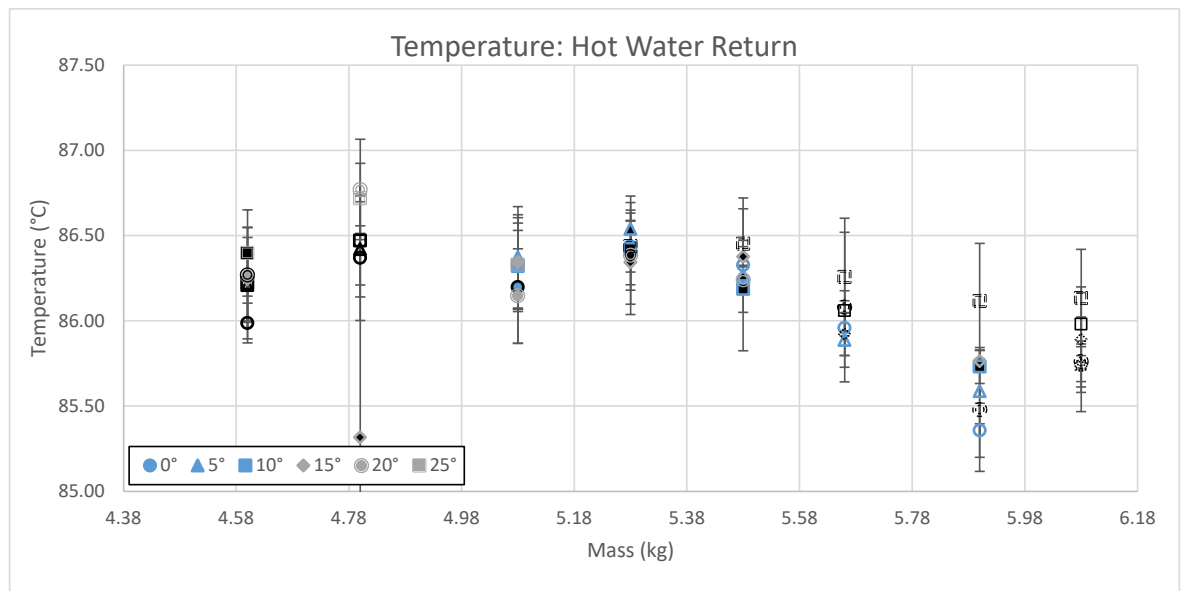
Figure 186: Hot water return temperature for various system charges and multiple bypass valve postitions at 1000 rpm pump speed. Above 5.08kg of system charge and upto 15° bypass opening angle there is no substantial change in hot water return temperature with increasing bypass opening angle. Further increase in opening angle results in increase in hot water return temperature. Below 5.08kg of system charge there is no obvious trend with increasing bypass opening angle.

The expander inlet and outlet temperature are shown in Figure 187 and Figure 188 respectively. In both cases above 5.08kg of system charge there is no significant change in temperature with increasing bypass angle. Any further increase results in a reduction in temperature. Below 5.08kg of system charge there is no observable consistent trend between increasing bypass angle and temperature.
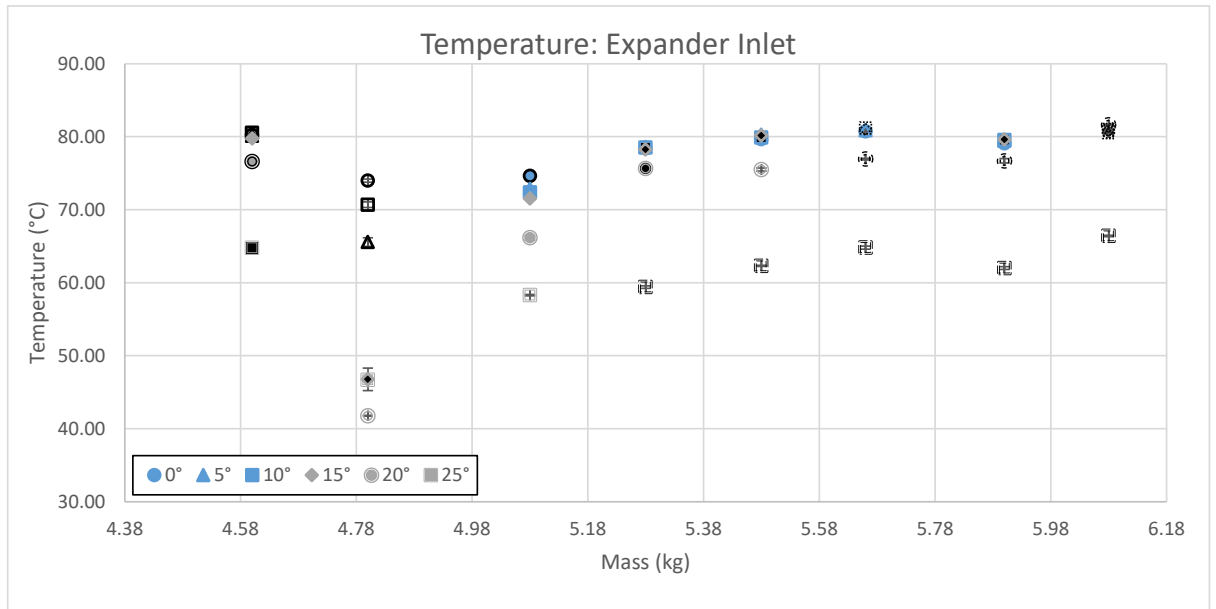
Figure 187: Expander inlet temperature for various system charges and multiple bypass valve postitions at 1000 rpm pump speed. Above 5.08kg of charge there is no significant change in expander inlet temperature with increasing bypass opening angle. Futher increase in bypass angle results in a decrease in temperature. Below 5.08kg of charge there is no obvious trend with increasing bypass angle.

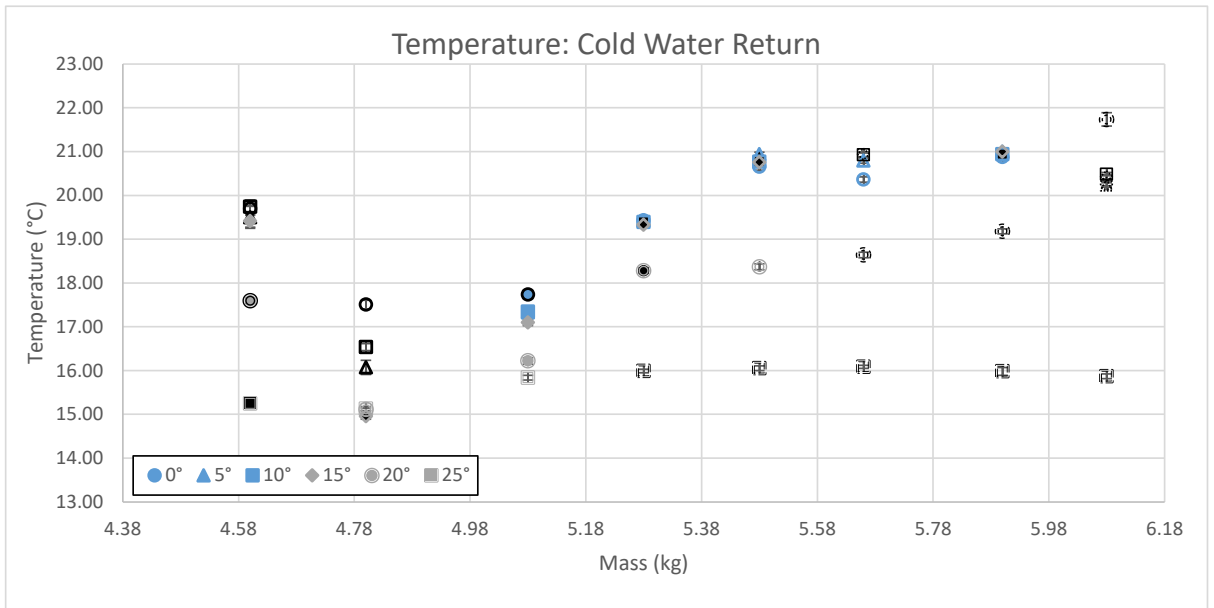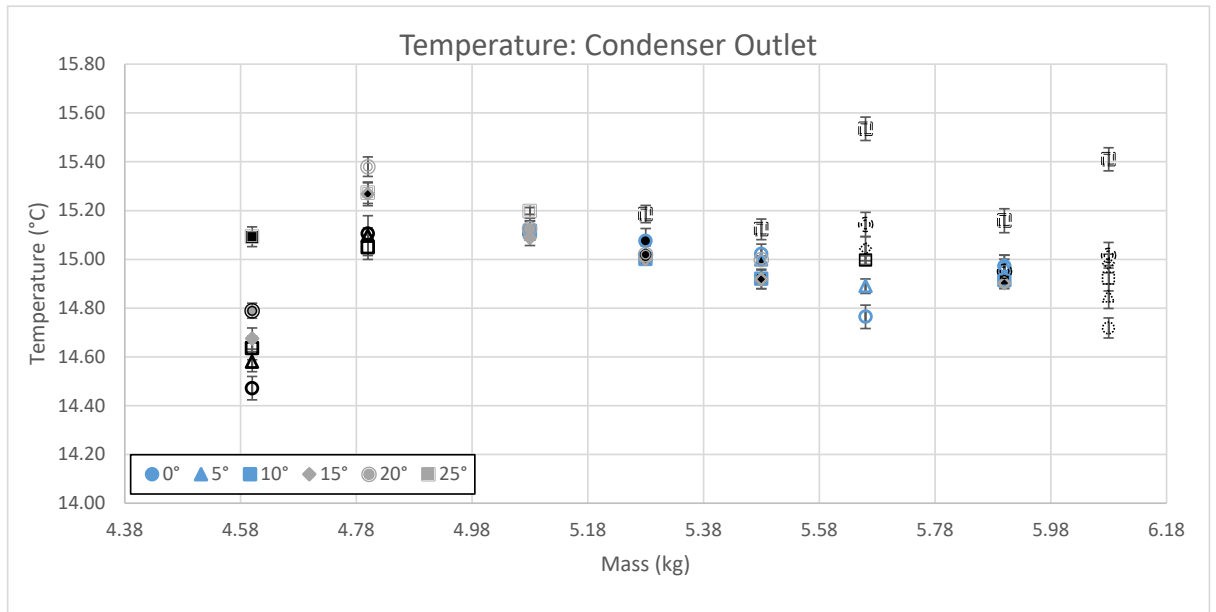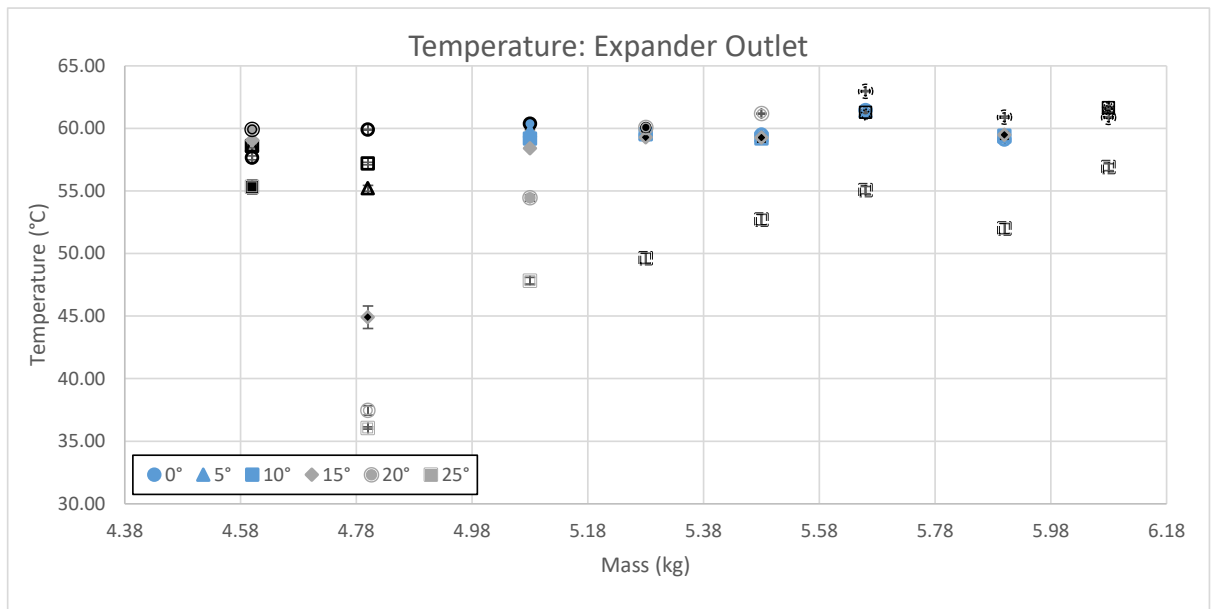Figure 188: Expander outlet temperature for various system charges and multiple bypass valve postitions at 1000 rpm pump speed. Above 5.08kg of system charge upto 15° bypass opening angle there is no significant change with increasing bypass angle. Futher increase results in a reduction in expnader outlet tmperature. Below 5.08kg of system charge there is no obvious trend in increaseing bypass angle.

6.3. **Experimental Results: 1200 Rpm pump speed**

Experimental results observation summary: Above 5.08kg of system charge and upto 15° bypass angle there is no significant change in overall system performance, high and low side pressure and the majority of temperatures. Further increase in bypass angle results in a deterioration in system parameters. Below 5.08kg of system charge there is no real observable trend with increasing bypass angle.

Overall Performance:

The overall performance of the ORC system at the maximum pump speed of 1200rpm, at varying degrees of bypass angle and system charge are shown in Figure 189, Figure 190 and Figure 191: The expander rotational speed, generated electrical output and consumed pump power. Above 5.08kg of system charge and upto 15° degrees bypass angle there is no significant change between increasing bypass angle and expander rotational speed. A further increase in bypass angle results in a deterioration in expander rotational speed. The generated electrical output follows a very similar trend with the exception that below 5.48kg of charge the expander rotational speed is below the synchronization speed of the generator. Resulting in no electrical output. Below 5.48kg of system charge the pump consumes 0.1kW of energy in all test cases which then increase to between 0.11 and 0.13 kW above 5.48kg of charge.
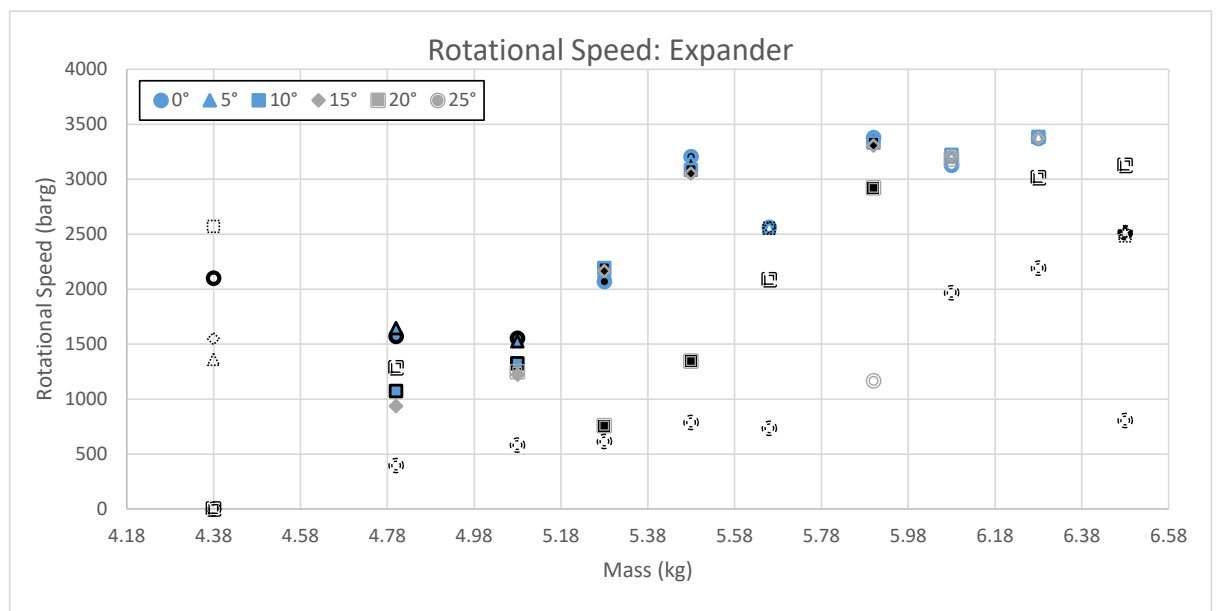
Figure 189: Expander rotational speed for various system charges and multiple bypass valve postitions at 1200 rpm pump speed. Above 5.08kg of charge and upto 15° bypass opening angle there is no significant change in expander rotational speed with increasing bypass angle. Further increase in bypass opening results in a decrease in expander rotational speed. Below 5.08kg of charge there is no obvious trend with increaseing bypass angle.

Figure 190: Expander power output for various system charges and multiple bypass valve postitions at 1200 rpm pump speed. Below 5.48kg of system charge the expander rotational speed is below the synchronisation speed of the generator and therefore the electrical output power is registered as 0W. Above 5.48kg of system charge and upto 15° opening angle there is no significant change with incrreasing bypass angle. Further increase results in a reduction in expander output power.
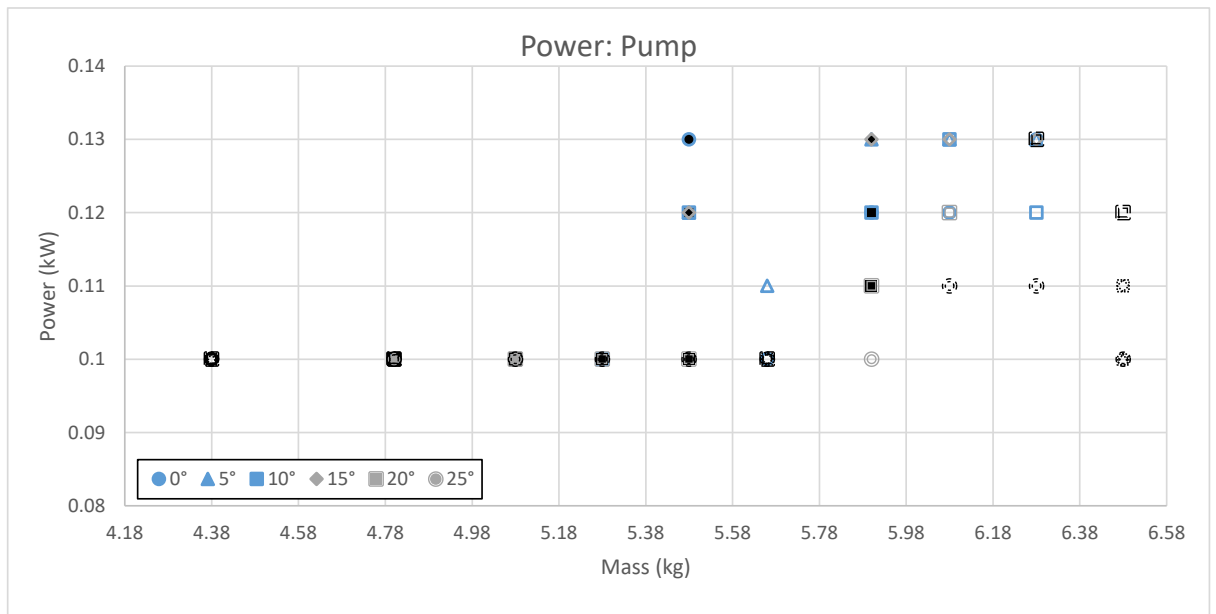
Figure 191: Consumed pump power for various system charges and multiple bypass valve postitions at 1200 rpm pump speed. Below 5.48kg of system charge there is no change in consumer pump power. Above 5.48kg there is no discerable trend with increasing bypass opening angle.

Pressure:

The pressure in the high side of the system recorded at the pump outlet and expander inlet are shown in Figure 192 and Figure 193 respectively. The pressure in both cases follows a very similar trend with a significant increase in system pressure occurring at 4.58kg of system charge for a bypass angle less than 15°. An increase in angle above 15° results in a significant reduction in high side system pressure.
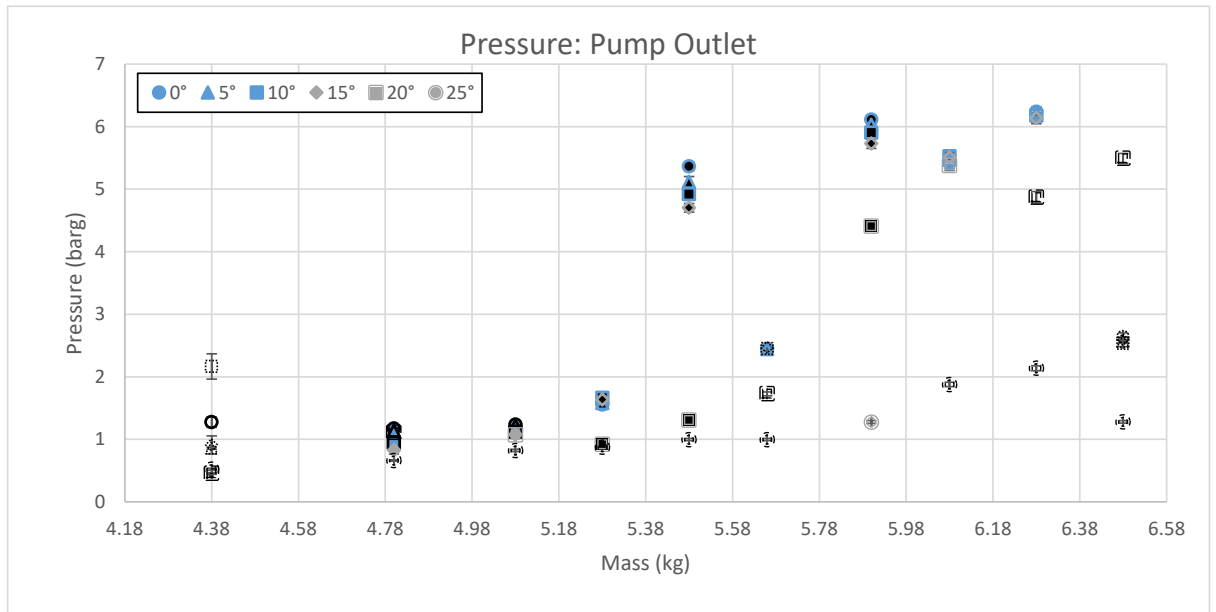
Figure 192: Pump outlet pressure for various system charges and multiple bypass valve postitions at 1200 rpm pump speed. Below 5.48kg of system charge the maximum pump outlet pressure is around 2 barg. Above 5.48kg there is a significant jump upto around 5barg. Upto 15° opening angle there is potentially a slight decrease in presure with increasing bypass opening angle. Above 15° there is a significant decreasing in pressure with increasing bypass anlge.
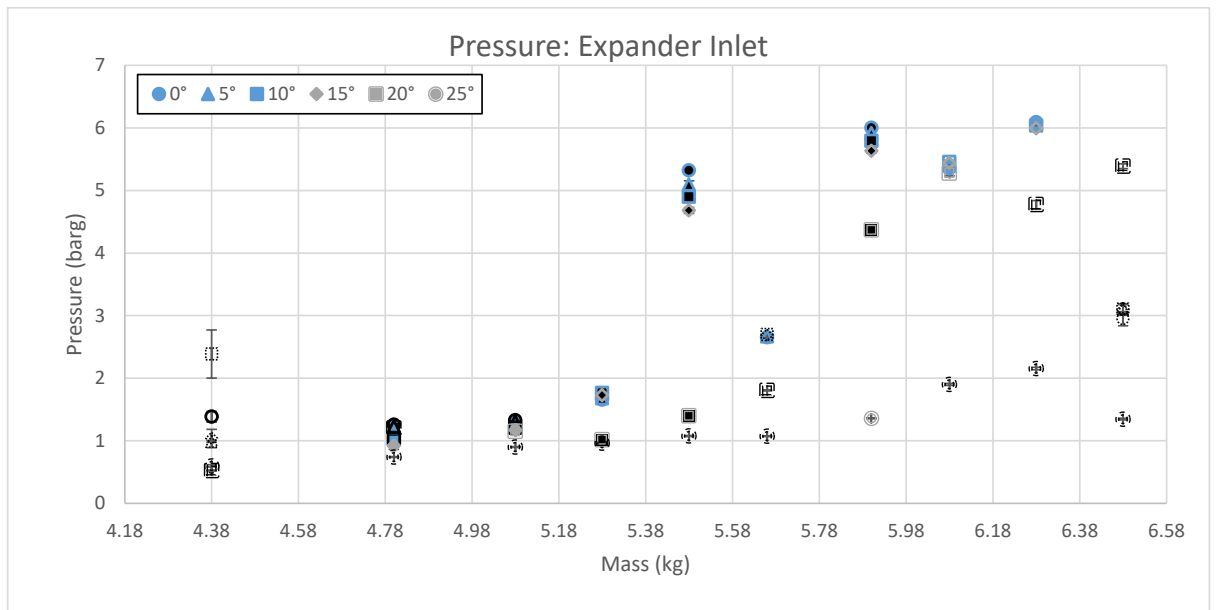
Figure 193: Expander inlet pressure for various system charges and multiple bypass valve postitions at 1200 rpm pump speed. The trend of the expander inlet pressure is the same as the pump outlet pressure in Figure 192.

The low pressure side of the system is shown in Figure 194, Figure 195, Figure 196 and Figure 197: the expander outlet, condenser outlet, sub cooler inlet and pump inlet pressure respectively. In all four cases there is no significant change in low side pressure with increasing bypass angle with the exception of above 15° bypass angle at the subcooler inlet and pump inlet. In both cases there is a respective increase in pressure with further increasing bypass angle.
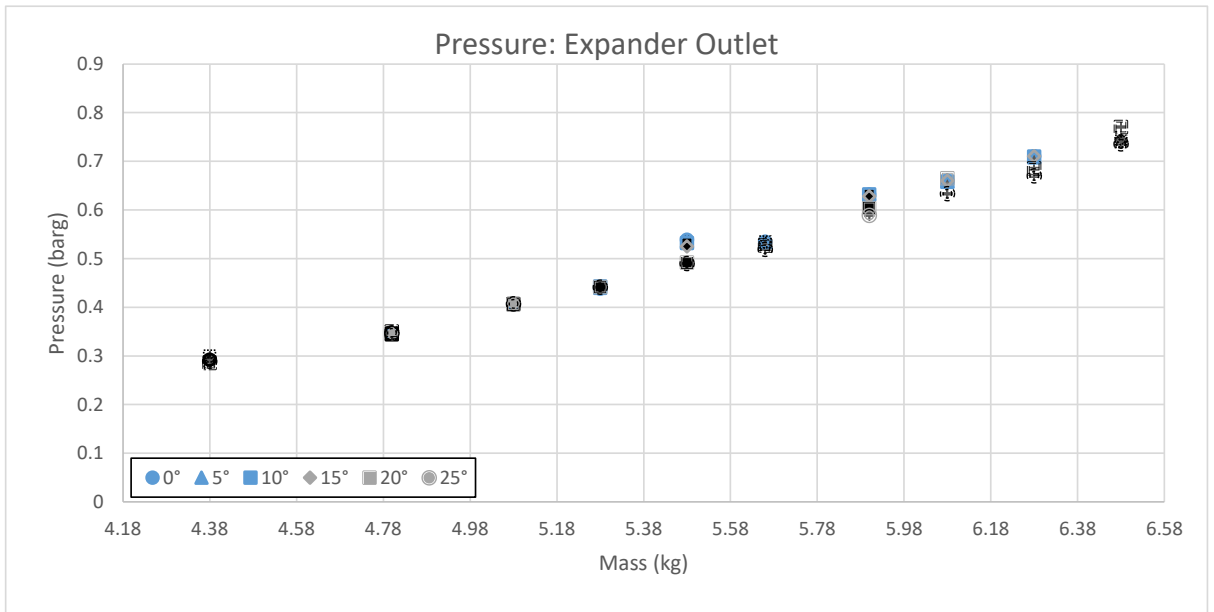
Figure 194: Expander outlet pressure for various system charges and multiple bypass valve postitions at 1200 rpm pump speed. In comparision to the effect of increasing mass the bypass opening angle has ngeligiable effect on the expander outlet presure.
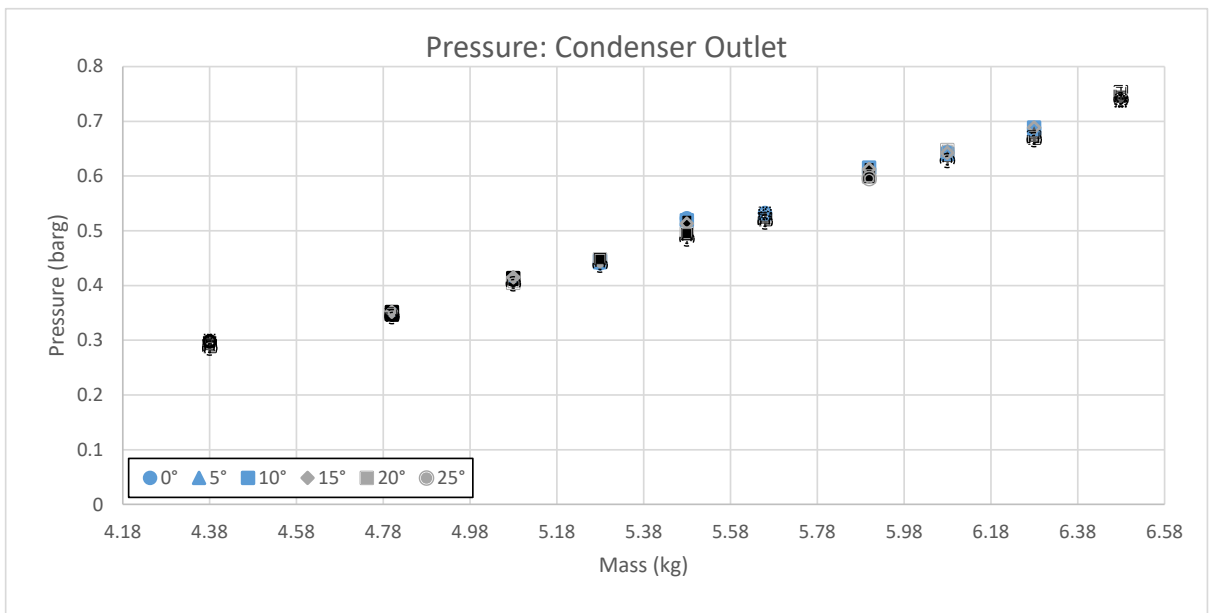
Figure 195: Condenser outlet pressure for various system charges and multiple bypass valve postitions at 1200 rpm pump speed. In comparision to the effect of increasing mass the bypass opening angle has negligable effect on the condenser outlet pressure.
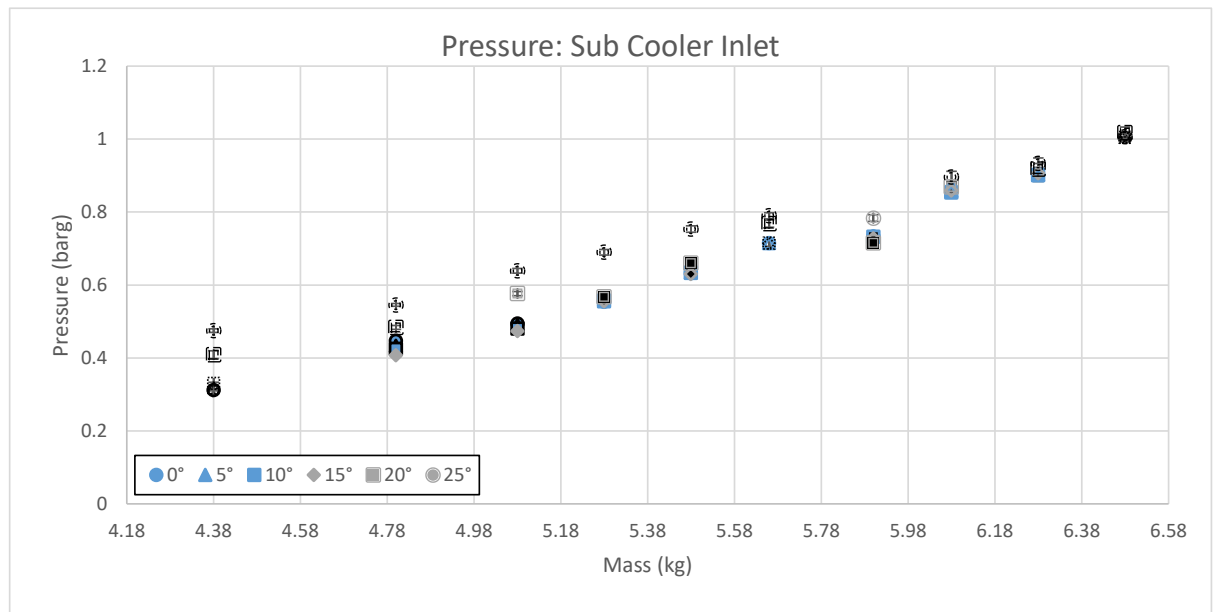
Figure 196: Sub cooler inlet pressure for various system charges and multiple bypass valve postitions at 1200 rpm pump speed. Upto 15° opening angle there is no singificant change in sub cooler inlet pressure with increasing degree of bypass. Further increase results in an increase in subcooler inlet pressure.
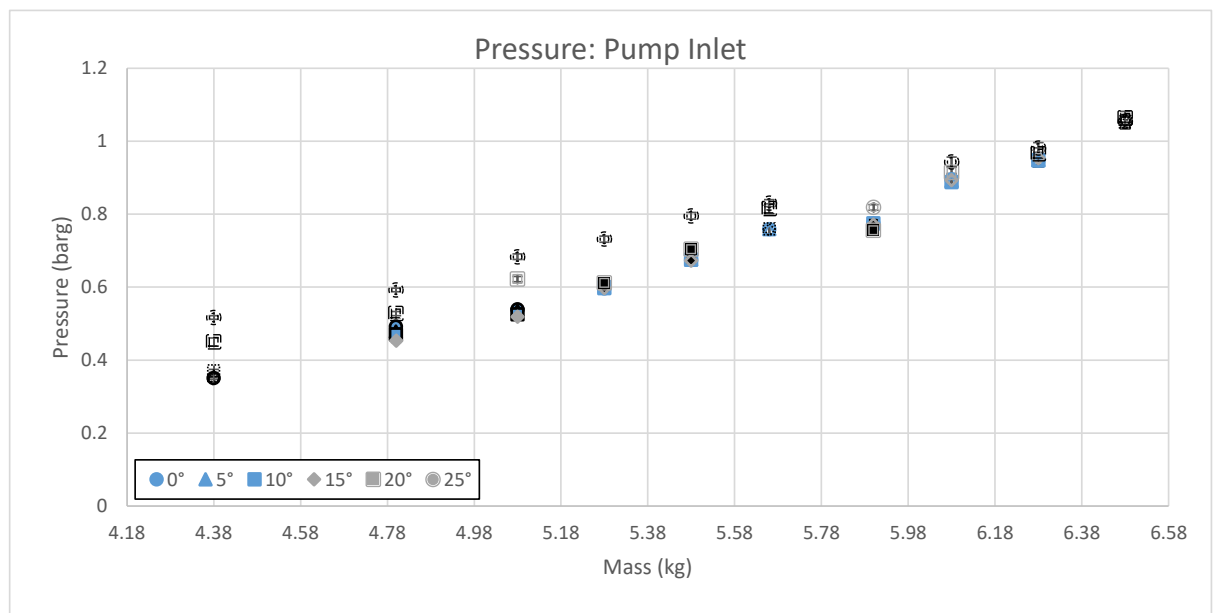
Figure 197: Pump inlet pressure for various system charges and multiple bypass valve postitions at 1200 rpm pump speed. Upto 15° opening angle there is negligable change in pump inlet pressure. Further increase in bypass angle results in an increase in pump inlet pressure.

Temperature:

The cold water feed, cold water return and condenser outlet temperature are shown in Figure 198, Figure 199 and Figure 200. The controlled cold water feed and condenser outlet temperature follow a very similar trend with a variation of less than 1°C over the entire test range and significantly less for each individual mass increment. There is a significant jump in cold water return temperature initial at 4.58kg of system charge and

again at 5.88kg. However, in all cases there is no significant change in temperature with increasing bypass angle upto 15°, a further increase results in a reduction in temperature.
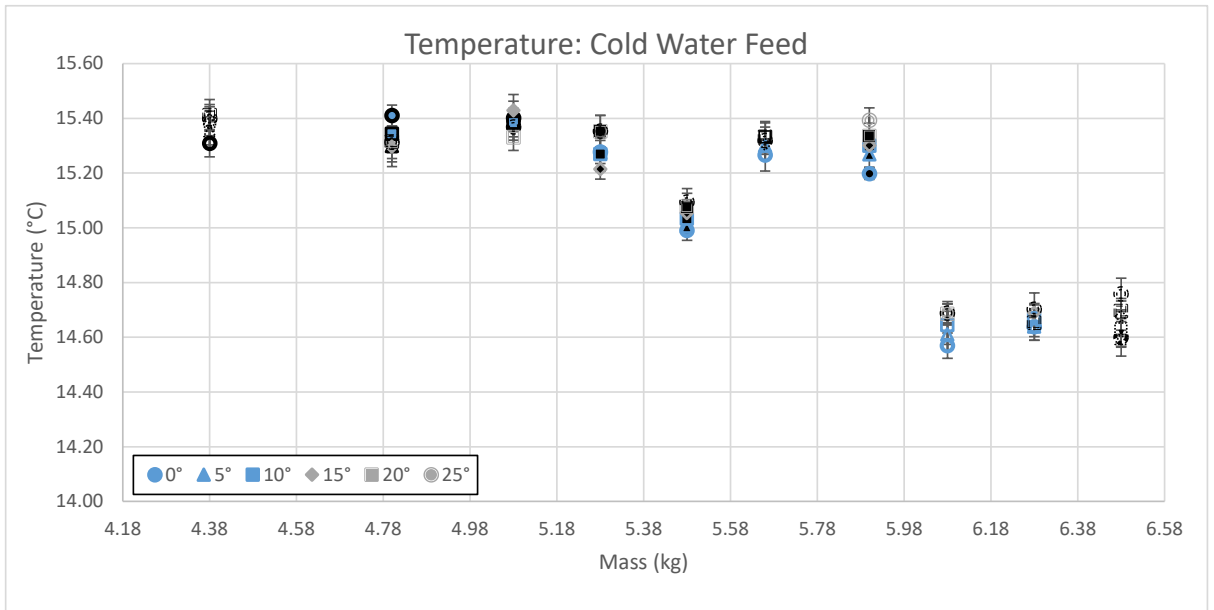
Figure 198: Cold water feed temperature for various system charges and multiple bypass valve postitions at 1200 rpm pump speed. The cold water feed is externally controlled and has less than 1°C variation in temperature across the entire test range. For each individual mass test run the variation is significantly less.

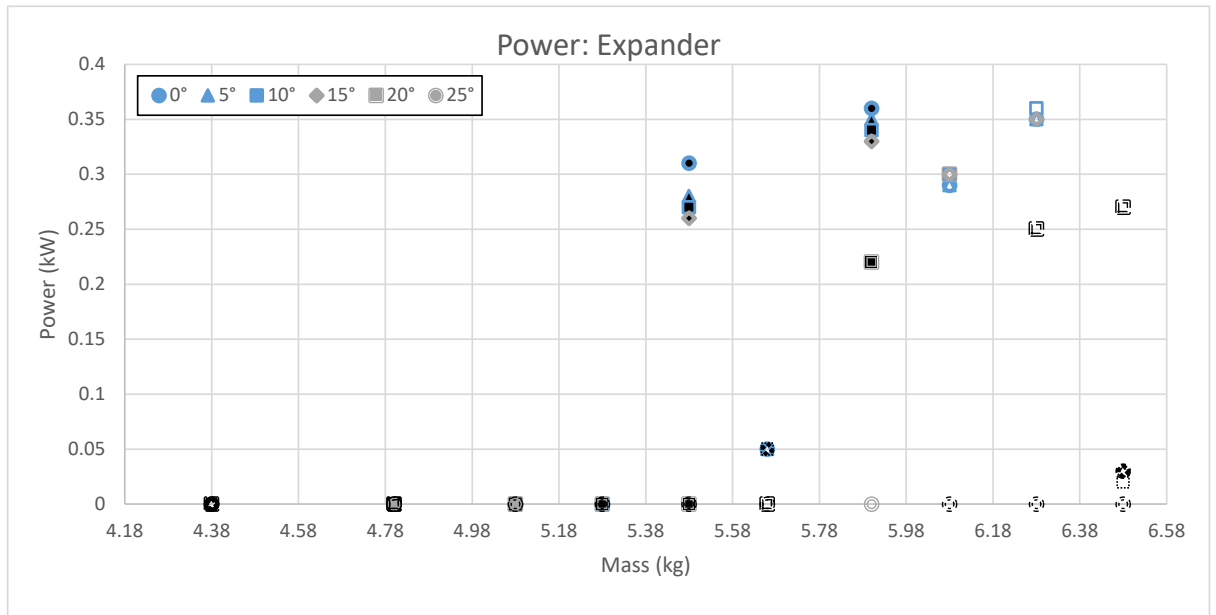*Figure 199: Cold water return temperature for various system charges and multiple bypass valve postitions at 1200 rpm pump speed. Below 5.48kg of system charge the cold water return temperature remains below 18°C. Above 5.48kg of charge there is a significant increase in return temperature. Upto 15° opening angle there is no signficant change. Further increase results in a reduction in the cold water return temperature.*
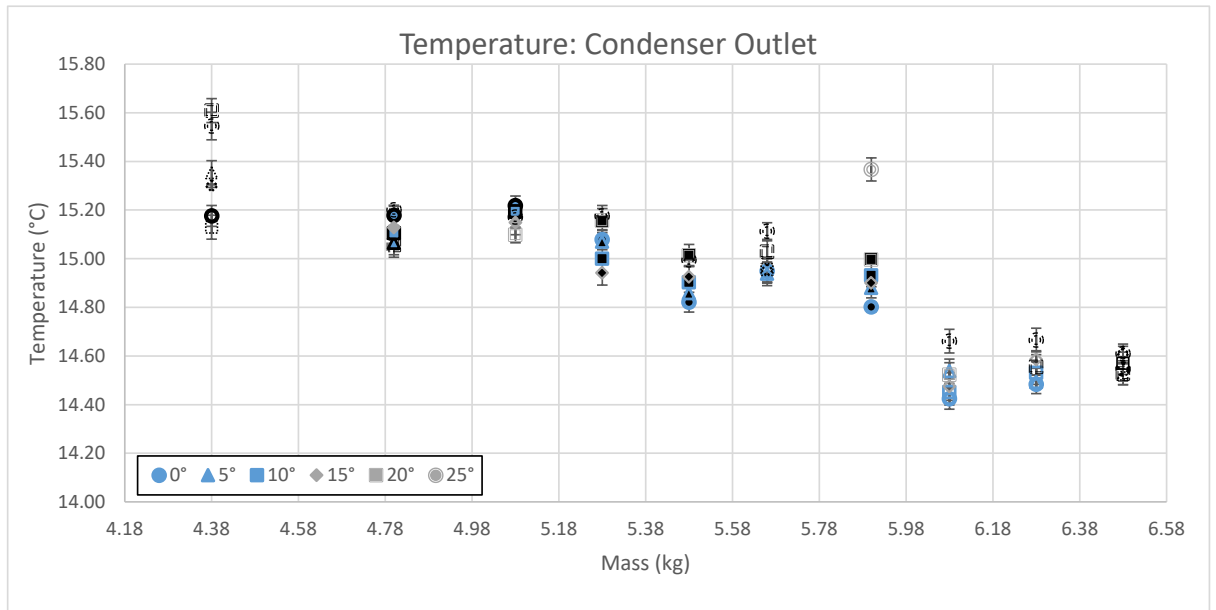
Figure 200: Condenser outlet for various system charges and multiple bypass valve postitions at 1200 rpm pump speed. With the exception of the first mass run the remaining test points have a relatively minnor change in temperature with bypass opening angle.

The pump inlet, pump outlet temperature is shown in Figure 201 and Figure 202 respectively. In both cases upto 15° bypass angle results in no significant change in temperature. A slight increase in temperature is observable in some cases at 20° bypass angle with a more significant increase observable for the 25° case.
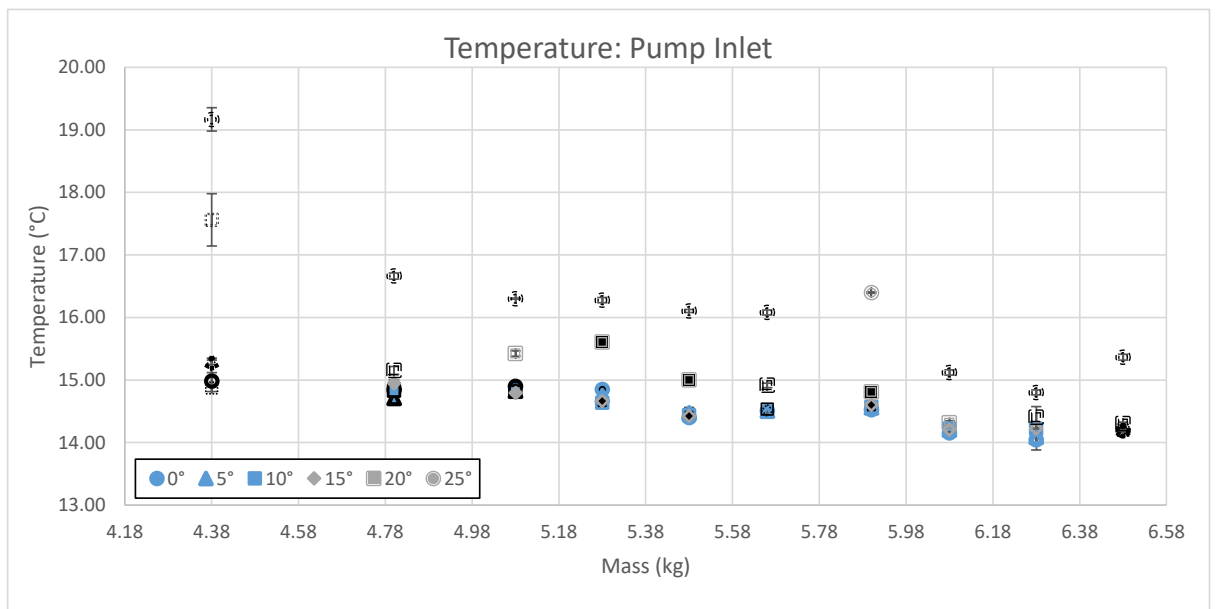
Figure 201: Pump inlet temperature for various system charges and multiple bypass valve postitions at 1200 rpm pump speed. Upto 15° opening angle there is no significant change with increasing opening angle. Further increase results in an increase in pump inlet pressure.
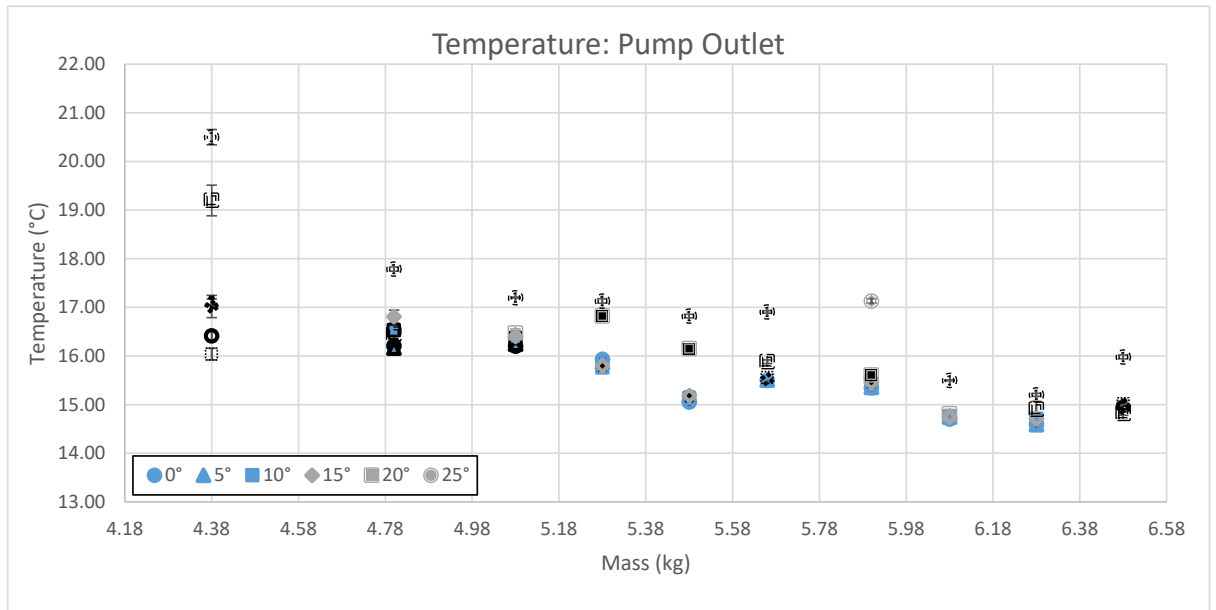
Figure 202: Pump outlet temperature for various system charges and multiple bypass valve postitions at 1200 rpm pump speed. Upto 15° there is no significant change in pump outlet temperature with increasing bypass angle. Further increse results in an increase in pump outlet temperature.

The evaporator inlet temperature is shown in Figure 203, below 5.28kg of system charge in this case there is no consistent trend between evaporator inlet and bypass angle. Above 5.28kg of system charge and upto 15° bypass angle there is no significant change in temperature with increasing bypass angle. For the most part in this system charge range a further increase in bypass angle results in an increase in evaporator inlet temperature. The unexpectedly high temperatures are a result of temperature sensor location and give an indication of ORC system flow.
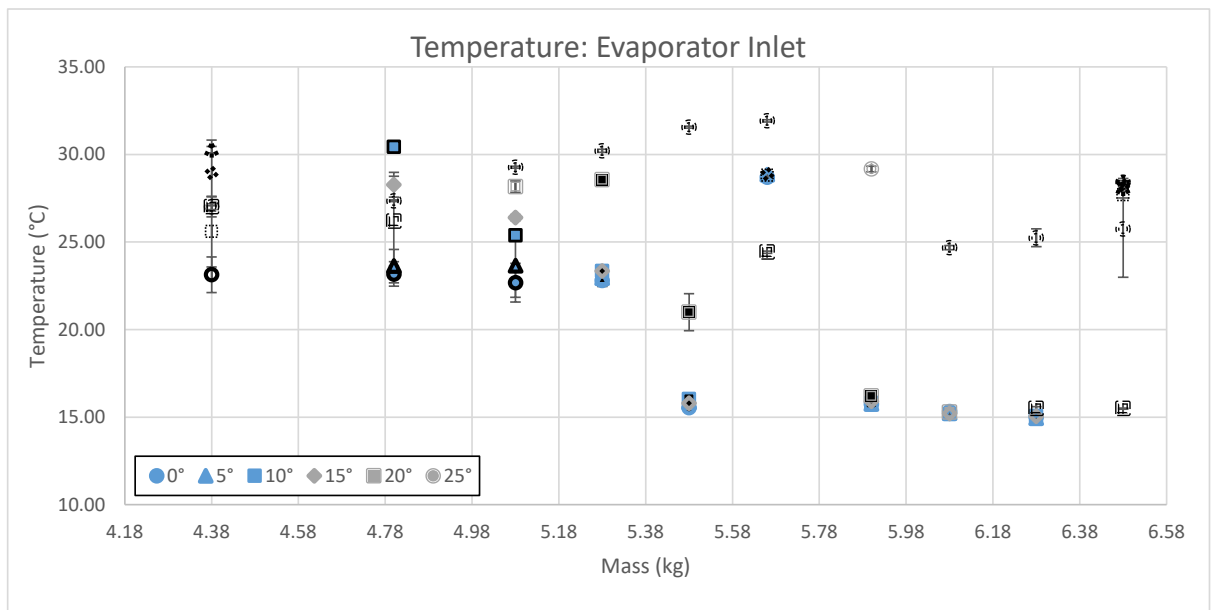
*Figure 203: Evaporator inlet temperature for various system charges and multiple bypass valve postitions at 1200 rpm pump speed. **Note: the location of the temperature sensor effects the measurement at the evaporator inlet and gives an indication of system flow.** Above 5.08kg and upto 15° opening angle there is no significant change in evpaorator inlet*

temperature with increasing opening angle. Further increase in opening angle results in an increase in evaporator inlet temperature. Below 5.08kg there is no obvious trend with increasing bypass opening angle.

The hot water feed and hot water return temperature are shown in Figure 204 and Figure 205. The controlled water feed temperature has an overall variation of less than 3°C with the exception of one outlying data point. In a similar manner to other data presented in this section, below 5.48kg of system charge there is only a small variation in temperature between the majority of data points. This changes at 5.48kg of system charge and again above 5.88kg where there is no significant change in temperature upto 15° bypass angle with further increase resulting in a rise in temperature.
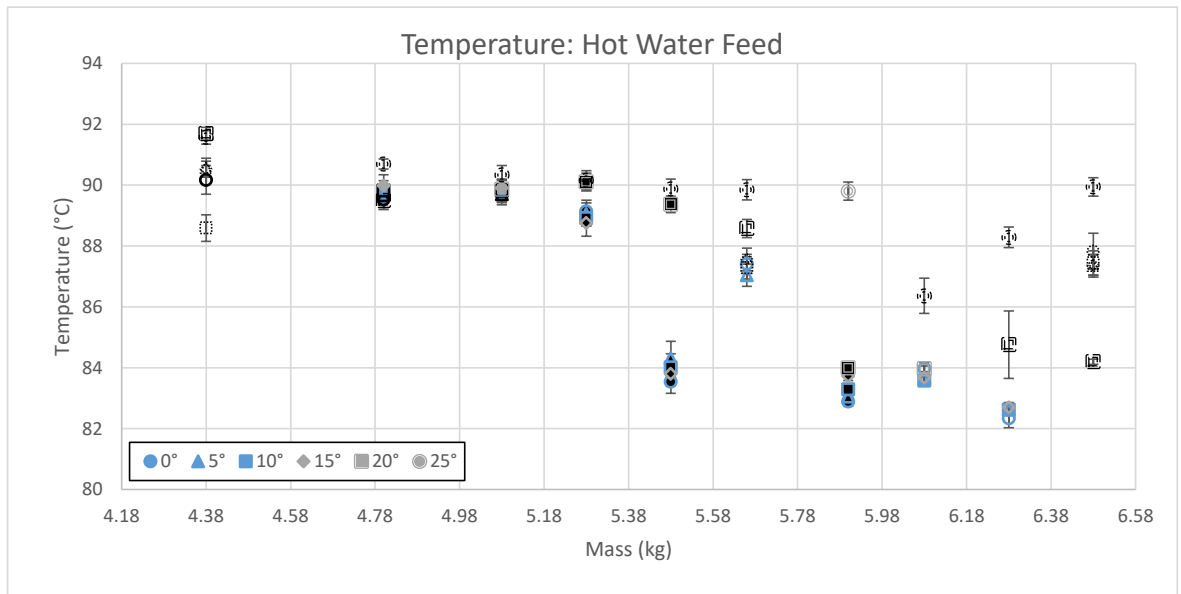
Figure 204: Hot water feed temperature for various system charges and multiple bypass valve postitions at 1200 rpm pump speed. The extrenally controlled hot water feed temperature has a higher than normal overall variation across the entire test range of 4°C. For each individual mass run the variation is in the most part significantly less.
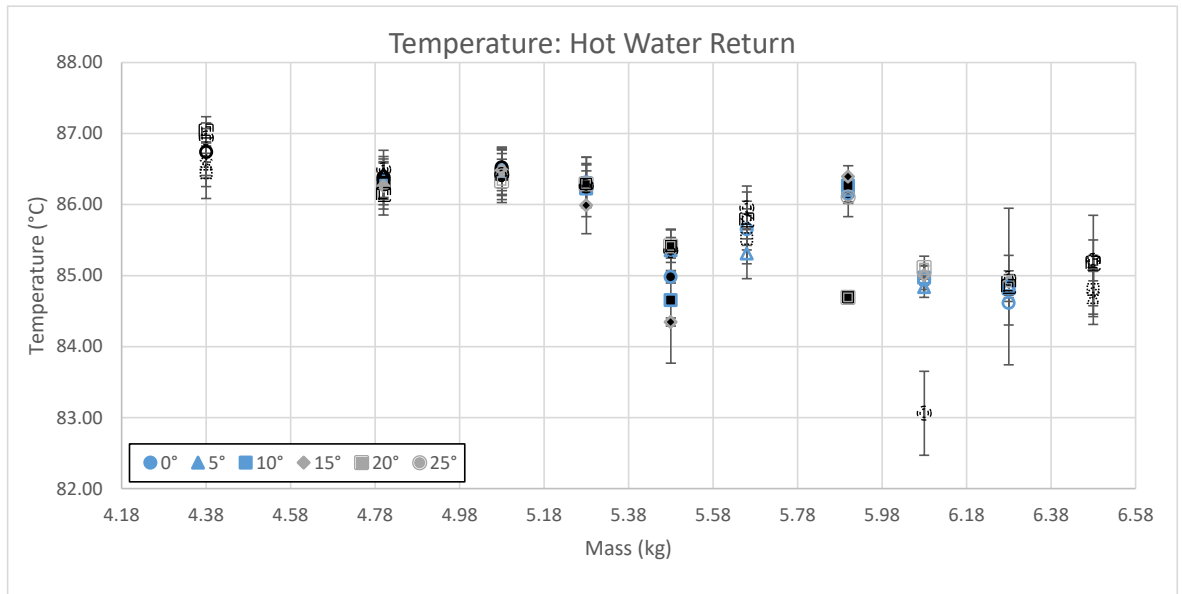
Figure 205: Hot water return temperature for various system charges and multiple bypass valve postitions at 1200 rpm pump speed. The higher degree of variation in the feed temperature is reflected in hot water return temperature data.

The expander inlet and outlet temperature are shown in Figure 206 and Figure 207. In both cases above 5.08kg of charge and upto 15° bypass opening angle there is no significant change in temperature. Further increase in bypass angle results in a larger variation in temperature.
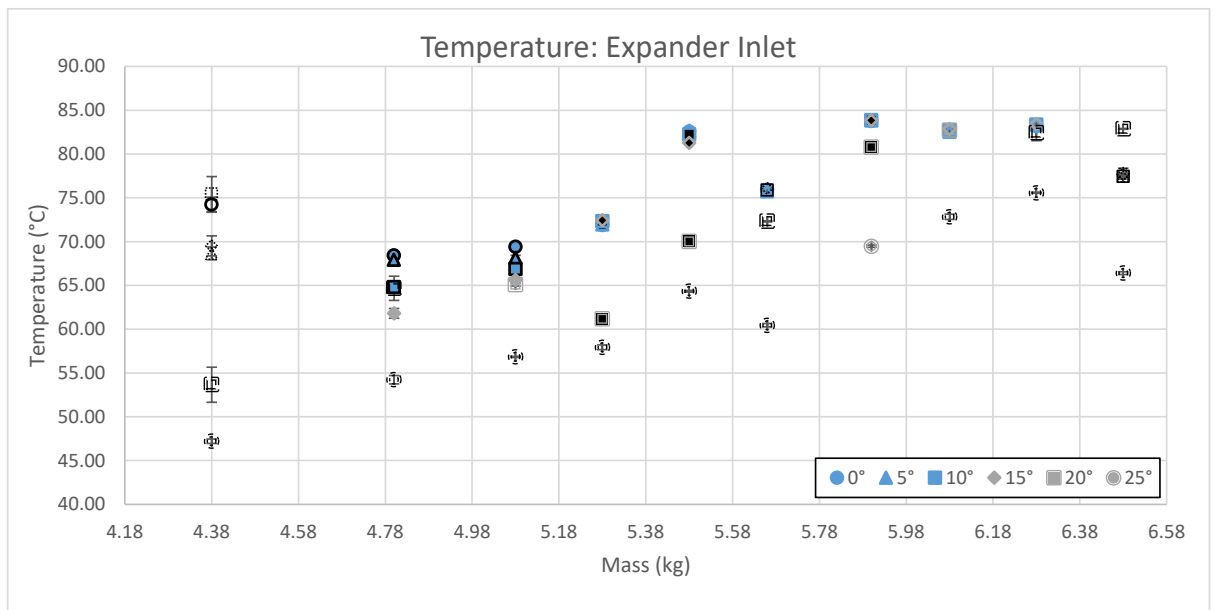
Figure 206: Expander inlet temperature for various system charges and multiple bypass valve postitions at 1200 rpm pump speed. Above 5.08kg of system charge and upto 15° opening angle there is negligiable change in expander inlet temperature with increasing opening angle. Further increase in opening angle results in a reduction in expander inlet temperature. below 5.08kg of system charge there is no obvious trend with bypass opening angle.

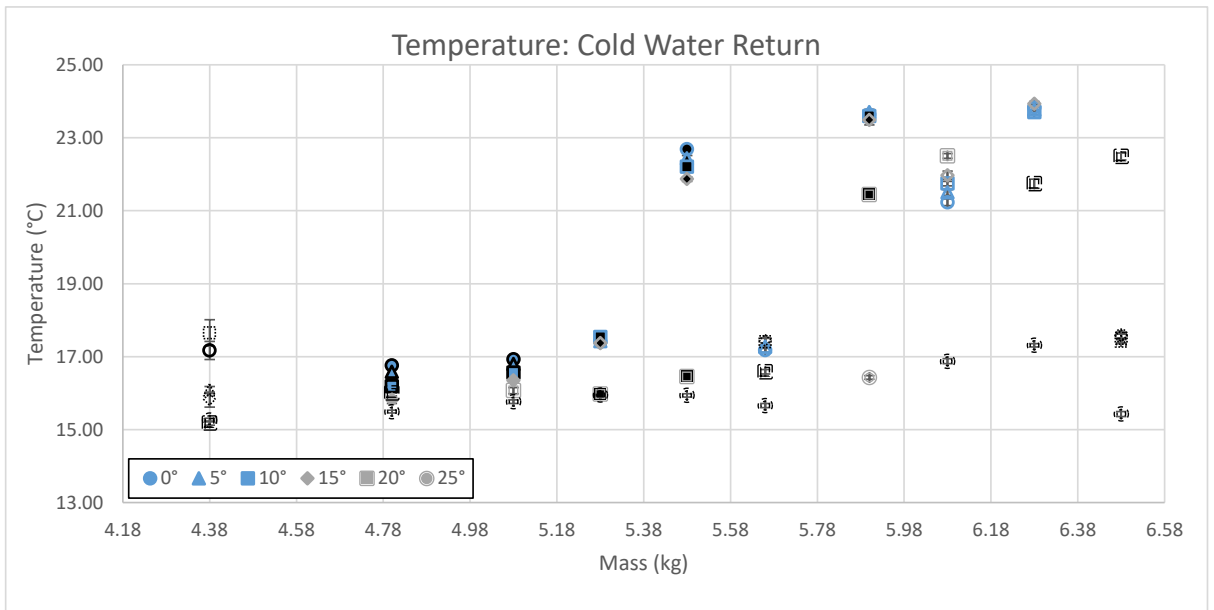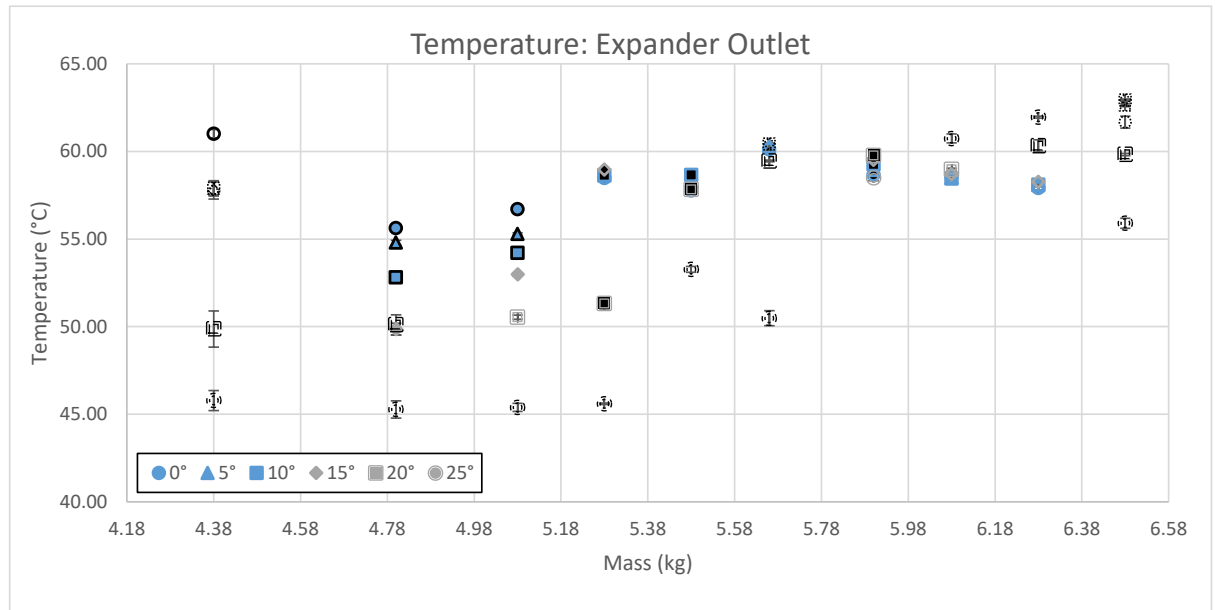*Figure 207: Expander outlet temperature for various system charges and multiple bypass valve postitions at 1200 rpm pump speed. Above 5.08kg of system charge an upto 15° opening angle there is negligable change in expander outlet temperature with increasing bypass angle. Below 5.88kg of charge and above 15° opening angle results in a decrease in expander outlet temperature, and above 5.88kg results in an increase in expander outlet temperature.*

6.4. **Analysis and Discussion**

The experimental effects of a combined pump bypass and liquid column height approach to cavitation mitigation was examined in this chapter at three pumps speeds of 800, 1000 and 1200 rpm. The results show that the addition of a bypass valve doesn't help mitigate the impacts of pump cavitation in this case and only results in a detrimental impact on the ORC system parameters.

The addition of the bypass valve for the 800rpm pump speed case provided no improvement in the overall performance of the ORC system. The opening of the bypass valve results in an increase in pressure at the subcooler inlet and pump inlet but this increase in pressure does not help the system. It is likely that the system charge and resulting liquid column height at the lowest system mass charge was sufficient to meet the Net Suction Head requirement of the pump. Therefore any reduction in high side pressure as a result of flow bypass would result in the observed deterioration in system performance.

6.5. **Summary**

The effect of liquid column height and pump bypass where tested at different operational pump speeds to determine the combined influence on the performance of the ORC pump. The liquid column height alone performed in the same manner as the results in Chapter four, with the addition of the pump bypass having no positive influence on the ORC performance.

Chapter 7 - Conclusions and Outlook

The worldwide burning of fossil fuels is having a direct impact on the rising global temperature as a result of greenhouse gases. The UK government along with other countries has set ambitious targets to reach net zero carbon emissions. In order to reach these targets, reducing our energy consumption with increased system efficiency and better utilization of energy plays an important role. Large amounts of waste heat is produced in many of our domestic and industrial processes, which in most cases is discarded to atmosphere. In order to recover energy from waste heat various solutions have been developed one of which is the organic Rankine cycle (ORC). The ORC is based off the traditional steam power plant except organic fluids are used instead of steam, usually refrigerants. The cycle pump is normally a commercially sourced component, not designed specifically for ORC application. This can cause numerous issues one of which is pump cavitation. Pump cavitation in ORC systems can cause various problems including, noise, vibration, damage and mass flows problems.

This work set out to investigate the effects of cavitation on the performance of microscale ORC systems and evaluate the main techniques and their combined interaction for mitigating cavitation. Initially, a micro scale ORC system was designed and constructed to test the effects of liquid column height on the performance of the pump. The system was designed with a significant vertical distance between the condenser outlet and the pump inlet (2.3m). It became apparent when testing begin that the design of the liquid column was extremely sensitive to mass variations, which lead to an unstable system with significant surging followed by collapse. In order to improve the stability of the system, the liquid column was modified to increase the mass storage capacity. Resulting in a significantly more stable system. However, a 3°C variation in condenser chilled water supply led to significant error in the data analysis. The chilled water system was also then modified to produce significantly more stable temperatures.

The system was then tested under various conditions to investigate the influence of mass and liquid column height on the ORC performance. Firstly the system was tested at a single set of system temperatures with increasing system mass at four pump speeds of 600, 800, 1000 and 1200rpm. In the 600, 800 and 1000 rpm case the system trends where the same. Increasing mass resulted in an increase in performance up to a peak value, any further increase in system mass resulted in a deterioration in output. The experimental data indicates that as the mass/liquid column is increased the operation of the pump improves.

Once the increase in mass no longer improves the pump output, the continued increase in low side pressure reduces the pressure difference across the expander, reducing system output. The highest tested pump speed of 1200 rpm did not conform to this trend. The maximum output of the system was significantly less than the 1000 rpm case and the stability of the system was questionable. Although, the calculated required liquid column height for the 1200 rpm case (2.5m) could not be achieved due to physical limits. The available net positive suction head measured at the pump inlet was significantly above the manufactured stated requirement. However, at this rotational speed the available liquid height alone was not sufficient to ensure stable operation of the pump.

In order to test the potential effects of other system parameters on the liquid column. Three cold side supply temperatures and three expander loads where tested at a single pump speed, with increasing system mass. The results produced a significant amount of repetition. The change in expander load had significant effect on the high pressure side of the system and the expander output. However, changes in expander load had negligible effect on the liquid column height and the pump inlet pressure, and therefore has no effect on the available NPSH of the ORC cycle. Likewise, changing the condenser temperature of the ORC system had no effect on the stored liquid column height. There is however a change in the pump inlet pressure as a result of changes in saturation temperature. As a result an increase in temperature corresponds with a small increase in NPSH.

Due to the inability of the pump to operate at the highest pump speed of 1200 rpm at the limits of test system 1. The ORC rig was modified to include a subcooler and a pump bypass to test the combined effects of mass, subcooling and pump bypass on the performance of the pump. A reduction in subcooler temperature in 2°C increments from 14°C to 6°C and bypass valve opening angle increments of 5° from 0 to 25°C, was tested at three pump speeds of 800, 1000 and 1200rpm in a single increasing mass test run. The test has be carried out in this manner to allow direct comparison between the mass, subcooling and bypass.

The experimental data concluded that a pump bypass valve provided no positive benefit to the ORC system and only resulted in a deterioration in the performance of the ORC system.

The subcooling of the liquid entering the pump provided no discernible benefit to the 800 rpm test case. Due to decrease in expander performance with increasing mass during the test range. It is strongly suspected that the lower end of the tested range was already above

the optimum mass point and therefore subcooling the liquid would provide no further benefit. The interaction between the subcooling and liquid column height was significantly more visible for the 1000 rpm and 1200rpm case. The addition of subcooling resulted in stable operation of the pump at the 1200rpm case. However, the increased output at the 1200 rpm case resulted in a system efficiency of 3.6% compared with 3.7% from test system 1 and 1000rpm. It is fairly evident from this that the increased cost and complexity of adding a sub cooler does not provide any benefit to the tested ORC system.

The issue of pump operation and feasibility of micro scale ORC systems remains a persistent challenge. Based on the findings of this work a number of areas require further work. Firstly: there remains a significant discrepancy between the required NPSH outlined by the manufacture for the chosen pump and the required level for the pump to operate effectively. Various attempts were made to find the underlying reason behind this during this work however one could not be found. Secondly, in order to achieve full operation of the pump a stored liquid column height of approximately 2m and significant subcooling was required. Neither of these additions are practically convenient and therefore significantly restrict the adoption of ORC systems into commercial settings. Further work is needed in the design, of diaphragm pumps in this case, to improve the system feasibility. Thirdly: Information produced from direct comparisons of different ORC pumps remains scare in the ORC literature. Future work in comparing different types of pumps and their required system requirements would be beneficial.

References

[1]   United Nations, "Paris Agreement," 2015.

[2]   HM Government, "Net Zero Strategy: Build Back Greener," UK Government, 2021.

[3]   S. Quoilin, V. Lemort and J. Lebrun, "Experimental study and modeling of an Organic Rankine Cycle using scroll expander," *Applied Energy,* vol. 87, pp. 1260-1268, 2010.

[4]   A. Landelle, N. Tauveron, R. Revellin and P. Haberschill, "Performance investigation of reciprocating pump running with organic fluid for organic rankine cycle," *Applied Thermal engineering,* vol. 113, pp. 962-969, 2017.

[5]   X. Yang, J. Xu, Z. Miao, J. Zou and C. Yu, "Operation of an organic Rankine cycle dependent on pumpin flow rates and expander torques," *Energy,* vol. 90, pp. 864-878, 2015.

[6]   D. Ziviani, S. Gusev, S. Lecompte, E. Groll, J. Braun, W. Horton, M. van den Broek and M. De Paepe, "Optimizing the performance of small-scale organic Rankine cycle that utilizes a single-screw expander," *Applied Energy,* vol. 189, pp. 416-432, 2017.

[7]   M. Bianchi, L. Branchini, N. Casari, A. De Pascale, F. Melino, S. Ottaviano, M. Pinelli, P. Spina and A. Suman, "Experimental anlaysis of a micro-ORC driven by piston expander for low-grade heat recovery," *Applied Thermal Engineering,* vol. 148, pp. 1278-1291, 2019.

[8]   C. E. Brennen, Cavitation and Bubble Dynamics, Cambridge: Cambridge University Press, 2014.

[9]   Y. Jang and J. Lee, "Comprehensive assessment of the impact of operating parameters on sub 1-kW compact ORC performance," *Energy Conversion and Management,* vol. 182, pp. 369-382, 2019.

[10] Z. Miao, J. Xu, X. Yang and J. Zou, "operation and performance of a low temperature organic Rankine cycle," *Applied Thermal Engineering,* vol. 75, pp. 1065-1075, 2015.

[11] L. Liu, T. Zhu and J. Ma, "Working fluid charge oriented off-design modeling of a small scale Organic Rankine Cycle system," *Energy Conversion and Management,* vol. 148, pp. 944-953, 2017.

[12] A. Leontaritis, P. Pallis, S. Karellas and A. Papastergiou, "Experimental Study On a Low Temperature ORC Unit for onboard waster heat recovery from marine Diesel Engines," in *3rd International Seminar On ORC Power Systems*, Brussels, 2015.

[13] L. Liu, T. Zhu, T. Wang and N. Gao, "Experimental investigation on the effect of working fluid charge in a small-scale Organic Rankine Cycle under off-design conditions," *Energy,* vol. 174, pp. 664-677, 2019.

[14] R. B. Peterson, H. Wang and T. Herron, "Performance of a small-scale regenerative Rankine power cycle employing a scroll expander," *Proceedings of the Insituate of Mechanical Engineers, Part A: Journal of Power and Energy,* vol. 222, pp. 271-282, 2008.

[15] G. Pei, J. Li, D. Wang and J. Ji, "Construction and dynamic test of a small-scale organic rankine cycke," *Energy,* vol. 36, no. 5, pp. 3215-3223, 2011.

[16] S. Cao, X. Ji and J. Xu, "R245fa condenstation heat transfer in a phase separation condenser," *Experimental Thermal and Fluid Science,* vol. 98, pp. 346-361, 2018.

[17] B. F. Tchanche, G. Lambrinos, A. Frangoudakis and G. Papadakis, "Low-grade heat conversion into power using organic Rankine cycles - A review of various applications," *Renewable and Sustainable energy Reviews,* vol. 15, no. 8, pp. 3963-3979, 2011.

[18] H. Zhai, L. Shi and Q. An, "Influence of working fluid properties on system performance and screen evaluation indicators for geothermal ORC (organic Rankine cycle) system," *Energy,* vol. 74, no. 2, pp. 2-11, 2014.

[19] I. Vaja and A. Gambarotta, "Internal Combustion Engine (ICE) bottoming with Organic Rankine Cycles," *Energy,* vol. 35, no. 2, pp. 1084-93, 2010.

[20] U. Drescher and D. Bruggemann, "Fluid selection for the Organic Rankine Cycle (ORC) in biomass power and heat plants," *Applied Thermal Engineering*, vol. 27, pp. 223-228, 2007.

[21] A. Rentizelas, S. Karellas, E. Kakaras and I. Tatsiopoulos, "Comparative techno-economic analysis of ORC and gasification for bioenergy applications," *Energy Conversion and Management,* vol. 50, pp. 674-681, 2009.

[22] Turboden, "Turboden supplies 6.5 MW ORC biomass unit in U.K," biomassmagazine, 2015.

[23] "Electratherma," [Online]. Available: https://electratherm.com/case-studies/biomass-in-the-uk/. [Accessed 18 04 2020].

[24] S. Canada, G. Cohen, R. Cable, D. Brosseau and H. Price, "Parabolic trough organic Rankine cycle solar power plant," DOE solar energy technologies program review meeting., USA: Denver, 2004.

[25] S. Qouilin, M. Orosz, H. Hemond and V. Lemont, "Performance and design optimization of a low-cost solar organic Rankine cycle for remote power generation," *Solar Energy,* vol. 85, no. 5, pp. 955-66, 2011.

[26] D. Burnett, E. Barbour and G. P. Harrison, "The Uk solar energy resource and the impact of climate change," *Renewable Energy,* vol. 71, pp. 333-343, 2014.

[27] J. Freeman, K. Hellgardt and N. Markides, "An assessment of solar-powered organic Rankine cycle systems for combined heating and power in UK domestic applications," *Applied Energy,* vol. 138, pp. 605-620, 2015.

[28] E. Barbier, "Geothermal energy technology and current status: an overview.," *Rewnewable and Sustainable Energy Reviews,* vol. 6, pp. 3-65, 2002.

[29] "UK Goverment (2)," [Online]. Available: https://www.gov.uk/government/consultations/consulting-on-ending-the-sale-of-new-petrol-diesel-and-hybrid-cars-and-vans. [Accessed 15 04 2020].

[30] M. R. Gillespie, E. J. Crane and H. F. Barron, Deep geothermal energy potetnial in Scotland., Nottingham: British Geological Survey, 2013.

[31] H. Zhai, Q. An, L. Shi, V. Lemort and S. Quoilin, "Categorization and analysis of heat sources for organic Rankine cycle systems," *Renewable and Sustainable Energy reviews,* vol. 64, pp. 790-805, 2016.

[32] T. Engin and V. Ari, "Energy auditing and recovery for a dry type cement rotary kiln systems- A case study," *Energy Conversion and Management ,* vol. 46, no. 4, pp. 551-562, 2005.

[33] S. Allardyce, E. Baster, C. Kirk and W. Lamond, "Balmenach Distillery Case Study," [Online]. Available: http://www.esru.strath.ac.uk/EandE/Web_sites/10-11/Whisky/downloads/case_study.pdf. [Accessed 13 04 2020].

[34] R. E. Chammas and D. Clodic, "Combined Cycle for Hybrid Vehicles," SAE International, Warrendale, 2005.

[35] J. Song, Y. Song and C. Gu, "Thermodynamic analysis and performance optimization of an Organic Rankine Cycle (ORC) waste heat recovery system for marine diesel engines," *Energy,* vol. 82, pp. 976-985, 2015.

[36] A. T. Hoang, "Waste heat recovery from diesel engines based on Organic Rankine Cycle," *Applied Energy,* vol. 231, pp. 138-166, 2018.

[37] SEPA, "Supporting Guidance (WAT-SG-85) Application of Standards to Thermal Discharges," Scottish Environment Protection Agency, 2016.

[38] H. Chen, D. Goswami and E. K. Stefanakos, "A review of thermodynamic cycles and working fluids for the conversion of low-grade heat.," *Renewable and Sustainable Energy Reviews,* vol. 14, pp. 3059-3067, 2010.

[39] B. F. Tchanche, G. Papadakis, G. Lambrinos and A. Frangoudakis, "Fluid Selection for a low-temperature solar organic Rankine cycle," *Applied Thermal Engineering,* vol. 29, pp. 2468-2476, 2009.

[40] B. Saleh, G. Koglbauer, M. Wendland and J. Fischer, "Working fluids for low-temperature organic Rankine cycles," *Energy ,* vol. 32, pp. 1210-1221, 2007.

[41] J. Bao and L. Zhao, "A review of working fluid and expander selections for organic Rankine cycle," *Renewable and Sustainable Energy Reviews,* vol. 24, pp. 325-342, 2013.

[42] T. Guo, H. X. Wang and S. J. Zhang, "Selection of working fluids for a novel low-temperature geothermally-powered ORC based cogeneration system," *Energy Conversion Management,* vol. 52, pp. 2384-2391, 2011.

[43] J. Larjola, "Electricity from industrial waste heat using high-speed organic Rankine cycle (ORC)," *International Journal of Production Economoics ,* vol. 41, pp. 227-235, 1995.

[44] United Nations Enviromental Programme, Handbook for the Montreal Protocol on Substances that Deplete the Ozone Layer, Nairobi: Ozone Secretariat, 2018.

[45] V. Lemort, S. Quoilin, C. Cuevas and J. Lebrun, "Testing and modeling a scroll expander integrated into an Organic Rankine Cycle," *Applied Thermal Engineering,* vol. 29, pp. 3094-3102, 2009.

[46] J. A. Mathias, J. R. Johnston, J. Cao, D. K. Priedeman and R. N. Christensen, "Experimental Testing of Geroter and Scroll Expanders Used in, and Energetic and Exergetic Modeling of, an Organic Rankine Cycle," *Journal of Energy Resources Technology,* vol. 131, p. 012201, 2009.

[47] Uk Goverment, "Uk Goverment," [Online]. Available: https://www.gov.uk/guidance/uses-of-f-gas-hfcs-exempt-from-the-phase-down. [Accessed 03 04 2020].

[48] R. Zanelli and D. Favrat, "Experimental Investigation of a Hermetic Scroll Expander-Generator," in *International Compresor Engineering Conference*, West Lafayette, 1994.

[49] D. Manolakos, G. Papadakis, S. Kyritsis and K. Bouzianas, "Experimental evaluation of an autonomous low-temperature solar Rankine cycle system for reverse osmosis desalination," *Desalination,* vol. 203, pp. 366-374, 2007.

[50] D. Wei, X. Lu, Z. Lu and J. Gu, "Performance analysis and optimization of organic Rankine cycle (ORC) for waste heat recovery," *Energy Conversion and Management,* vol. 48, pp. 1113-1119, 2007.

[51] A. M. Delgado-Torres and L. Garcia-Rodriguez, "Preliminary assessment of solar organic Rankine cycles for driving a desalination system," *Desalination,* vol. 216, pp. 252-275, 2007.

[52] X. Yang, J. Xu, Z. Miao, J. Zou and C. Yu, "Operation of an organic Rankine cycle dependent on pumping flow rates and expander torques," *Energy,* vol. 90, pp. 864-878, 2015.

[53] T. Saitoh, N. Yamada and S. Wakashima, "Solar Rankine Cycle System using scroll Expander," *Journal of Enviroment and Engineering,* vol. 2, no. 4, pp. 708-719, 2007.

[54] D. Kim, J. Lee, J. Kim, M. Kim and M. Kim, "Parametric study and performance evaluation of an organic Rankine cycle (ORC) system using low-grade heat at temperatures below 80°C," *Applied Energy,* vol. 189, pp. 55-65, 2017.

[55] U. Muhammad, M. Imran, D. Hyun Lee and B. Sik Park, "Design and experiemtnal investigation of a 1 kW organic Rankine cycle system using R245fa as working fluid for low-grade waste heat recovery from steam," *Energy Conversion and Management,* vol. 103, pp. 1089-1100, 2015.

[56] T. Li, J. Zhu, W. Fu and K. Hu, "Experimental comparision of R245fa and R245fa/R601a for organic Rankine cycle using scroll expander," *International Journal of Energy Research,* vol. 39, pp. 202-214, 2015.

[57] G. Qiu, Y. Shao, J. Li, H. liu and S. B. Riffat, "Experimental investigation of a biomass-fried ORC-based micro-CHP for domestic applications," *Fuel,* vol. 96, pp. 374-382, 2012.

[58] B. Musthafah, M. Tahir, N. Yamada and T. Hoshino, "Efficiency of Compact Organic Rankine Cycle System with Rotary-Vane-Type Expander for Low-Temperature Waste Heat Recovery," *International Journal of Mechanical and Mechatronics Engineering,* vol. 4, pp. 105-110, 2010.

[59] Z. Gnutek and P. Kolasinski, "The Application of Rotary Vane Expanders in Organic Rankine Cycle Systems- Thermodynamic Description and experimental results," *Journal of Engineering for Gas Turbines and Power,* vol. 135, pp. 1-10, 2013.

[60] S. Cao, Z. Miao and J. Xu, "The effect of liquid charge ratio on organic Rankine cycle operation," *Applied Thermal Engineering,* vol. 162, 2019.

[61] S. Cao, J. Xu, Z. Miao, X. Liu, X. Xie, Z. Li, X. Zhao and G. Tang, "Steady and transient operation of an organic Rankine cycle power system," *Renewable Energy,* vol. 133, pp. 284-294, 2019.

[62] W. Gu, Y. Weng, Y. Wang and B. Zheng, "Theoretical and experimental investigation of an organic Rankine cycle for a waste heat recovery system," *Journal of Power and Energy,* vol. 223, pp. 523-533, 2009.

[63] H. A. Ingley, D. Y. Goswami and R. Reed, "Optimization of a Scroll Expander Applied to an Ammonia/Water Combined Cycle System for Hydrogen Production," in *Proceedings of the ISES solar World Congress ,* Orlando, 2005.

[64] G. Qui, H. Liu and S. Riffat, "Expanders for micro-CHP systems with organic Rankine cycle," *Applied Thermal Engineering,* vol. 31, pp. 3301-3307, 2011.

[65] K. Rahbar, S. Mahmoud, R. K. Al-Dadah, N. Moazami and S. A. Mirhadizadeh, "Review of organic Rankine cycle for small-scale applications," *Energy Conversion and Management,* vol. 134, pp. 135-155, 2017.

[66] V. Lemort, S. Declaye and S. Quoilin, "Experimental characterization of a hermetic scroll expander for use in a micro-scale Rankine cycle," *Power and Energy,* vol. 226, pp. 126-136, 2011.

[67] E. H. Kane, "Intégration et optimisation thermoéconomique & environomique de centrales thermiques solaires hybrides," Phd Thesis, Laboratoire d'Energétique Industrielle, Ecole polytechnique Fédérale de Lausanne, Suisse, 2002.

[68] T. Yanagisawa, M. Fukuta, Y. OGI and T. Hikichi, "Performance of an oil-free sroll-type air expander," IMechE, Hamamatsu, 2001.

[69] B. Aoun and D. Clodic, "Theoretical and Experimental Study of an Oil-Free Scroll Vapor Expander," in *International Compressor Engineering Conference*, West Lafayette, 2008.

[70] G. Fanti, D. Romao, R. Barbosa de Almeida and P. Batista de Mello, "Influence of flank clearance on the performance of a scroll expander prototype," *Energy,* vol. 193, 2020.

[71] H. J. Kim, J. M. Ahn, I. Park and P. C. Rha, "Scroll Expander for power generation from low-grade steam source," *Journal of Power and Energy,* vol. 221, pp. 705-712, 2007.

[72] S. Quoilin, M. Van De Broek, S. Declaye and P. Dewallef, "Techno-economic survey of Organic Rankine Cycle (ORC) Systems," *Renewable and Sustainable Energy Reviews,* vol. 22, pp. 168-186, 2013.

[73] G.Vetter, Leak-free pumps & compressors, Oxford: Elsevier Science Ltd, 1995.

[74] R. Davies, Cavitation In Real Liquids, Warren: Elsevier Publishing Company, 1962.

[75] Hydraulic Institute, "Rotodynamic Pumps for Hydraulic Perfromance Acceptance Tests," American National Standards Insitute, Net Jersey, 2016.

[76] Wanner, "www.hydra-cell.co.uk," [Online]. Available: https://www.hydra-cell.co.uk/docs/Sales-Lit-Extranet-Datasheets/G20-Datasheet.pdf. [Accessed 17 07 2022].

[77] G. Carraro, P. Pallis, A. D. Leontaritis and S. Karellas, "Experimental performance evaualion of a multi-diaphragm pump of a micro-ORC system," *Energy Procedia,* vol. 129, pp. 1018-1025, 2017.

[78] H. Zhai, I. Shi and Q. An, "Influence of working fluid properties on system performance and screen evaluation indicators for geothermal ORC (organic Rankine cycle) system," *Energy,* vol. 74, pp. 2-11, 2014.

[79] R. Long, Y. Bao, X. Huang and W. Liu, "Exergy analysis and working fluid selection of organic Rankine cycle for low grade waste heat revovery," *Energy,* vol. 73, pp. 475-483, 2014.

[80] S. Quoilin and V. Lemont, "Technological and Economical Survey of Organic Rankine Cycle," in *5th European Conference Economics and Management of Energy in Industry*, Belgium, 2009.

[81] A. Algieri and P. Morrone, "Techno-economic analysis of biomass-fired ORC systems for single-family combined heat and power (CHP) applications," *Energy Procedia,* vol. 45, pp. 1285-1294, 2014.

[82] D. Ziviani, B. Woodland, E. Georges, E. Groll, J. Braun, W. Horton, M. van den Broek and M. De Paepe, "Development and Validation of a Charge Sensitive Organic Rankine Cycle (ORC) Simulation Tool," *Energies,* vol. 9, 2015.

[83] Y. Feng, T. Hung, Y. He, Q. Wang, S. Chen, S. Wu and C. Lin, "Experimental investigation of lubricant oil on a 3 kW organic Rankine cycle (ORC) using R123," *Energy Conversion and Management,* vol. 182, pp. 340-350, 2019.

[84] O. Dumont, A. Parthoens, R. Dickes and V. Lemort, "Experimental investigation ad optimal performance assessment of four volumetric expanders (scroll, screw,piston and roots) tested in a small-scale organic Rankine cycle system," *Energy,* vol. 165, pp. 1119-1127, 2018.

[85] S. Quoilin, S. Declaye, B. Tchanche and V. Lemort, "Thermo-economic optimization of waste heat recovery Organic Rankine Cycles," *Applied Thermal Energy,* vol. 31, pp. 2885-2893, 2011.

[86] J. Sun and W. Li, "Operation optimization of an organic Rankine cycle (ORC) heat recovery plant," *Applied Thermal Energy,* vol. 31, pp. 2032-2041, 2011.

[87] M. Bamgbopa and E. Uzgoren, "Quasi-dynamic model for an organic Rankine cycle.," *Energy Conversion Management,* vol. 72, pp. 117-124, 2013.

[88] R. Dickes, O. Dumont, A. Legros, S. Quoilin and V. Lemort, "Analysis and comparison of different modeling approaches for the simulation of a micro-scale organic Rankine cycle power plant," in *3rd International Seminar on ORC Power Systems*, Brussels, 2015.

[89] R. Dickes, O. Dumont, R. Daccord, S. Quoilin and V. Lemort, "Modelling of organic Rankine cycle power systems in off-design conditions: An experimentally-validated comparative study," *Energy,* vol. 123, pp. 710-727, 2017.

[90] Hydra-Cell, "www.hydra-cell.com," [Online]. Available: http://www.hydra-cell.com/product/F20-hydracell-pump.html. [Accessed 03 02 2020].

[91] O. Kaska, "Energy and Exergy analysis of an organic Rankine for power generation from waste heat recovery in steel industy," *Energy Conversion and Management,* vol. 77, pp. 108-117, 2014.